Evaluation of Cucurbitacin B Isolated from *Corallocarpus epigaeus,* as a Candidate Drug against Malignant Melanoma

Thesis submitted to
the University of Calicut in partial fulfillment
for the award of

DOCTOR OF PHILOSOPHY IN BIOTECHNOLOGY

By

AISWARYA U S

DEPARTMENT OF BIOTECHNOLOGY
UNIVERSITY OF CALICUT
KERALA- 673635
INDIA

August 2022

DECLARATION

I hereby declare that the work presented in this Thesis entitled **'Evaluation of Cucurbitacin B Isolated from *Corallocarpus epigaeus*, as a Candidate Drug against Malignant Melanoma'** submitted to the University of Calicut, as partial fulfilment of Ph.D. programme for the award of the degree of Doctor of Philosophy in Biotechnology, is original and carried out by me under the supervision of Dr. Smitha V B, Department of Biotechnology, University of Calicut and co-guidance of Dr. Ruby John Anto, Scientist G, Division of Cancer Research, Rajiv Gandhi Centre for Biotechnology, Thiruvananthapuram. This has not been submitted earlier either in part or full for any degree or diploma of any University and there is no plagiarism using the software approved by UGC/University.

Aiswarya U S

CU Campus

Date: 29/8/2022

കാലിക്കറ്റ് സർവ്വകലാശാല
ജൈവ സാങ്കേതികവിദ്യാ പഠനവിഭാഗം
കാലിക്കറ്റ് യൂണിവേഴ്സിറ്റി പി.ഒ., മലപ്പുറം
കേരള - ഇന്ത്യ - 673 635

ഫോൺ നമ്പർ :
വകുപ്പ് തലവൻ - 0494 2407403
ഓഫീസ് - 0494 2407404

UNIVERSITY OF CALICUT
DEPARTMENT OF BIOTECHNOLOGY
Calicut University (P.O.), Malappuram (Dist.),
Kerala - India - 673 635

Tel. No : Head - 0494 2407403
Office - 0494 2407404
e-mail : biotechhod@uoc.ac.in

Re-Accredited by NAAC with "A" Grade

Certificate

This is to certify that the Thesis entitled **"Evaluation of Cucurbitacin B Isolated from *Corallocarpus epigaeus*, as a Candidate Drug against Malignant Melanoma"** submitted to University of Calicut, as partial fulfilment of Ph.D. programme for the award of the degree of Doctor of Philosophy in Biotechnology, by **Aiswarya U S**, embodies the results of bonafide research work carried out by her under my guidance and supervision at the Department of Biotechnology, University of Calicut. This Thesis has not previously formed the basis for the award of any degree, diploma, associateship, fellowship or other similar titles or recognition and that there is no plagiarism using the software approved by UGC/University. The candidate has also successfully completed the course work of the Ph.D. programme in accordance with the UGC regulations.

Dr. Smitha V B

(Research Supervisor)

Assistant Professor,
Department of Biotechnology
University of Calicut
Kerala - 673635

Date: 29/8/2022
C.U. Campus

Dr. SMITHA.V.B
Asst. Professor
Dept. of Biotechnology
University of Calicut
Malapuram 673635, KERALA, INDIA

RGCB
DISCOVERIES FOR A BETTER TOMORROW

Rajiv Gandhi Centre for Biotechnology, Thiruvananthapuram 695014, Kerala State, India.
An Autonomous National Institute for Discovery, Innovation & Translation in Biotechnology and Disease Biology,
Government of India, Ministry of Science & Technology, Department of Biotechnology.

राजीव गाँधी जैव प्रौद्योगिकी केन्द्र, तिरुवनन्तपुरम 695 014, केरल, भारत.
जैवप्रौद्योगिकी और रोग जीवविज्ञान में आविष्कार, नवीनता एवं अनुवाद की स्वायत्त राष्ट्रीय संस्थान,
भारत सरकार विज्ञान एवं प्रौद्योगिकी मंत्रालय, जैवप्रौद्योगिकी विभाग.

CERTIFICATE

This is to certify that **Ms. Aiswarya U S** has carried out the research work embodied in this thesis under my supervision and co-guidance for the full period prescribed under the Ph.D. ordinance of University of Calicut. I recommend her thesis entitled, **"Evaluation of Cucurbitacin B Isolated from *Corallocarpus epigaeus*, as a Candidate Drug against Malignant Melanoma"**, for submission for the degree of Doctor of Philosophy in Biotechnology of the University of Calicut.

Dr. Ruby John Anto, Ph.D, FNASc, FAS.
(Co-Guide)
Scientist-G
Division of Cancer Research

Dr. RUBY JOHN ANTO PhD, FNASc, FAS
Scientist G
Division of Cancer Research
Rajiv Gandhi Centre for Biotechnology,
Thiruvananthapuram-695 014

കാലിക്കറ്റ് സർവ്വകലാശാല
ജൈവ സാങ്കേതികവിദ്യാ പഠനവിഭാഗം
കാലിക്കറ്റ് യൂണിവേഴ്സിറ്റി പി.ഒ., മലപ്പുറം
കേരള - ഇന്ത്യ - 673 635
ഫോൺ നമ്പർ :
വകുപ്പ് തലവൻ - 0494 2407403
ഓഫീസ് - 0494 2407404

UNIVERSITY OF CALICUT
DEPARTMENT OF BIOTECHNOLOGY
Calicut University (P.O.), Malappuram (Dist.),
Kerala - India - 673 635
Tel. No : Head - 0494 2407403
Office - 0494 2407404
e-mail : biotechhod@uoc.ac.in

Re-Accredited by NAAC with "A" Grade

CERIFICATE

This is to certify that **Ms. Aiswarya U S** has carried out the research work embodied in this thesis under the supervision and guidance of Dr. Smitha V B, Assistant Professor, Department of Biotechnology, University of Calicut and the co-guidance of Dr. Ruby John Anto, Scientist G, Division of Cancer Research, and Rajiv Gandhi Centre for Biotechnology, Thiruvananthapuram for the full period prescribed under the Ph.D. ordinance of this University. I recommend her thesis entitled '**Evaluation of Cucurbitacin B Isolated from *Corallocarpus epigaeus*, as a Candidate Drug against Malignant Melanoma**', for submission for the degree of Doctor of Philosophy in Biotechnology of the University of Calicut.

Head of the Department

Prof.(Dr.)K.K ELYAS
Head and coordinator
Department of Biotechnology
University of Calicut,Kerala 673635

Date: 30/8/22

C.U Campus

DEPARTMENT OF BIOTECHNOLOGY ★ CALICUT UNIVERSITY ★ Date.....

ACKNOWLEDGEMENTS

I take this opportunity to owe a deep sense of gratitude to my guide, Dr. Smitha V B, Assistant Professor, Department of Biotechnology for her invaluable and inspiring guidance, enthusiastic-timely advice & stimulating criticism to materialize and successfully complete my Ph.D. work and to my Co-guide, Dr. Ruby John Anto, Scientist G, Division of Cancer Research, Rajiv Gandhi Centre for Biotechnology for her patience, motivation, enthusiasm, and encouragement to successfully complete my Ph.D. work.

I express my gratitude to Prof. (Dr). K. K. Elyas, Head of the department, for providing the facilities at the department as well as for his encouragement and kindness.

I am extremely thankful to Dr. Ravi Shankar Lankalapalli, Principle Scientist, Organic Chemistry Division, NIIST, Pappanamcode, who has always been very supportive with his exemplary guidance in the natural compound purification and characterization work. I express my sincere thanks to Dr. Sankar Sundaram, Head, Department of Pathology, Medical College, Kottayam for the histopathological verification of the tissue samples.

I thank Dr. ManishKumar, Dr. C. Gopinathan, members of the teaching faculty of the department and Dr. Tara Menon, technical assistant for their support. I hereby extend my sincere appreciation to all members of the non-teaching staff of the department, Iqbalkka - our librarian, Biju sir - section officer, Srikanth sir and Sudheesh sir – section assistants, Lalitha chechi and Shambhu chettan – lab attendees and Ramani chechi and Usha chechi – for all technical help during my research period. I also thank Dr. Pradeep A. K., Department of Botany for the help rendered for herbarium preparation and sample deposition.

My appreciation and love to all my lab mates – Faizal, Remya Chechi and Meghna. I treasure your friendship close to my heart and thank you for all the warm memories.
I would like to acknowledge all my seniors at Dr, Ruby's lab, especially, Dr. Jayesh Antony, Dr. Lekshmi R Nath, Dr. Haritha H Nair, Dr. Minakshi Saikia, Dr. Mohan Shankar G, Dr. Shabna A, Dr. Liju V B, Dr. Archana P R, Dr. Padma Krishnan, and Dr. Kalishwaralal Kalimuthu from whom I have learned most of the techniques during the initial stages of my Ph.D. work. I should especially thank Ms. Rayginia P Tenyison and Ms. Keerthana C K who have helped me at various stages of the preparation of the thesis. I appreciate the helpful nature of Jannet chechi, Devika and Shilpa for providing the routine necessities in the lab. I am very grateful to Haritha chechi, Shabna Chechi, Jannet Chechi, Swetha, Rayginia, Keerthana, Devika and Shilpa for their constant support during my low times. I find myself immensely lucky to have come across each of you.

I also thank all the co-authors and reviewers of my publication. I especially thank Dr. Nikhil P Anto, for all the support rendered during the publication of my work.

I am very much thankful to Dr. Archana S, Dr. Arya Aravind, Dr. Vishnu Sunil Jaikumar, the veterinary surgeons and all staff of the Animal Research Facility, RGCB especially, Mr. Anwar and Mr. Dileep for their valuable help in conducting of animal experiments. I am immensely indebted to all the laboratory animals who sacrificed their lives during the course of this work.

I thank all members of the Institutional Animal Ethics Committee, all members of instrumentation, animal house facility, stores and purchase, library, and security departments of RGCB, for the indispensable help rendered by them. I acknowledge the financial assistance provided by Kerala State Council for Science Technology and Environment for my project/Ph.D. work.

I express my gratitude to my seniors and friends in the Dept. of Biotechnology, for all the support and warmth. I thank all my friends at the University, my hostel mates and my roommates at the convent for your love and support, I would like to thank each and every friend of mine and their families for directly or indirectly supporting me in completing this thesis. I bow to all the wonderful people in my life for making this thesis a reality.

I cherish the unstinted support, care, and encouragement I received from my Achan, husband, Amma, my sweet Aadhuttan, Chinnu, my in-laws, grandparents, brother-in-law, and sister-in-law for which, I am highly indebted. Without their unconditional encouragement and love, I would never have been able to complete this thesis.

I am grateful to Achan for his unwavering care and devotion. He was always there for me and always supported me. I can't express my gratitude to him in a single phrase since he is everything to me and I am nothing without him.

I am grateful to my husband for his unwavering support throughout my Ph.D. tenure. Throughout these years, he was always by my side. During this difficult time, he provided me with emotional support and held my hand at the most needed time.

I'm also grateful to my son Aadhuttan, who modified and managed his daily routine to accommodate my schedule. I appreciate my mum taking better care of my son, better than I could have done. I thank her for holding my hand at the most needed time. I am grateful to my sister for always being there for me and for her unconditional support.

I thank Goddess Attukal Devi and the Lord Sri Mahadevan for providing me the grace and blessings. This work wouldn’t have been possible but for the blessings, I received from my most beloved Achan and his benediction, which has always been with me.

Aiswarya U S

CONTENTS

LIST OF TABLES

LIST OF FIGURES

ABBREVIATIONS

AIF	: Apoptosis Inducing Factor
ALP	: Alkaline phosphatase
AO	: Acridine Orange
ALT	: Alkaline transaminase
AST	: Aspartate aminotransferase
BAK	: Bcl-2 homologous antagonist/killer
BAX	: Bcl-2 associated X protein
BIM	: Bcl-2 interacting mediator of cell death
B-RAF	: B-rapidly accelerated fibrosarcoma
BRN2	: Brain specific homeobox/POU domain protein2
BSA	: Bovine serum albumin
C	: Celsius
Caspase	: Cysteine aspartase
Cu-B	: Cucurbitacin B
DAPI	: 4’6-diamidino-2-phenylindole
DMEM	: Dulbeco’s modified eagle medium
DNA	: Deoxyribose nucleic acid
DTIC	: Dacarbazine
DTT	: Dithioltreitol
ECF	: Ethyl acetate cytotoxic fraction
ECL	: Enhanced chemiluminescence
EDTA	: Ethylene diamine tetra acetic acid
ERK	: Extracellular signal regulated kinase
EtBr	: Ethidium Bromide
FADD	: Fas ligand associated death domain
FACS	: Fluorescence activated cell sorting
FBS	: Fetal bovine serum
FDA	: Food and drug administration
FITC	: Fluorescein isothiocyanate

H&E	: Haematoxylin and Eosin staining
HEPES	: (4-(2-hydroxyethyl)-1-piperazineethanesulfonic acid)
HPLC	: High performance liquid chromatography
HRP	: Horse radish peroxidase
hr	: Hour
IAEC	: Institutional animal ethical committee
IC50	: Inhibitory concentration 50
IHC	: Immunohistochemistry
IL-2	: Interleukin-2
kDa	: Kilo dalton
MAPK	: Mitogen activated protein kinase
MEK	: Mitogen activated extracellular signal regulated kinase
MEKi	: MEK inhibitor
mg	: Milligram
min	: Minute
MITF	: Microphthalmia associated transcription factor
ml	: Milliliter
MTT	: (3-(4, 5-Dimethylthiazol-2-yl)-2, 5-Diphenyltetrazolium Bromide)
MS	: Mass spectrometry
MYC	: Proto oncogene c-Myc
NF-1	: Neurofibromatosis type-1
NOD SCID	: Non-obese diabetic severe combined immune deficient
nM	: Nano molar
NMR	: Nuclear magnetic resonance
PARP	: Poly (ADP-ribose) polymerase
PBS	: Phosphate buffered saline
PCNA	: Proliferating cell nuclear antigen
PKC	: Protein kinase C
PMSF	: Phenyl methyl sulfonyl fluoride
PVDF	: Poly vinylidene didluride

RAF	: Rapidly accelerated fibrosarcoma
ROS	: Reactive oxygen species
SDS-PAGE	: Sodium dodecyl sulphate poly acrylamide gel electrophoresis
STAT3	: Signal transducers and activator of transcription 3
TBS	: Tris buffered saline
TBST	: Tris buffered saline with tween 20
TMZ	: Temozolomide
TNF	: Tumor necrosis factor
TRIS	: 2-amino-2 hydroxy methyl-propane-1-3- diol
UHPLC	: Ultra high performance liquid chromatography
UV	: Ultraviolet
WB	: Western blotting
WHO	: World health organization
µg	: Microgram
µl	: Microliter
µM	: Micro molar

Chapter 1

INTRODUCTION

INTRODUCTION

1.1. CANCER

Cancer is the term used for a broad spectrum of over a hundred types of diseases characterized by uncontrolled cell proliferation that can spread to adjacent or distinct tissue via invasion or metastasis. The multistep process of tumorigenesis begins with cellular transformation, progresses to hyperproliferation, and culminates in the acquisition of invasive potential and angiogenic properties and the establishment of metastatic lesions.

The incidence of cancer usually increases with age, inherited predisposing mutations, and exposure to various carcinogens. According to WHO, cancer is the second leading cause of death globally and is responsible for an estimated 9.6 million deaths in 2018 (Sung et al., 2021). Globally, about 1 in 6 deaths is due to cancer. The most common causes of cancer death are cancers of the Lung (1.76 million deaths), Colorectal (862 000 deaths), Stomach (783 000 deaths), Liver (782 000 deaths), Breast (627 000 deaths) (World Cancer Report 2018).

1.1.1. Cancer Classification

Cancer is classified in two ways: by its primary site of origin or by its histological or tissue types. By primary site of origin, cancer may be classified as breast cancer, lung cancer, colon cancer, liver cancer, prostate cancer, oral cancer, skin cancer, cervical cancer, etc.

Based on the tissue type, cancer may be classified as **Carcinoma** (originates from the epithelial tissue), **Sarcoma** (originates in connective and supportive tissues), **Myeloma** (originates in the plasma cells of the bone marrow), **Leukaemia** (cancer of white blood cells, especially granulocytes) and **Lymphoma** (cancer of lymphocytes).

1.1.2. Causes of Cancer

The causes of cancer are very complex, involving both the cell and factors in the environment.

- ✓ **Chemical and other Substances**

  Being exposed to substances such as certain chemicals, metals, or pesticides can increase the risk of cancer. Asbestos, Nickel, Cadmium, Uranium, Radon, vinyl chloride, benzidine, Ethyl Methane Sulfonate (EMS), Dimethyl sulfate (DMS), nitrogen mustard and benzene are examples of well-known carcinogens. These may act alone or along with another carcinogen, such as cigarettes smoke, to increase the risk of cancer.

- ✓ **Tobacco**

  Tobacco consumption is the major preventable cause of cancer (Knowles and Selby, 2005). Tobacco smoke is known to contain at least 60 carcinogens and 6 developmental toxicants. The carcinogens in tobacco smoke include benzo (a) pyrene, dimethyl nitrosamine, and nickel compounds (Cooper et al., 2007). In addition, to be responsible for 80 to 90 percent of lung cancer, cigarette smoking is also associated with cancers of the mouth, pharynx, larynx, esophagus, pancreas, kidney, and bladder. Chewing betel quid and tobacco is also an important risk factor for cancer of the mouth and pharynx. Exposure to environmental tobacco smoke (passive smoking) is also carcinogenic (Knowles and Selby, 2005).

- ✓ **Radiation**

  Certain types of radiation, such as x- rays, rays from radioactive substances, and ultraviolet rays from exposure to the sun, can produce damage to the DNA of cells, which might lead to cancer.

- ✓ **Infections**

  The viruses that cause cancer can be broadly divided into two large groups; DNA tumor viruses and RNA tumor viruses. Among the DNA viruses capable of transforming cells are polyomavirus, simian virus 40 (SV40), adenovirus, and herpes-like viruses. RNA tumor viruses are retroviruses. Other viruses linked to human cancers include hepatitis B virus, which is associated with liver cancer; Epstein-Barr virus, which is associated with Burkitt's lymphoma. Certain gastric lymphomas are associated with chronic infection by the stomach-dwelling bacterium *Helicobacter pylori*, which is also responsible for ulcers (Karp, 2009). Infestation with the Water-borne trematode, *Schistosoma haematobium* is associated with an increased risk of squamous cell carcinoma of the bladder. Food-Borne trematodes (liver Flukes) such as *Opisthorchis viverrini*, and *Opisthorchis felineus* are an established cause of cancer of the bile ducts (Knowles and Selby, 2005).

- ✓ **Dietary-related factors**

  Several dietary factors, such as fat and meat, have been suggested to increase cancer risk. Overweight and obese increase the risk of colon cancer and the risk of breast cancer in post-menopausal women. A high intake of alcoholic beverages increases the risk of cancer. Aflatoxin contaminated foods contribute to the causation of liver Cancer (Knowles and Selby, 2005).

- ✓ **Hormonal Imbalances**

  Some hormones can act similarly to non-mutagenic carcinogens that may stimulate excessive cell growth. A well-established example is the role of hyperestrogenic states in breast cancer and endometrial cancer.

- ✓ **Immune system Dysfunction**

  HIV is associated with several malignancies, including Kaposi's sarcoma, non-Hodgkin's lymphoma, and HPV-associated malignancies such as anal cancer and cervical cancer.

- ✓ **Heredity**

  Some inherited mutations in the genes BRCA 1 and BRCA 2 are associated with an elevated risk of breast cancer and ovarian cancer. Li-Fraumeni syndrome (various tumors such as osteosarcoma, breast cancer, soft tissue sarcoma, brain tumors) due to mutations of p53. Hereditary Non-Polyposis Colorectal Cancer (HNPCC, also known as Lynch syndrome) can include familial cases of colon cancer, uterine cancer, gastric cancer, and ovarian cancer. Retinoblastoma, when occurring in young children, is due to a hereditary mutation in the retinoblastoma gene.

- ✓ **Ageing**

  Aging is another fundamental factor in the development of cancer. The incidence of cancer rises dramatically with age, most likely due to a build-up of risks for specific cancers that increase with age. The overall risk of accumulating mutations is combined with the tendency for cellular repair mechanisms to be less effective as a person grows older.

1.1.3. Cancer therapy

Surgery, radiation therapy and chemotherapy are the three main treatment modalities adopted in the clinic for cancer therapy. Surgery and radiation therapy is the treatment of choice for solid tumors that are localised. However, liquid cancers, locally advanced and metastasised cancer cases require chemotherapy, sometimes in combination with surgery or radiation therapy. A variety of other treatment modalities like Immunotherapy, Targeted therapy, Hormone therapy and stem cell transplantation are also employed (DeVita et al., 2008).

Surgery: involves the Removal of the tumor tissues by surgery

Radiation therapy: uses High-powered energy beams, such as X-rays or protons to kill cancer cells.

Hormone therapy: Hormones or hormone analogues used to slow or stop the growth of cancer cells.

Stem cell transplantation: Transplantations of blood and marrow stem cells are considered the most effective for blood cancers such as leukaemia, lymphoma and myeloma

Chemotherapy: Involves the use of Cytotoxic chemical agents that destroy cancer cells. Platinum derivatives, nucleoside analogues, topoisomerase inhibitors, plant-derived -taxanes and vinca alkaloids are the old generation anticancer chemotherapy agents, that target processes such as DNA replication, and microtubule dynamics which block cell division and eventually drives cells to apoptosis.

Targeted therapy/ Precision medicine: Targeted therapy is a type of cancer treatment that uses drugs or other substances to precisely identify and attack certain types of cancer cells. A targeted therapy can be used by itself or in combination with other treatments, such as traditional or standard chemotherapy, surgery, or radiation therapy. Use chemicals that targets proteins involved in cells growth, division, and spread. The proteins that targeted may be different for each type of cancers. The protein that functions abnormally and is targeted. It is a type of precision medicine.

1.2. CHEMOTHERAPY

Chemotherapy is the application of a series of chemical compounds, natural or synthetic, which leads to the induction of cell death or cell cycle arrest in cancer cells. More than 100 chemo drugs are used to treat cancer, either alone or in combination with other drugs or treatments. Chemotherapeutic drugs are classified based on their mode of action, their chemical structure, their relationships to other drugs and their source of isolation. Most drugs target cells with high proliferating propensity and also exploit deficiencies in checkpoint control, defects in DNA repair and altered apoptosis. Many anti-cancer drugs used today are very effective; however, they have undesirable side effects like stomatitis, myelosuppression, thromboembolism, infertility, cardiac dysfunction, Secondary leukemia, immune suppression, excessive hair loss, nausea and loss of appetite (Partridge et al., 2001). Another hurdle to successful chemotherapy is chemoresistance. Cancers initially respond to chemotherapeutic drugs, however, there is a decline associated with resistance to anti-cancer drugs. When continuously exposed to a particular drug for a long time, tumor cells acquire an ability to develop resistance to a broad range of structurally and functionally unrelated drugs (Vinod et al., 2013).

1.3. APOPTOSIS

Apoptosis is one of the major mechanisms by which chemotherapeutic drugs induce cell death in cancer cells. Apoptosis or programmed cell death is a normal occurrence in which an orchestrated sequence of events leads to the death of a cell. Death by apoptosis is a neat, orderly process characterized by the overall shrinkage in volume of the cell and its nucleus, the loss of adhesion to neighbouring cells, the formation of blebs at the cell surface, the dissection of the chromatin into small fragments, and the rapid engulfment of the "corpse" by phagocytosis (Karp, 2009).

Apoptosis can be triggered by both internal stimuli, such as abnormalities in the DNA, and external stimuli, such as certain cytokines (proteins secreted by cells of the immune system).

1.3.1. Extrinsic Pathway

The stimulus for apoptosis by extrinsic pathway is carried by a variety of chemicals and molecules, for e.g. extracellular messenger protein called TNF (Tumour Necrosis Factor), which was named for its ability to kill tumour cells. TNF is produced by certain cells of the immune system in response to adverse conditions, such as exposure to ionizing radiation, elevated temperature, viral infections, or toxic chemical agents such as those used in cancer therapy. TNF evokes its response by binding to a transmembrane receptor, TNFR1.TNFR1 is a member of a family of related "death receptors" that turns on the apoptotic process. The TNF receptor is present in the plasma membrane as a preassembled trimer. The cytoplasmic domain of each TNF receptor subunit contains a segment of about 70 amino acids called a death domain that mediates protein-protein interactions. The binding of TNF to the trimeric receptor produces a change in conformation of the receptor's death domain, which leads to the recruitment of a number of proteins.

The last proteins to join the complex that assembles at the inner surface of the plasma membrane are two procaspase-8 molecules. These proteins are called "procaspases" because each is a precursor of caspases; it contains an extra portion that must be removed by proteolytic processing to activate the enzyme. The synthesis of caspases as proenzymes protects the cell from accidental proteolytic damage. Unlike most proenzymes, procaspases exhibit a low level of proteolytic activity. According to one model, when two or more caspases are held in close association with one another, they are capable of cleaving one another's polypeptide chain and converting the other molecules to fully active caspases. The final mature enzyme contains four polypeptide chains, derived from two procaspases precursors.

Caspase-8 is described as an initiator caspase because it initiates apoptosis by cleaving and activating downstream, or executioner, caspases that carry out the controlled self-destruction of the cell. Another initiator caspase associated with the extrinsic pathway is caspase 10, which is activated in the same way as caspase 8.

1.3.2. Intrinsic Pathway

Internal stimuli, such as irreparable genetic damage, lack of oxygen (hypoxia), extremely high concentrations of cytosolic ca2+, viral infection, or severe oxidative stress (I.e, the production of large numbers of destructive free radicals,) trigger apoptosis by the intrinsic pathway. Activation of the intrinsic pathway is regulated by members of the Bcl-2 family of proteins, which are characterized by the presence of one or more BH domains. Bcl-2 family members can be subdivided into three groups: (1) proapoptotic members that promote apoptosis (e.g, Bax and Bak) (and 2) anti-apoptotic members that protect cells from apoptosis (e.g, Bcl-xL, Bcl-W, and Bcl-2)3 and (3) BH3- only proteins (so-named because they share only one small domain-the BH3 domain- with other Bcl-2 family members), which promote apoptosis by an indirect mechanism. According to the prevailing view, BH3-only proteins (e.g, Bid, Bad, Puma, and Bim) can exert their proapoptotic effect in two different ways, depending on the particular proteins involved. In some cases, they apparently promote apoptosis by inhibiting anti-apoptotic Bcl-2 members, whereas in other cases they apparently promote apoptosis by activating proapoptotic Bcl-2 members. In either case, the BH3-only proteins are the likely determinants as to whether a cell follows a pathway of survival or death. In a healthy cell, the BH3-only proteins are either absent or strongly inhibited, and the antiapoptotic Bcl-2 proteins are able to restrain proapoptotic members. It is only in the face of certain types of stress that the BH3-only proteins are expressed or activated, thereby shifting the balance in the direction of apoptosis. In these circumstances, the restraining effects of the anti-apoptotic Bcl-2 proteins are overridden, and certain proapoptotic members of the Bcl-2 family, such as Bax, are free to translocate from the cytosol to the outer mitochondrial membrane. Although the mechanism is not entirely clear, it is thought that Bax (and/or Bak) molecules undergo a change in conformation that cause them to insert into the outer mitochondrial membrane and assemble into a multi-subunit, protein-linked channel. Once formed, this channel dramatically increases the permeability of the outer mitochondrial membrane and promotes the release of certain mitochondrial membrane, and promotes the release of certain mitochondrial proteins, most notably cytochrome c which resides in the intermembrane space. Mitochondrial membrane permeabilization may be accelerated by a rise in cytosolic Ca+ levels following the release of

the ion from the ER. Nearly all of the cytochrome c molecules present in all of a cell's mitochondria can be released from an apoptotic cell in a period as short as five minutes.

The release of pro-apoptotic mitochondrial proteins such as cytochrome c is apparently the "point of no return", that is, an event that irreversibly commits the cell to apoptosis. Once in the cytosol, cytochrome c forms part of a multiprotein complex called the apoptosome that also includes several molecules of the initiator caspase associated with the intrinsic pathway, procaspase-9. Proscaspase-9 molecules are thought to become activated by simply joining the multiprotein complex and do not require proteolytic cleavage. Like caspase-8, which is activated by the receptor-mediated pathway described above, caspase-9 is an initiator caspase that activates downstream executioner caspases, which bring about apoptosis. The extrinsic (receptor-mediated) and intrinsic (mitochondria-mediated) pathways ultimately converge by activating the same executioner caspases (caspases 7 and caspase 3), which cleaves the same cellular targets that eventually bring about the characteristic features of apoptosis.

As cells execute the apoptotic program, they lose contact with their neighbours and start to shrink. Finally, the cell disintegrates into a condensed, membrane-enclosed apoptotic body. This entire apoptotic program can be executed in less than an hour. The apoptotic bodies are recognized by the presence of phosphatidylserine on their surface. Phosphatidylserine is a phospholipid that is normally present only on the inner leaflet of the plasma membrane. During apoptosis, a phospholipid "scramblase" moves phosphatidylserine molecules to the outer leaflet of the plasma membrane where they are recognized as an "eat me" signal by specialized macrophages. Apoptotic cell death thus occurs without spilling cellular content into the extracellular environment. This is important because the release of cellular debris can trigger inflammation, which can cause a significant amount of tissue damage.

1.4. MELANOMA

Skin cancer is the most common cancer around the world and the incidence is alarmingly on the rise. According to WHO 2020, 1.20 million new cases are reported every year (WHO, 2020). Skin cancer is the uncontrolled growth of cells in any of three layers of skin that grow and spread to another part of the body through the bloodstream where it may grow and form secondary tumors. Skin cancer is mainly classified into melanoma and non–melanoma. Melanoma develops from the pigment-producing cells known as melanocytes and is the most aggressive of all skin cancer types. Non-melanoma is of two types, basal cell carcinoma and

squamous cell carcinoma, named based on the types of skin cells from which cancer develops.

Melanoma, caused by the malignant transformation of melanocytes is the deadliest the skin cancer due to its high metastatic potential (Chan et al., 2017). The overall incidence of the disease is 324635 cases with 57,043 death per year (Sung et al., 2021). Major causes of melanoma are exposure to UV radiation, hereditary disposition and poor or compromised immune system.

1.4.1. Common molecular Pathways involved in melanoma

Cancer is caused by the accumulation of mutations in the genes regulating cell growth, division death and survival. The development and progression of each type of cancer is associated with specific mutations in the particular cell signalling pathways involved in the growth and division of the tissue or cell type in which cancer originates. The major signaling pathway involved in the initiation and progression of melanoma is the MAPK pathway. β-catenin and MITF signalling are also implicated in the progression of melanoma (Paluncic et al., 2016).

1.4.1.1. MAPK Pathway

Mitogen-activated protein kinase (MAPK) pathway has an important role in cell proliferation, differentiation, and apoptosis. Three main kinases are involved in this pathway, MAPK kinase kinase, MAPK kinase and MAPK, which activate and phosphorylate downstream proteins. The best characterized MAPK pathway is ERK/MAPK pathway. Several reports have showcased the importance of MAPK signaling in melanoma (Amann et al., 2017). This pathway is activated through the interaction of growth factors with receptors present on their cell surface, which will subsequently activate RAS and its downstream effectors, RAF (A-RAF, B-RAF, and C-RAF). These will result in the consecutive activation of MEK1/2 that in turn activates ERK1/2. Activated ERK either activates cytoplasmic targets or migrates to the nucleus and phosphorylate transcription factors like p-STAT, MITF-M, c-MYC, etc (Becker et al., 2014).

Continuous hyperactivity of the MAPK pathway is observed in 90% of clinical melanoma specimens (Cohen et al., 2002). 15-20% of melanoma cases occur due to N-RAS mutation whereas about 60% of melanoma is due to B-RAF mutation (Patel et al., 2021). In fact, elucidation of the key mutations that drive melanoma progression has resulted in targeted therapies using small-molecule inhibitors of B-RAF and MEK either alone or in combination

and has made significant progress in the treatment of melanoma (Fecher et al., 2007). However, acquired resistance poses serious limitations to the success of these small-molecule kinase inhibitors in the clinic (Amann et al., 2017). Therefore, natural agents which can selectively inhibit B-RAF, MEK and other key members of the signaling cascade and suppress the deregulated MAPK signalling may produce a better therapeutic efficacy with limited toxicity.

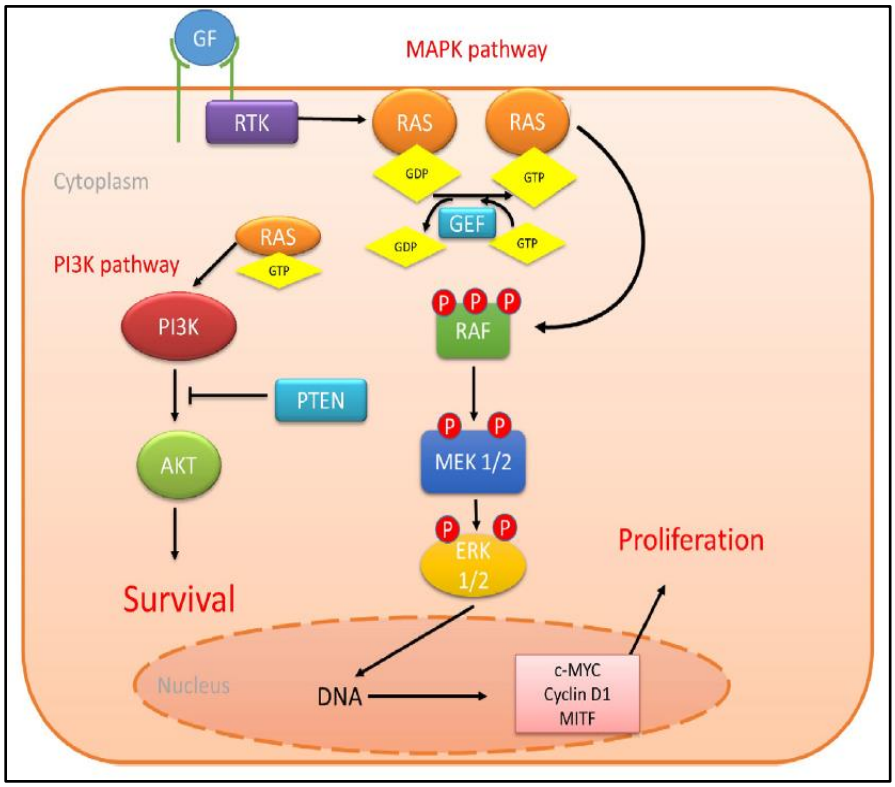

Figure: 1.4.1.1: Cellular events during MAPK signaling pathway (Paluncic et al., 2016)

1.4.1.2. Wnt/β-Catenin pathway

The Wnt signaling pathway controls cell polarity, proliferation, and migration. The initiation of intracellular signal transduction in Wnt signaling is by the binding of glycoproteins, secreted by the Wnt family proteins, to the seven-transmembrane Frizzled receptor (FZD) proteins (Komiya and Habas, 2008). There are three possible pathways activated upon this interaction; (i) a canonical β-catenin-dependent pathway; (ii) a non-canonical β-catenin independent pathway for cell polarity signaling; and (iii) a Wnt-dependent, protein kinase-C (PKC)-dependent pathway (Mosimann et al., 2009). The canonical pathway contributes to melanoma formation, while the non-canonical pathway is involved in metastasis (Kulikova et al., 2012). The key role of this pathway is the accumulation and translocation of the adherent junction complex molecule, β-catenin, into the nucleus, which interact with

other transcription factors to activate Wnt target gene expression (Figure 1.4.1.2). The presence of nuclear β-catenin in melanoma cells proves the activation of the canonical WNT/β-catenin pathway in melanoma development. Additionally, constitutively activated canonical Wnt signaling can act synergistically with the MAPK cascade, with both signaling pathways resulting in the induction of melanoma formation and development (Delmas et al., 2007). Wnt signaling is also required for the development of melanocytes from their neural crest precursors to pigment forming cells by binding β- catenin with the homeobox gene, MITF, which encodes the transcription factor, MITF(Chien et al., 2009).

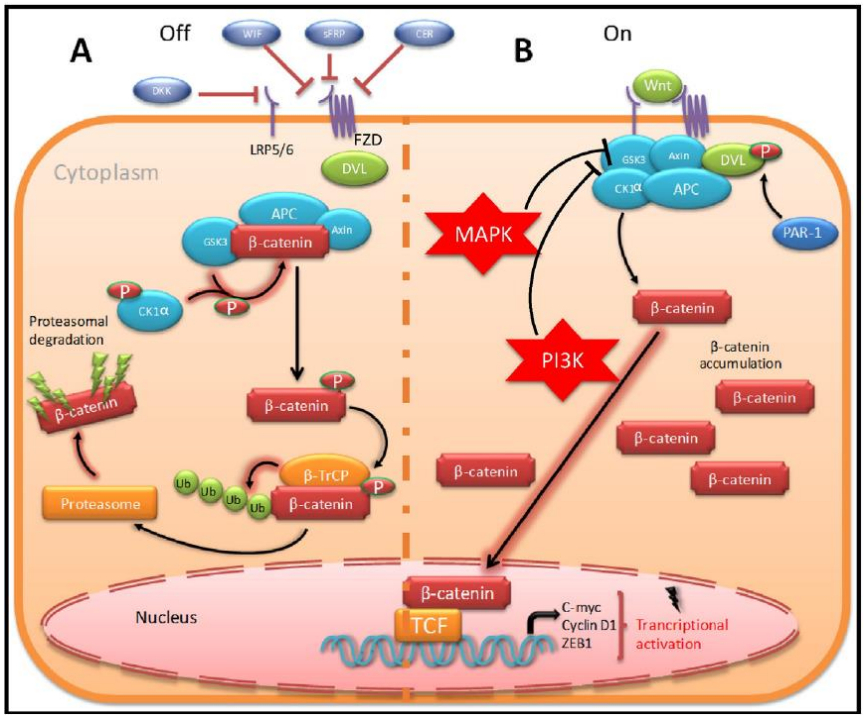

Figure 1.4.1.2: The canonical Wnt signal transduction cascade (Paluncic et al., 2016).

1.4.1.3. MITF-M signaling pathway

Microphthalmia-associated transcription factor (MITF) is commonly known as the master melanocyte transcription factor. MITF represents a distinct class of lineage survival or lineage addiction oncogene required for both tissue-specific cancer development and tumor progression. There are several pathways that regulate melanogenesis and interestingly all pathways converge at the regulatory molecule MITF-M. MITF controls the differentiation and development of melanocytes and has a critical role in melanocyte survival and proliferation. There are five isoforms for MITF, differing in their N-termini and expression patterns, they are MITF-A, MITF-B, MITF-C, MITF-H and MITF-M. The common inducer

of MITF is the Wnt signaling molecule β-Catenin and also B-RAF mediates MITF regulation by Brn-2, which is involved in melanoma proliferation (Larue and Delmas, 2006).

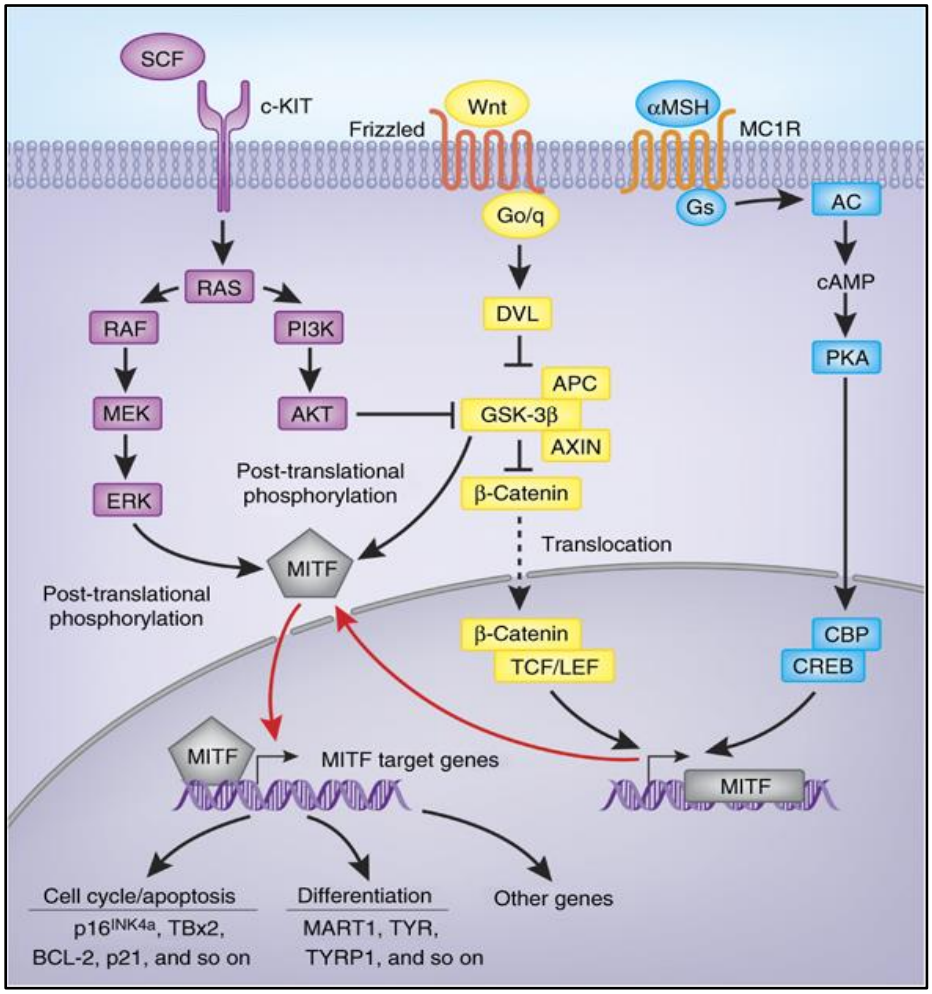

Figure 1.4.1.3: Pathways mostly activated in melanogenesis (Hocker et al., 2008).

1.4.2. Treatment of Melanoma

Treatment for early-stage cutaneous melanoma involves surgery, however, treatment of metastatic melanoma involves the use of chemotherapeutic drugs as a single agent or as multi-drug combinations. Since 1970, the FDA-approved pro drug Dacarbazine (DTIC) was used as a standard chemotherapy drug for stage IV metastasis patients. A combination of temozolomide (TMZ) (Alkylating agent) and dacarbazine (DTIC) was used for last-stage melanoma patients with progressive, refractory or relapsed disease. For stage II/III patients, high doses of interferons α-2b (INF α-2b) and interleukin-2 (IL-2) were administered as a single dose, both of which was approved by FDA in 2011 and 1998 respectively (Yang and Chapman, 2009, Omata et al., 2017).

The B-RAF mutations in melanoma cases was discovered in 2002 which was a breakthrough in melanoma treatment. The mutations in serine/threonine kinase B-RAF lead to the constitutive activation of the MAPK pathway in more than 50% of melanoma cases. Hence various targeted therapies in melanoma target B-RAF mutation. Vemurafenib was the first FDA-approved B-RAF inhibitor that was administered in patients with advanced melanoma in 2011. Another FDA-approved B-RAF-specific inhibitor is Dabrafenib, which had fewer side effects and higher potency as compared to Vemurafenib (Menaa, 2013). In 2013, Trametinib, another inhibitor that targets MEK was developed (Alcalá and Flaherty, 2012). A combination of B-RAF and MEK1/2 inhibitors was found to be more effective compared to monotherapy with any of these inhibitors. A combination of Encorafenib (B-RAFi)/ Binimetinib (MEKi) is yet another FDA-approved targeted therapy for advanced-stage melanoma which appears to efficiently delay chemoresistance (Dummer et al., 2018). Dabrafenib is often used with trametinib, a MEK inhibitor, the combination of which has been approved by FDA for the treatment of melanoma (Subbiah et al., 2020).

1.5. *Corallocarpus epigaeus*

Corallocarpus epigaeus

Taxonomic classification

Kingdom- Plantae

Phylum- Tracheophyta

Class- Magnoliopsida

Order- Cucurbitales

Family- Cucurbitaceae

Genus- Corallocarpus

Species- epigaeus

Corallocarpus epigaeus belongs to cucurbitaceae family which is commonly known by the name Bryonia, Akasha gaddah or Akashagarudankizhang. These plants are monoecious, climbers that grow up to 4m long with tuberous root. Stem is angular, tendrils simple and leaves lobed (Chandrakala et al., 2013, Cragg and Pezzuto, 2016). Roots of this species are yellowish white, marked externally with circular rings. It has a bitter and sub-acid taste, credited with alterative and laxative properties (Sivkumar et al., 2009). They are found in the dry evergreen to dry deciduous forests. They are globally distributed in the regions of India, Tropical Africa and West Asia. In India they are distributed in Andhra Pradesh, Gujarat, Karnataka, Punjab, Rajasthan and Tamil Nadu (Umadevi and Kamalam, 2012)The parts of the plant used in traditional medicine include the roots and rhizomes. *C. epigaeus* is used by tribals of Rajasthan to cure various ailments related to digestive tracts like indigestion, constipation, abdominal pain, dysentery and typhoid. It is also used to cure skin diseases like tumors, boils, sunburns, cuts and injury (Choudhary et al., 2008). The plant is also used against syphilis, chronic dysentery, chronic mucus enteritis and rheumatism (Kirtikar and Basu, 1935). It is a siddha (a system of traditional medicine) remedy for chronic eczema (Umadevi and Kamalam, 2012). The traditional healers from the rural areas of Mysore district, Karnataka use the extracted juice of the entire root for curing eczema (Jagdeepchandra et al., 2014).

Chapter 2

REVIEW OF LITERATURE

REVIEW OF LITERATURE

2.1. *Corallocarpus epigaeus*

Corallocarpus epigaeus (Cucurbitaceae) is a prostrate or climbing monoecious herb that has been known for its therapeutic potential for centuries. The root and rhizomes of the plant are yellowish white with a bitter taste and possess laxative properties (Gnananath et al., 2013; Kirtikar & Basu, 1935). The plant is indigenously known as 'Akasgaddah' in Hindi, 'Akashagarudan' in Tamil (Kirtikar & Basu, 1935; Nadkarni & Nadkarni, 1976), and 'Kilimukkan kizhangu' in Malayalam[http://indiabiodiversity.org/species/show/249147]. The parts of the plant used in traditional medicine include the roots, rhizomes and leaves. These are especially used as a remedy for syphilitic disorders and venereal complaints, chronic mucous enteritis characterized by dysentery (Swarnkar & Katewa, 2008), chronic rheumatism (Ganesan, Pandi, & Banumathy, 2007), snake bite (Kottaimuthu, 2008), and asthma (Reddy, Reddy, & Trimurthulu, 2006). Decoction of the tuber is also used as an anthelmintic (Nadkarni, 1982).

The plant extracts have been reported to possess a broad range of pharmacological properties (Jamuna, Karthika, & Paulsamy, 2015). The tuber extracts of *Corallocarpus epigaeus* are reported to have significant anti-helminthic, anti-fungal, anti-snake venom, anti-diabetic, analgesic, antipyretic and anti-inflammatory activities (Kothawade & Siddiqui, 2018).

Priyadarshini et al have reported the antibacterial activity of the hexane, petroleum ether, chloroform, acetone and methanol extracts of *Corallocarpus epigaeus* leaf, stem and tuber against various pathogenic bacteria. Among the various crude extracts, methanol extracts of the plant parts of *Corallocarpus epigaeus* were found to be the most effective against all the tested pathogens(Priyavardhini, Vasantha, TresinaSoris, & Mohan, 2012). Vasantha et al. 2012 have also reported the antibacterial activity of the Methanol extract of *C. epigaeus* leaf, stem and tuber against various pathogens such as Staphylococcus aureus, *Escherichia coli*, *Klebsiella pneumoniae*, *Serratia marcescens* and *Pseudomonas aeruginosa* (Vasantha, Priyavardhini, Tresina, & Mohan, 2012).

The same group has also investigated the anti-fungal activity of *Corallocarpus epigaeus* (Vasantha et al., 2012). Antifungal activity of petroleum ether, hexane, chloroform, acetone and methanol extracts of leaf, stem and tuber of *C. epigaeus* against *Candida albicans, C. tropicalis*, *Aspergillus niger*, *A. flavus* and *A. versicolor* by disc diffusion method was investigated. Methanol extract of *C. epigaeus* tuber exhibited maximum activity against most

of the tested fungi. The petroleum ether and hexane extracts obtained from *C. epigaeus* stem was found to be active only against *A. niger*, *A. flavus* and *A. versicolor*. All the crude extracts exhibited activity against *A. niger* and *A. flavus*. The tuber extract of *C. epigaeus* showed a higher inhibitory effect than leaf and stem.

An *in vivo* study using the crude extracts of the roots of *Corallocarpus epigaeus* revealed the analgesic, anti-oxidant, anti-inflammatory and anti-arthritic activity (Uthrapathy et al., 2011). The acute toxicity study conducted by the same group observed the LD 50 of the 85% methanolic extract of the roots to be 500 mg/Kg body weight of experimental rats.

Studies on an ethanol extract of the whole plant in Wistar albino rats have reported the anti-oxidant, anti- inflammatory, anti-hyperlipidaemic, anti-diabetic and hepatoprotective activities(Jeyaseelan, Arumugam, & Thangaraj, 2014; KB & NVNA, 2015; Mahesh, Babu, Narayana, Naik, & Malothu, 2012). In 2012, Mahesh et al., reported that ethanol and aqueous extracts showed a protective effect against toxicity induced by CCl4, which may be attributed to the individual or combined effect of hepatoprotective activity of the phytoconstituents present in it (Mahesh et al., 2012). Corallocarpus exhibited 23.19% of anti-inflammatory activity and 33.59% of anti-arthritic effect in complete Freund's adjuvant-induced paw edema (Uthrapathy et al., 2011). Ponna et al. have investigated the antivenom activity of ethanolic extracts of *C. epigaeus* and reported the neutralising effect on venom to some extent by depleting envenomated rat tissue of MDA levels (Ponna, Ranjani, Rao, & Sundarsanam, 2013). Dhanapal et al., 2006 has reported anti-steroidogenic activity of the ethanol extract of *C. epigaeus* tubers in female mice ovaries that showed a positive response (Dhanapal et al., 2006) (Dhanapal et al., 2006)

Chetty et al., in 2004 have recognized and Gnananath et al in 2013 scientifically reported the anti-diabetic activity of the rhizomes of this plant(Chetty, Shivaji, & Tulasi, 2004; Gnananath et al., 2013). Comparing the statistically significant action of a higher dose of plant extract with the standard glibenclamide group, it is clear that the extract is capable of inhibiting the elevation of blood glucose levels to the extent of action shown by the standard glibenclamide groups. Gnananath et al., concluded that the ethanolic extract of *C. epigaeus* rhizomes possesses an anti-diabetic action that is comparable with that of the standard glibenclamide drug employed(Gnananath et al., 2013).

A mitogen-associated antigen from *C. epigaeus* tuber extract was able to activate peripheral blood mononuclear cells from healthy and allergic individuals, thereby demonstrating sensitization to probably highly conserved plant antigens (Chandrakala et al., 2013).

In 2017, a pilot study was conducted to evaluate the haemopoietic activity of the Rhizome of *Corallocarpus epigaeus*. At the end of the clinical study, they observed an increase in average haemoglobin concentration from 103 g/l to 129.89g/l. they also reported a significant reduction in the degree of signs and symptoms of Pandu Rogam like Exertional tiredness, Palpitation, Paleness and Tachycardia (Saranya, Sivakanesan, & Varnakulendran, 2017). Karthic et al., in 2019 has reported potential phytotherapeutics from *Corallocarpus epigaeus* for treating urticarial. in-silico molecular docking analysis showed that all the four bioactive compounds screened *In-silico* has the tendency to bind to the most significant active site amino acid residue present in the Histamine 1 receptor, Prostaglandin H2 synthase, Cyclooxygenase I and it was also observed that none of the compounds possessed a binding affinity for Cyclooxygenase 2 (Karthic, Poongodi, Shanmugapriya, & Sivaraman, 2019).

Silver Nanoparticles synthesized by Sowmiya et al., Using Aqueous Rhizome Extract of *Corallocarpus epigaeus* exhibited bacteriostatic activity against Pseudomonas aeuginosa, *Escherichia coli*, *Proteus mirabilis, Bacillus cereus*, and *Staphylococcus aureus*.the nanoparticles also displayed fungicidal activity of Mucor species, *Aspergillus niger, Aspergillus flavus*, and Rhizopus species (Sowmiya, Aishwarya, Navamathavan, Kim, & Nirmala, 2021).

In 2020, Ishnava identified bioactive compounds n-hexadecanoic acid and 1-octadecanoic acid from ethyl acetate extract of *C. epigaeus* which was used for the treatment of helminthiasis (Ishnava & Konar, 2020).

Chitra et al., studied the Anti-acetylcholinesterase activity of *Corallocarpus epigaeus* tuber using In vitro kinetics, in silico docking and molecular dynamics analysis. They used the active constituents-rich fraction of methanol solvent extract which was obtained by silica column chromatography (Chitra et al., 2022). Kandasamy and his team synthesized gold nanoparticles from *Corallocarpus epigaeus* rhizome extract which exhibited superior antioxidant and antidiabetic activity(Kandasamy, Chinnappan, Thangaswamy, & Balakrishnan, 2020).

Although some studies have indicated the cytotoxic property of the solvent extracts of the plant on cancer cells, a thorough investigation of the anticancer potential of the plant is lacking. The cytotoxic effects of the ethanolic extract of the whole plant against the K562 cell line and methanolic root extract of *Corallocarpus epigaeus* against HT-29 and MCF-7 have been reported (Banotha et al.; Bhavani & Leelavathi, 2015). Ethanolic extract *of C. epigaeus* has appreciable growth inhibitory activity on K562 cell lines with an IC50 of 78.84µg/ml (Banotha et al.). The methanolic root extract of the plant *C. epigaeus* has yielded an IC50 value of 183.33+0.7 µg/ml and <62.5µg/ml respectively for two human cancer cell lines (MCF7, Human breast adenocarcinoma and HT human colon carcinoma.

Corallocarpus epigaeus is a rich source of phytochemical compounds with high nutritive value (Uthrapathy et al., 2011). The phytochemical analysis of *Corallocarpus epigaeus* have shown that they are rich in alkaloids, flavonoids, triterpenoids and steroids (Shri, Balaji, Venkatramanan, & Madhumathi, 2010). Petroleum ether extract of *C. epigaeus* was reported to have large number of flavonoids which plays an important role in the antioxidant activity of the plant (Jeyaseelan et al., 2014).

N-methylasparagine from the seeds, essential oils ishwarane and ishwarone from the roots have been reported (Dunnill & Fowden, 1965; Gupta et al., 1997). GC-MS analysis were compared with standard phytochemical libraries to identify volatile compounds from the roots and rhizomes (Gupta et al., 1997; Karthic et al., 2017; Kandasamy et al., 2020). Ali et al. reported a pyridine carboxylic ester, corallocarpenoyl ester; an aliphatic C32 keto diol, dotriacont-22,25-diol-10-one; a sesquiterpene lactone, corallocarpscalarolide; a p-hydroxybenzoyl ester, designated as epigaeusyl ester from the roots (Ali & Gupta, 1996). A glycoside bryonin was reported from the roots (Dymock, Warden, & Hooper, 1893), however, bryonin is a general name referred to glycosides that are structurally elucidated partially from Bryonia dioica (cucurbitaceae family), which were later reported with complete structural characterization as glycosides of a triterpene Cucurbitacin known as bryodulcosigenin (Hylands & Kosugi, 1982; Tunmann & Stapel, 1966)

It is evident from the literature that not many studies have been done on the anticancer property of the plant. Moreover, despite its traditional significance, there are no comprehensive reports of the isolation of phytochemical constituents of *C. epigaeus* with structural details.

Although some studies have indicated the anti-proliferative activity of the plant extracts (Banotha et al.; Bhavani & Leelavathi, 2015) none of the studies have explored the anticancer

property of *C. epigaeus* in detail. The present study was designed to explore the anticancer property of the rhizome of the plant *Corallocarpus epigaeus* and isolate and characterize the anticancer principle/s.

2.2. Cucurbitacin B

Cucurbitacins are highly oxygenated triterpenoids, characterized by the presence of a tetracyclic cucurbitane (triterpene hydrocarbon) nucleus skeleton 19-(10"9β)-abeo-5α-lanostane base, varied by the positional substitution of an oxygen atom. They are found mainly in the plants of Cucurbitaceae family and up to 40 cucurbitacins are known. These and their derivatives are classified into 12 groups. Cucurbitacins are usually crystalline in nature, purgative, hydrophobic and easily soluble in organic solvents.

Among the Cucurbitacins, Cucurbitacin B (Cu-B) has been the one most explored for its role in biological systems. Cucurbitacin B (C32H46O8, molecular weight 558.712 g/mol, 19-(10"9β)-abeo-10-lanost-5-ene triterpene) is found in the plants of cucurbitaceae and other plant families like Brassicaceae. It is a steroid with peculiar bitter taste and cytotoxic properties. Its bitterness helps the host plant by protecting against predators and parasites (Clericuzio, Mella, Vita-Finzi, Zema, & Vidari, 2004). Previous reports showed that Cucurbitacin is effective against various illnesses notably generalized inflammation and algesia, carbon chloride-induced hepatotoxicity and profound cholestasis, CD18-mediated disorders, infestation of insects, cell adhesion and leukemic disorders, immune mediated and angiogenic disorders (J. C. Chen, Chiu, Nie, Cordell, & Qiu, 2005; Clericuzio et al., 2004; Wiart, 2012).

2.2.1. Cytotoxic/antiproliferative potential of Cucurbitacin B isolated from various sources

Cucurbitacin B has been extracted from plants of various families and genera around the world for research purpose. *Helicteres angustifolia* derived cucurbitacin B was effective on a variety of cancer cells especially in bone osteosarcoma cells at nanomolar doses (K. Li et al., 2016). In 2001, Oberlies et al., reported that Cucurbitacin B fractionated from the methanolic extract of *Licaniaintra petiolaris*, induced at the dose <0.01 μg/ml, >50% cell death in human oral epidermoid carcinoma cells (Oberlies et al., 2001). Cucurbitacin B isolated from root extract of *Casearia arborea* showed potent cytotoxicity against gliosarcoma and melanoma cell lines (Beutler et al., 2000). Cucurbitacin B isolated from the chloroform- methanol extracts of *Cucumis prophetarum* showed cytotoxicity against tumour derived and virally transformed mouse cancer cells (Ayyad, Abdel-Lateff, Basaif, & Shier, 2011). Cucurbitacin B isolated from the fruiting bodies of the fungal mushroom *Leucopaxillus gentianeus* showed very strong

cytotoxicity against NSCLC, RCC, HCC and HER2-/ER+ breast carcinoma cells (Clericuzio et al., 2004). Cucurbitacin B derived from the stems of *Cucumis melo* it showed significant cytotoxicity against NSCLC and HCC *in vitro* via activation of phospho-STAT3. Cucurbitacin B derived from the methanolic extract of *Trichosanthes kirilowii* and its close relatives demonstrated potent anticancer activities mediated through HIF-1α a nd N F-κB suppression (Dat, Jin, Hong, & Lee, 2010). Air-dried rhizomes of *Begonia nantoensis* derived cucurbitacin B, showed cytotoxicity against NSCLC, HER2-/ER+ breast carcinoma, gastric adenocarcinoma and non-neoplastic nasopharyngeal epithelial cell carcinoma cells (Wu et al., 1999)

2.2.2. Anti-melanoma activity of Cucurbitacin B

Group B cucurbitacins possess a wide spectrum of biological activities, including potent anticancer activity against cancers of the lung, pancreas, prostate, breast, brain, liver, cervical and blood (Garg, Kaul, & Wadhwa, 2018). However, only a limited number of studies have been reported on the efficacy of Cucurbitacin B, towards melanoma as well as their ability to target the MAPK pathway, a target for the treatment of melanoma. Detailed here are the international publications on the studies of Cucurbitacin B in melanoma.

In 1994, Fuller et al., reported a similar differential cytotoxicity profile by extracts of *Zberis amara*, *Begonia plebeja* and *Gonystylus keithii* towards renal carcinoma, brain tumor and melanoma cell lines in the NCI human disease-oriented tumor screening panel. The active principle in the extracts was identified as Cucurbitacins (Fuller, Cardellina, Cragg, & Boyd, 1994). Another group, while analysing the antitumor activity of compounds from *Helicteres angustifolia*, identified that cucurbitacins, elicit significant inhibitory activities against the growth of both hepatocellular carcinoma BEL-7402 cells and malignant melanoma SK-MEL-28 cells (Z.-T. Chen, Lee, & Chen, 2006). Siqueira et. al in 2009 had used murine melanoma cells in the *in vitro* and *in vivo* models to establish the antitumor efficacy of Dihydrocucurbitacin B, isolated from *Wilbrandia ebracteata* and demonstrated the antitumor effect, due to a decrease in the expression of cyclins, mainly cyclin-B1 and disruption of the actin cytoskeleton (Siqueira Jr et al., 2007). Zhang et al., in 2011, explored the potential anticancer mechanism of Cu-B in murine B16F10 melanoma cells and found that the compound caused cell membrane blebbing and deformation and multiploidy, via ROS induction resulting in dose-dependent G2/M phase growth arrest. They identified induction of rapid depletion of the G-actin pool through ROS-dependent actin aggregation, which they described as partial explanation for its anti-tumor activity. They also demonstrated

antimelanoma activity in an in vivo murine subcutaneous melanoma model (Y. Zhang et al., 2011). Another work undertaken by Zhang et al., in 2013, used both human A375 and murine B16F10 melanoma cell lines. They established that Cu-B-induced formation of cofilin-actin rods was mediated by slingshot homolog 1 (SSH1)-dependent but chronophin (CIN) - independent cofilin hyper activation (Y. T. Zhang, Ouyang, Xu, Zha, & He, 2013). Further studies by Zhang, et. al in 2014, explored the role of vasodilator-stimulated phosphoprotein (VASP) in Cu-B-induced disruption of actin cytoskeleton in human A375 and mouse B16F10 melanoma cell lines. Their results provided evidence that Cu-B induces actin aggregation and cofilin-actin rod formation through activation of the Gα13/RhoA/PKA/VASP pathway (Y.-T. Zhang et al., 2014). Li. et. al in 2012 has reported that Cu B –induces STAT3 activation via both JNK and Jak2 signalling and they demonstrated that blocking STAT3 activation enhanced the cytotoxicity of Cu-B in murine B16F10 melanoma cells (J. Li et al., 2012). Ouyang et al in 2011 has evaluated the anti-cancer effect of Cu-B as a single agent and in combination with valproic acid, an inhibitor of histone deacetylase, in B16F10, the mouse melanoma cell line and demonstrated the synergistic effect of the combination in inducing apoptosis (Ouyang et al., 2011). In 2014, a group reported the ability of Cu-B to inhibit B-Raf and MEK by binding to the hydrophobic pocket of B-Raf receptor and allosteric site of MEK via molecular docking studies and indicated the anti-melanoma potential of Cu-B by targeting the MAPK pathway (Ahmed, Kopel, & Halaweish, 2014).

As is evident from the literature review, although, there are several *in vitro* and *in vivo* studies reporting the efficacy of Cu-B, against various cancers through various mechanisms, only very limited studies have yet been reported on the anti-melanoma efficacy of Cu-B. Among these, most of them are basic studies reporting the anti-proliferative/cytotoxic effect in murine melanoma cell lines. Only a couple of studies have explored the molecular mechanism of anti-melanoma activity of Cu-B in human melanoma cells (Ahmed & Halaweish, 2014; Y.-T. Zhang et al., 2014). Moreover, none of the studies have explored in detail the effect of Cu-B on the RAS/RAF/MEK/ERK signalling axis deregulated in melanoma and so far, no in vivo studies have been conducted to analyse the effect of Cu-B against human melanoma.

2.2.6. Cucurbitacin B – toxicity

cucurbitacin B has not been listed as toxic or restricted use by any of the world's drug and safety bureaus, nor is there any report claiming its toxic role in vivo anywhere in the world, with the exception of an FDA report from 1955 and a follow-up in 1983, where the authors reported that the median lethal dose of cucurbitacin B via intraperitoneal route was 1 mg/kg in male albino mice at the end of three doses caused death due to acute pulmonary edema and respiratory arrest (David & Vallance, 1955). In 2000 Smit et al reported that the median lethal dose of cucurbitacin B after intravenous administration in rabbits was 0.5 mg/kg body weight (WHO 2009).

Ferguson et al. also observed toxicity after 700 g of commercially produced *Cucurbita pepo* L. was consumed by a human within a 6-hour period. Bitter mouth taste, cramping in the abdomen, diarrhoea, and occasionally syncope and vertigo were the toxic effects (Ferguson, Fischer, & Metcalf, 1983). The Australian Therapeutic Goods Administration has approved cucurbitacin B for use in combination with other agents and encourages its use (Therapeutic Goods Association, 2011).

Median lethal dose of Cucurbitacin B in its pure form was 5 mg/kg via oral route (LeMen et al., 1969) and 1 mg/kg by intraperitoneal in mice. Likewise, median lethal dose reported in rabbit was 0.5 mg/kg (intravenous) (Enslin, 1954), and 0.32 mg/kg (intravenous) in cat (Gry J, et al., 2006).

HYPOTHESIS

Bioprospecting for the identification of active compounds has contributed significantly to anticancer drug discovery. An ideal cancer chemotherapeutic drug is a biologically safe compound, which destroys the rapidly dividing cancer cells without affecting the normal cells. Many drugs currently used in cancer chemotherapy, were discovered as a part of systematic screening of plants for potent anticancer compounds (Choudhary et al., 2008). The present study aims to analyze the anticancer property and isolate the anticancer principle from the medicinal plant, *Corallocarpus epigaeus*. *Corallocarpus epigaeus* (Cucurbitaceae) is a prostrate or climbing monoecious plant that has been known for its therapeutic potential for centuries. It is used as a remedy for acute dysentery, venereal diseases, skin diseases, and snake bite (Kirtikar and Basu, 1935). Despite its significance in traditional medicine, there are no comprehensive reports on the isolation of phytochemical constituents from *C. epigaeus* and although a couple of studies have indicated the cytotoxic effect of the plant extracts in cancer cells (Banotha et al., Bhavani and Leelavathi, 2015), none of the studies have analyzed the anticancer property of the plant. Considering the known therapeutic efficacy of the plant *Corallocarpus epigaeus*, it has the potential for being investigated for its anticancer activity. The ability of plant-derived compounds to influence cell signalling pathways and induce cell cycle arrest or programmed cell death in cancerous cells in an attempt to arrest their proliferation has been the topic of much research. The expected outcome of the present study is such an anticancer principle, from the plant *Corallocarpus epigaeus* could be developed into a potent anticancer drug.

OBJECTIVES

- To analyze the cytotoxic potential of organic solvent extracts prepared from dried rhizome powder of *Corallocarpus epigaeus*.

- To isolate, identify and characterize anticancer principle/s from the rhizome of the medicinal plant *Corallocarpus epigaeus.*

- To study the mechanism of cell death induced by the compound and the signaling pathways regulated by the compound/s.

- To study the pharmacological safety of the anticancer compound isolated in the *in vivo* condition

- To study the mechanism of anti-tumor activity of the compound *in vivo*

Chapter 3

MATERIALS AND METHODS

MATERIALS AND METHODS

3.1. MATERIALS

3.1.1. Reagents and antibodies

Cell culture reagents such as Dulbecco's Modified Eagle Medium (DMEM) (GIBCO, 12800-017) and streptomycin sulphate (GIBCO, 11860-038) were obtained from Invitrogen Corporation (Grand Island, USA). Poly Excel HRP/ DAB detection system universal kit (PathnSitu Biotechnologies Pvt. Ltd, India, OSH001) was used for immunohistochemistry experiments. Cucurbitacin B and MTT reagent were purchased from TCI Chemicals (India) Pvt. Ltd (D0801) and Amersham ECL Plus™ Western blotting reagents (PRPN 2132) were purchased from GE Healthcare Life Sciences (Piscataway, USA). Annexin V apoptosis detection kit (sc4252AK) was purchased from Santa Cruz Biotechnology (Santa Cruz, CA, USA). Antibodies against, Caspase 9 (9508S), Caspase 8 (4790S), Caspase 7 (12827S), Bid (2002S), p-P53 (9281S), PARP (9532S), p-ERK1/2 (4370S), ERK (9108S), p-STAT3 (9136S), β-actin (12620S) and p-MEK1/2 (9121S) were obtained from Cell Signalling Technologies (Beverly, MA, USA) and the antibody against C-MYC (sc764), Cyclin-D1 (sc8396), PCNA (sc25280) were purchased from Santa Cruz Biotechnology (Santa Cruz, CA, USA).Antibody against Caspase 3 (74T2) and ECL reagent (PierceTM ECL western blotting substrate 32109)were purchased from ThermoFisher Scientific (Waltham, Massachusetts, United States) Antibody against MITF-M (ab12039) and Cellular ROS kit (ab113851) were purchased from Abcam (Cambridge, United Kingdom). Anti-caspase 10 (BD 51-9000066) antibody was purchased from BD Bioscience. DeadEnd™ Colorimetric TUNEL System from Promega (G7132) was procured from Addgene (Cambridge, MA, USA). An antibody against B-RAFV600E (SAB 5600047), anti-rabbit antibody, anti-mouse antibody, and silica gel for column chromatography were obtained from Sigma Chemicals (St. Louis, MO, USA). EGF was purchased from Genscript (New Jersey, U.S). Organic solvents and TLC sheets were purchased from Merck (Germany). All other chemicals and an antibody against Vinculin (V9131) were purchased from Sigma Chemicals (St. Louis, MO, USA) unless otherwise mentioned.

3.1.2. Cell lines

The lung cancer cell line, H1299, and normal skin fibroblast, FS were gifts from Prof. B.B. Agarwal to RJA. The cancer cell lines viz. colon (HCT-116), breast (MDA-MB-231), liver (HEP 3B), and cervical (HeLa) were procured from NCCS, Pune, India. Melanoma cell lines

with different mutation status viz. A375 (B-RAF), SK-MEL-2 (N-RAS), and SK-MEL-28 (B-RAF) were procured from NCCS, Pune, India. All the cells were routinely maintained in a complete medium, which contained DMEM, 10% FBS, and 2mg/ml Amphotericin B. The cells were incubated at 370 C and 5% CO2 atmosphere. Mycoplasma tests were performed on parent cell lines every 6 months. Cell lines passage between 3 - 6 times post- revival, were used for all experiments.

3.1.3. Plant specimens

Fresh Rhizomes of *C. epigaeus* collected in January 2017 from Nagamalai, Madhurai were identified and authenticated by Dr. Pradeep Kumar, Curator, Department of Botany, University of Calicut, and a voucher specimen has been deposited at the Department of Botany, University of Calicut (VOUCHER NO: CALI 6891).

3.2. METHODS

3.2.1. Preparation of extracts and isolation of ECF

3.2.1.1. Extraction from the tuber of *Corallocarpus epigaeus* (Rottl.) C.B.Clark

The tuber of the plants was washed thoroughly and shade-dried at room temperature (25-30 °C) for 14 days. The well-dried samples were powdered, and a defined quantity (100 g) was serially extracted using solvents with increasing polarity viz; hexane (0.0), ethyl acetate(4.4) and methanol (6.7) at 37°C, 120 rpm, 24 h at room temperature. The individual solvent extracts were concentrated separately under vacuum using rotary evaporator (BuchiRotavapor R-210), the resulting crude extracts were dissolved in a minimal volume of DMSO and were stored in -20 °C freezer as stock solutions (100 mg/mL or 50 mg/mL).

3.2.1.2. Bioassay-guided fractionation of the active fraction using Column chromatography

The crude ethyl acetate extract (EA-1.5g) was subjected to Silica gel Column Chromatography (230-400 mesh size, column size 40 cm × 20 cm) using hexane/ethyl acetate (100/0, 95/5, 90/10, 80/20, 75/25, 60/40, 50/50, 25/75, 0/100), ethyl acetate/methanol (100/0, 95/5, 90/10, 0/100). Total of 11 fractions were collected, visualized with UV chamber (256 nm and 365 nm) and the fractions possessing similar TLC profile were pooled together. Chromatographic separations were carried out by conventional column chromatography on silica gel (100-200 and 230-400 mesh).We tested the cytotoxic activity of each fraction among which, four fractions (Fraction 6 to 9) were found to be highly cytotoxic. As they showed similar cytotoxic

profile as well as TLC pattern, we pooled them together and designated them as ECF (Ethyl acetate Cytotoxic Fraction).

3.2.2. Nuclear Magnetic Resonance (NMR) spectroscopic analysis

1H and 13C NMR were recorded on a Bruker ASCENDTM-500 spectrometer at 500 and 125 MHz, respectively using CDCl3 and acetone-d6 solvents. TOCSY spectrum was acquired with an 80 ms mix time. NMR data are reported as follows: chemical shifts in ppm (δ) with integration, coupling constants in Hz. 1H, 13C, and 2D NMR data were used to elucidate the structure of the compounds. Mass spectrometry Higher Resolution Mass Spectrometry (HRMS) analysis was recorded to determine the molecular formula of the compounds using a Thermo Scientific Exactive-Liquid Chromatography-Mass Spectrometry (LCMS) instrument by electrospray ionization method with ions given in m/z using Orbitrap analyzer.

Prior to NMR analysis, the sample was dried under vacuum. Immediately, the sample was dissolved in an adequate NMR solvent depending on the solubility nature of the pure isolated compounds. The sample should be without any foreign particles in a 15 cm NMR sampler tube. The 1H NMR (500 MHz) spectra and 13C NMR (75 MHz) spectra were recorded on Bruker Avance 500 Nuclear Magnetic Resonance spectrometer in CDCl3 or CD3OD using TMS as an internal standard.

The chemical shifts (δ) were reported in parts per million (ppm) downfield from TMS.

3.2.2.1. Proton (^{1}H) NMR

The fundamental analysis for the structure elucidation of any molecule is the measurement of its ^{1}H NMR. Based on the results, further decision to analyze the two-dimensional NMR measurements would be considered. For the compounds already in literature, analysis of ^{1}H NMR is enough to depict the structure of a compound. Proton NMR spectra of most organic compounds are characterized by chemical shifts in the range +14 to -4 ppm and by spin-spin coupling between protons. Simple NMR spectra are recorded in solution, and solvent protons must not be allowed to interfere. Deuterated (deuterium = 2H, often symbolized as D) solvents especially for use in NMR are preferred, e.g. deuterated water, D2O, deuterated acetone, (CD3)2CO, deuterated methanol, CD3OD, deuterated dimethyl sulfoxide, (CD3)2SO, and deuterated chloroform, CDCl3.

3.2.2.2. Carbon (^{13}C) NMR

It is analogous to proton NMR (^{1}H NMR) and allows the identification of carbon atoms in an organic molecule just as proton NMR identifies hydrogen atoms. Varying to ^{1}H NMR experiment, the ^{13}C NMR measurement needs more quantity of sample. This is due to the ratio of ^{13}C to ^{12}C isotopes abundance in the nature is less than the ratio of ^{1}H to ^{2}H isotopes. ^{13}C chemical shifts follow the same principles as those of 1H, although the typical range of chemical shifts is much larger than for 1H (by a factor of about 20). The chemical shift reference standard for ^{13}C is the carbons in tetramethyl silane (TMS), whose chemical shift is considered to be 0.0 ppm.

3.2.2.3. Mass Spectrometry

The molecular weight of a compound is mainly determined via Mass spectrometer. Fundamentally, mass spectrometer is divided into three parts, ionization source, analyzer and detector that should be maintained under high vacuum condition in order to maintain the ions travel through the instrument without any hindrance from air molecules. Once a sample is injected into the ionization source, the molecules are ionized. The ions are then passed and extracted into the analyzer. In the analyzer, the ions were separated according to their mass (m) to charge (z) ratio (m/z). Once the separated ions flow into the detector, the signals are then transmitted to the data system where the mass spectrum is recorded. There are many different methods of ionization used in mass spectrometry and the method to be used depend on the type of sample to be analysed. Some of the commonly known ionization methods include:

Fast Atom Bombardment (FAB)

• Electro-Spray Ionisation (ESI)

• Matrix Assisted Laser Desorption Ionisation (MALDI)

The mass spectrum shows a plot of the relative intensity versus mass to charge ratio (m/z) and gives the information about molecular weight and relative abundance of the components in the sample. The most intense peak in the spectrum is called the base peak and others are reported relative to the base peak intensity. The fragments which are formed follow the simple and predictable chemical pathways and reflect the most stable ions or radicals. The highest molecular weight peak observed in a spectrum represents the typical parent molecule. In general, small peaks are also observed above the calculated molecular weight due to the natural isotopic abundance of ^{13}C and ^{1}H. Mass measurements were carried out on CEC-21-110B double focusing mass spectrometer operating at 70 eV using direct inlet systems and are given in mass units (m/z) under Electron Spray Ionization conditions preparing sample solution in

methanol. The spectra obtained were subsequently analyzed in order to determine the molecular mass and possible fragments of the compounds.

All the spectral analyses of isolated compounds, Cucurbitacin B was conducted by Dr. Ravi Shanker Lankalapalli, Scientist, Organic chemistry division, National Institute for Interdisciplinary Science and Technology, Pappanamcode, Thiruvananthapuram.

3.2.3. Ultra-High Performance Liquid Chromatography (UHPLC) profiling of ECF extract from *C. epigaeus*

The sample was injected into the analytical Nexera UHPLC system equipped with a reverse-phase Shim-pack GWS 5µ C18 column 250 × 4.6 mm ID connected to a PDA detector (SPD-M20A) and an autosampler (SIL-30AC). ECF fraction (3 mg/ml) and the isolated pure compound (2 mg/ml) were dissolved in acetonitrile: water (1:1) and filtered through a 0.2 µm nylon filter. The sample injection volume was 20 µL, and the C18 column temperature was 35 °C. The mobile phase system consisted of water: acetic acid (100:1) (A) and acetonitrile (B). A step gradient program was used for this analysis as follows: 0% B at 0 min to 40% B at 20 min, 40 to 50% at 30 min, 50 to 60% at 40 min, 60 to 80% at 50 min, 80 to 100% at 60 min, then maintaining at 100% B from 60 to 65 min at a flow rate of 1 ml/min, monitored at 254 nm.

3.2.4. Mode of drug treatment

Stocks of crude extracts and isolated compounds from *Corallocarpus epigeaus* was prepared in DMSO for the *in vitro* studies and stored at -20^{0}C. The DMSO concentration in all experiments, including controls, was ≤ 0.2%. Cell viability assay was performed after 72h of drug treatment while whole cell lysate preparation and cell cycle analysis were done after 24h and 48h of drug treatment. For Annexin V staining, cells were incubated with compound/s for 16h. For acridine orange-ethidium bromide staining, cells were incubated with compound/s for 24h.

3.2.4. MTT assay

MTT assay is based on the metabolic activities of the viable cells. In this assay a tetrazolium salt MTT (3-(4,5-Dimethyl-2-thiazolyl)-2,5-diphenyl-2H-tetrazolium bromide) is used which is cleaved by Succinate Dehydrogenase-that is present in metabolically active cells, into water insoluble dark blue formazan crystals. These water insoluble formazan crystals can be solubilized using 20% SDS in 50% DMF. After it is solubilized, the formazan formed can easily and rapidly be quantitated in a conventional ELISA plate reader at 570nm.

The cells were seeded in 96-well plates (2000 cells/well), incubated overnight, and treated with different concentrations of plant extracts, ECF and Cu-B. After 72 h the sample solution was flicked off and Fresh media containing 25 µL of 3-(4, 5-Dimethylthiazol-2-yl)-2,5-Diphenyltetrazolium Bromide (MTT) solution (5 mg/mL in PBS) was added to the wells and incubated for 2h. At the end of incubation, lysis buffer (20% sodium dodecyl sulphate in 50% dimethylformamide) was added to the wells (0.1 mL/well) and incubated for another 1 h at 37°C. At the end of incubation, the optical density was measured at 570 nm using an ELISA plate reader (Bio-Rad). The relative cell viability in percentage was calculated as (A570 of treated cells/A570 of untreated cells) X 100. The IC50 values were extrapolated from polynomial regression analysis of experimental data.

3.2.5. Acridine orange/ethidium bromide staining

Acridine orange/ethidium bromide (AO/EB) staining is used to visualize cell-death in response to cytotoxic agents. Acridine orange stains both live and dead cells green, while Ethidium bromide will stain only cells that have lost membrane integrity and so dying cells appear green and orange. Briefly, cells were seeded in 48-well plates and treated with active extract ECF for 24h. After washing once with PBS, the cells were stained with 100 µL of a 1:1 mixture of acridine orange (100 µg/mL) /ethidium bromide (100 µg/mL) solution for 5min at RT. The cells were immediately washed with PBS, viewed under Nikon inverted fluorescent microscope (TE-Eclipse 300) and photographs were taken.

3.2.6. Clonogenic assay

Clonogenic assay or colony formation assay is an in vitro cell survival assay based on the ability of a single cell to grow into a colony. The colony is defined to consist of at least 50 cells. The assay essentially tests every cell in the population for its ability to undergo "unlimited" division. Clonogenic assay is the method of choice to determine cell reproductive death after treatment with ionizing radiation, but can also be used to determine the effectiveness of other cytotoxic agents. Only a fraction of seeded cells retains the capacity to produce colonies. After drug treatment, cells are seeded out in appropriate dilutions to form colonies in 1–3 weeks in the drug containing media. Colonies are fixed with glutaraldehyde (6.0% v/v), stained with crystal violet (0.5% w/v) and counted.

Briefly, 500 cells were seeded in 6-well plates and treated with different concentrations of ECF. After 72 h, media along with ECF was removed, supplied with fresh medium, and incubated for 1 week. The developed clones were fixed in glutaraldehyde (6%) and stained using crystal violet (0.5%). The plate was incubated for 30 min at room temperature, followed by rinsing

with tap water. After drying the plate, colonies were counted and compared with the untreated control.

3.2.7. Scratch wound assay

A scratch was made on the monolayer of confluent cells using a sterile micropipette tip to create a wound. Cell debris was gently removed by washing the cells with 1X PBS followed by the addition of complete medium in the wells maintained as control. In the treatment wells, medium containing the required concentrations of the compound was added. Images were taken at the start of the assay and at required time intervals under a phase contrast microscope.

3.2.8. Chromatin condensation

DAPI staining was used to analyse the dense chromatin formed as a consequence of apoptosis induced by the compound. 5000 cells were seeded on coverslips placed in a 24 well plate and were treated with different concentrations of the compound. After desired period of incubation, the cells were washed with PBS and were fixed using a mixture of Methanol- EDTA. The nuclei of the cells were stained with 1 µg/ml of DAPI for 5 min and were mounted on gelatine coated glass slides using fluoromount. The cells were then viewed under a fluorescent microscope for nuclear condensation and the images were captured.

3.2.9. Annexin V-Propidium Iodide staining

Apoptosis causes changes in membrane permeability, there is a transient leakage of phosphatidylserine to the membrane, which is considered to be an early marker of apoptosis. Annexin V preferentially binds to phosphatidylserine as it is a negatively charged phospholipid. Hence, using Fluorescein isothiocyanate (FITC) conjugated Annexin V. Apoptotic cells were detected with the help of a fluorescent microscope by Annexin V apoptosis detection kit according to the manufacturer's protocol (Santa Cruz, CA, USA). Briefly, the cells were seeded in 96-well plates and treated with ECF as in the MTT assay, but for 16 h. The cells were then washed with PBS, followed by 1X assay buffer, after which, 5 µL of Annexin V FITC and 10 µL of propidium iodide per 100 µL assay buffer was added, followed by incubation in the dark for 15min. The cells were then washed with PBS and immediately photographed using a fluorescent microscope, Nikon inverted fluorescent microscope (TEEclipse 300).

3.2.10. Fluorescent Activated Cell Sorting (FACS) analysis for Apoptosis

Phosphatidylserine (PS) is a membrane phospholipid which is usually located in the inner side of the plasma membrane. During apoptosis, membrane flip-flop occurs during which PS is externalized to the outer cell surface. When the cells are stained with FITC conjugated Annexine V- propidium iodide mixture, bright green fluorescence is imparted to the membrane, as Annexine V has a strong affinity towards PS, indicating membrane flip-flop, marking the early stages of apoptosis. The nucleus is stained by adding propidium iodide (PI), which has binding affinity towards DNA. Depending upon the extent of nuclear membrane damage, nuclear contents will exert red fluorescence, due to the penetration of PI. Hence, the cell population, which shows only green fluorescence indicates early stage of apoptosis as indicated in the bottom right of the quadrant (Q4) and those stained with both green and red fluorescence are the population which underwent late apoptosis, since they will be taking up PI as well, they are represented in the top right of the quadrant (Q2).

The extent of apoptosis induced by ECF and Cu-B was estimated by FACS using Annexin V FITC apoptosis kit (Santa Cruz, CA, USA). Briefly, the cells were seeded in 60mm culture plates, and incubated with different concentrations of ECF and Cu-B. After 16 h, cells were trypsinized and the pellets were washed with PBS and suspended in 100 µL 1 X assay buffer. To the buffer, 5 µL of FITC conjugated Annexin V and 10 µL of propidium iodide were added and incubated for 15 min in dark at room temperature. The cells were then analyzed by flow cytometry to get the percentage of apoptotic cells (FACS AriaTM, BD Bioscience)

3.2.11. Flow cytometry and cell cycle analysis

Cell cycle analysis helps in differentiating the distribution of a population of cells to the different stages of the cycle. Cell cycle analysis using flow cytometry was done to investigate the cell cycle arrest induced by the isolated compound/s. Cell cycle analysis is done by quantitative measurement of nuclear DNA content in a cell by staining DNA with Propidium iodide. Propidium iodide is a DNA binding dye which intercalates into the major groove of double stranded DNA and its excitation and emission peaks are at 488nm and around 600nm. When propidium iodide is added to a suspension of permeabilized cells, its incorporation will be proportional to the DNA content and the stage of cell cycle can be determined by measuring total fluorescence emission using a flow cytometer. Briefly, cells were treated with different concentrations of Cu-B and incubated for different time periods (24 h and 48 h). After incubation, the cells were trypsinized and the pellets were washed with PBS, and fixed in 70%

ice-cold ethanol treated with 100 mg/ml RNAase A and 50 mg/ml propidium iodide, followed by flow cytometric analysis (BD Biosciences).

3.2.12. Fluorescent microscopy for Reactive Oxygen Species (ROS)

ROS levels within the cells in response to Cu-B were determined by staining the cells using H2DCF-DA according to the manufacturer's protocol. Briefly, the cells were seeded in 60 mm plates, kept overnight, and treated with different concentrations of Cu-B for 6 h followed by trypsinization. The cell pellets were washed with PBS, re-suspended in DCFDA containing assay buffer, and incubated for 30 min. After incubation, the cells were washed with PBS and observed and quantified using a Nikon inverted fluorescent microscope (TEEclipse 300).

3.2.13. Immunoblot analysis

3.2.13.1. Whole cell lysis

Whole cell extract from cells/tissues were prepared using lysis buffer (Appendix). $0.5x10^6$ cells/tumor tissues were exposed to ECF/Cu-B as indicated for the desired time. After removing the spent medium, the cells were craped out in ice cold 1XPBS and pelleted down at 13000 rpm for 2min. Resuspended the pellet in 150µl of ice-cold whole cell lysis buffer and kept on ice for 30 min with intermittent vortexing every 5min. After incubation, the lysate was centrifuged at 13000 rpm for 10min at 4^{o}C and the supernatant was collected. The total protein content in the lysate was estimated by Bradford's method, and was then denatured by boiling with 5X sample buffer and kept at -80^{o}C until analysis.

50mg of tumor tissues were weighed on an aluminium foil and immediately dip in a pre-cooled mortar containing ~500 µl of WCL buffer. The tissue was gently smashed using a pestle till it becomes a paste. Then transferred into fresh 1.5ml vials and kept in ice for 90 min with intermittent vortexing every 10 min. After incubation, the homogenate was centrifuged at 13000 rpm for 30 min at 4^{o}C and the supernatant was collected. The total protein content in the lysate was estimated by Bradford's method and was then denatured by boiling with 5X sample buffer and the protein samples were either loaded onto SDS-PAGE gels or stored at -80°C until use.

3.2.13.2. SDS-PAGE

Resolving gel containing 8, 10, 12 or 15% acrylamide were used according to the molecular weight of the protein to be probed. Samples were run along with the pre-stained board range molecular weight marker (New England Biolabs, UK) at 40mA through the stacking gels, and at 60mA through the resolving gels.

3.2.13.3. Western Blotting

Western blotting analysis were carried out using specific antibodies as described earlier (Towbin, Staehelin and Gordon 1979). Following electrophoresis, the polyacrylamide gel and a PVDF membrane were equilibrated with Towbins buffer (Appendix) for 15-30 min and the separated proteins were electro-transferred to PVDF membrane (Hybond-P, GE Healthcare Life science) using Bio-Rad Mini PROTEAN III wet blot apparatus at 100 V for 2h at room temperature or 40V for 16h at cold room conditions. After the transfer, the membrane was rinsed with TBST buffer and stained with Ponceau-S to ensure uniform transfer. After washing off the Ponceau stain with TBST, the membrane was exposed to 5% fat free milk in TBST buffer for 1hour at room temperature or 2h at cold condition to block the nonspecific binding of antibodies, followed by overnight incubation with the primary antibody (1:1000 dilution) in 3% BSA in TBST buffer at 4^{o}C. Excess antibody was washed off with TBST buffer and incubated with corresponding secondary antibody (1:5000 dilution) coupled with horse radish peroxidase (HRP) in 5% fat free milk in TBST buffer. The bands were visualized using enhanced chemiluminescence kit (PierceTM ECL western blotting solution) following manufacturer's protocol.

3.2.14. Animal experiments

3.2.14.1. Toxicological Analyses

The toxicological analysis of the active fraction ECF and Cu-B were performed in 6-8 weeks old male Swiss albino mice as per protocol (IAEC/669/RUBY/2018 and IAEC/849/Ruby/2021) approved by the Institutional Animal Ethics Committee, Rajiv Gandhi Centre for Biotechnology.

Dose calculation and liposome encapsulation

The dose of drug to be administered *in vivo* was calculated using Castanas method. Briefly, the amount of drug to be injected per dose (mg/Kg/animal) was obtained by multiplying the values X and Y, in which 'X' is the desired dose (IC50) x molecular weight of the compound and 'Y' is the body weight of the animal x water content of the animal (Sreekanth et al., 2011). ECF/Cu-B was encapsulated into uni-lamellar liposome formulation containing phosphatidyl choline and cholesterol. For 1 mg ECF/Cu-B, 9 mg phosphatidyl choline and 1.16 mg cholesterol were dissolved in 3:1 mixture of chloroform and methanol 9 (10 ml). After dissolving completely, the solvent was removed using vacuum rotary evaporator and the residue was suspended in

PBS and kept as stock solution. the concentrations were prepared from the stock solution using PBS.

Acute toxicity: Doses of 0, 0.25, and 1.25mg/Kg of active fraction ECF and 0, 0.05, and 0.15 mg/Kg of Cu-B were given as a single intraperitoneal injection to each group of 5 animals. The mice were observed continuously for 1 h, for any gross behavioural changes and death, and then intermittently for the next 6 h and 24 h. The behavioural parameters monitored were convulsion, hyperactivity, sedation, grooming, food and water intake, etc. The animals were observed routinely for the next 7 days from the day of treatment, after which, the animals were euthanized in a CO_2 chamber. The blood serum was collected for analysing biochemical parameters of liver function, the abnormal values of which are indicative of toxicity. The liver was fixed in 10% buffered formalin and the thin cryostat sections (LEICA CM 1850UV Cryostat) were stained with haematoxylin and eosin for histopathological evaluation. The weight of the animals as well as that of the individual vital organs were also recorded (Antony et al., 2015).

Sub-chronic toxicity: Doses of 0, 0.25, and 1.25mg/Kg of active fraction ECF and 0, 0.05, and 0.15 mg/Kg of Cu-B were given as intraperitoneal injections on alternate days for 3 months. Each group consists of 5 animals. Animals were euthanized after 3 months. Liver tissues were collected and toxicity was measured as described above.

3.2.14.2. *In vivo* Xenograft Model

A melanoma xenograft study was performed in male NOD-SCID mice following the approved guidelines of the Institute Animal Ethics Committee of Rajiv Gandhi Centre for Biotechnology, Thiruvananthapuram (IAEC/818/RUBY/2020). A375 cells ($1X10^6$) were subcutaneously injected into the flank region of the mice. 5 days post the cell injection, the animals were divided into 3 groups. Cu-B being hydrophobic was encapsulated in the liposomal formulation, which was prepared by vacuum rotary evaporation of a mixture of 1 mg Cu-B, 9 mg phosphatidylcholine, and 1.16 mg cholesterol, dissolved in a 3:1 mixture of chloroform and methanol. 0.05 mg/Kg of liposomal Cu-B (corresponding to the IC50 in A375), was prepared by dissolving the liposome in 1X PBS and administered intradermally and intraperitoneally to the animals in groups 2 and 3 respectively, on alternative days for a period of 4 weeks. Group 1 was kept as vehicle control. The tumor size was measured weekly and the corresponding tumor volume was calculated as per the formula, (length x width2)/2 (Sreekanth et al., 2011). At the end of the experiment, the animals were euthanized and tumor tissues were collected.

3.2.14.3. Tissue sample collection

At the end of the animal studies, all the animals were sacrificed in the CO2 chamber. Tumor and the organs from the different groups were excised and washed in ice-cold PBS and subjected to *ex vivo* imaging. One part of the tissue to be used for protein extraction was snap frozen in liquid nitrogen and stored at -80°C. Another portion of the tissue was fixed in 4% PFA for histopathological analysis and immunohistochemistry.

3.2.14.4. Preparation of tissue cryosections

Tissues obtained from animals of different groups were excised and fixed in 4% PFA overnight, transferred to 30% sucrose solution till they sink. The sunken tissues were kept immersed in O.C.T (Optimal Cutting Temperature, Tissue-Tek) and allowed to freeze in the cryostat (Leica CM 1850 UV) set at -20°C. Sections of ~7µm thickness were cut from the frozen tissue sample using cryostat on ply L-lysine coated micro slides (Leica) and were kept at -80°C until histopathological or immunohistochemical analyses.

3.2.14.5. H & E Staining

The tissue sections were thawed in room temperature followed by dipping in 1X PBS and distilled water for 5 min each, stained using Mayer's haematoxylin for 5 min. Excess satin was washed off and the slides were dipped in tap water for bluing and dehydrated using increasing concentrations of isopropyl alcohol and counter stained with eosin solution for 1 min. The sections were kept in 100% isopropyl alcohol for 5 min, cleared in xylene and mounted using DPX mountant. Stained sections were observed under a light microscope and images were captured. Histopathological verifications were done by Dr. Sankar Sundaram, HOD of pathology, Kottayam Medical College.

3.2.14.6. Immunohistochemistry

Immunolocalization of specific proteins in the tissue sections was done using the Poly Excel HRP/ DAB detection system universal kit (PathnSitu Biotechnologies Pvt. Ltd, India. Cryosections were thawed in room temperature followed by dipping in 1X PBS followed by steam induced antigen retrieval in citrate buffer. Non-specific antibody binding sites on tissue sections and endogenous peroxidase activity were blocked by appropriate reagents supplied with the kit. The pre-diluted primary antibody was added enough to cover the sections. After incubating for overnight at 4°C, the unbound primary antibody was washed off with PBS. The sections were then covered with polymer-horseradish peroxidase conjugate, incubated for 30 min at room temperature, rinsed with PBS. Immunostaining was visualized using

diaminobenzidine chromogen, counterstained with Mayer's hematoxylin and the sections were cleared in xylene and mounted using DPX. The tissues were subjected to an immunohistochemical analysis against, PCNA (Proliferating Cell Nuclear Antigen), B-RAFV600E, p-MEK1/2, p-ERK1/2, p-STAT3, c-MYC, Cyclin-D1 and β-Catenin. All the immunohistochemistry images were taken in DMi8 Inverted Fluorescence Research Microscope with a DMC 2900 Digital Camera. The verification of IHC was done by Dr. Sankar Sundaram, HOD of pathology, Kottayam Medical College.

3.2.14.7. TUNEL assay

TUNEL assay was performed to detect apoptosis in formalin-fixed, paraffin-embedded xenograft tumor tissue sections using Dead End Colorimetric TUNEL System (Promega). During apoptosis, fragmentation of DNA occurs. Biotinylated nucleotide binds to the 3'-OH ends of DNA using Terminal Deoxynucleotidyl Transferase, Recombinant (rTdT) enzyme. Then Horseradish peroxidase labelled streptavidin binds to this complex, which are detected using stable chromogen, diaminobenzidine (DAB). Apoptotic nuclei are stained dark brown and visualized with light microscope. Briefly, the sections were washed with 0.85% NaCl for 5min at room temperature and washed using PBS. After washing fixed the tissues by 4% paraformaldehyde for 15 min followed by PBS wash. Then added 100 µl of the 200 µg/ml Proteinase K to each section and incubated the slides for 15 min and washed off using PBS. Re-fixed the sections in 4% PFA for 5 min and washed using PBS. Then added equilibrating buffer for 10 min, after incubation, blotted the areas with tissue paper and added 100 µl of rTdT reaction mix to the sections. Cover the sections with plastic cover slip and incubate at 37°C for 60 min inside a humidified chamber. Then remove the plastic cover slip and terminated the reactions by immersing the slides in 2X SSC reagent for 15 min. then washed the sections by PBS and block the tissue sections by 0.3% hydrogen peroxide in PBS for 5 min. Wash the sections by PBS and add 100 µl of Streptavidin HRP (dilute 1:500in PBS) for 30 min at room temperature. Wash the sections by PBS and incubate the sections with 100 µl of DAB for 30 min, rinse the sections by deionized water, mounted the sections and Observe the staining by light microscope.

3.2.15. Statistical analysis

For the flow cytometry, data analysis was performed using the BD FACS Diva software version 5.0.2. The statistical analysis was performed using Graph Pad Prism software Inc. (version 6.0, San Diego, CA, USA) and the quantification of Western blot was carried out using ImageJ software, version1.8.0. the comparison of mean data among multiple groups was analyzed by ANOVA. Statistical significance was defined as ****P <0.0001, ***P ≤0.001, **P ≤0.01, *P <0.1 and ns ≥ 0.05. The error bars represent SD, taken from three independent experiments.

Chapter 4

RESULTS

4. 1. Isolation & Identification of Anti-cancer Principle from *Corallocarpus epigaeus*

4.1.1. Evaluation of the Cytotoxic Potential of crude tuber extracts of *Corallocarpus epigaeus (C. epigaeus)*

To investigate the potential anti-cancer property of *C. epigaeus*, the rhizome part was preferred, due to its multiple applications in traditional medicine against various ailments. A polarity gradient extraction of the dried rhizome powder of *C. epigaeus* was performed and the cytotoxicity analysis of the three organic extracts (hexane, ethyl acetate, and methanol) was conducted in cancer cell lines of various tissue origins. The cells were treated with different concentrations of the three extracts (0.25-1 µg/ml) for 72h. The cell viability was assessed by MTT, as described in "Materials and Methods". The assessment of cell viability in various cancer cells demonstrated the ethyl acetate extract as the most potent fraction which exhibited substantial cytotoxicity with an IC50 around 0.05µg/ml, particularly in the melanoma cell line, A375. The methanol extract also possessed the ability to induce cell death, most notably in A375 (IC50 of 0.15 µg/ml), whereas the hexane fraction was found to be non-toxic to all the cell lines studied (Figure 4.1.1 A-C).

A

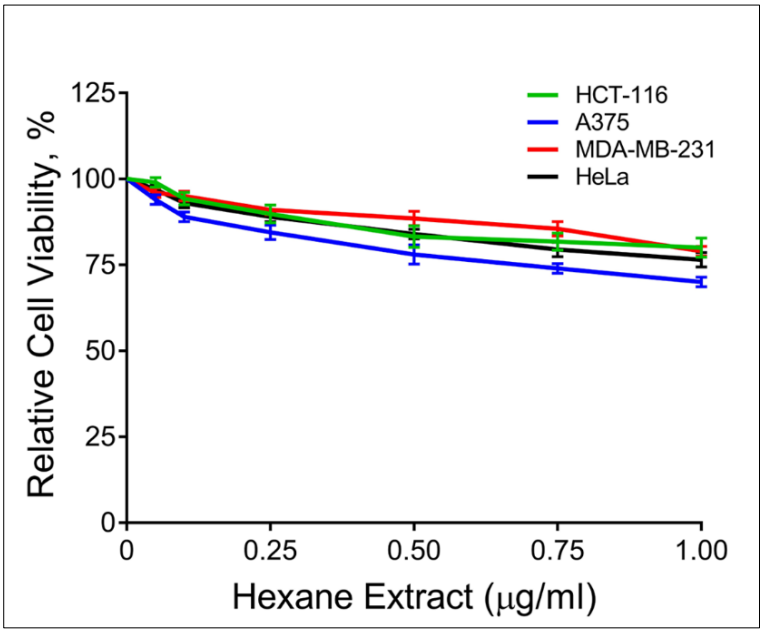

B

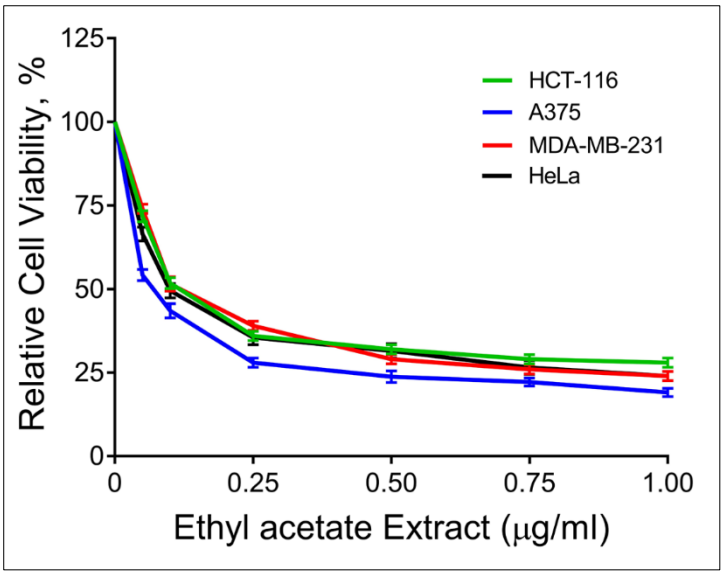

C

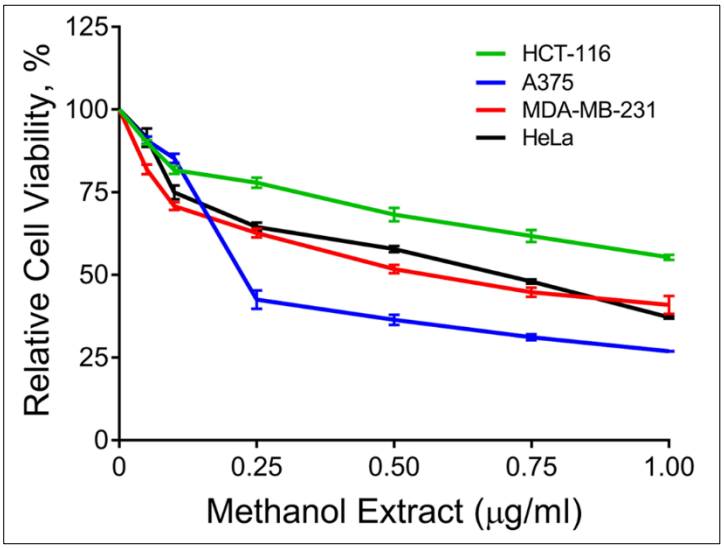

Figure 4.1.1 A-C: Evaluation of the cytotoxicity of organic extracts of *C. epigaeus* in a panel of four cancer cell lines. (A-C) The cancer cells were treated with indicated concentrations of hexane extract, ethyl acetate extract and methanol extract, incubated for 72h and the cell viability was assessed by MTT assay as described in "Materials and Methods". Relative cell viability was determined as % absorbance over untreated control. Data represent three independent sets of experiments. The error bars represent ± S.D.

4.1.2. Isolation of active fractions from the crude ethyl acetate tuber extract

As ethyl acetate extract was found to be the most cytotoxic, it was considered further for the isolation and purification of one or more potential anticancer principle (s). The ethyl acetate extract was subjected to silica gel column chromatography, (60–120 mesh size, column size 40 cm 20 cm) using n-hexane as the solvent and 1.5g of crude ethyl acetate extract was loaded on the top of silica gel. The column was eluted stepwise with 100 ml of hexane, hexane: ethyl acetate (100ml) (100/0, 95/5, 90/10, 80/20, 75/25, 60/40, 50/50, 25/75, 0/100), ethyl acetate: methanol (100ml) (100/0, 95/5, 90/10) in different ratios. A total of 11 fractions were collected and the fractions were evaluated for their cytotoxic potential in the colon cancer cell line HCT-116 using an MTT assay. Two cytotoxic concentrations (0.05µg/ml and 0.1µg/ml) were used for this study. Among the 11 fractions screened, four fractions (F6, F7, F8, and F9) showed potent cytotoxicity with an IC_{50} value of around 0.05µg/ml (Figure 4.1.2A). As these four fractions showed similar cytotoxic profiles and TLC patterns, they were pooled together and were designated as "ECF" (Ethyl acetate Cytotoxic Fraction).

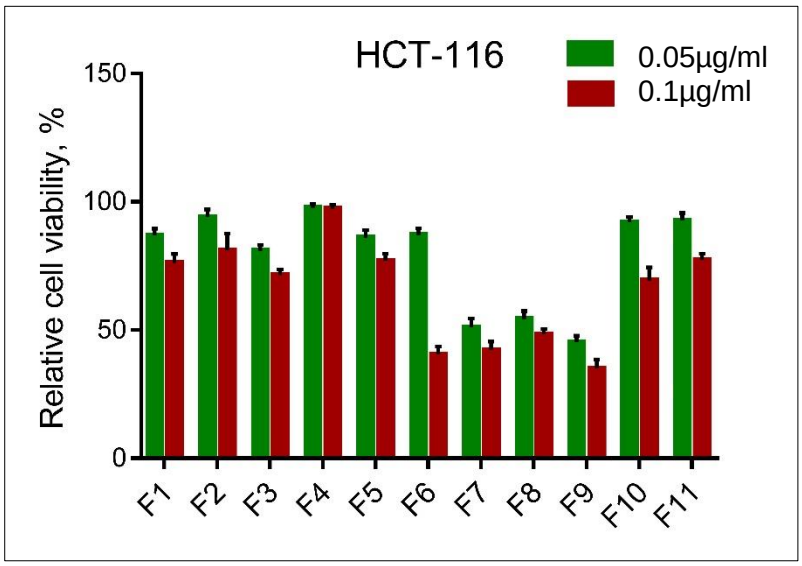

Figure 4.1.2A: Evaluation of the cytotoxicity of fractions obtained from ethyl acetate extract of *C. epigaeus* in HCT-116 cells. HCT-116 cells were treated with two concentrations of column fractions as indicated, incubated for 72h and cell viability were assessed by MTT as described in "Materials and Methods". Relative cell viability was determined as % absorbance over untreated control. Data represent three independent sets of experiments. The error bars represent ± S.D.

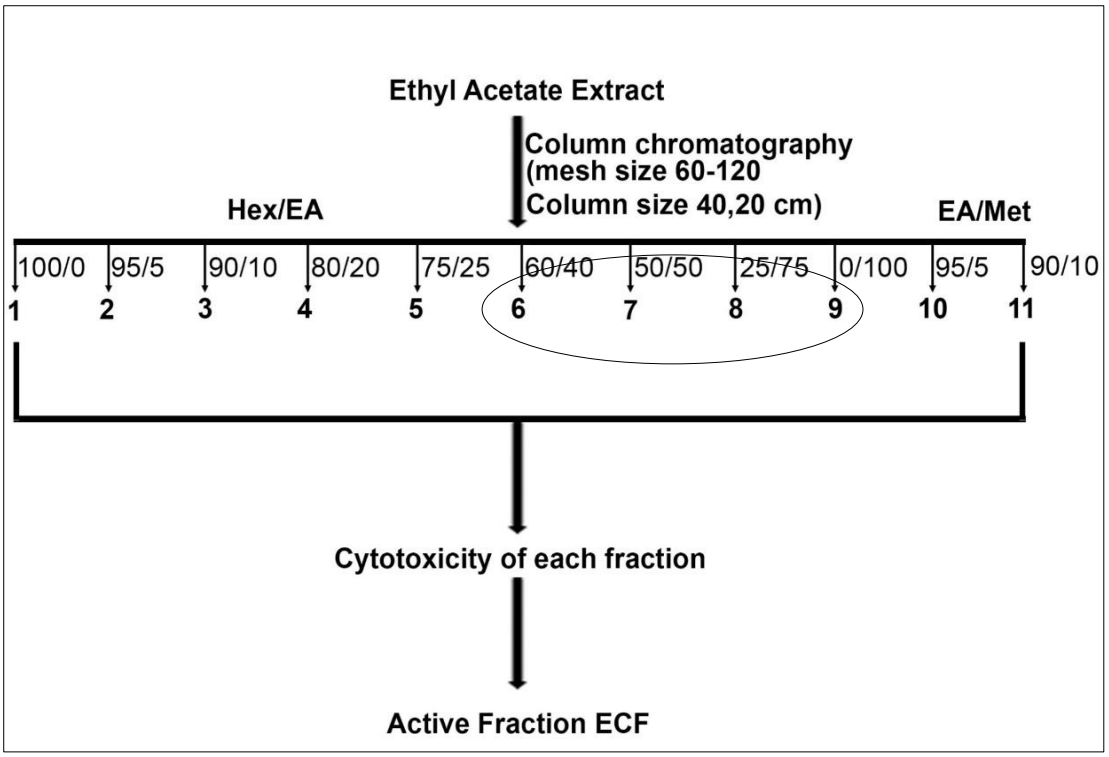

Figure 4.1.2B: Schematic representation of the isolation of the cytotoxic fraction ECF from EA ex of *C. epigaeus* rhizome

4.1.3. Screening of the ECF fraction in cancer cell lines of various tissue origins to identify the most sensitive cell line to the fraction

The cytotoxic fraction obtained from ethyl acetate extract (ECF) was evaluated for its efficacy against various human cancer cell lines, viz. HCT116 (Colon Cancer cell line), H1299 (Lung cancer cell line), A375 (Melanoma cell line), MDA-MB-231 (Breast cancer cell line), Hep-3B (Liver Cancer cell line), and HeLa (Cervical cancer cell line), using MTT assay. To study the effect of ECF on cancer cells of different origins, the cells were treated with different concentrations of ECF (0.01-0.05 µg/ml) for 72h. Among the various cancer cell lines screened, the melanoma cell line, A375, displayed maximal sensitivity towards ECF (IC50- 0.015 µg/ml) followed by Hep-3B, HeLa, MDA-MB-231, HCT116, and H1299 (Figure 4.1.3).

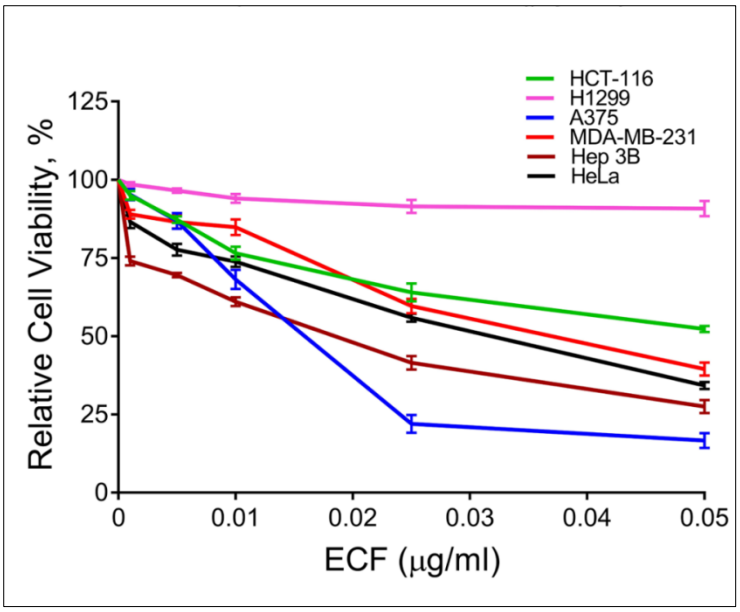

Figure 4.1.3: ECF, the cytotoxic fraction from the ethyl acetate extract of *C. epigaeus* induces maximum cytotoxicity in melanoma cells. The cancer cells were treated with indicated concentrations of ECF incubated for 72h and the cell viability was assessed by MTT assay as described in "Materials and Methods". Relative cell viability was determined as % absorbance over untreated control. Data represent three independent sets of experiments. The error bars represent ± S.D.

4.1.4. Evaluation of the cytotoxic potential of ECF in various melanoma cell lines

To validate the anti-melanoma efficacy of ECF, the cytotoxic potential of ECF was evaluated against different melanoma cell lines viz. A375, SK-MEL-2, and SK-MEL-28, using MTT assay. Interestingly, all the melanoma cell lines selected for this study displayed considerable sensitivity towards ECF. Cell line, A375 was repeatedly observed as the most sensitive to ECF with an IC50 of 0.015µg/ml followed by SK-MEL-2 (IC50 -0.02µg/ml) and SK-MEL-28 (IC50 -0.025µg/ml). Hence, A375 was picked for further studies.

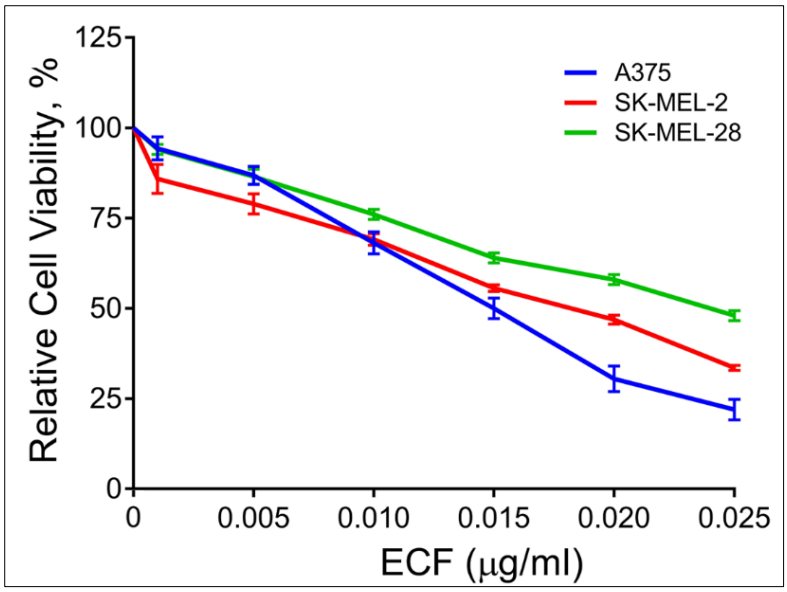

Figure 4.1.4: ECF is highly cytotoxic to different melanoma cell lines studied. The melanoma cell lines, A375, SK-MEL-2, and SK-MEL-28 were treated with ECF as indicated, incubated for 72h and the Cell viability was assessed by MTT assay as described under "Materials and Methods". Relative cell viability was determined as % absorbance over untreated control. Data represent three independent sets of experiments. The error bars represent ± S.D.

4.1.5. Evaluation of the cytotoxic effect of ECF in normal skin fibroblast

Before going for the detailed anti-cancer studies in melanoma cells, the biological safety of ECF was analyzed, by studying the effect of ECF in the normal skin fibroblast cells, FS, using an MTT assay. The cells were treated with different concentrations (0.015-0.06 µg/ml) of ECF for a period of 72 h (Figure 4.1.5). The result revealed that at 0.015µg/ml, the IC50 concentration of ECF in A375 cells, 95% of normal skin fibroblasts were live.

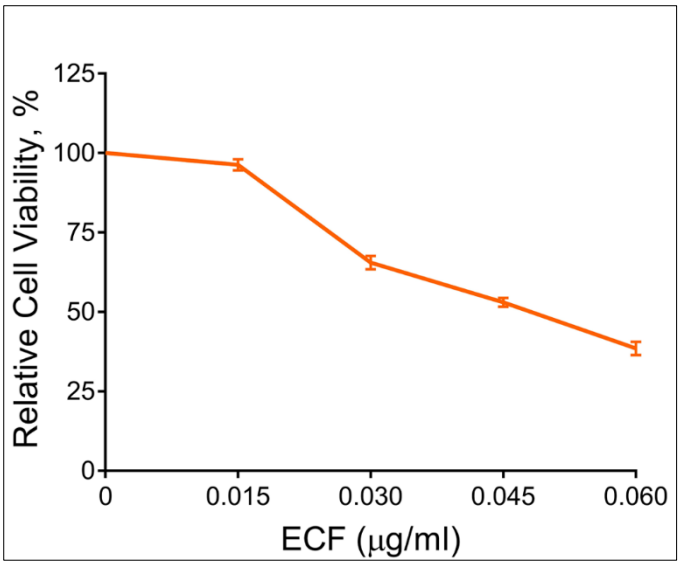

Figure 4.1.5: Assessment of ECF-induced cytotoxicity in normal skin fibroblast cells. Normal skin fibroblast (FS) cells were treated with ECF as indicated, incubated for 72h and the cell viability was assessed by MTT assay as described under "Materials and Methods". Relative cell viability was determined as % absorbance over untreated control. Data represent three independent sets of experiments and results are shown as the mean± SD.

4.1.6. Evaluation of the cytotoxic potential of ECF in A375 cells by Acridine orange/Ethidium Bromide staining

The cytotoxic potential of ECF in A375 cells was analyzed by Acridine orange/Ethidium Bromide staining. A375 cells were treated with 0.01 and 0.015 µg/ml of ECF, incubated for 24h, and stained with acridine orange/ethidium bromide as described in "Materials and Methods". All the cells take up AO and appear green while the dead cells take up ethidium bromide as well, due to cell membrane damage, and appear green and red. The number of dual-stained cells showed a dose-dependent increase indicating the cytotoxic potential of ECF (Figure 4.1.6).

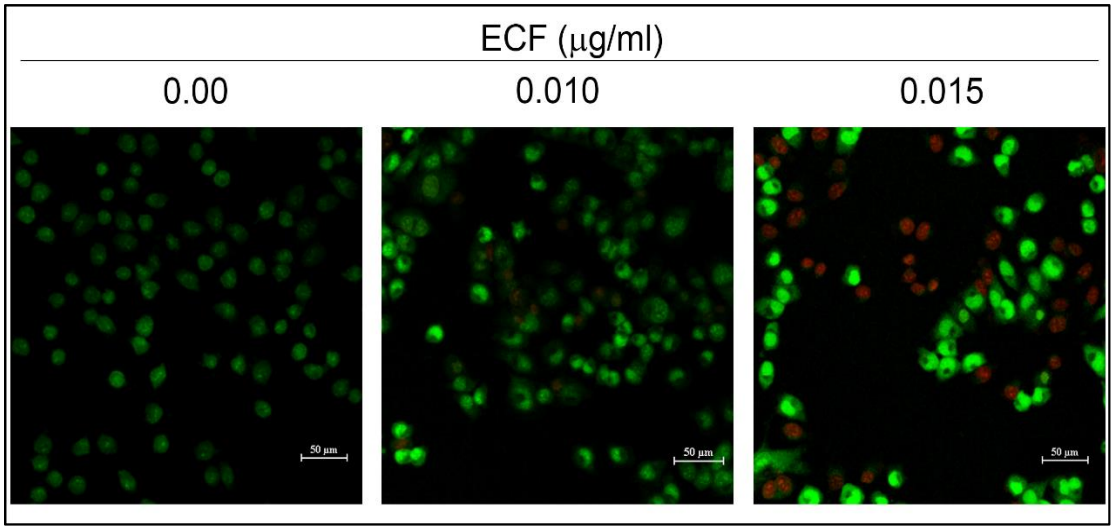

Figure 4.1.6: Evaluation of the cytotoxic potential of ECF in A375 cells by Acridine orange/Ethidium Bromide staining. A375 cells were treated with ECF as indicated, incubated for 24h and stained with acridine orange/ethidium bromide as described under "Materials and Methods". Apoptotic cells with membrane damage take ethidium bromide and appear green and red. Data represent three independent sets of experiments.

4.1.7. Evaluation of the anti-proliferative effect of ECF by clonogenic assay and scratch assay

(A) Clonogenic assay

The ability of ECF to inhibit the proliferative propensity of A375 cells was assessed using the clonogenic assay. Two concentrations, 0.010 and 0.015 µg/ml of ECF were used for this study. The widely studied bio-active phytochemical, curcumin (9 µg/ml), was used as the positive control. The result indicated a significant reduction in the number and size of the colonies formed in a dose-dependent manner, in response to 0.010 and 0.015µg/ml ECF. This reduction in colony number and size is essentially evidence of the ability of ECF in destroying the dividing cells in the population and hamper the potential of these cells to grow and proliferate (Figure 4.1.7A).

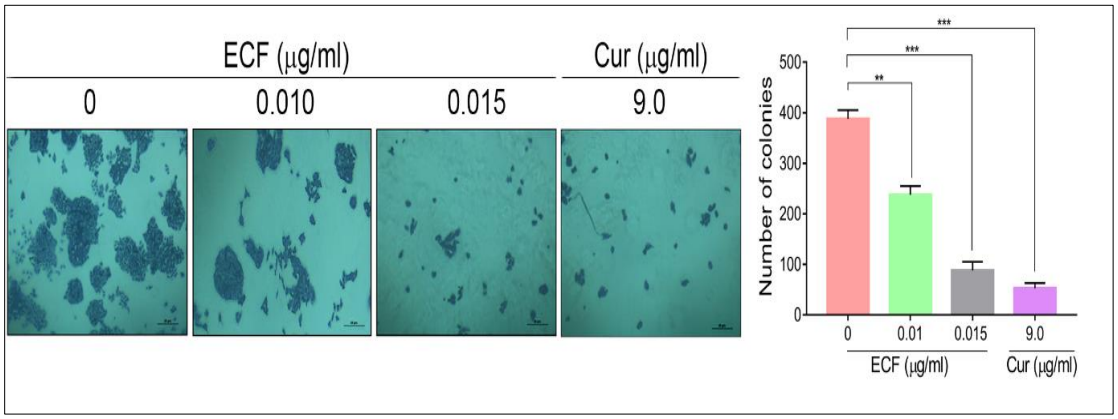

Figure 4.1.7A: ECF inhibits the proliferative potential of A375 cells as assessed by clonogenic assay. Cells were treated with different concentrations of ECF for 72h followed by replacement with fresh media for 1 week as described under "Materials and Methods". Curcumin (9 µg/ml) was used as positive control. Clones were counted and compared with the control. More than four cells containing a colony were counted as one clone. Representative histograms indicate the number of colonies formed. Data represent three independent experiments (Mean± SEM) and P-values are calculated using one-way ANOVA. ***P ≤0.001 and **P ≤0.01

(B) Scratch assay

The effect of ECF on cell proliferation of A375 cells was further analyzed using scratch assay, and cell migration at 24th and 48thh over 0thh were determined for both untreated and drug-treated cases. At the 24th hour of drug treatment, only 40% and 16% migration was observed in plates treated with 0.010 and 0.015 µg/ml of ECF respectively, while 63% migration was observed in the untreated control. At the 48th hour, 53% of migration was observed at 0.01µg/ml and 23% of migration was observed at 0.15µg/ml, whereas 88 % of migration was observed in the untreated control (Image J software). Results revealed that the wound closure was much slower in the wells treated with ECF, compared with control (Figure 4.1.7B).

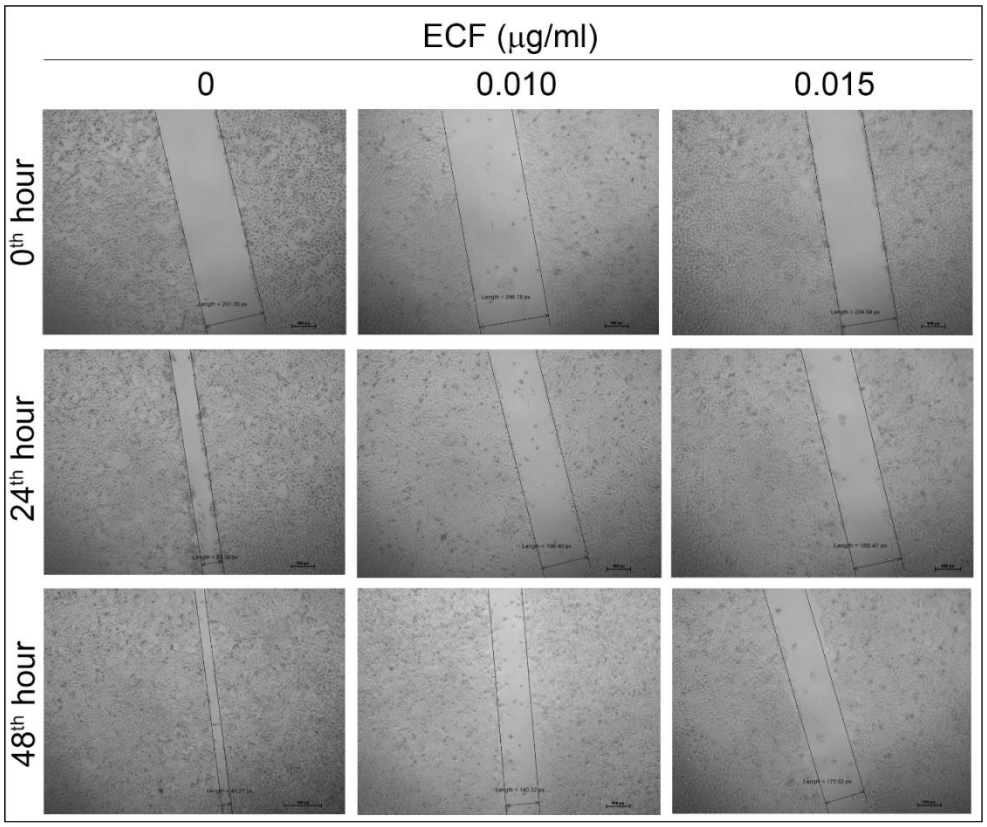

Figure 4.1.7B: ECF inhibits the proliferative potential of A375 cells as assessed by scratch assay. A wound was created in the cell containing plate. Cells were treated with different concentrations of ECF and cell migration at 24th and 48th h over 0th h were determined for both untreated and drug-treated cases as described under "Materials and Methods. Wound closure was calculated using ImageJ software. Representative histograms indicate the number of colonies formed. Data represent three independent experiments (Mean± SEM). P-values were calculated using one-way ANOVA.

4.1.8. Evaluation of apoptosis in response to ECF in the melanoma cell line by Annexin V-FITC/PI staining

To analyze if apoptosis is involved in the cytotoxic mechanism of ECF in melanoma cells, FITC-Annexin V/PI staining was used. Annexin is a family of calcium-dependent phospholipid-binding proteins that preferentially bind to phosphatidyl serine (PS). Under normal physiological conditions, PS is predominantly located in the inner leaflet of the plasma membrane. Upon induction of apoptosis, PS loses its asymmetric distribution across the phospholipid bilayer and is translocated to the outer leaflet of the cell membrane, and can be detected by fluorescent-labelled Annexin V. In the early stages of apoptosis, the cells will stain with annexin V but not PI, as membrane integrity is intact and appears green. In the late stages of apoptosis, the cell membrane integrity is lost and cells stain PI in addition to Annexin V, making the cells appear red/orange with a green outline. ECF treatment (0.01

and 0.015 µg/ml) resulted in a significant hike in the number of FITC/PI-positive apoptotic cells in comparison to the untreated control (Figure 4.1.8A).

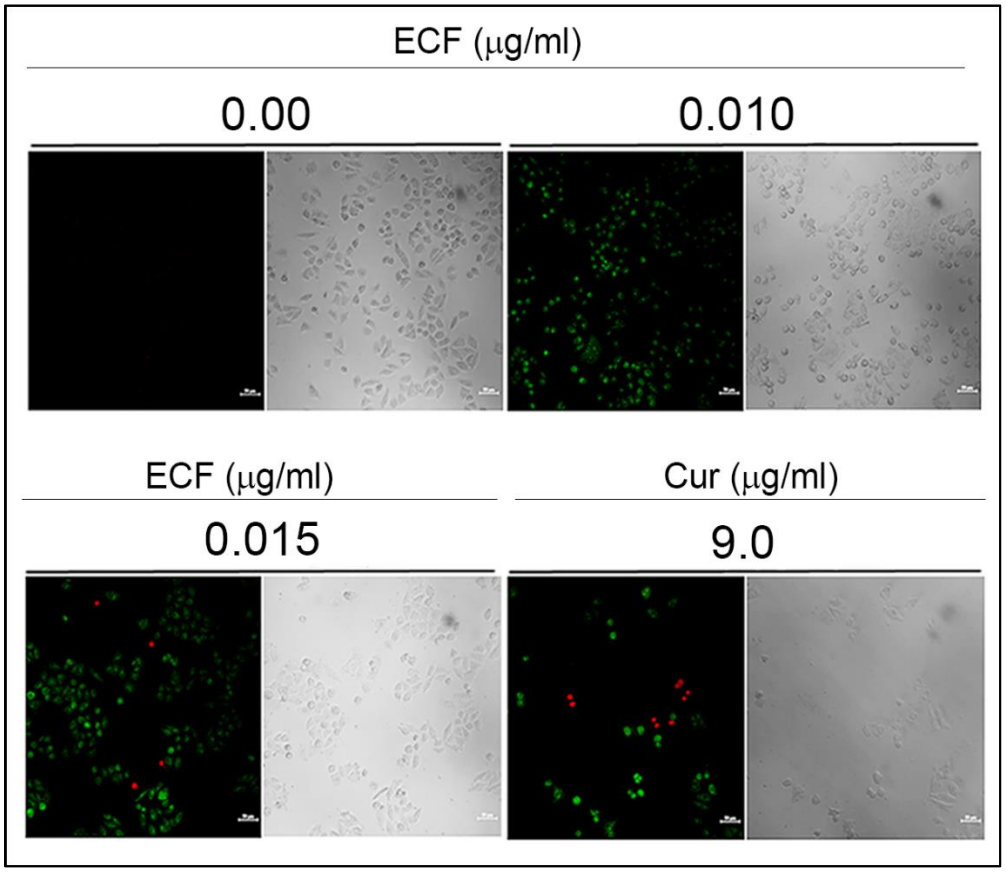

Figure 4.1.8A: ECF induces apoptosis in A375 cells as assessed by Annexin V-FITC/PI staining. A375 cells were treated with ECF as indicated for 16h and stained with Annexin V-FITC/PI. The green colour indicates cells at the early stage of apoptosis and the red colour indicates cells at the late stage of apoptosis. Curcumin (9µg/ml) was used as positive control. Data represent three independent sets of experiments.

The extent of apoptosis induced by ECF was estimated by FACS analysis of the Annexin V–FITC/PI double-stained cells. The apoptotic cell population was found to increase from 2.4% to 6.3% and 34.3% when treated for 16 h with 0.01µg/ml and 0.015µg/ml of ECF respectively. A375 cells treated with curcumin (9µg/ml) were used as a positive control (Figure 4.1.8B).

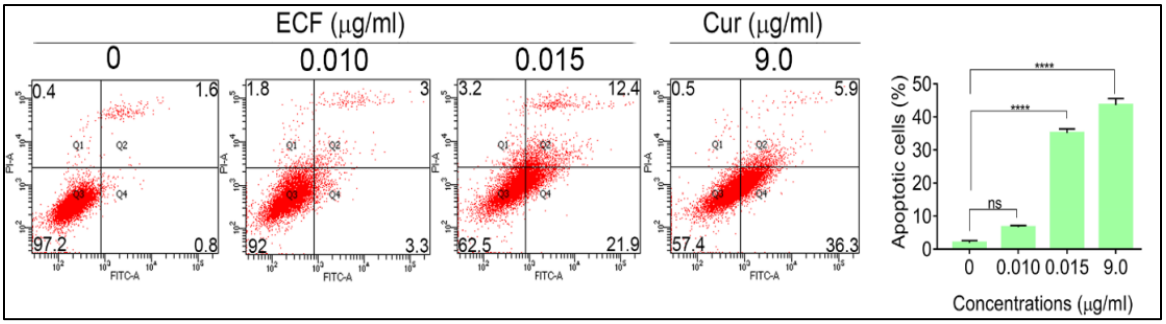

Figure 4.1.8B: FACS analysis for ECF-induced apoptosis in A375 cells. A375cells were treated with ECF as indicated for 24 h and Annexin V-FITC/propidium iodide (PI) positive cells were quantitated by FACS analysis. Curcumin (9 µg/ml) was used as positive control. Data are representative of three independent experiments (Mean± SEM). P-values were calculated using one-way ANOVA. ****P <0.0001, and ns ≥ 0.05.

4.1.9. Evaluation of apoptosis in response to ECF in the melanoma cell line by DAPI staining

During apoptosis, a phase change in chromatin (from a heterogeneous, genetically active network to an inert, highly condensed form) is observed. DNA binding nuclear dye such as DAPI can stain the condensed chromatin, which will be brighter than the chromatin from non-apoptotic cells so that the condensed nuclei can be easily identified by fluorescence microscopy. DAPI staining was performed to substantiate apoptosis in ECF-treated A375 cells, and the result revealed a dose-dependent increase in the number of cells with condensed chromatin, as assessed by enhancement in fluorescence intensity in the ECF-treated wells of the plate (0.010 and 0.015 µg/ml) (Figure 4.1.9).

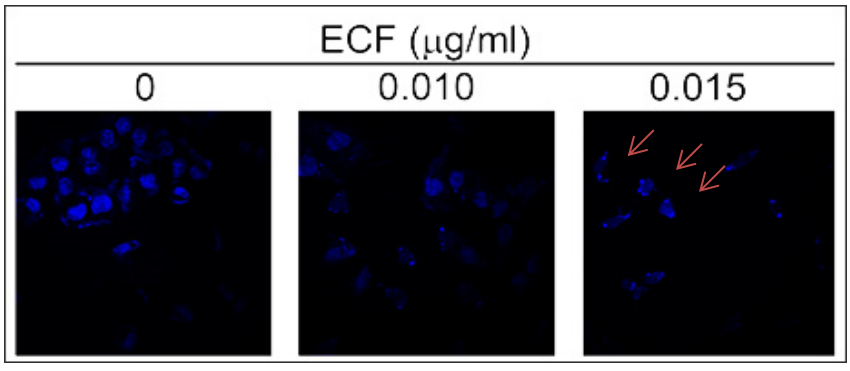

Figure 4.1.9: ECF-induced chromatin condensation in A375 cells as assessed by DAPI staining. A375 cells were treated with ECF as indicated for 24h and stained with DAPI. The presence of intense blue fluorescent spots indicates chromatin condensation which is observed in cells undergoing apoptosis. Data are representative of three independent experiments.

4.1.10. Delineation of the apoptotic pathway induced by ECF in A375 cells

Apoptosis in cells is mediated by cysteine proteases, termed caspases, which are functionally classified into initiators and executioners. Initiator caspases 8 and 9, are activated by intrinsic or extrinsic apoptotic stimuli, subsequently activating the executioner caspases, which in turn cleave the cellular death substrates, eventually resulting in apoptosis. ECF treatment led to the cleavage of the initiator caspase 9 (Figure 4.1.10A) while caspase 8, associated with extrinsic stimuli, remained unaffected (Figure 4.1.10B). To rule out the involvement of the extrinsic pathway, the activation of BID was tested. The protein BID is a specific proximal substrate of caspase 8 in the death receptor-mediated extrinsic apoptotic signaling pathway and a mediator of caspase 8-induced mitochondrial membrane damage (Li, Zhu, Xu, & Yuan, 1998). Strikingly, an activation of BID upon ECF treatment was observed, even in the absence of activation of caspase 8 (Figure 4.1.10C). Previous reports have indicated the ability of caspase-10, yet another initiator caspase in the extrinsic pathway, to cleave and activate BID (Milhas et al., 2005). Interestingly, immunoblot analysis revealed the ability of ECF to activate caspase 10 (Figure 4.1.10C). Furthermore, ECF induced the cleavage of executioner caspases, 7and 3, as well as the substrate of executioner caspases, Poly ADP-Ribose Polymerase (PARP) (Figure 4.1.10D-F). Together, these data confirm that the cytotoxicity induced by ECF in melanoma cells involves caspase-dependent apoptosis.

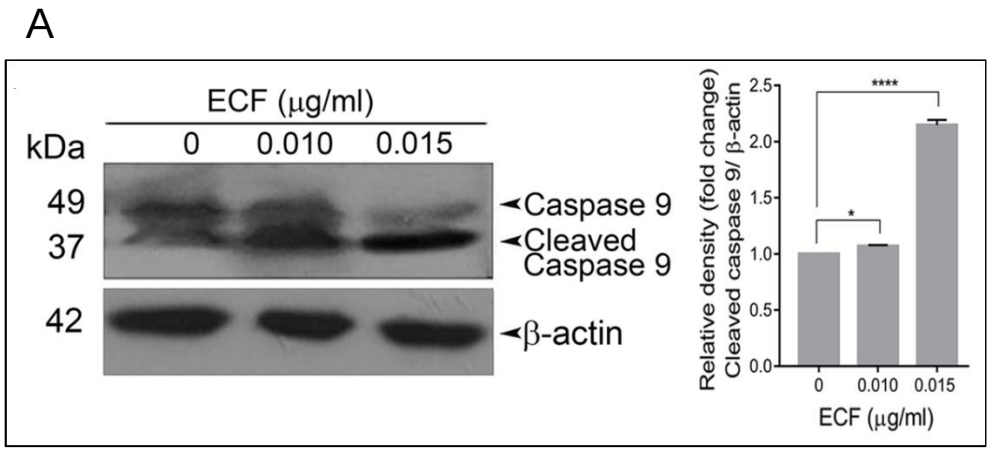

Figure 4.1.10A: ECF triggers cleavage of caspase 9 indicating the apoptotic mode of cell death in A375 cells. Immunoblot analysis was conducted for detecting cleavage of procaspase 9 in A375 cells. A375 cells were treated with ECF for 48 h, and whole-cell lysates prepared were electrophoresed and immunoblotted against anti-caspase-9. Bands were developed using ECL reagent and quantified by Image J software. Data are representative of three independent experiments (Mean± SEM). P-values were calculated using one-way ANOVA. ****P <0.0001 and *P <0.1.

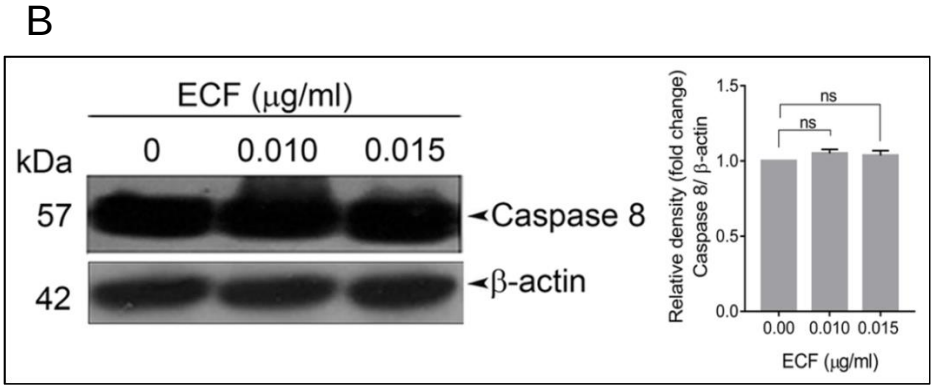

Figure 4.1.10B: ECF triggers cleavage of caspase 8 indicating the apoptotic mode of cell death in A375 cells. Immunoblot analysis was conducted for detecting cleavage of procaspase 8 in A375 cells. A375 cells were treated with ECF for 48 h, and whole-cell lysates prepared were electrophoresed and immunoblotted against anti-caspase-8. Bands were developed using ECL reagent and quantified by Image J software. Data are representative of three independent experiments (Mean± SEM). P-values were calculated using one-way ANOVA. ns ≥ 0.05.

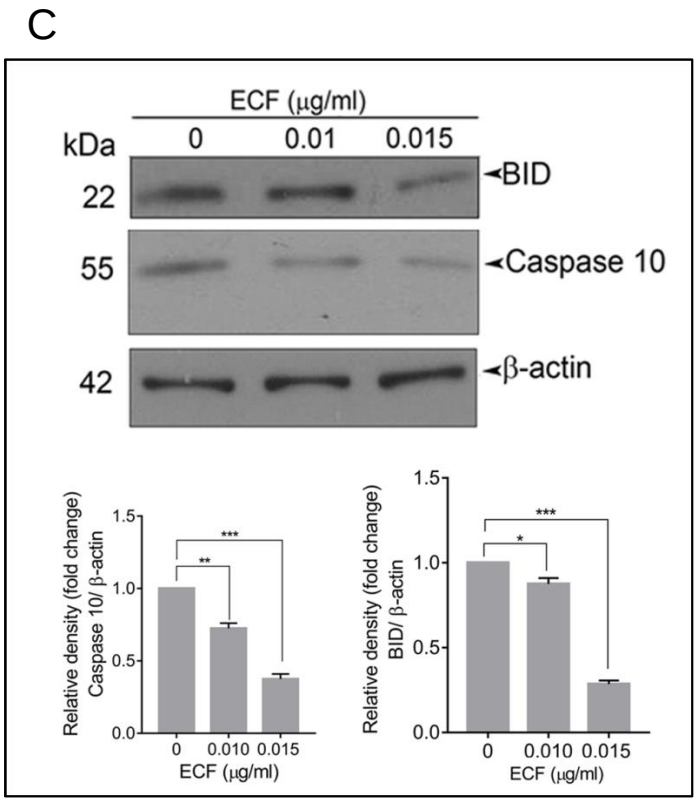

Figure 4.1.10C: ECF induces cleavage of caspase 10 and BID confirming the apoptotic mode of cell death in A375 cells. Immunoblot analysis was conducted to detect cleavage of procaspase 10 and BID in A375 cells. A375 cells were treated with ECF for 48 h, and whole-cell lysates prepared were electrophoresed and immunoblotted against anti-caspase-10 and BID. Bands were developed using ECL reagent and quantified by Image J software. Data are representative of three independent experiments (Mean± SEM). P-values were one-way using one-way ANOVA. ***P ≤0.001, **P ≤0.01 and *P <0.1.

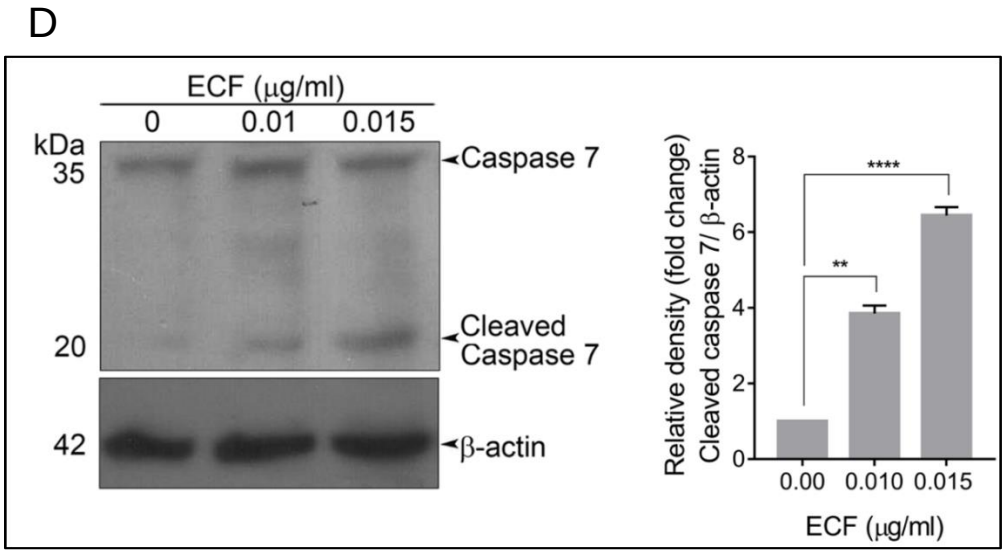

Figure 4.1.10D: ECF induces cleavage of caspase 7 indicating the apoptotic mode of cell death in A375 cells. Immunoblot analysis was conducted to detect cleavage of procaspase 7 cleavage in A375 cells. A375 cells were treated with ECF for 48 h, and whole-cell lysates prepared were electrophoresed and immunoblotted against anti-caspase-7. Bands were developed using ECL reagent and quantified by Image J software. Data are representative of three independent experiments (Mean± SEM) and P-values are calculated using one-way ANOVA. ****P <0.0001 and **P ≤0.01.

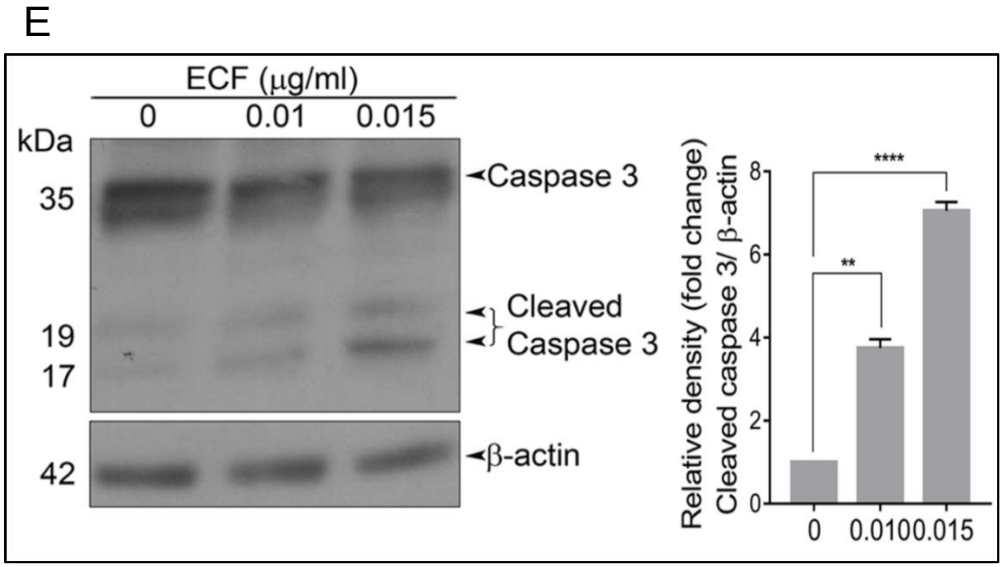

Figure 4.1.10E: ECF triggers cleavage of caspase 3 indicating the apoptotic mode of cell death in A375 cells. Immunoblot analysis was conducted to detect cleavage of procaspase 3 cleavage in A375 cells. A375 cells were treated with ECF for 48 h, and whole-cell lysates prepared were electrophoresed and immunoblotted against anti-caspase-3. Bands were developed using ECL reagent and quantified by Image J software. Data are representative of three independent experiments (Mean± SEM) and P-values are calculated using one-way ANOVA. ****P <0.0001 and **P ≤0.01.

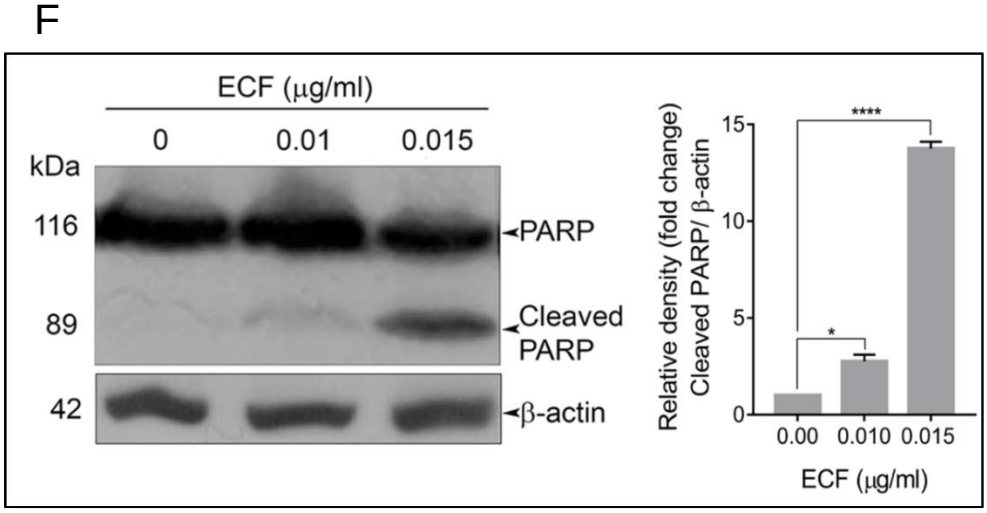

Figure 4.1.10F: ECF induces cleavage of PARP confirming the apoptotic mode of cell death in A375 cells. PARP cleavage was detected in A375 cells by immunoblot analysis. A375 cells were treated with ECF for 48 h, and whole-cell lysates prepared were electrophoresed and immunoblotted against anti-PARP. Bands were developed using ECL reagent and quantified by Image J software. Data are representative of three independent experiments (Mean± SEM) and P-values are calculated by using one-way ANOVA. ****P <0.0001 and *P <0.1.

4.1.11. Toxicological evaluation of ECF in *Swiss albino* mice

To ascertain the biological safety of ECF, acute and sub-chronic toxicity studies were conducted in Swiss albino mice. Two doses of ECF, the optimal dose and five times the optimal dose (0.25 and 1.25 mg/kg), were used for the drug-induced toxicity evaluation. A mass spectrometry analysis of the ECF fraction was done and the molecular weight corresponding to the base peak obtained as 581, which corresponds to a sodium adduct of 558 was selected, based on the assumption that the compound corresponds to this peak is responsible for the cytotoxic effect of the fraction. At the end of the experiment, murine blood was collected to quantitate AST, ALT, and ALP, the elevated levels of which are indicative of liver toxicity. Histopathological analysis of mice liver tissues was also performed using H & E staining. Notably, no behavioural changes such as convulsion, hyperactivity, sedation, grooming, food and water intake, etc. were observed in the mice upon ECF treatment. In addition, no significant changes were observed in the body weight of the animals. The serum analysis, as well as histopathological evaluation of liver sections of the mice studied, did not show a significant toxicological change in any of the parameters studied (Figure 4.1.11A-F), indicating that ECF is pharmacologically safe, *in vivo*.

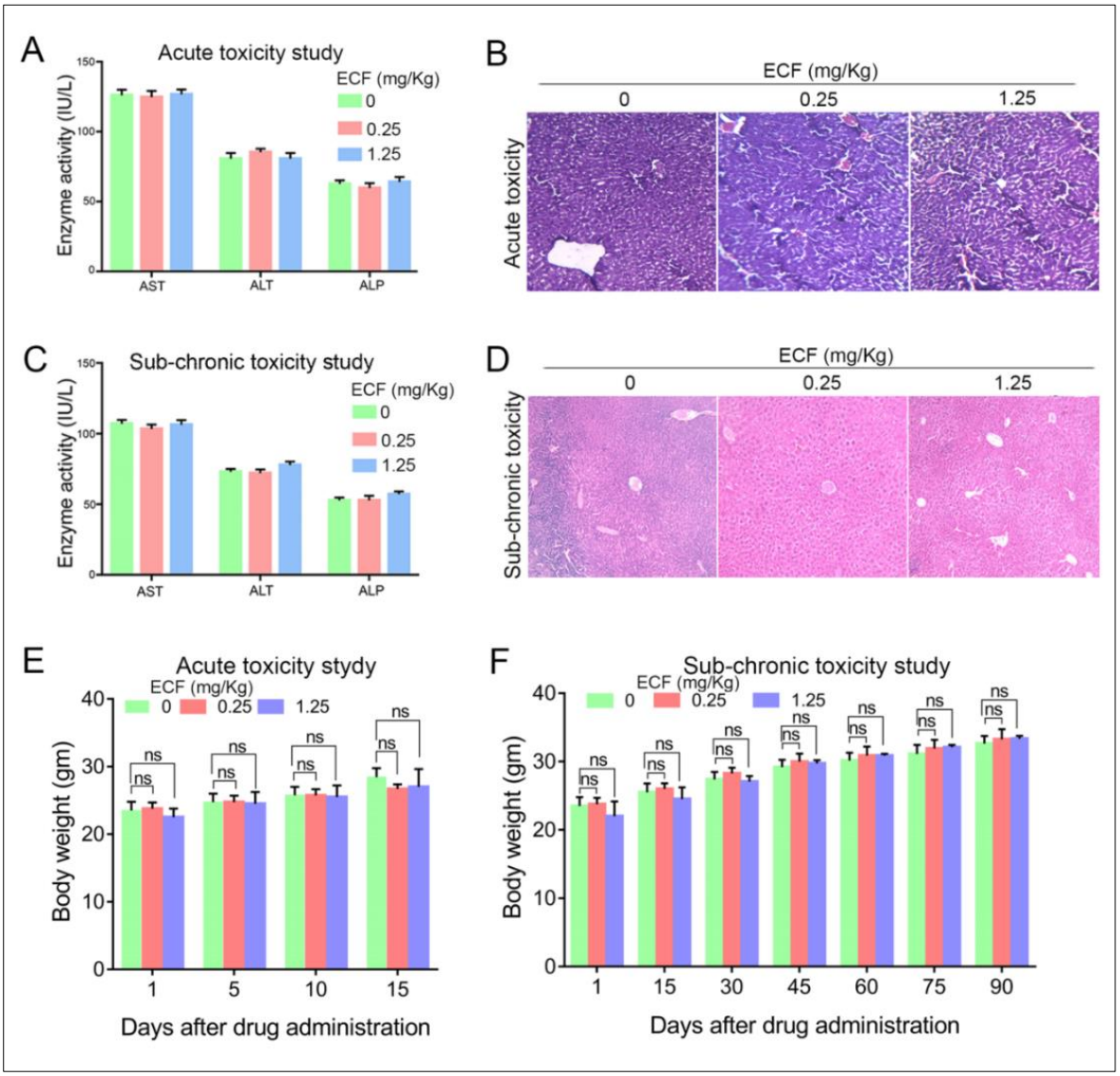

Figure 4.1.11A-F: Pharmacological safety of ECF, (A-D) Acute and sub-chronic toxicity analysis upon ECF treatment in *Swiss albino* mice. The figure denotes graphical representations of AST, ALT, and ALP activities, in response to ECF treatment. H&E stained liver tissues of mice treated with ECF. (E) Representation of body weight (5 days intervals) of animals of the acute toxicity study. (F) Representation of body weight (14 days interval) of animals of the sub-chronic toxicity study.

4.1.12. Characterization and identification of the anti-cancer compound from ECF

To isolate and purify the anticancer compound from ECF, column chromatography was done, finally leading to the isolation of a major product with polar characteristics. An initial observation by 1H NMR indicated a triterpene pattern with polar functional groups for the isolated compound (Figure 4.1.12A). The compound was found to have structural similarities with cucurbitacins, which are abundantly oxygenated triterpenes. Initially, an HR-ESI-MS analysis was carried out to match the list of already isolated cucurbitacins from the family of Cucurbitaceae. The molecular formula of the *C. epigaeus*-derived cucurbitacin was determined as $C_{32}H_{46}O_8$ as per the HR-ESI-MS analysis which exhibited ions at 581.3113 (M+Na)+ along with a corresponding dimer peak at 1139.6336 (2M+Na)+ (Figure 4.1.12B). The 13C NMR exhibited three ketone functional groups at δC 202.50, 212.19, and 213.08 ppm, and one among these three carbonyls is a part of α, βa -unsaturated system that appears at δH 6.4 (d, J = 16.5 Hz) and 7.0 (d, J = 16 Hz) in the 1H NMR (Figure 4.1.12C). The presence of δC 170.32 indicated the presence of an ester group and the presence of nine methyl groups in ^{13}C NMR. Together, the spectral data indicated the identity of the polar compound as cucurbitacin B (purity 99.99%) (Figure 4.1.12D). Gratifyingly, the ^{1}H and ^{13}C NMR were found to be in perfect agreement with published literature (Table 4.1.12) for Cu-B (Jacobs, Singh, Reynolds, & McLean, 1990). This is the first report indicating the presence of Cu-B from *C. epigaeus.*

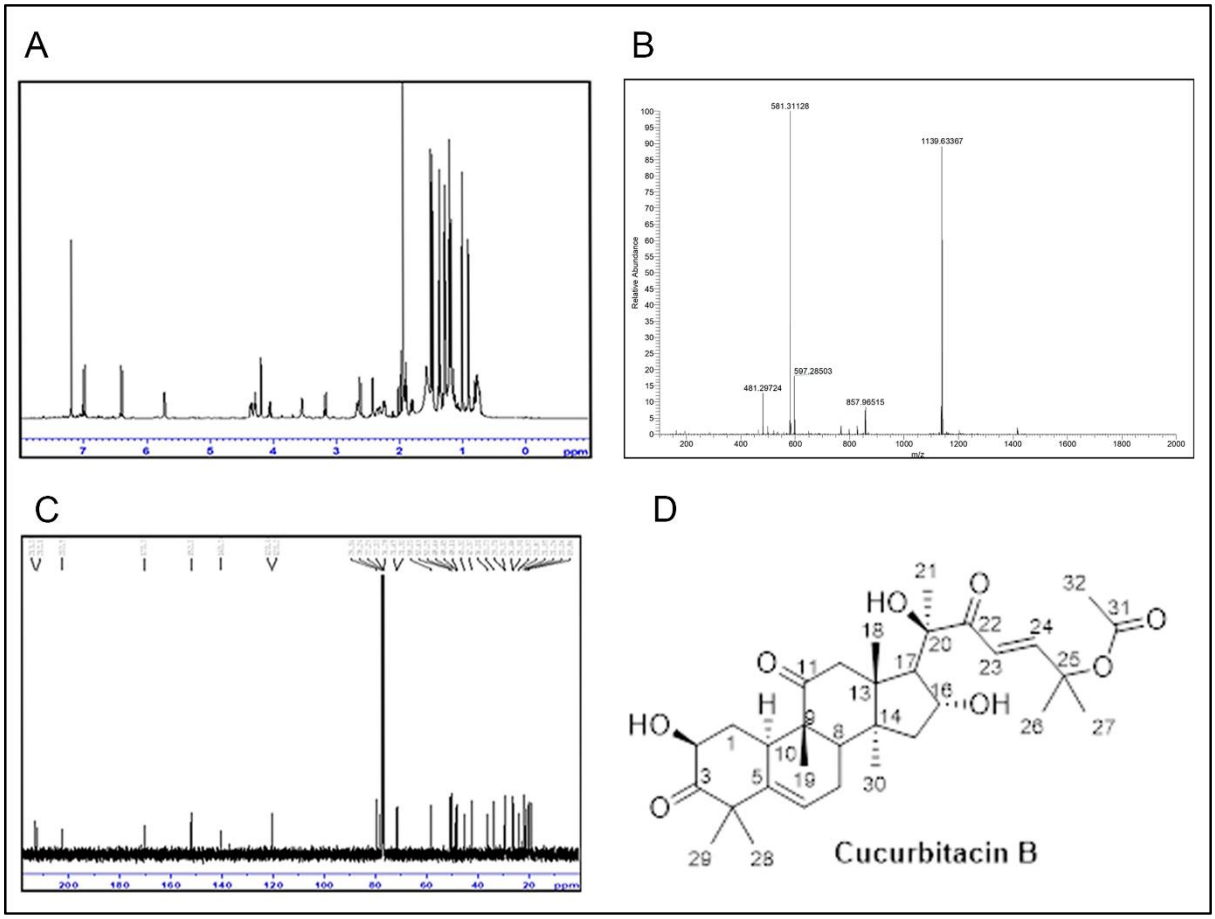

Figure 4.1.12A-D: Purification and structural elucidation of Cu-B from ECF fraction of *C. epigaeus* rhizome (A-D) 1H NMR, HR-ESI-MS, 13C NMR data, and structure of *C. epigaeus*-derived Cu-B.

UHPLC profiling was conducted to ascertain the purity of the isolated Cu-B, which exhibited a peak at 31.8 min at 254 nm. The chromatograms of Cu-B and its presence in ECF were confirmed by spiking the bioactive fraction with pure cucurbitacin B (Figure 4.1.12.E).

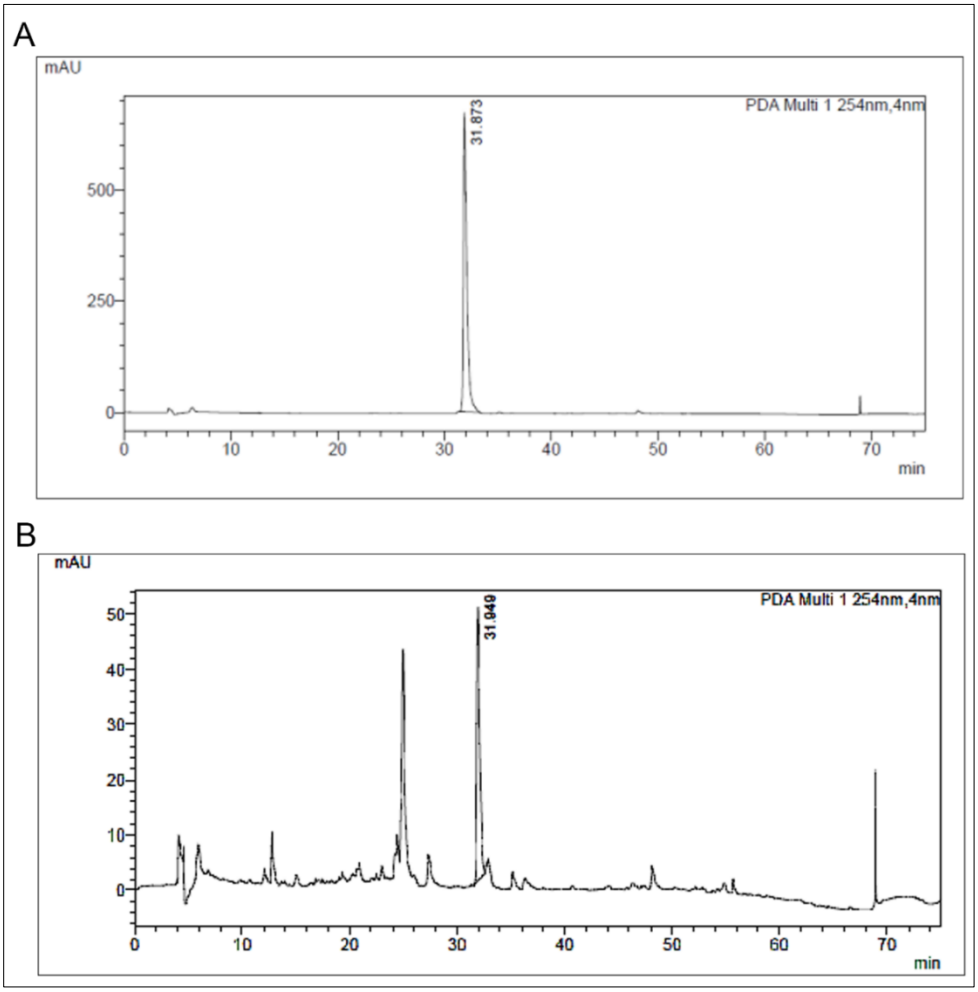

Figure 4.1.12.E: UHPLC chromatograms of cucurbitacin B and its presence in ECF fraction, (A-B) ECF fraction (3 mg/ml) and the isolated pure compound (2 mg/ml) were dissolved in acetonitrile:water (1:1) and filtered through a 0.2 µm nylon filter. The sample injection volume was 20 µL, and the C18 column temperature was 35 °C. The mobile phase system consists of water:acetic acid (100:1) (A) and acetonitrile (B). A step gradient program was used for this analysis as follows: 0% B at 0 min to 40% B at 20 min, 40 to 50% at 30 min, 50 to 60% at 40 min, 60 to 80% at 50 min, 80 to 100% at 60 min, then maintaining at 100% B from 60 to 65 min at a flow rate of 1 ml/min, monitored at 254 nm.

The cytotoxic activity of Cu-B isolated from *C. epigaeus* was compared with that of a commercially available one, purchased from TCI Chemicals Pvt. Ltd, India. The melanoma cell line, A375 was treated with Cu-B from different sources (1-10nM) for 72h, and the cell viability was assessed by MTT assay, as described in "Materials and Methods". The result revealed that irrespective of the source, Cu-B exhibited substantial cytotoxicity in A375 cells and the IC50 value was found to be around 5nM for both cases.

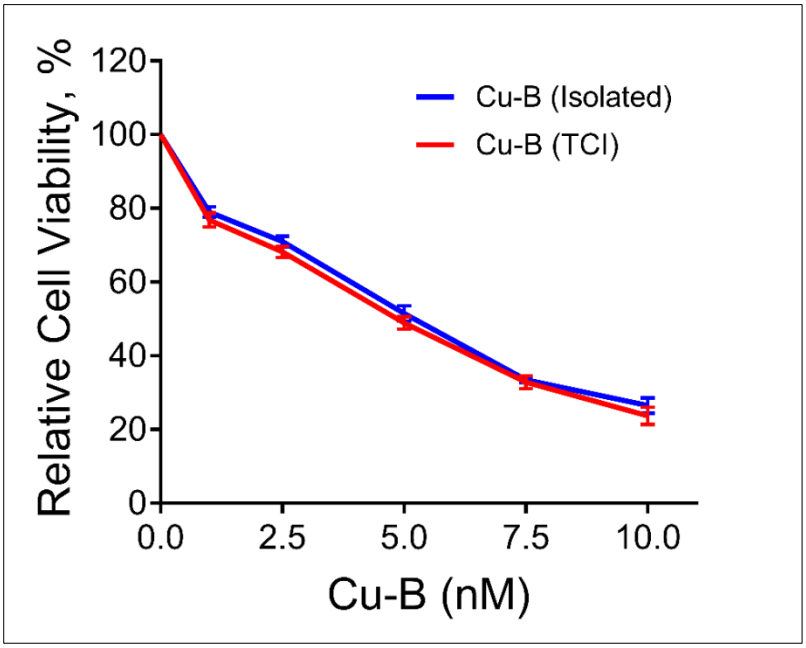

Figure 4.1.12F: Comparative analysis of the cytotoxic potential of Cu-B isolated from *C. epigaeus* and Cu-B purchased from TCI. A375 cells were treated with different concentrations of Cu-B, incubated for 72 h and cell, viability was assessed by MTT assay as described under "Materials and Methods". Relative cell viability was determined as % absorbance over untreated control. Data represent three independent sets of experiments. The error bars represent ± S.D.

Carbon No.	**^{1}H (ppm)**	**^{13}C (ppm)**
1	2.30, 1.24	36.01
2	4.36	71.65
3	-	213.08
4	-	50.25
5	-	140.36
6	5.7 (t, *J* = 3.5 Hz, 1H)	120.46
7	1.90 (d, *J* = 7 Hz), 2.42 (d, *J* = 7 Hz)	23.87
8	1.98	42.37
9	-	48.45
10	2.67	33.73
11	-	212.19
12	3.17 (d, *J* = 14.5 Hz), 2.62 (d, *J* = 14.5 Hz)	48.66
13	-	50.69
14	-	48.11
15	1.89, 1.47	45.32
16	4.36	71.3
17	2.5	58.2
18	0.91 (s, 3H)	19.86
19	1.01 (s, 3H)	20.06
20	-	78.24
21	1.35 (s, 3H)	23.93
22	-	202.5
23	6.39 (d, *J* = 16.5 Hz)	120.29
24	7.0 (d, *J* = 16.0 Hz)	152.03
25	-	79.34
26	1.50 (s, 3H)	26.46
27	1.57 (s, 3H)	25.91
28	1.2 4(s, 3H)	29.37
29	1.28 (s, 3H)	21.26
30	1.3 (s, 3H)	18.91
31	-	170.32
32	1.94 (s, 3H)	21.95

Table 4.1.12: ^{1}H and ^{13}C NMR of cucurbitacin B, in $CDCl_3$, isolated from the ethyl acetate extract of *Corallocarpus epigaeus.*

4. 2. Evaluation of the anti-melanoma efficacy of Cucurbitacin B, isolated from *Corallocarpus epigaeus*

The previous section of this study (4.1) has analyzed the anticancer property of the plant, *Corallocarpus epigaeus* and the isolated anticancer compound, Cucurbitacin B (Cu-B) from the cytotoxic fraction, ECF derived from the ethyl acetate extract of the rhizome. As ECF exhibited potent anti-melanoma activity, the present chapter has focused on the anti-melanoma efficacy of ECF derived Cu-B.

4.2.1. Screening of cancer cell lines of various tissue origins for their sensitivity towards Cu-B

To study the cytotoxic effect of Cu-B, a panel of five cancer cells of different origins, HCT-116 (Colon cancer cell line), H1299 (Lung cancer cell line), A375 (Melanoma), MDA-MB-231 (Breast cancer cell line), Hep 3B (Liver cancer cell line) and HeLa (Cervical cancer cell line) were used. These cell lines were treated with different concentrations of Cu-B (1-15nM) for 72 h, and cell viability was determined by MTT assay as described in "Materials and Methods". In line with the results obtained with ECF fraction (refer to Figure 4.1.3), increased sensitivity of the melanoma cells to Cu-B in comparison to cancer cells of other tissue origins was observed followed by Hep-3B, HCT116, MDA-MB-231, HeLa, and H1299(Figure 4.2.1).

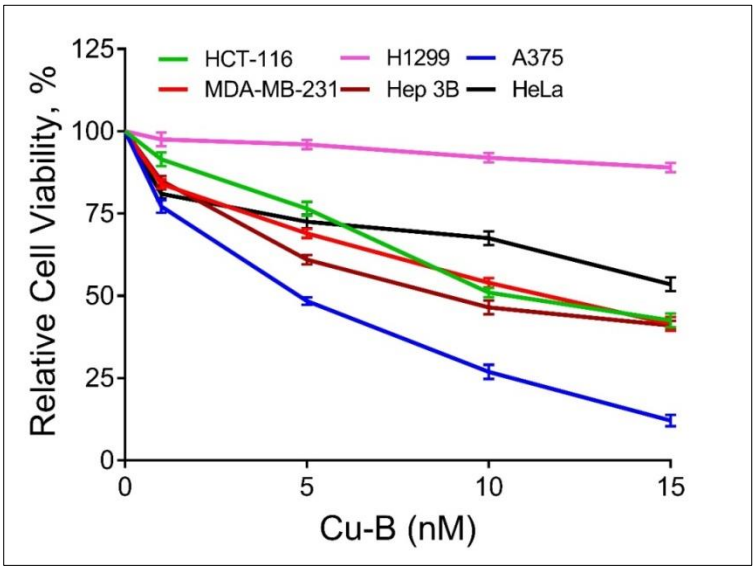

Figure 4.2.1: Screening of cancer cell lines of various tissue origins for their sensitivity towards Cu-B. Cancer cell lines HCT-116, H1299, A375, MDA-MB-231, Hep 3B and HeLa were treated with Cu-B as indicated, incubated for 72h and the cell viability was assessed by MTT assay as described under "Materials and Methods". Relative cell viability was determined as % absorbance over untreated control. Data represent three independent sets of experiments and results are shown as the mean± SD.

4.2.2. Evaluation of the cytotoxic potential of Cu-B in various melanoma cell lines to select the most sensitive cell line

The potent cytotoxic activity exhibited by Cu-B in melanoma cells was further evaluated in other melanoma cell lines, SK-MEL-2 and SK-MEL-28. Melanoma is classified into several molecular subgroups based on genomic alterations, among which, B-RAF and NRAS mutated melanomas are the most common (Amann et al., 2017). Therefore, we selected melanoma cell lines, which belong to the two molecular subgroups, with B-RAF/ NRAS mutation status viz. A375 cells [B-RAF mutation], SK-MEL-2 [NRAS mutation] and SK-MEL-28 [B-RAF mutation]. Cells were treated with different concentrations of Cu-B for 72 h and the cell cytotoxicity was evaluated by MTT assay. The results indicated that Cu-B induced potent cytotoxicity in all the three melanoma cell lines chosen for the study, irrespective of the mutation status (Figure 4.2.2). A375 cell line emerged as the most sensitive to Cu-B (IC50-5nM) and this cell line was selected for further studies.

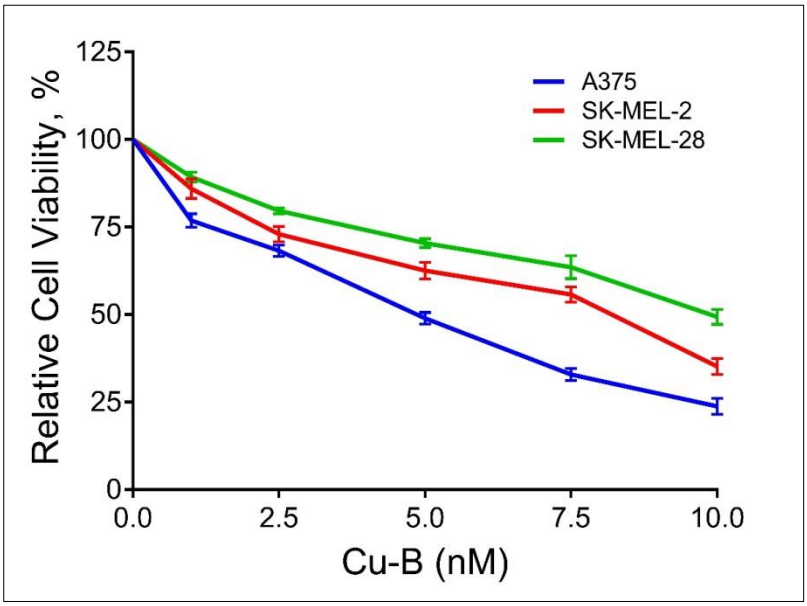

Figure 4.2.2: Dose-dependent effect of Cu-B on different melanoma cells. A375, SK-MEL-2 and Sk-MEL-28 were treated with Cu-B as indicated, incubated for 72h and the cell viability was assessed by MTT assay as described under" Materials and Methods". Relative cell viability was determined as % absorbance over untreated control. Data represent three independent sets of experiments and results are shown as the mean± SD.

4.2.3. Comparative analysis of the cytotoxic potential of Cu-B, Dacarbazine and Vemurafenib in the A375 cells

Dacarbazine (DTIC), is the most common drug used in melanoma chemotherapy. Hence, a comparative analysis of the cytotoxicity of Cu-B and Dacarbazine in A375 cells was done. Cells were treated with different concentrations of the drugs for a period of 72 h. interestingly, it was observed that Cu-B induced 50% cytotoxicity in A375 at 5nM (0.005µM) whereas dacarbazine induced 50% cytotoxicity only at around 25 µM. Recently, FDA-approved a B-RAF inhibitor, vemurafenib for the treatment of melanoma. However, a previous study conducted in human melanoma cell lines has shown that vemurafenib induces 50% cytotoxicity in A375 cells, only at 0.8 µM (Liu et al., 2020).

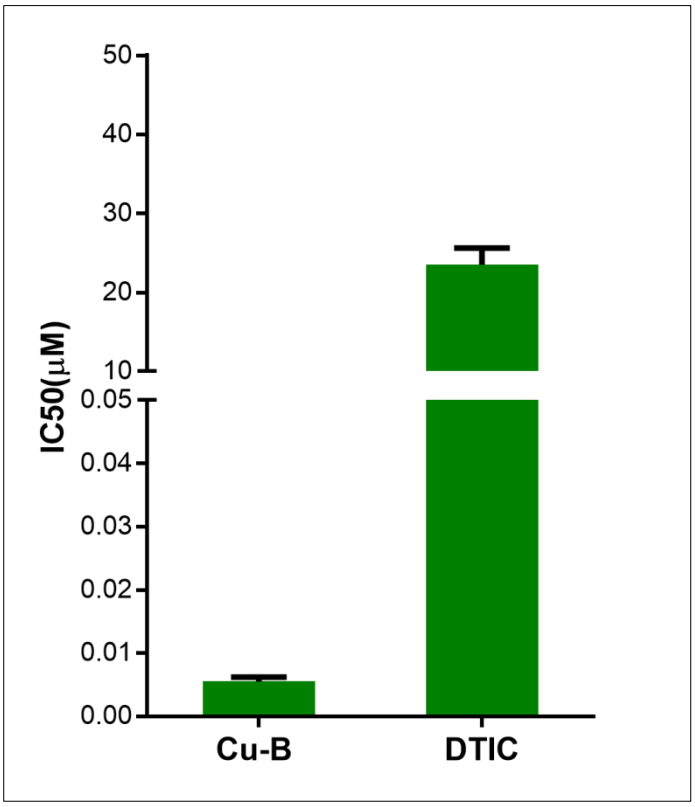

Figure 4.2.3: Comparison of IC50 of Cu-B with dacarbazine. The melanoma cell line A375 was treated with Cu-B and DTIC as indicated, incubated for 72h and the cell viability was assessed by MTT assay as described under "Materials and Methods". Relative cell viability was determined as % absorbance over untreated control. Data represent three independent sets of experiments and results are shown as the mean± SD.

4.2.4. Evaluation of the cytotoxic potential of Cu-B in normal skin fibroblasts

Since Cu-B was found to be highly efficacious against melanoma cells, the cytotoxic effect of the compound was analyzed in normal skin fibroblasts. Cells were treated with different concentrations of the compound for a period of 72 h and the cell viability was assessed by MTT assay. The results revealed that at 5nM, which is the IC50 concentration of Cu-B in A375 cells, 90% of normal skin fibroblast cells were live and at 10nM, 78% of cells were live, indicating the comparative safety of Cu-B to normal skin fibroblasts (Figure 4.2.4).

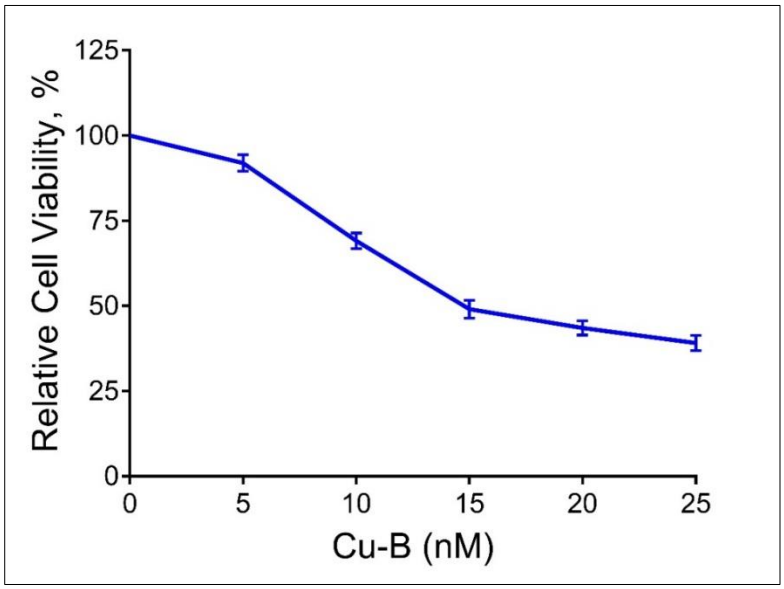

Figure 4.2.4: Assessment of Cu-B induced cytotoxicity in normal skin fibroblast cells. Normal skin fibroblast (FS) were treated with various concentrations of Cu-B, incubated for 72h and the cell viability was assessed by MTT assay as described under "Materials and Methods". Relative cell viability was determined as % absorbance over untreated control. Data represent three independent sets of experiments and results are shown as the mean± SD.

4.2.5. FACS analysis for cell cycle arrest in response to Cu-B in A375 cells

To explore whether the growth-inhibitory effect of Cu-B on A375 cells is mediated through cell cycle arrest, the distribution of cells in different phases of the cell cycle was analyzed by measuring intracellular DNA content in each phase by FACS analysis (BD FACS AriaTM). The results revealed that Cu-B did not interfere with any phases of the cell cycle even after prolonged treatment for 48 h (Figure 4.2.5), while curcumin (25µM) readily induced G2/M arrest at 24h. Notably, there was an augmentation in the number of cells at the sub G0 phase, upon treatment with Cu-B, indicating an apoptotic mode of cell death in response to Cu-B.

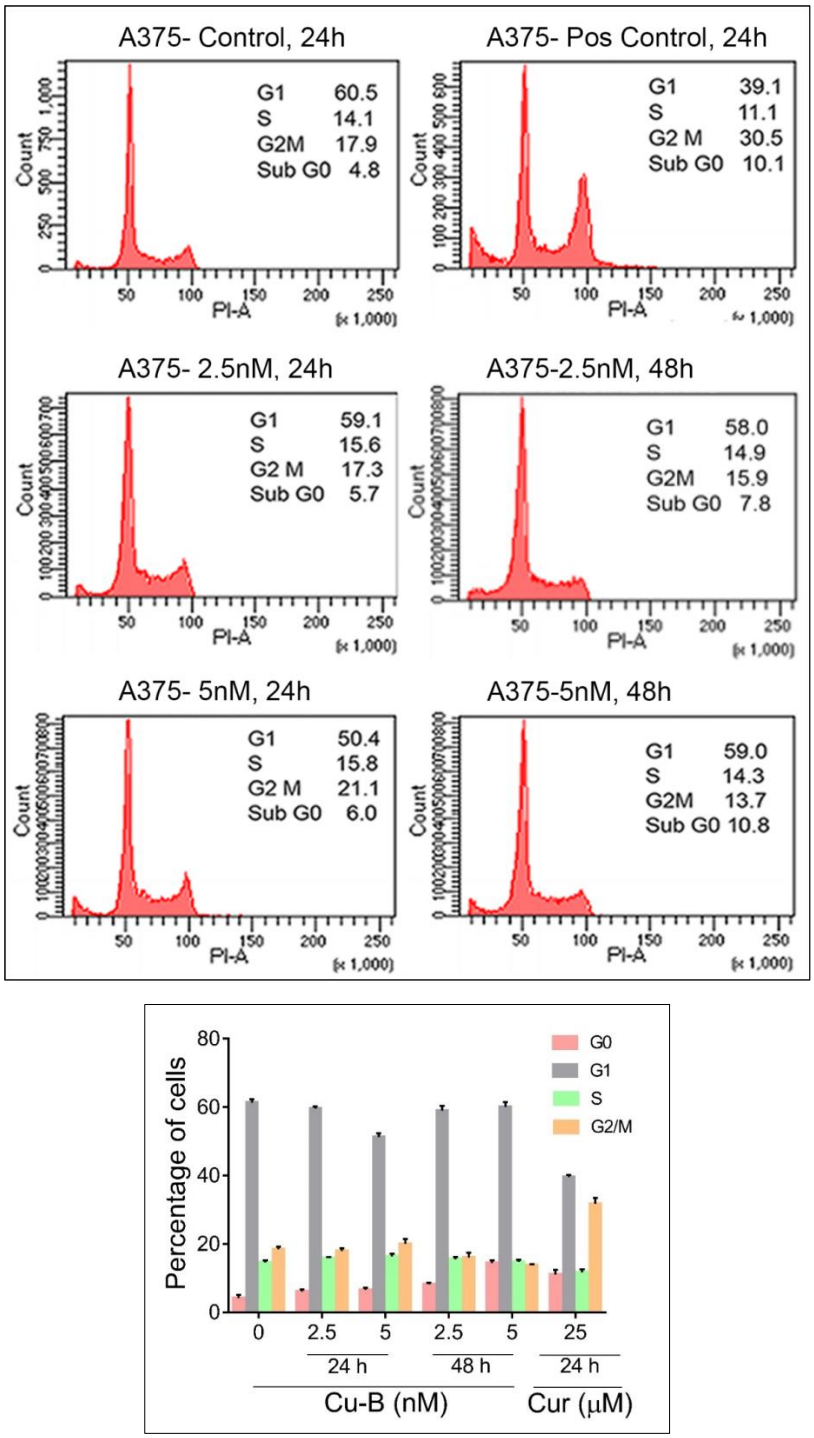

Figure 4.2.5: FACS analysis for Cu-B mediated cell cycle arrest in A375 cells. Cells were harvested after 24h &48 h of treatment with Cu-B, fixed in alcohol, stained with propidium iodide, and assayed for DNA content by flow cytometry as described in "Materials and Methods". Curcumin (25μM) was used as the positive control. Representative histograms indicate the percentages of cells in G1, S, G2/M and sub-G0 phases of the cell cycle. The percentage of cells with sub-G0 DNA content indicates the apoptotic cell population. The data provided is representative of three independent experiments.

4.2.6. FACS analysis for Annexin V-FITC/PI-positive apoptotic cells in response to Cu-B

To assess apoptosis and to quantitate the extent of apoptosis induced by Cu-B, FACS analysis of the Cu-B treated A375 cells stained with Annexin V-FITC/ PI was done. From the results, it is evident that Annexin V–FITC/PI double-stained apoptotic cell population increased from 1.6% to 35% and 43.6% when treated with 2.5nM and 5nM of Cu-B for 16 h, respectively. A375 cells treated with 25 µM curcumin were used as a positive control (Figure 4.2.6A-B).

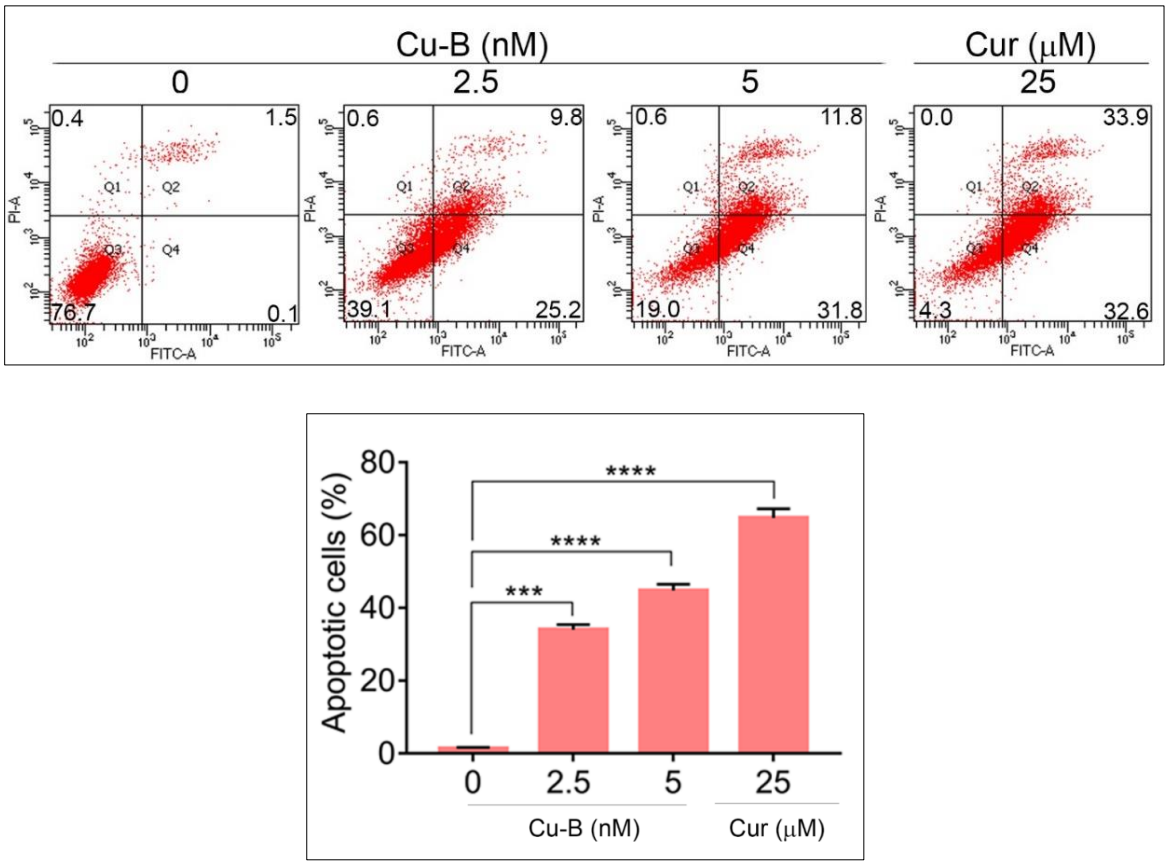

Figure 4.2.6: The extent of apoptosis induced by Cu-B was quantitated by Annexin V/PI FACS analysis. A375 cells were treated with Cu-B for 16h and stained with Annexin V-FITC/ PI to detect apoptotic cells. Representative histograms indicate the percentage of Annexin V-FITC/PI-positive cells. 25µM curcumin was used as a positive control. Data are representative of three independent experiments (Mean± SEM) and P-values are calculated using one-way ANOVA. ****P <0.0001 and ***P ≤0.001.

4.2.7. Delineation of the apoptotic pathway induced by Cu-B in A375 cells

To ascertain apoptosis and to delineate the Cu-B-mediated apoptotic pathway in A375 cells, immunoblot analysis was conducted to detect cleaved fragments of the activated caspases and PARP. A dose-dependent cleavage of the initiator caspase 9 as well as the effector caspases, 3 and, 7 was observed, clearly demonstrating mitochondria-mediated apoptosis (Figure 4.2.7A, C-D). Interestingly, Cu-B failed to induce the cleavage of caspase 8, as observed upon ECF treatment (Figure 4.2.7B), and in line with the data obtained with ECF, activation of caspase 10 and BID in A375 cells was observed, indicating the involvement of the death receptor pathway in Cu-B induced apoptosis (Figure 4.2.7E). Furthermore, Cu-B triggered a noticeable cleavage of PARP, marking apoptotic cell death (Figure 4.2.7F).

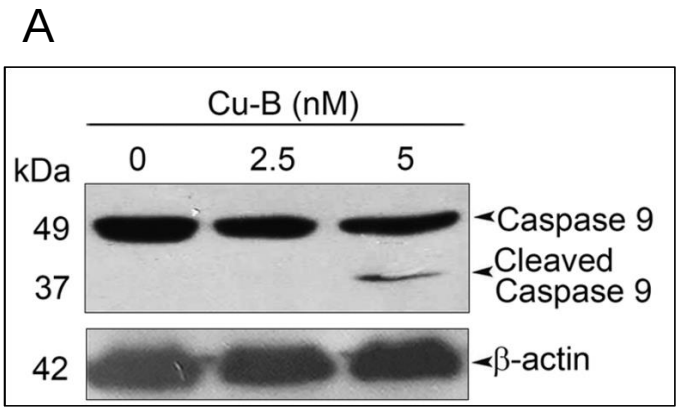

Figure 4.2.7A: Cu-B induces an apoptotic mode of cell death in A375 cells. Immunoblot analysis was conducted for detecting cleavage of procaspase 9 in A375 cells. A375 cells were treated with Cu-B for 24 h, and whole-cell lysates prepared were electrophoresed and immunoblotted against anti-caspase-9. Bands were developed by ECL and quantified by Image J software. Data are representative of three independent experiments (Mean± SEM). P-values were calculated using one-way ANOVA.

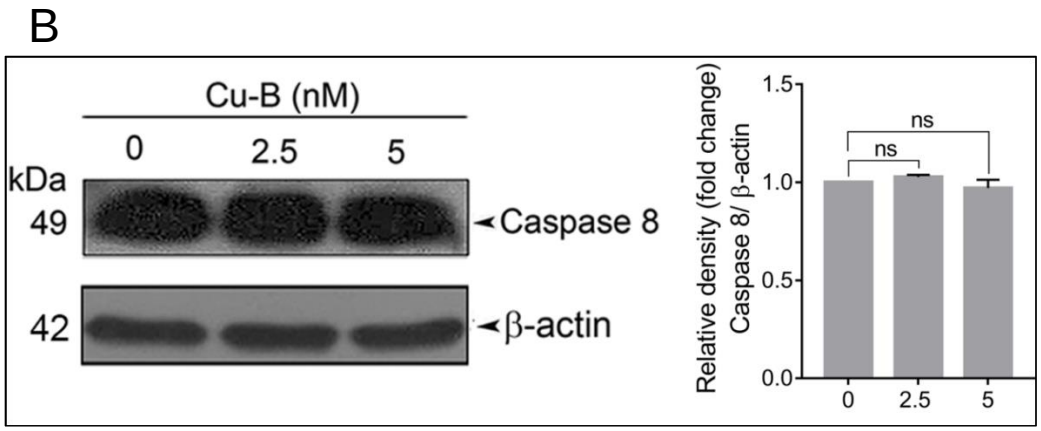

Figure 4.2.7B: Cu-B induces an apoptotic mode of cell death in A375 cells. Immunoblot analysis was conducted for detecting cleavage of procaspase 8 in A375 cells. A375 cells were treated with Cu-B for 24 h, and whole-cell lysates prepared were electrophoresed and immunoblotted against anti-caspase-8. Bands were developed by ECL and quantified by Image J software. Data are representative of three independent experiments (Mean± SEM). P-values were calculated using one-way ANOVA. ns ≥ 0.05.

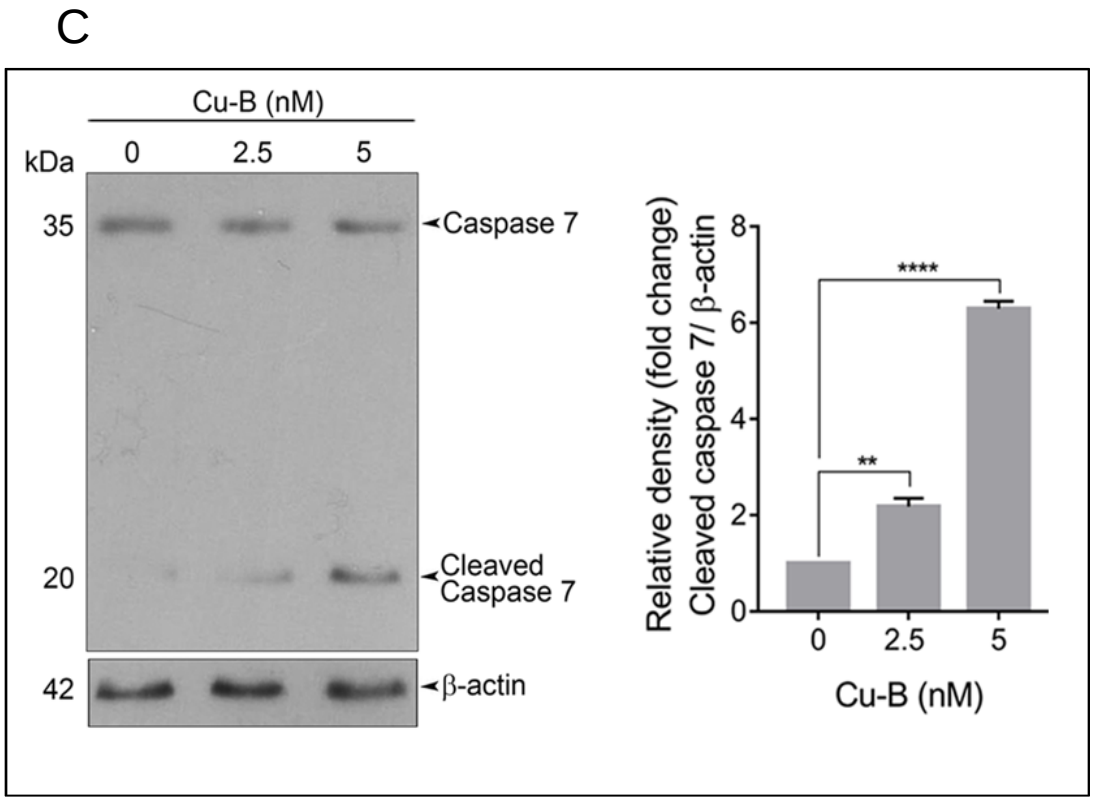

Figure 4.2.7C: Cu-B induces an apoptotic mode of cell death in A375 cells. Immunoblot analysis was conducted to detect cleavage of procaspase 7 cleavage in A375 cells. A375 cells were treated with Cu-B for 24 h, and whole-cell lysates prepared were electrophoresed and immunoblotted against anti-caspase-7. Bands were developed by ECL and quantified by Image J software. Data are representative of three independent experiments (Mean± SEM). P-values were calculated using one-way ANOVA. ***P ≤0.001and **P ≤0.01.

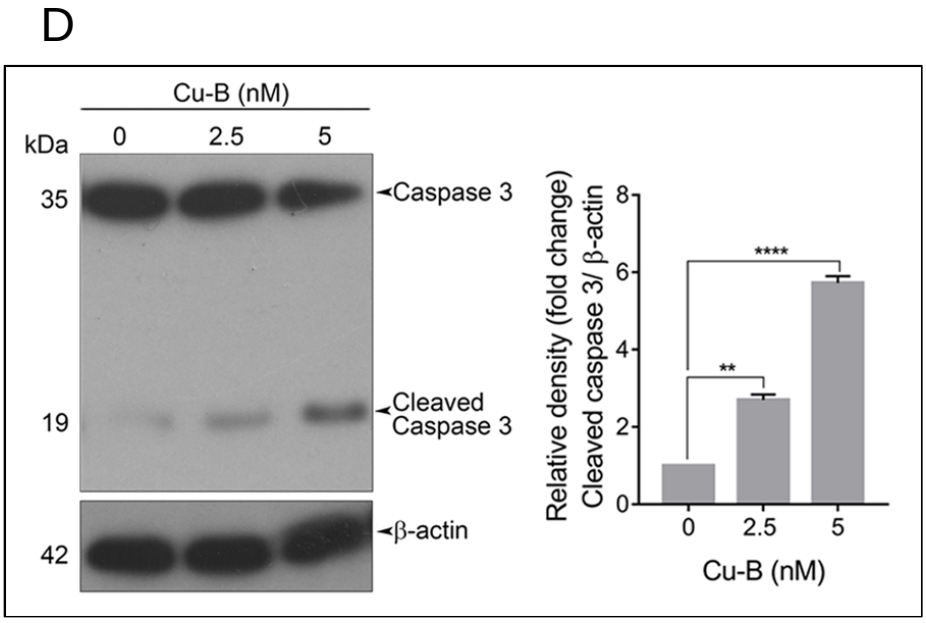

Figure 4.2.7D: Cu-B induces an apoptotic mode of cell death in A375 cells. Cleavage of procaspase 3 in A375 cells was detected and quantified by immunoblot analysis. A375 cells were treated with Cu-B for 24 h, and whole-cell lysates prepared were electrophoresed and immunoblotted against anti-caspase-3. Bands were developed by ECL and quantified by Image J software. Data are representative of three independent experiments (Mean± SEM). P-values were calculated using one-way ANOVA. ****P <0.0001 and **P ≤0.01.

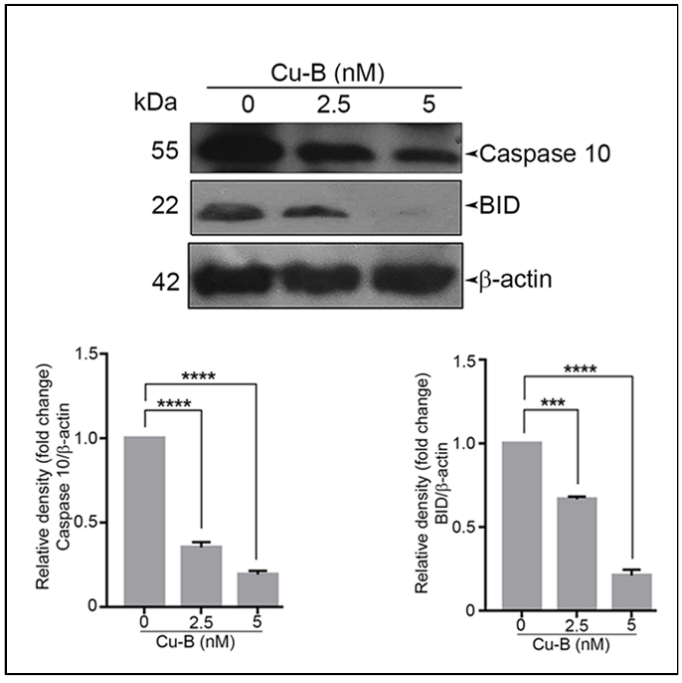

Figure 4.2.7E: Cu-B induces an apoptotic mode of cell death in A375 cells. Immunoblot analysis was conducted to detect cleavage of procaspase 10 and BID in A375 cells. A375 cells were treated with Cu-B for 24 h, and whole-cell lysates prepared were electrophoresed and immunoblotted against anti-caspase-10 and BID. Bands were developed by ECL and quantified by Image J software. Data are representative of three independent experiments (Mean± SEM). P-values were calculated using one-way ANOVA. ****P <0.0001 and ***P ≤0.001.

F

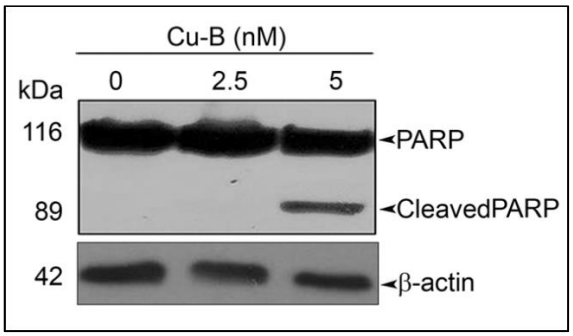

Figure 4.2.7F: Cu-B induces an apoptotic mode of cell death in A375 cells. PARP cleavage was detected in A375 cells by immunoblot analysis. A375 cells were treated with Cu-B for 24 h, and whole-cell lysates prepared were electrophoresed and immunoblotted against anti-PARP. Bands were developed by ECL and quantified by Image J software. Data are representative of three independent experiments (Mean± SEM). P-values were calculated using one-way ANOVA.

4.2.8. Evaluation of ROS generation and p53 activation in response to Cu-B in A375 cells

Previous reports have demonstrated the ability of chemotherapeutic drugs to induce apoptosis in cancer cells by triggering DNA damage as a result of increased ROS production (Zaidieh, Smith, Ball, & An, 2019). To investigate whether Cu-B elevates ROS production in A375 cells, a ROS-sensitive H2DCF-DA assay was employed. Cu -B treatment in A375 cells triggered the oxidation of H2DCF-DA by ROS to dichlorofluorescein (DCF), which further led to the generation of green fluorescence, the intensity of which was quantified by confocal microscopy (Figure 3P). Moreover, an increase in the phosphorylation of p53 in response to Cu-B was observed (Figure 3Q). These results indicate that Cu-B augments ROS production in A375 cells, subsequently leading to intrinsic apoptosis, signaled by DNA damage-induced p53 signaling. The data demonstrate the cell death mechanism through which *C. epigaeus*-derived Cu-B targets melanoma cells.

A

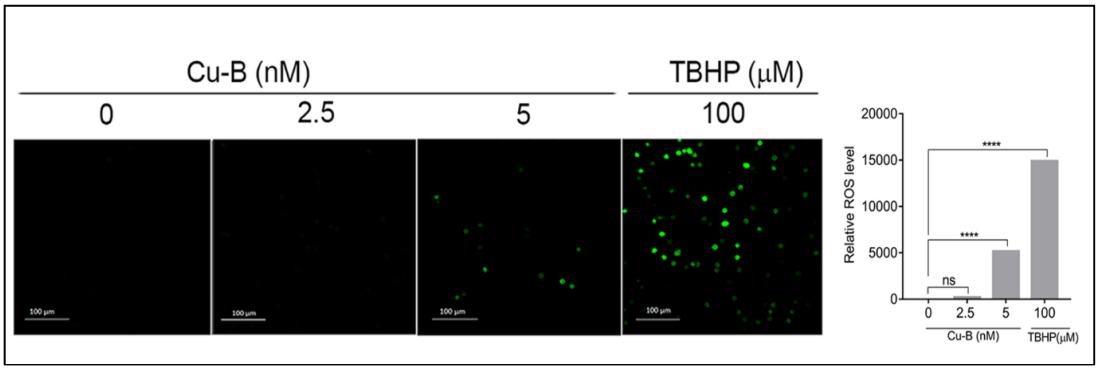

Figure 4.2.8A: Measurement of ROS generated in response to Cu-B in A375 cells by fluorescence microscopy. A375 cells were treated with Cu-B for 6 h and stained with DCFDA as described under "Materials and Methods". The green fluorescence generated produced was imaged and quantified. Data representative of three independent experiments (Mean± SEM) and P-values are calculated using one-way ANOVA. ****P <0.0001.

B

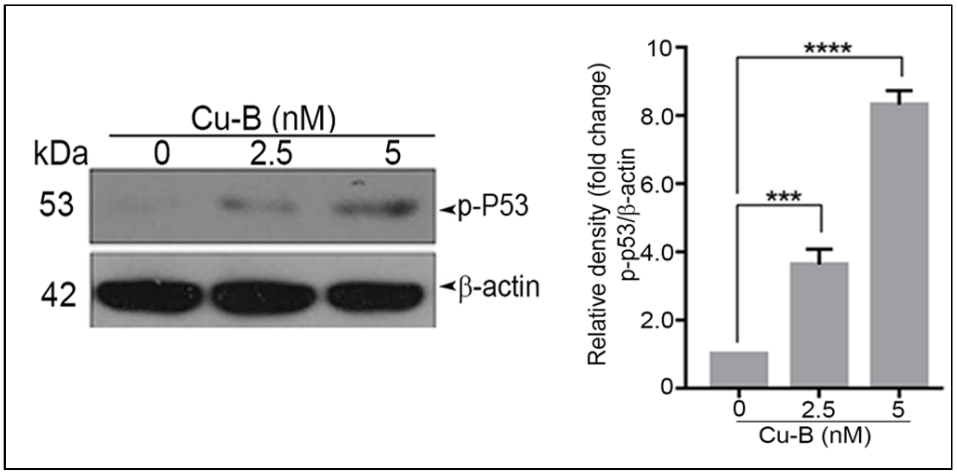

Figure 4.2.8B: Cu-B potentiates p53 activation in A375 cells. A375 cells were treated with Cu-B for 24 h, whole-cell lysates prepared were electrophoresed and immunoblotted against anti-pP53. Bands were developed by ECL and quantified by Image J software. Data are representative of three independent experiments (Mean± SEM). P-values were calculated using one-way ANOVA. ****P <0.0001, and ***P ≤0.001.

4.2.9. Toxicological evaluation of Cu-B in *Swiss albino* mice

To rule out the chance of any adverse effect of Cu-B *in vivo*, an acute toxicity study for 7 days and a sub-chronic toxicity study for 3 months in Swiss albino mice were conducted. At the end of the experiment, Blood and liver tissues were collected for biochemical and histopathological evaluation. The serum was analyzed for the levels of AST, ALT and ALP, elevated levels of which are indicative of hepatotoxicity. The levels of urea, creatinine and uric acid, elevated levels of which are indicative of renal toxicity were also analyzed. Histopathological analysis of the liver tissue was conducted, using H and E staining for toxicological changes. No behavioural changes were noted in the mice at any concentrations of Cu-B studied, till the end of the experiment (Figure 4.2.9A-F). The serum analysis, as well as histopathological evaluation of liver sections from Cu-B-treated mice, did not reveal any noticeable toxicological changes in any of the parameters tested, indicating the pharmacological safety of Cu-B.

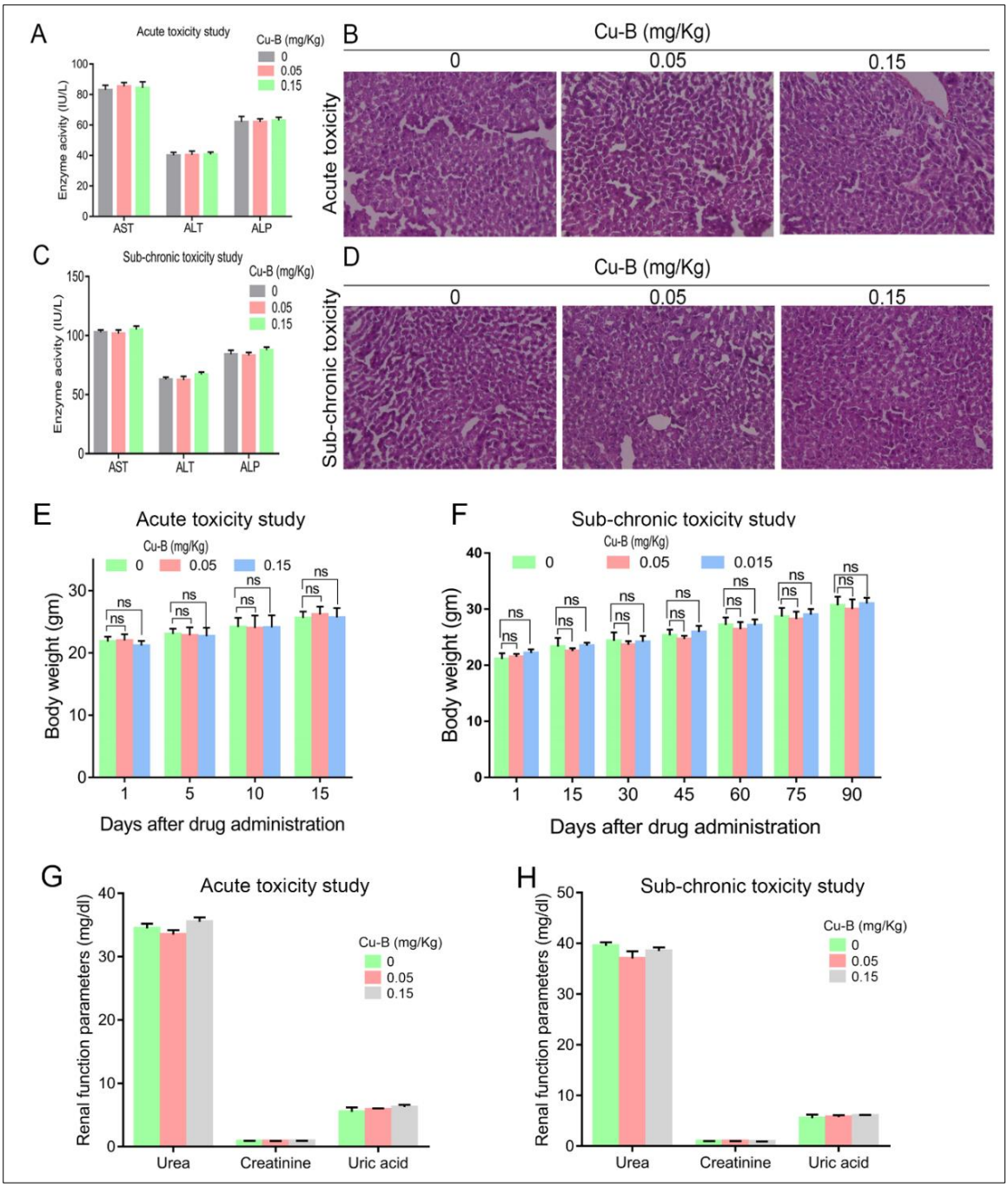

Figure 4.2.9: Pharmacological safety of Cu-B, (A-D) Acute and sub-chronic toxicity analysis upon Cu-B treatment in *Swiss albino* mice. The figure denotes graphical representations of AST, ALT, and ALP activities, in response to Cu-B treatment. H&E stained liver tissues of mice treated with Cu-B. (E) Representation of body weight (5 days intervals) of animals of the acute toxicity study. (F) Representation of body weight (14 days interval) of animals of the sub-chronic toxicity study. (G-H) Graphical representation of urea, creatinine, and uric acid levels in response to Cu-B treatment in acute and sub-chronic toxicity studies respectively.

4.2.10. Analysis of the Cu-B induced regulation of MAPK signaling in A375 cells

The constitutive activation of RAS-RAF-MEK-ERK signaling axes has been widely implicated in the initiation and development of melanoma via the activating mutations of RAF and RAS genes (Paluncic et al., 2016). Therefore, the effect of Cu-B on MAPK signaling was studied by analyzing the expression status of B-RAF^{V600E} protein in A375 cells, which endogenously harbour a B-RAF mutation. The result revealed a significant down-regulation of the mutant B-RAF^{V600E} protein (Figure 4.2.10A). Further, the activation of MEK and ERK, which are downstream of B-RAF, was analyzed by immunoblot analysis of MEK1/2 and ERK1/2 phosphorylation. Notably, Cu-B treatment significantly ablated the constitutive phosphorylation of MEK1/2 as well as ERK1/2 (Figure 4.2.10B-C), indicating Cu-B-mediated suppression of B-RAF^{V600E} downstream kinase activity. Phospho-STAT3 is a major transcription factor that stays downstream of the RAF pathway and maintains cell proliferation and survival in melanoma (Becker et al., 2014). Active ERK is reported to phosphorylate Ser727 residue of STAT3 (Carpenter & Lo, 2014). Analysis of phospho-STAT3 by immunoblotting revealed a significant down-regulation upon Cu-B treatment of A375 cells (Figure 4.2.10D). Further, the effect of Cu-B on the expression status of c-MYC, and Cyclin-D1, the major downstream targets in the MAPK pathway was studied. Notably, the Cyclin-D1 protein levels remained unaltered; however, a down-regulation in the c-MYC levels was observed (Figure 4.2.10E).

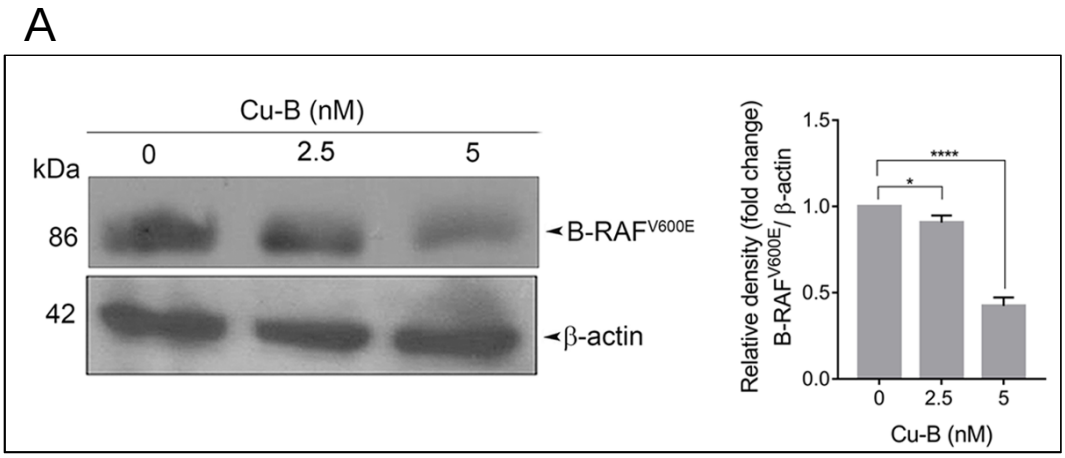

Figure 4.2.10A: The effect of Cu-B on the key survival signaling pathway in melanoma. Cu-B diminishes B-RAF^{V600E} expressions in A375 cells as analyzed by immunoblotting. A375 cells were treated with Cu-B for 24 h, whole-cell lysates prepared were electrophoresed and immunoblotted against anti-B-RAF^{V600E}. Bands were developed by ECL and quantified by Image J software. Data are representative of three independent experiments (Mean± SEM). P-values were calculated using one-way ANOVA. ****P <0.0001 and *P <0.1.

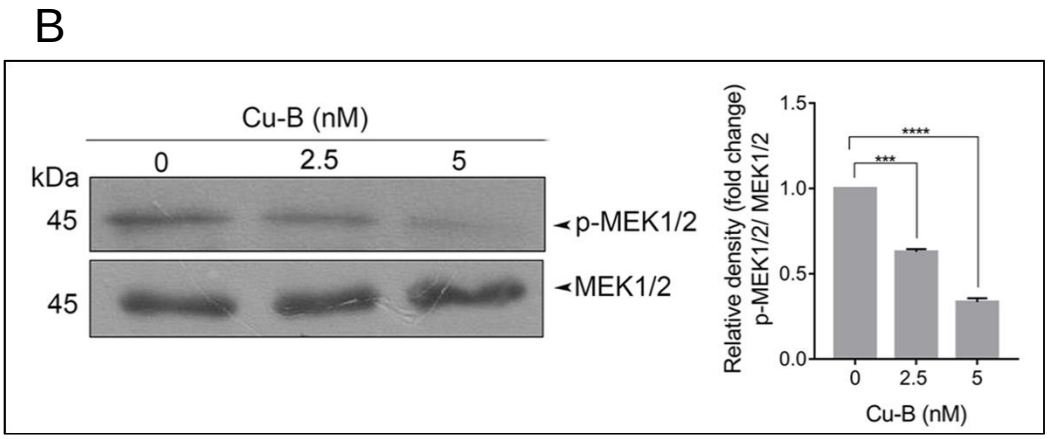

Figure 4.2.10B: The effect of Cu-B on the key survival signals in melanoma. Cu-B down-regulates the expression of phosphorylated MEK1/2 in A375 cells. A375 cells were treated with Cu-B for 24 h, whole-cell lysates prepared were electrophoresed and immunoblotted against anti-p-MEK1/2. Bands were developed by ECL and quantified by Image J software. Data are representative of three independent experiments (Mean± SEM). P-values were calculated using one-way ANOVA. ****P <0.0001 and ***P ≤0.001.

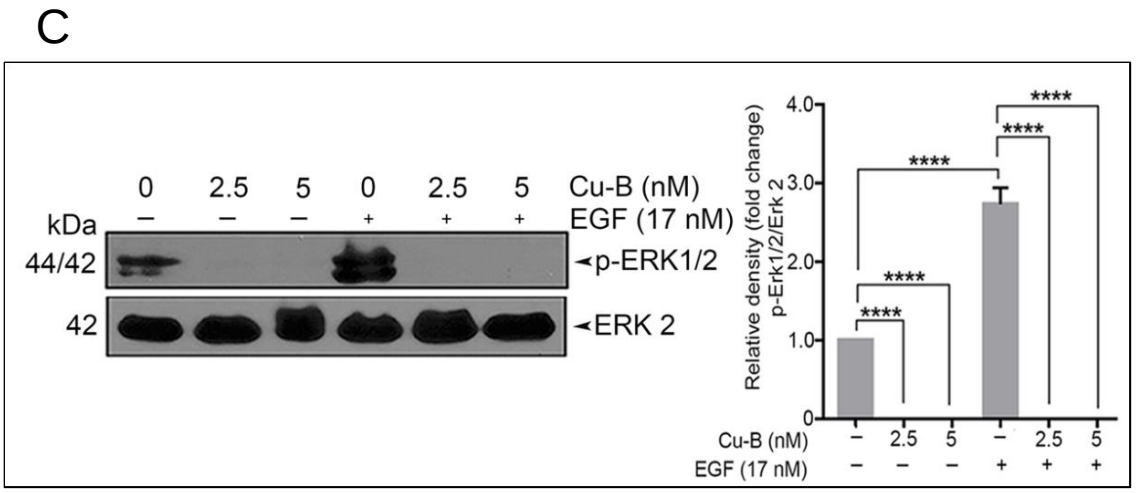

Figure 4.2.10C: The effect of Cu-B on the key survival signals in melanoma. Cu-B down-regulates the constitutive and EGF-induced phosphorylation of ERK1/2 in A375 cells. A375 cells were treated with Cu-B for 24 h, and whole-cell lysates prepared were electrophoresed and immunoblotted against anti-p-ERK1/2. Bands were developed using ECL and quantified by Image J software. Data are representative of three independent experiments (Mean± SEM). P-values were calculated using one-way ANOVA. ****P <0.0001.

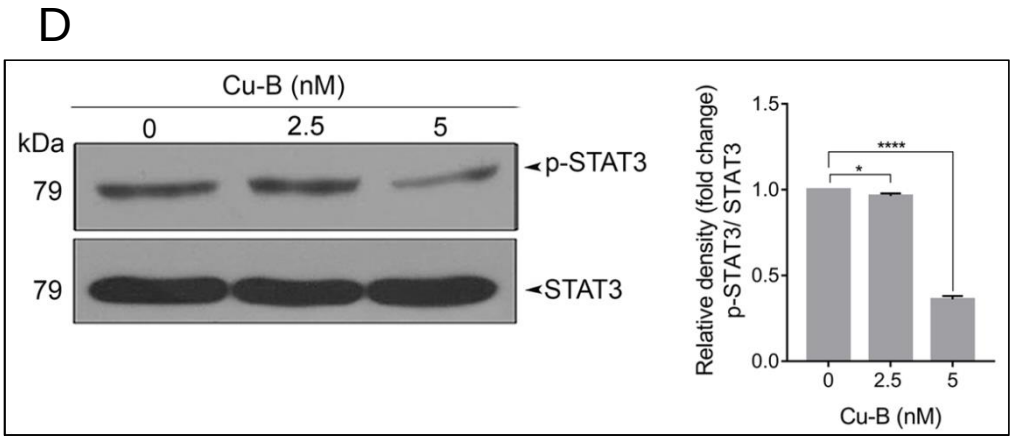

Figure 4.2.10D: The effect of Cu-B on the key survival signals in melanoma. Cu-B down-regulates the phosphorylation of STAT3 in A375 cells. A375 cells were treated with Cu-B for 24 h, and whole-cell lysates prepared were electrophoresed and immunoblotted against anti-p-STAT3. Bands were developed by ECL and quantified by Image J software. Data are representative of three independent experiments (Mean± SEM) and P-values were calculated using one-way ANOVA. ****P <0.0001 and *P <0.1.

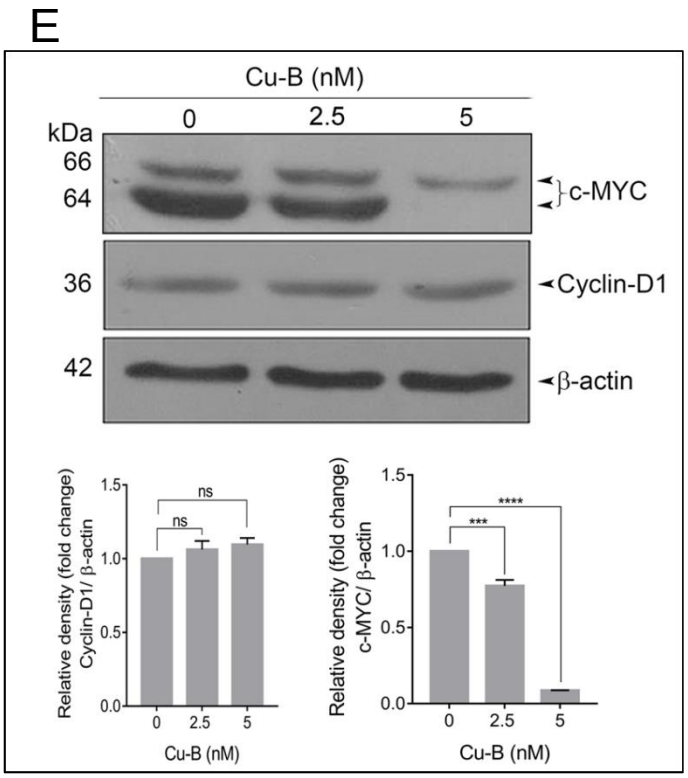

Figure 4.2.10E: The effect of Cu-B on the key survival signals in melanoma. Cu-B inhibits the expression of c-MYC, but Cyclin-D1 expression remains unaffected. A375 cells were treated with Cu-B for 24 h, whole-cell lysates prepared were electrophoresed and immunoblotted against anti-c-MYC and Cyclin D1. Bands were developed by ECL and quantified by Image J software. Data are representative of three independent experiments (Mean± SEM). P-values were calculated using one-way ANOVA. ****P <0.0001, ***P ≤0.001, and ns ≥ 0.05.

4.2.11. Analysis of the Cu-B induced regulation of Wnt signaling in A375 cells

Wnt signaling is yet another proliferation signaling pathway that is deregulated in melanoma (Sanders et al., 1999; Silye et al., 1998). The nuclear accumulation of β-catenin is a key feature of the Wnt signaling. Therefore, to study whether Cu-B has any effect on Wnt signaling melanoma cells, the expression status of β-catenin in A375 cells was analyzed. However, Cu-B treatment did not affect β-catenin status in A375 cells (Figure 4.2.11), indicating that Cu-B mediates the anti-melanoma efficacy by regulating MAPK signaling.

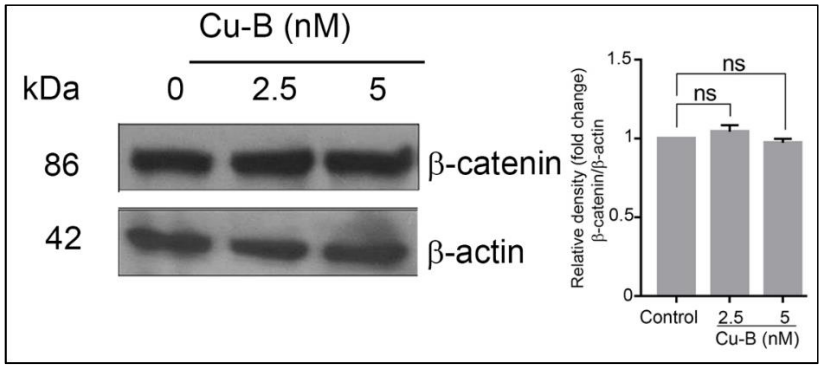

Figure 4.2.11: Cu-B treatment does not affect β-catenin levels in A375 cells. A375 cells were treated with Cu-B for 24 h, whole-cell lysates prepared were electrophoresed and immunoblotted against anti-β-catenin. Bands were developed using ECL and quantified by Image J software. Data are representative of three independent experiments (Mean± SEM). P-values were calculated using one-way ANOVA. ns ≥ 0.05.

4.2.12. Analysis of the Cu-B induced regulation of MITF-M signaling in A375 cells

In melanoma cells harboring B-Raf^{V600E} mutation, MITF-M down-regulated by B-Raf signaling is considered a crucial event for the progression of melanoma (Wellbrock & Marais, 2005). Therefore, the effect of Cu-B on expression and MITF-M signaling was analyzed However, Cu-B, at the concentrations investigated, did not alter the expression of MITF-M in A375 cells.

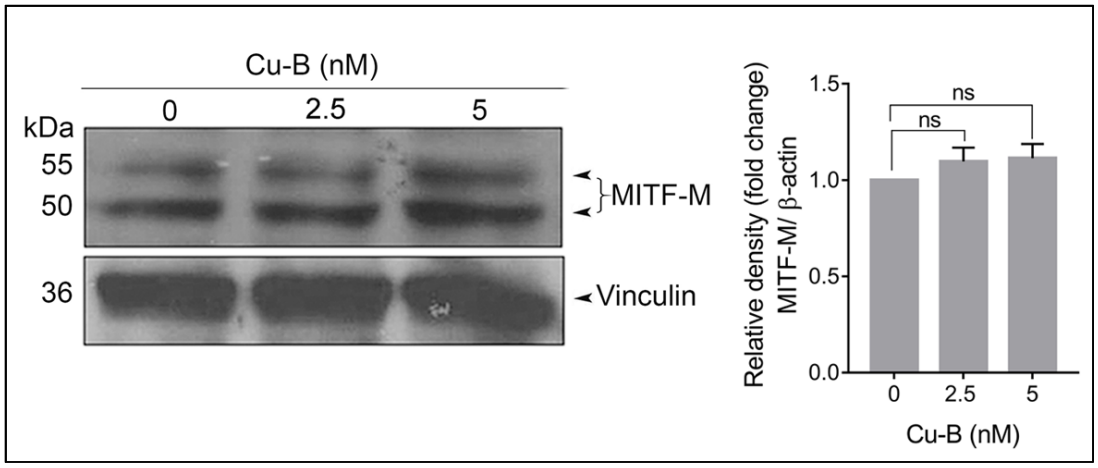

Figure 4.2.12: Cu-B treatment does not affect MITF-M levels in A375 cells. A375 cells were treated with Cu-B for 24 h, whole-cell lysates prepared were electrophoresed and immunoblotted against anti-MITF-M. Bands were developed by ECL and quantified by Image J software. Data are representative of three independent experiments (Mean± SEM). P-values were calculated using one-way ANOVA. ns ≥ 0.05.

4.2.13. Evaluation of the anti-tumor efficacy of Cu-B *in vivo*

The anti-melanoma efficacy of Cu-B was tested *in vivo* using a xenograft model of human melanoma in NOD-SCID mice using A375 cells. The method of tumor development and drug treatment regimen in the NOD-SCID murine model has been detailed in the methodology section. The experimental plan is shown as a schematic representation (Figure 4.2.13A). Following the regimen, the tumors from the animals were excised and various parameters were analyzed. It was observed that the ID administration of Cu-B was more effective, as evidenced by the significant reduction in tumor volume, compared to that of IP drug administration (Figure 4.2.13 B-C). The body weights of the animals were routinely checked and no significant change between the groups was observed (Figure 4.2.13D). Histopathological analysis indicated substantial destruction of tumor cells in Cu-B-treated mice-derived tissues, which correlated with the considerable tumor reduction (Figure 4.2.13E). Immunohistochemical analysis for the expression of PCNA in tumor sections derived from Cu-B-treated (ID) animals showed a significant decline in the PCNA expression, which authenticated the ability of Cu-B to inhibit tumor cell proliferation (Figure 4.2.13F). Further, the Induction of apoptosis in the tissue sections in response to Cu-B was analyzed by PARP cleavage and confirmed by the TUNEL assay (Figure 4.2.13G-H).

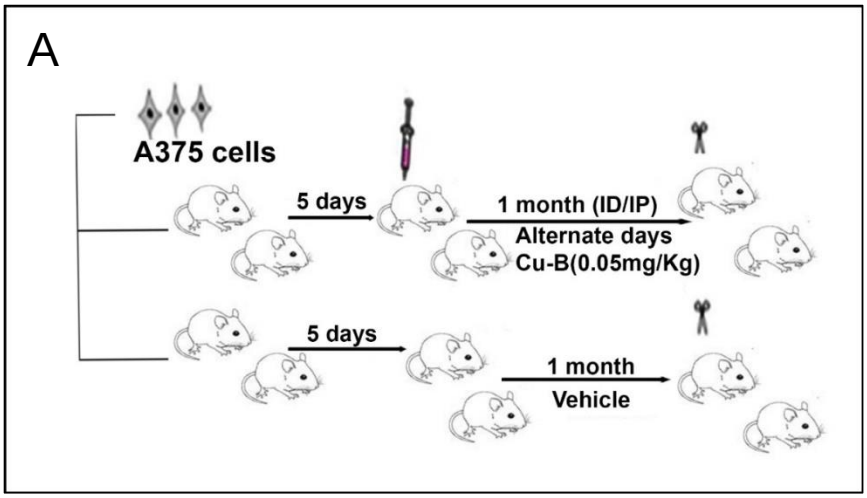

Figure 4.2.13A: Schematic diagram illustrating the NOD-SCID mice experiment to validate the anti-melanoma efficacy of Cu-B.

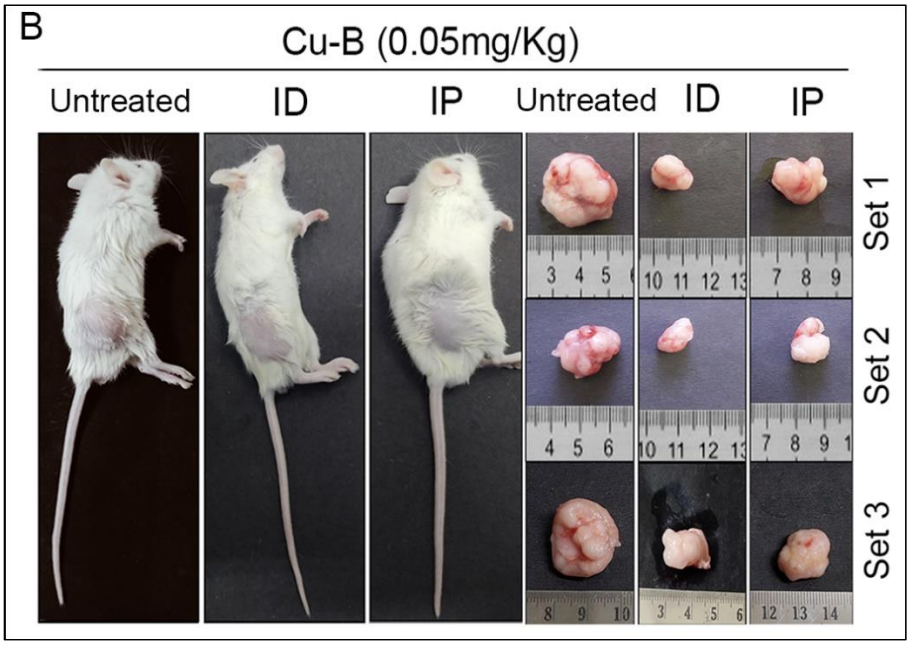

Figure 4.2.13B: Cu-B suppresses tumor growth in a NOD-SCID murine model of human melanoma. Representative photographs of Cu-B- treated NOD-SCID mice bearing A375 xenografts and the excised tumors. The result reveals that the ID mode of drug administration is more effective than IP.

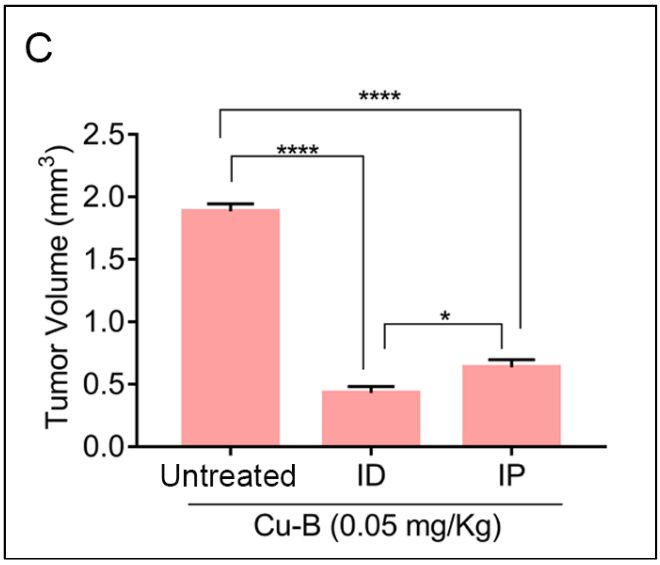

Figure 4.2.13C: Cu-B exhibits significant anti-tumor efficacy against human melanoma xenograft in NOD-SCID mice. Cu-B-treatment leads to the reduction of tumor volume in melanoma-bearing NOD-SCID mice. Data are representative of three independent experiments (Mean± SEM). P-values were calculated using one-way ANOVA. ****P <0.0001 and *P ≤0.1.

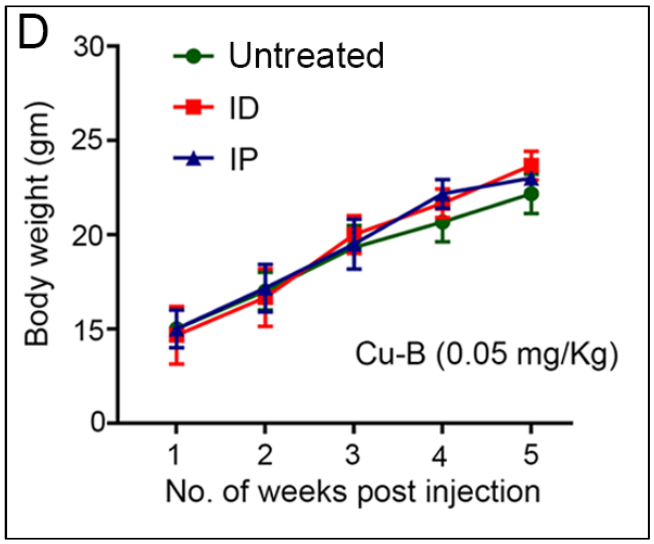

Figure 4.2.13D: Cu-B treatment does not affect the bodyweight of mice throughout the study period. None of the animals in any of the group show significant loss of weight till the end of the experiment.

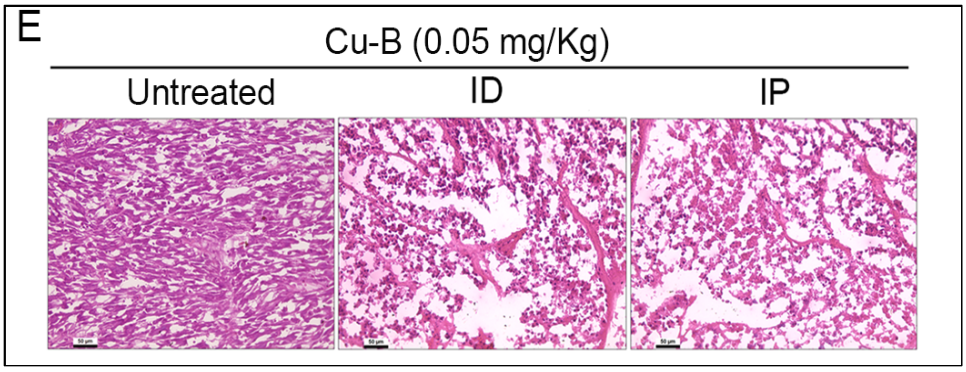

Figure 4.2.13E: Cu-B inhibits the growth of A375 xenograft tumor. Histopathological evaluation of tumor tissue isolated from mice from untreated and drug treated groups. Formalin-fixed cryosections were stained with Haematoxylin and Eosin and tumor pathology was verified.

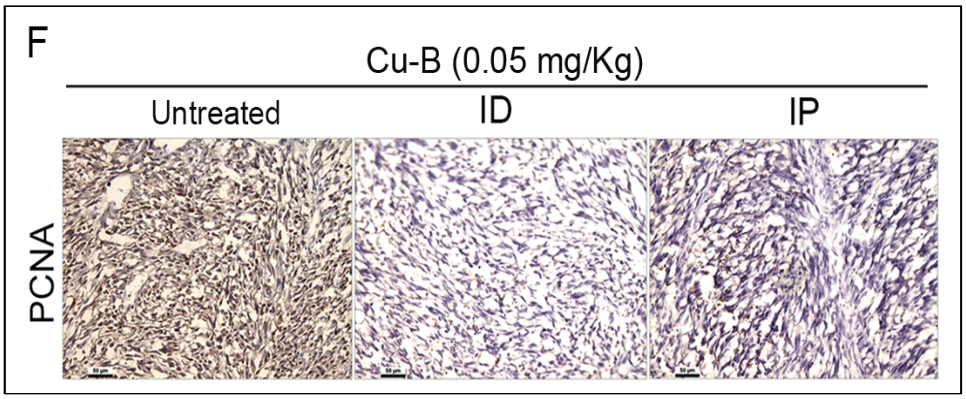

Figure 4.2.13F: Cu-B exhibits significant *in vivo* anti-proliferative efficacy in human melanoma xenografts tumors in NOD-SCID mice. IHC analysis on the expression of PCNA in tumor tissues of mice from untreated and drug-treated groups. Formalin-fixed cryosections were incubated with PCNA antibody and visualized by Poly Excel HRP/ DAB detection system universal kit.

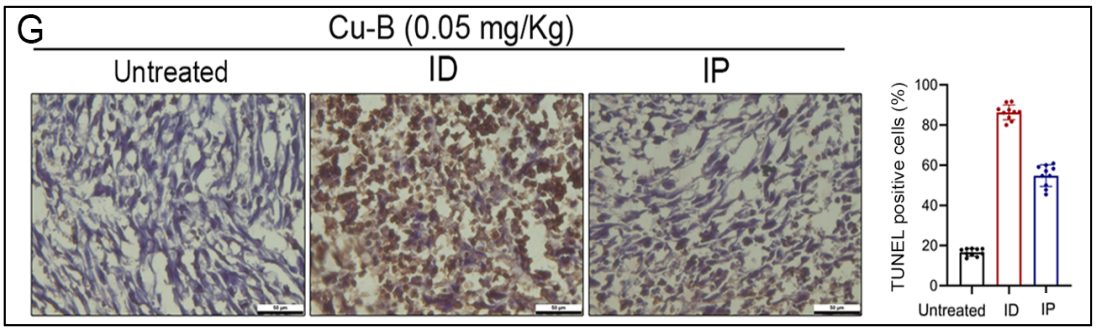

Figure 4.2.13G: The apoptosis induced by Cu-B in the tumor tissues as assessed by TUNEL assay. TUNEL assay was performed to detect apoptosis in formalin-fixed, paraffin-embedded xenograft tumor tissue sections using Dead End Colorimetric TUNEL System. The blue indicates the nucleus counterstained by haematoxylin and the brown colour indicates the presence of fragmented DNA which is a hallmark of apoptosis.

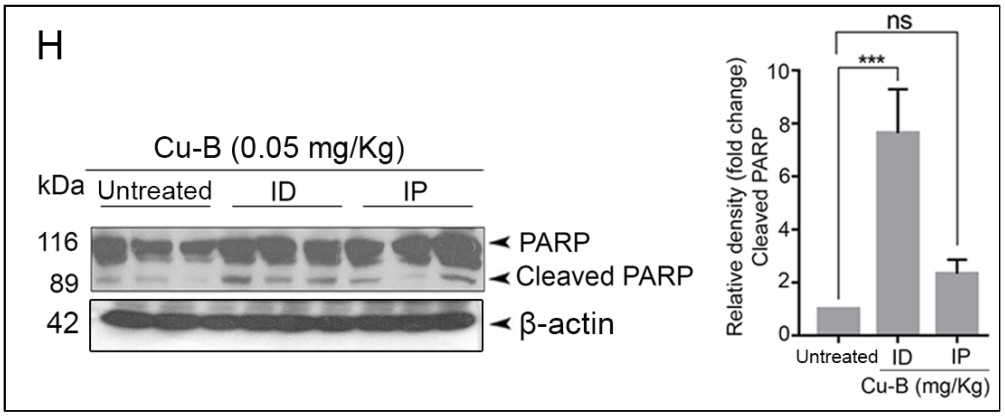

Figure 4.2.13H: Immunoblot analysis of PARP cleavage for Cu-B induced apoptosis in tumor tissues. Immunoblot analysis demonstrating apoptosis as evidenced by enhanced cleavage of PARP in the tumor lysates of Cu-B treated mice. Data are representative of three independent experiments (Mean± SEM). P-values were calculated using one-way ANOVA. ***P <0.001 and ns ≥ 0.05.

4.2.14. Analysis of the Cu-B-induced regulation of MAPK signaling in xenograft tumor tissue

The decisive role of the MAPK pathway as observed *in vitro* was validated in the *in vivo* tumor samples. In line with the data obtained from *in vitro* studies, a significant down-regulation in the expression of the key components of the MAPK pathway, p-ERK1/2, and p-MEK1/2, was observed by immunohistochemical analysis in the tissue sections of Cu-B-treated mice tissues in comparison to the vehicle control (Figure 4.2.14A). In line with this observation, a strong inhibition in the expression of c-MYC and p-STAT3, a critical downstream target of ERK, supported the earlier *in vitro* data (Figure 5I). The results obtained from immunohistochemical analysis of the tissue sections were further confirmed by Immunoblot analysis (Figure 4.2.14B-F).

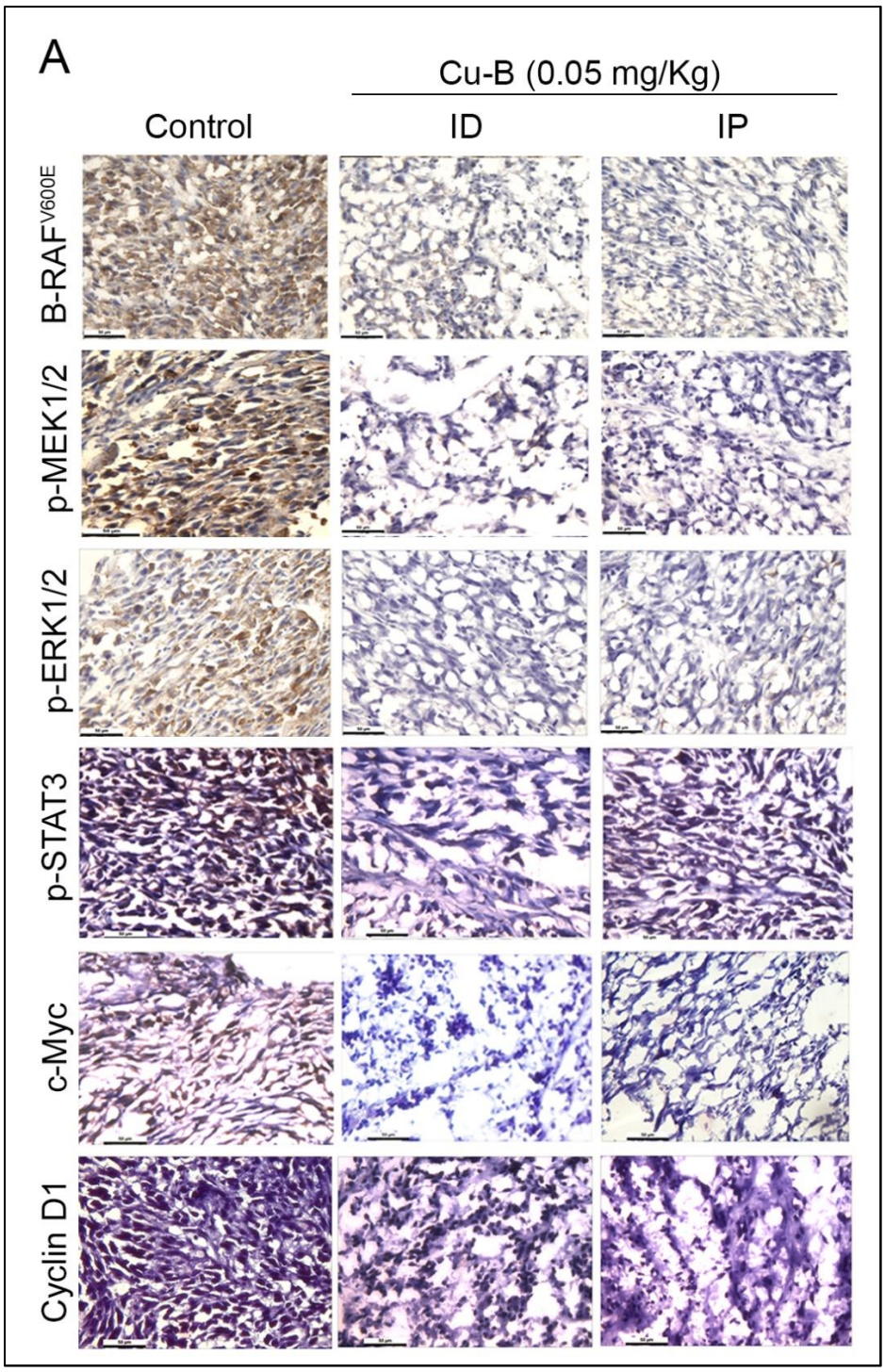

Figure 4.2.14A: IHC analysis of proteins in the MAPK signaling pathway in the tumor tissues: Formalin-fixed cryosections of tumor tissues from untreated and drug-treated mice, were incubated with B- RAF^{V600E}, p-MEK1/2, p-ERK1/2, p-STAT3, c-MYC and Cyclin D1 and visualized by Poly Excel HRP/ DAB detection system universal kit.

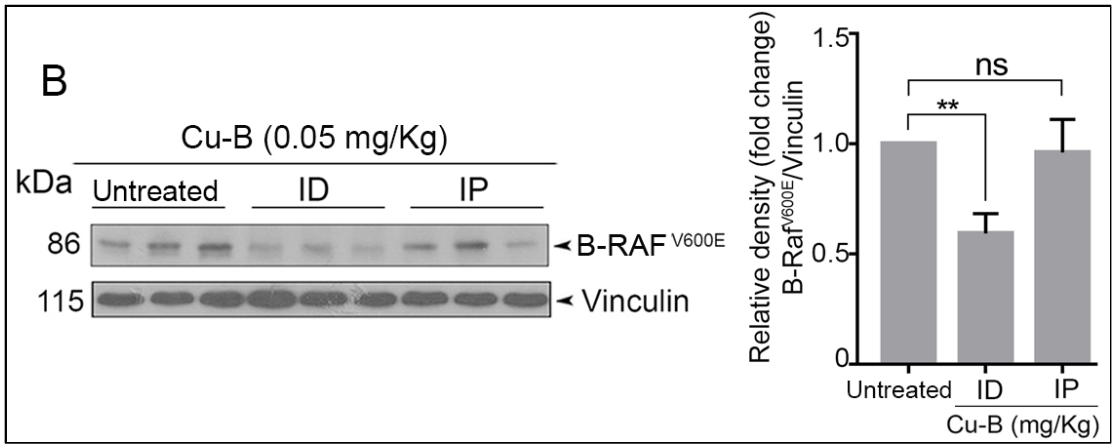

Figure 4.2.14B: Immunoblot analysis of proteins in the MAPK signaling pathway: Cu-B diminishes B-RAF^{V600E} expressions in tumor tissues as assessed by Immunoblot analysis. Tumor tissue lysates were prepared, electrophoresed and immunoblotted against anti-B-RAF^{V600E}. Bands were developed by ECL and quantified by Image J software. Data are representative of three independent experiments (Mean± SEM). P-values were calculated using one-way ANOVA. ****P <0.0001 and *P <0.1.

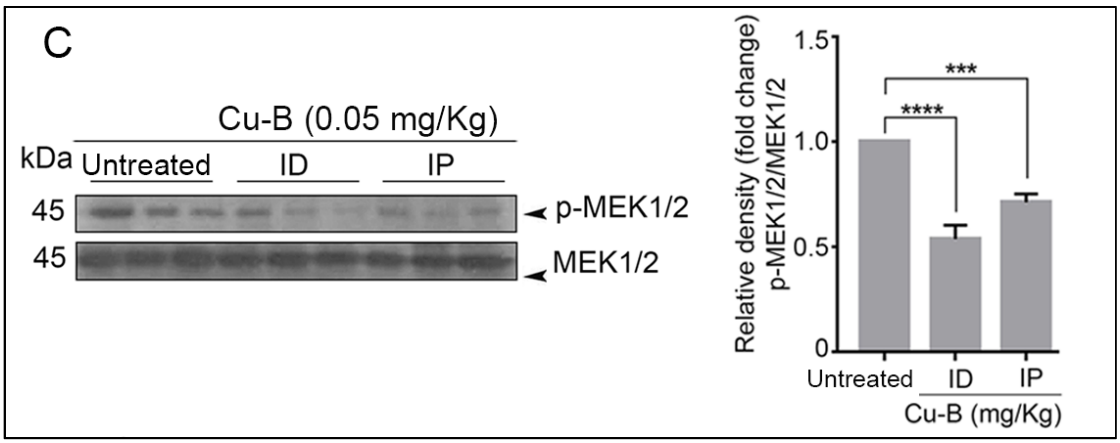

Figure 4.2.14C: Immunoblot analysis of proteins in the MAPK signaling pathway: Cu-B down-regulates p-MEK1/2 expressions in tumor tissues as assessed by Immunoblot analysis. Tumor tissue lysates were prepared, electrophoresed and immunoblotted against anti-p-MEK1/2. Bands were developed by ECL and quantified by Image J software. Data are representative of three independent experiments (Mean± SEM). P-values were calculated using one-way ANOVA. ****P <0.0001 and ***P ≤0.001.

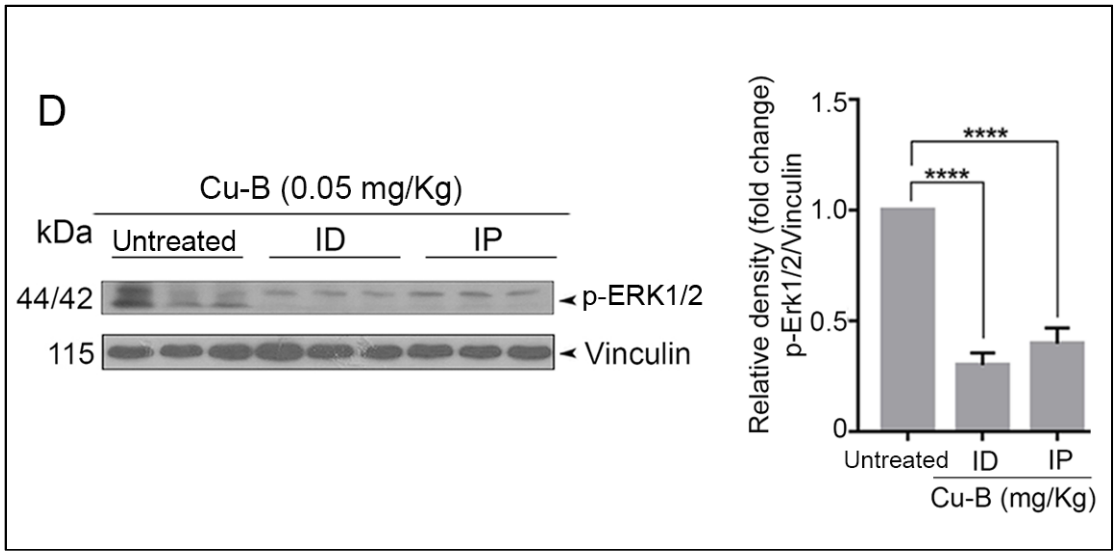

Figure 4.2.14D: Immunoblot analysis of proteins in the MAPK signaling pathway: Cu-B down-regulates p-ERK1/2 expressions in tumor tissues as assessed by Immunoblot analysis. Tumor tissue lysates were prepared, electrophoresed and immunoblotted against anti-p-ERK1/2. Bands were developed by ECL and quantified by Image J software. Data are representative of three independent experiments (Mean± SEM). P-values were calculated using one-way ANOVA. ****P <0.0001.

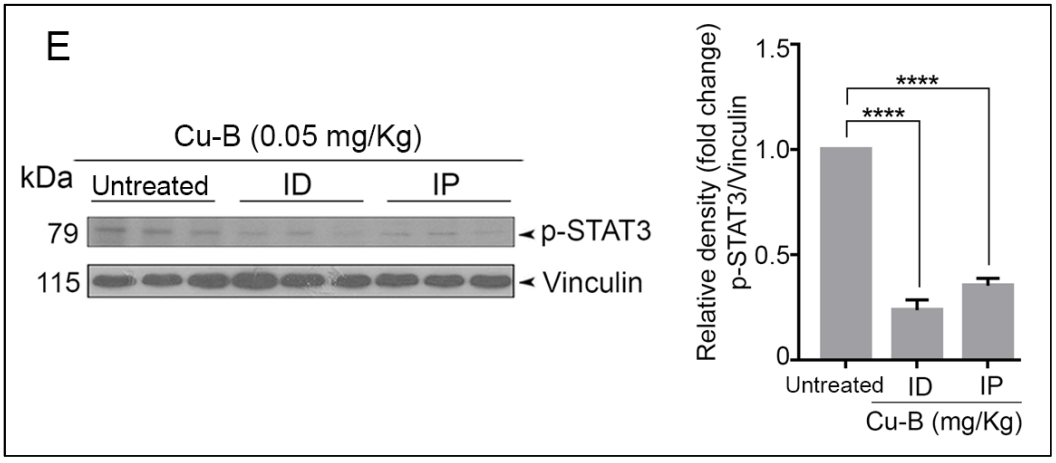

Figure 4.2.14E: Immunoblot analysis of proteins in the MAPK signaling pathway: Cu-B down-regulates p-STAT3 expression in drug-treated tumor tissues as assessed by Immunoblot analysis. Tumor tissue lysates were prepared, electrophoresed and immunoblotted against anti-p-STAT3. Bands were developed by ECL and quantified by Image J software. Data are representative of three independent experiments (Mean± SEM). P-values were calculated using one-way ANOVA. ****P <0.0001.

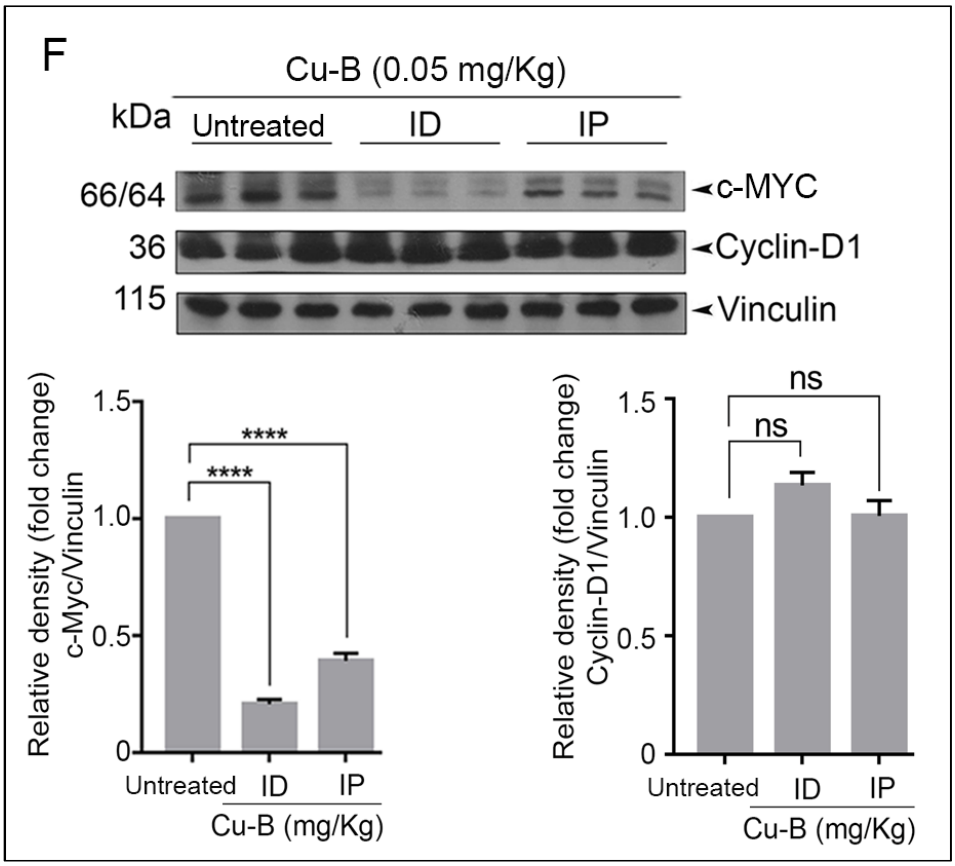

Figure 4.2.14F: Immunoblot analysis of proteins in the MAPK signaling pathway: Cu-B down-regulates c-MYC expression but Cyclin-D1 expression remains unaffected in drug-treated tumor tissues as assessed by Immunoblot analysis. Tumor tissue lysates were prepared, electrophoresed and immunoblotted against anti-c-MYC and Cyclin-D1. Bands were developed by ECL and quantified by Image J software. Data representative of three independent experiments (Mean± SEM) and P-values are calculated using one-way ANOVA. ****P <0.0001 and ns ≥ 0.05.

4.2.15. Analysis of the Cu-B induced regulation of Wnt and MITF-M signaling in xenograft tumor tissue

Corroborating the data obtained earlier from *in vitro* studies, Cu-B did not affect the Wnt pathway and MITF-M signaling in the *in vivo* conditions, as observed by the absence of changes in the level of β-catenin as well as MITF-M expression in the tumor tissues from mice treated with Cu-B and in the control tumor tissues (Figure 4.2.15A-B). (Figure 4.2.15C). This observation confirms that Wnt signaling as well as the MITF-M signaling pathway has no regulatory role in the anti-melanoma activity of Cu-B and is in line with our finding that the MAPK pathway is the key regulator of the anti-melanoma efficacy of Cu-B.

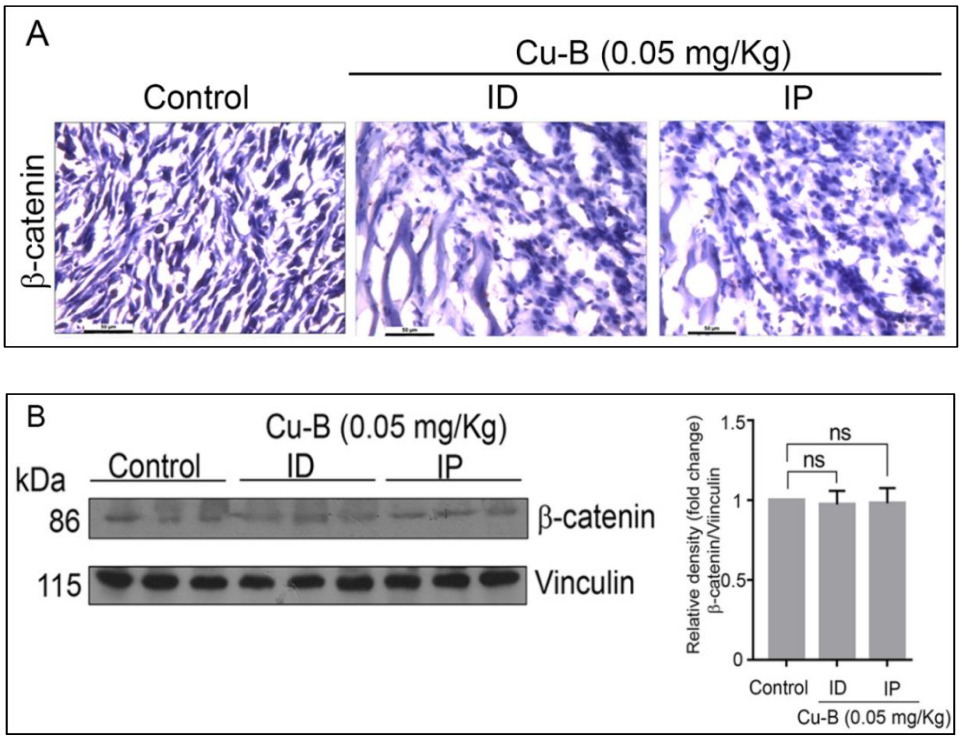

Figure4.2.15. Effect of Cu-B on the expression of β-catenin, the key protein in the Wnt signaling pathway. (A) IHC analysis of β-catenin expression in the tumor tissues of mice of untreated and drug-treated groups. Formalin-fixed cryosections were incubated with β-catenin and visualized by Poly Excel HRP/ DAB detection system universal kit. (B) Immunoblot analysis of β-catenin expression in tumor tissues from mice of drug-treated and untreated groups showed no variation Tumor tissue lysates were prepared, electrophoresed and immunoblotted against anti- β-catenin. Bands were developed by ECL and quantified by Image J software. Data are representative of three independent experiments (Mean± SEM). P-values were calculated using one-way ANOVA. ns ≥ 0.05.

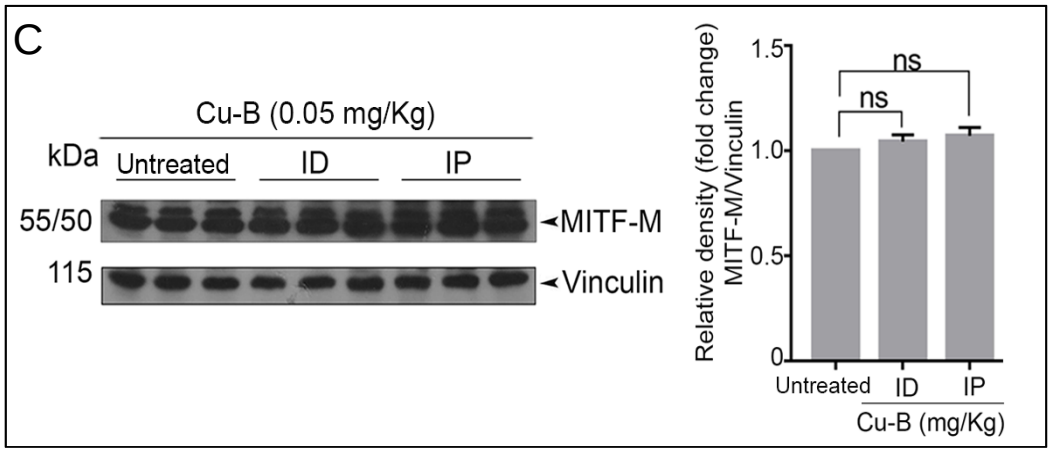

Figure 4.2.15C: The effect of Cu-B on the expression of a key protein in the MITF-M signaling pathway. Immunoblot analysis of MITF-M expression in tumor tissues shows no significant variation. Tumor tissue lysates were prepared, electrophoresed and immunoblotted against anti-MITF-M. Bands were developed by ECL and quantified by Image J software. Data are representative of three independent experiments (Mean± SEM). P-values were calculated using one-way ANOVA. ns ≥ 0.05.

Chapter 5

DISCUSSION

DISCUSSION

Systematic analysis of the bioactive compounds derived from plants of ethnobotanical significance has paved the way for novel lead structures and has largely progressed as drugs against many diseases including cancer (Dias et al., 2012). *Corallocarpus epigaeus* (Rottl. & Willd.) C. B. Clarke is a popular medicinal plant in the Cucurbitaceae family, notably prescribed in traditional medicine as a remedy for acute dysentery, venereal diseases, skin diseases, and snake bite (Kirtikar and Basu, 1935). Despite its significance in traditional medicine, there are no comprehensive reports on the isolation of phytochemical constituents from *C. epigaeus*. Reports on the isolation of N-methyl asparagine from *C. epigaeus* seeds and essential oils like ishwarane and ishwarone from the roots are documented (Dunnill and Fowden, 1965, Gupta et al., 1997). Volatile compounds from the roots and rhizomes of *C. epigaeus* have been detected by GC-MS analysis in comparison with standard phytochemical libraries for identification (Gupta et al., 1997, Kandasamy et al., 2020, Karthic et al., 2017). In addition, there are reports on the identification of a pyridine carboxylic ester (corallocarpenoyl ester), an aliphatic C32 keto diol (dotriacont-22, 25-diol-10-one), a sesterpene lactone (corallocarpscalarolide), and a p-hydroxy benzoyl ester (designated as epigaeusyl ester) from the roots of *C. epigaeus* (Ali and Gupta, 1996). Furthermore, a glycoside termed bryonin is purified from *C. epigaeus* roots (Dymock et al., 1893). Organic solvent extracts of various parts of the plant are shown to possess a broad range of pharmacological properties (Jamuna et al., 2015). A couple of reports indicate that the ethanol extracts of *C. epigaeus* induce cytotoxicity in cancer cells (Banotha et al., Bhavani and Leelavathi, 2015). However, a thorough investigation of the anti-cancer potential of *C. epigaeus* or its purified derivatives remains elusive. The present study was designed to explore the potential anti-cancer activity of *C. epigaeus* and to isolate the anticancer principle/s, focusing on the rhizome part which is widely being utilized in ethnomedicine.

The study has revealed the potent anticancer property of the ethyl acetate extract of *C. epigaeus* rhizome and isolated a cytotoxic fraction, ECF, which yielded Cu-B as the bio-active ingredient. Cancer cell lines of various tissue origins were screened to study their sensitivity towards organic extracts of the rhizome, ECF and Cu-B. Amongst the cancer cell lines of various tissue origins, employed for the drug screening, the melanoma cell line, A375 was found to be the most sensitive towards ECF and Cu-B. Hence, the cytotoxic potential of Cu-B was evaluated in melanoma cell lines belonging to two molecular subgroups, based on the difference in their mutation status in RAS and RAF genes. Interestingly, irrespective of the

mutation status, all the melanoma cell lines screened were found to be very sensitive to Cu-B. Moreover, in normal skin fibroblast, Cu-B was found to be non-toxic, at concentration that induced 50% cell death in the melanoma cell line, A375.

A literature survey shows that there are up to 40 known cucurbitacins or their derivatives which are essentially classified into 12 groups. Group B cucurbitacins have been shown to possess potent anticancer activity in a variety of cancers *in vitro* and *in vivo* (Garg et al., 2018). However, this is the first study demonstrating the molecular mechanism underlying the efficacy of Cu-B against human melanoma *in vitro* and *in vivo*. In the melanoma cell line A375, Cu-B induced potent cytotoxicity with an IC50 value of 5 nM. Analysis of Cu-B-induced cytotoxic mechanism in A375 cells showed that the drug potentiates apoptosis involving both the intrinsic and extrinsic pathways. Activation of initiator and executioner caspases, 9 7 and 3 respectively as well as cell-surface death receptor-mediated caspase 10 and Bid underscore the significant role of mitochondrial pathway in Cu-B induced apoptosis. Investigations into the underlying reason for the augmented sensitivity of melanoma cells to Cu-B revealed that the drug down-regulates MAPK signaling, involved in cell proliferation.

Melanoma is a subtype of skin cancer, partly driven by the MAPK signaling pathway through RAS-RAF-MEK-ERK signaling, which concludes in the activation of ERK, and regulates p-STAT3, MITF-M, c-MYC, and other transcription factors, resulting in alteration of cell proliferation and survival. The most prevalent gene mutations identified in melanoma are B-RAF, RAS, and NF-1, all of which cause constitutive MAPK signaling (Amann et al., 2017). Evaluation of the cytotoxic potential of Cu-B in melanoma cell lines viz. SK-MEL-2 and SK-MEL-28 with N-RAS and B-RAF mutation respectively revealed that the compound is highly efficacious against the melanoma cell lines, irrespective of the mutation status. In fact, elucidation of the key mutations that drive melanoma progression has resulted in targeted therapies using small-molecule inhibitors of B-RAF and MEK either alone or in combination and has made significant progress in the treatment of melanoma (Amann et al., 2017, Berger et al., 2018). However, acquired resistance poses serious limitations to the success of these small-molecule kinase inhibitors in the clinic (Long et al., 2016, Johannessen et al., 2010). A previous study conducted in the human melanoma xenograft model has shown that melanoma cells can transcriptionally up-regulate the B-RAF molecule to compensate for the inhibition by, the B-RAF^{V600E} inhibitor, vemurafenib (Das Thakur et al., 2013). The present study demonstrates the efficacy of Cu-B, in suppressing the expression of mutant B-RAF^{V600E} protein as well as inhibiting the B-RAF^{V600E} kinase activity as evidenced by inhibition of MEK1/2

phosphorylation. Moreover, Cu-B inhibited both the constitutive as well as EGF-induced ERK phosphorylation, indicating the role of MAPK signaling in regulating the chemotherapeutic potency of Cu-B against melanoma. As RAF inhibitors have been found to relieve the ERK1/2-dependent feedback inhibition of MAPK signaling, inhibition of MEK1/2 along with B-RAF is considered as a promising strategy in the treatment of B-RAF -mutated melanoma, while inhibition of MEK is proved to be beneficial for NRAS-mutated melanoma (Ascierto et al., 2013, Lito et al., 2012, Flaherty et al., 2012). Indeed, molecular docking studies have revealed that cucurbitacins show a significant binding towards the crystal structure of RAF and MEK, comparable to that of the standard B-RAF and MEK inhibitors, imparting cucurbitacins the ability to inhibit the ERK activation in melanoma cells (Ahmed et al., 2014). In line with the ability of Cu-B to inhibit MAPK signaling, the efficacy of Cu-B in down-regulating the downstream effector transcription factors of ERK, such as p-STAT-3 and c-MYC in A375 cells, has also been demonstrated in this study. In melanoma cells harbouring B- RAF^{V600E} mutation, MITF-M down-regulated by B-RAF signaling is considered a crucial event for the progression of melanoma (Wellbrock and Marais, 2005). However, in the present study, any significant variation in the expression of MITF-M in response to Cu-B was not observed. Furthermore, a study using a tumor xenograft model in NOD-SCID mice harbouring the B-RAF^{V600E} mutated A375 cells, resulted in substantial inhibition of tumor growth without any apparent toxicity and corroborated the *in vitro* data on the molecular mechanism underlying the anti-melanoma activity of Cu-B. Taken together, the data highlights the potent anti-melanoma activity of Cu-B, involving potentiation of apoptotic cell death and suppression of proliferation by the inhibition of MAPK signaling. Studies are in progress to elucidate the role of Cu-B in modulating key mutations in other genes which cause de-regulated MAPK signaling, viz. RAS and NF-1. Further, the anti-melanoma efficacy of Cu-B has to be evaluated using a patient-derived melanoma xenograft model and using patient-derived melanoma cells so that the compound can be effectively translated from bench to bedside.

The current study, involving the isolation and characterization of the anti-cancer principle, Cu-B, from *C. epigaeus* and its prospective anti-melanoma efficacy is briefed in a schematic representation (Figure 6). This is the first study reporting the isolation and identification of cucurbitacin B from *C. epigaeus.* Moreover, this is the first study demonstrating its anti-melanoma potential, *in vitro* and *in vivo*. The study demonstrates the necessity of advancing Cu-B, as a candidate drug against melanoma, which is the most aggressive and treatment-resistant cancer, and accounts for 75% of all skin cancer-related deaths (Ascierto et al., 2013).

CONCLUSIONS AND SUMMARY

CONCLUSIONS

- Ethyl acetate extract of the rhizome of *C. epigaeus* showed potent cytotoxic activity against cancer cell lines.
- The IC50 value of ethyl acetate extract in the most sensitive cell line, A375 was found to be 0.050ug/ml
- Fractionation of Ethyl acetate extract yielded a cytotoxic fraction (ECF), which was found to be highly efficacious against melanoma cell lines.
- ECF induced apoptotic mode of cell death in melanoma cells.
- The anti-cancer compound in the ECF was identified as the triterpenoid, Cu-B.
- Cu-B induced 50% cell death in the melanoma cell line, A375, at 5nM, while it was found to be non-toxic to normal skin fibroblast.
- Cu-B inhibited cell proliferation and induced apoptotic mode of cell death in A375 cells.
- Molecular investigations in to the potent anti-melanoma activity of Cu-B revealed suppression of proliferation by Cu-B-induced inhibition of MAPK signaling and induction of apoptotic cell death.
- Pharmacological safety of Cu B was confirmed *in vivo* using acute and sub-chronic toxicity models in Swiss albino mice.
- Analysis of the anti-melanoma efficacy of Cu-B using a tumor xenograft model in NOD-SCID mice resulted in a substantial inhibition of tumor growth corroborating our *in vitro* data on the molecular mechanism underlying the anti-melanoma activity of Cu-B.
- The study demonstrates the necessity of advancing Cu-B, as a candidate drug against melanoma, which is the most aggressive and treatment-resistant among the cancers, and accounts for 75% of all skin cancer-related deaths.

SUMMARY

The ethnomedicinal plant from the Cucurbitaceae family, *Corallocarpus epigaeus*, or its bioactive derivatives have been widely utilized in traditional medicine owing to their distinct applications against various human ailments and have lured the interest of ethnobotanists and biochemists. The present study has explored the anti-cancer potential of the plant and succeeded in isolating a bio-active fraction from the dried rhizome of *C. epigaeus*. The bioactive principle was identified as cucurbitacin B (Cu-B). The purification processes involving the utilization of multiple organic extracts of *C. epigaeus* rhizome powder, yielded Cu-B from the Ethyl acetate Cytotoxic Fraction (ECF), obtained by the chromatographic separation of the ethyl acetate extract. Amongst the various cancer lines tested, melanoma cells exhibited maximal sensitivity towards the Cu-B-containing ECF fraction. Cu-B induced an apoptotic mode of cell death initiated intrinsically as well as extrinsically in A375 melanoma cells whilst remaining comparatively less toxic to normal skin fibroblasts. *In vivo* studies involving a NOD-SCID murine model of human melanoma demonstrated the ability of Cu-B to attenuate tumor growth, while being pharmacologically safe *in vivo*, as assessed using acute and sub-chronic toxicity models in Swiss albino mice. Furthermore, Cu-B inhibited MEK 1/2 as well as the constitutive and EGF-induced ERK 1/2 activation, indicating a definitive involvement of MAPK signal transducers in regulating Cu-B-mediated anti-melanoma activity. The study has demonstrated the anti-cancer property of the plant, *C. epigaeus* and the anti-melanoma potential of *C. epigaeus*-derived Cu-B.

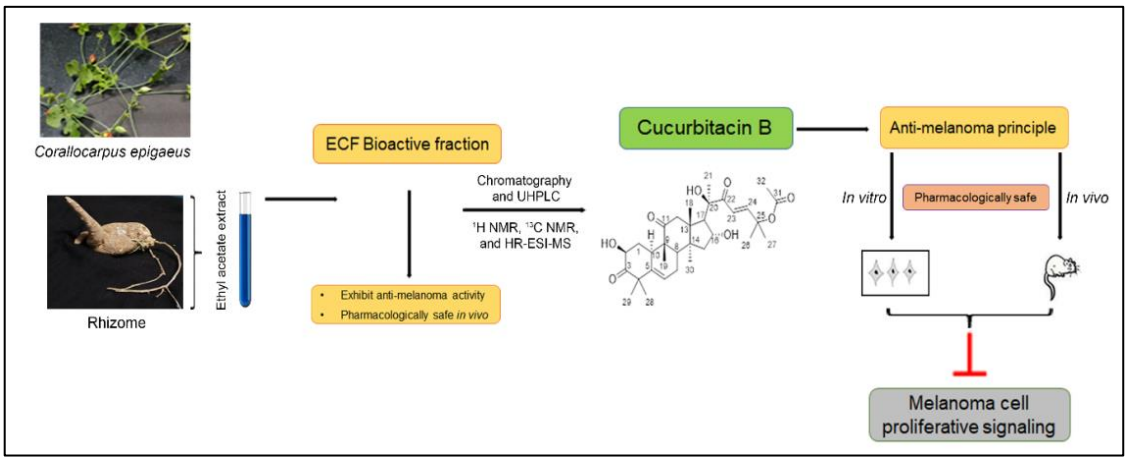

Figure 6: Schematic representation highlighting the process of isolation and characterization of the anti-melanoma principle Cucurbitacin B from the rhizome of *C. epigaeus*. Briefly, ethyl acetate extract of *C. epigaeus* rhizome, was fractionated using column chromatography, which yielded purified Cu-B and the isolated anti-cancer principle was characterized and verified using ^{1}H NMR, ^{13}C NMR and HR-ESI-MS analysis. *In vitro* and *in vivo* studies validated the potential of Cu-B to attenuate melanoma by targeting critical proliferative signals. The pharmacological safety of ECF and ECF-derived Cu-B were assured in *Swiss albino* mice.

RECOMMENDATIONS

Melanoma is alarmingly on the rise and the disease accounts for 75% of all skin cancer deaths (Ye et al., 2020). Dacarbazine, an alkylating agent is the most widely used chemotherapeutic drug for metastatic melanoma treatment. However, its efficacy in terms of survival is unsatisfactory (Pasquali et al., 2018). A recent trend in cancer treatment is targeted drug therapy, which exploits the specific molecular changes which are unique to particular cancer. The Ras/Raf/MEK/ ERK signalling pathway is a kinase receptor pathway widely implicated in melanoma due to mutations in RAF (50%), RAS (30%) and NF-1 genes (14%) (Amann et al., 2017). Elucidation of the key mutations involved in melanoma initiation and progression has resulted in targeted therapies using small-molecule inhibitors of B-Raf and NRAS either alone or in combination and has made progress in the treatment of melanoma. However, acquired resistance poses limitations to the success of these small-molecule kinase inhibitors in the clinic.

In this context, the development of a cost-effective chemotherapeutic drug, with a superior therapeutic index to, treat melanoma has become imperative.

The present study has resulted in the isolation and identification of an anticancer compound from the ethyl acetate extract of the rhizome of *Corallocarpus epigaeus*, possessing potent anti-melanoma activity. The compound induced 50% cell death in A375 melanoma cells and evoked apoptotic mode of cell death, involving intrinsic and extrinsic pathways. Exploration of the signalling pathways relevant to melanomagenesis has demonstrated the efficacy of Cu-B in inhibiting MAPK signalling, which has been validated in a tumour xenograft model. In this context, considering the ability of Cu-B to inhibit MAPK signalling and elicit apoptosis in melanoma cells, it is worth exploring the potential of the same as a candidate drug against melanoma.

Further studies are in progress to elucidate the role of Cu-B in modulating key mutations in other genes which cause de-regulated MAPK signalling, viz. RAS and NF-1. Further, the anti-melanoma efficacy of Cu-B has to be evaluated using a patient-derived melanoma xenograft model and using patient-derived melanoma cells so that the compound can be effectively translated from bench to bedside.

BIBLIOGRAPHY

AHMED, M. S. & HALAWEISH, F. T. 2014. Cucurbitacins: potential candidates targeting mitogen-activated protein kinase pathway for treatment of melanoma. Journal of enzyme inhibition and medicinal chemistry, 29, 162-167.

AHMED, M. S., KOPEL, L. C. & HALAWEISH, F. T. 2014. Structural optimization and biological screening of a steroidal scaffold possessing cucurbitacin-like functionalities as B-raf inhibitors. ChemMedChem, 9, 1361-1367.

ALCALÁ, A. M. & FLAHERTY, K. T. 2012. BRAF inhibitors for the treatment of metastatic melanoma: clinical trials and mechanisms of resistance. Clinical cancer research, 18, 33-39.

ALI, M. & GUPTA, J. 1996. Chemical Constituents of *Corallocarpus epigaeus* rhizomes. Journal of Medicinal and Aromatic plant sciences, 18, 791-794.

AMANN, V., RAMELYTE, E., THURNEYSEN, S., PITOCCO, R., BENTELE-JABERG, N., GOLDINGER, S., DUMMER, R. & MANGANA, J. 2017. Developments in targeted therapy in melanoma. European Journal of Surgical Oncology (EJSO), 43, 581-593.

ANTONY, J., SAIKIA, M., NATH, L., KATIKI, M. R., MURTY, M., PAUL, A., CHANDRAN, H., JOSEPH, S. M., PANAKKAL, E. J. & RAN, S. 2015. DW-F5: A novel formulation against malignant melanoma from *Wrightia tinctoria*. Scientific reports, 5, 1-15.

ASCIERTO, P. A., SCHADENDORF, D., BERKING, C., AGARWALA, S. S., VAN HERPEN, C. M., QUEIROLO, P., BLANK, C. U., HAUSCHILD, A., BECK, J. T. & ST-PIERRE, A. 2013. MEK162 for patients with advanced melanoma harbouring NRAS or Val600 BRAF mutations: a non-randomised, open-label phase 2 study. The lancet oncology, 14, 249-256.

AYYAD, S.-E. N., ABDEL-LATEFF, A., BASAIF, S. A. & SHIER, T. 2011. Cucurbitacins-type triterpene with potent activity on mouse embryonic fibroblast from Cucumis prophetarum, cucurbitaceae. Pharmacognosy research, 3, 189.

BANOTHA, C. S. K., NAYAKANTI, D., NANDYALAC, V. N. A. S. R., ORUGANTIC, S. K., KANALAD, J. R., SANAKATTULA, S. & ALA, S. Journal of Comprehensive Pharmacy.

BECKER, T., BOYD, S., MIJATOV, B., GOWRISHANKAR, K., SNOYMAN, S., PUPO, G., SCOLYER, R., MANN, G., KEFFORD, R. & ZHANG, X. 2014. Mutant B-RAF-Mcl-1 survival signaling depends on the STAT3 transcription factor. Oncogene, 33, 1158-1166.

BERGER, M., RICHTIG, G., KASHOFER, K., AIGELSREITER, A. & RICHTIG, E. 2018. The window of opportunities for targeted therapy in BRAFwt/NRASwt/KITwt melanoma: biology and clinical implications of fusion proteins and other mutations. Giornale Italiano di Dermatologia e Venereologia: Organo Ufficiale, Societa Italiana di Dermatologia e Sifilografia, 153, 349-360.

BEUTLER, J. A., MCCALL, K. L., HERBERT, K., HERALD, D. L., PETTIT, G. R., JOHNSON, T., SHOEMAKER, R. H. & BOYD, M. R. 2000. Novel cytotoxic diterpenes from Casearia arborea. Journal of Natural Products, 63, 657-661.

BHAVANI, M. & LEELAVATHI, S. 2015. Investigation on in vitro cytotoxic activity of a selected wild cucurbitaceae plant *Corallocarpus epigaeus* against cancer. International Journal of Pharmaceutical Sciences and Research, 6, 3554.

CARPENTER, R. L. & LO, H.-W. 2014. STAT3 target genes relevant to human cancers. Cancers, 6, 897-925.

CHAN, X. Y., SINGH, A., OSMAN, N. & PIVA, T. J. 2017. Role played by signalling pathways in overcoming BRAF inhibitor resistance in melanoma. International Journal of Molecular Sciences, 18, 1527.

CHANDRAKALA, A., HARINATHA, R., NAGESWARI, G., VANI SRI, D., SHABANA BEGUM, S. & VENKATAPPA, B. 2013. Anti-Venom and Immunomodulatory Functions of *Corallocarpus epigaeus* L. Int. J. Pharm. Biol. Sci, 4, 654-660.

CHEN, J. C., CHIU, M. H., NIE, R. L., CORDELL, G. A. & QIU, S. X. 2005. Cucurbitacins and cucurbitane glycosides: structures and biological activities. Natural product reports, 22, 386-399.

CHEN, Z.-T., LEE, S.-W. & CHEN, C.-M. 2006. Cucurbitacin B 2-sulfate and cucurbitacin glucosides from the root bark of Helicteres angustifolia. Chemical and pharmaceutical bulletin, 54, 1605-1607.

CHETTY, K., SHIVAJI, K. & TULASI, K. 2004. Flowering plants of Chittoor district Andhra Pradesh, India (pp 138). Tirupathi: Student offset printers.

CHIEN, A. J., MOORE, E. C., LONSDORF, A. S., KULIKAUSKAS, R. M., ROTHBERG, B. G., BERGER, A. J., MAJOR, M. B., HWANG, S. T., RIMM, D. L. & MOON, R. T. 2009. Activated Wnt/ß-catenin signaling in melanoma is associated with decreased proliferation in patient tumors and a murine melanoma model. Proceedings of the National Academy of Sciences, 106, 1193-1198.

CHITRA, L., PENISLUSSHIYAN, S., SOUNDARIYA, M., LOGESWARI, S., RAJESH, R. V. & PALVANNAN, T. 2022. Anti-acetylcholinesterase activity of *Corallocarpus epigaeus* tuber: in vitro kinetics, in silico docking and molecular dynamics analysis. Journal of Molecular Structure, 1255, 132450.

CHOUDHARY, K., SINGH, M. & PILLAI, U. 2008. Ethnobotanical survey of Rajasthan-An update. American-Eurasian Journal of Botany, 1, 38-45.

CLERICUZIO, M., MELLA, M., VITA-FINZI, P., ZEMA, M. & VIDARI, G. 2004. Cucurbitane Triterpenoids from Leucopaxillus g entianeus. Journal of natural products, 67, 1823-1828.

COHEN, C., ZAVALA-POMPA, A., SEQUEIRA, J. H., SHOJI, M., SEXTON, D. G., COTSONIS, G., CERIMELE, F., GOVINDARAJAN, B., MACARON, N. & ARBISER, J. L. 2002. Mitogen-actived protein kinase activation is an early event in melanoma progression. Clinical cancer research, 8, 3728-3733.

COOPER, G. M., HAUSMAN, R. E. & HAUSMAN, R. E. 2007. The cell: a molecular approach, ASM press Washington, DC.

CRAGG, G. M. & PEZZUTO, J. M. 2016. Natural products as a vital source for the discovery of cancer chemotherapeutic and chemopreventive agents. Medical Principles and Practice, 25, 41-59.

DAS THAKUR, M., SALANGSANG, F., LANDMAN, A. S., SELLERS, W. R., PRYER, N. K., LEVESQUE, M. P., DUMMER, R., MCMAHON, M. & STUART, D. D. 2013. Modelling vemurafenib resistance in melanoma reveals a strategy to forestall drug resistance. Nature, 494, 251-255.

DAT, N. T., JIN, X., HONG, Y.-S. & LEE, J. J. 2010. An isoaurone and other constituents from trichosanthes kirilowii seeds inhibit hypoxia-inducible factor-1 and nuclear factor-κB. Journal of natural products, 73, 1167-1169.

DAVID, A. & VALLANCE, D. 1955. Bitter principles of Cucurbitaceae. Journal of Pharmacy and Pharmacology, 7, 295-296.

DELMAS, V., BEERMANN, F., MARTINOZZI, S., CARREIRA, S., ACKERMANN, J., KUMASAKA, M., DENAT, L., GOODALL, J., LUCIANI, F. & VIROS, A. 2007. β-Catenin induces immortalization of melanocytes by suppressing p16INK4a expression and cooperates with N-Ras in melanoma development. Genes & development, 21, 2923-2935.

DEVITA, V. T., LAWRENCE, T. S. & ROSENBERG, S. A. 2008. DeVita, Hellman, and Rosenberg's cancer: principles & practice of oncology, Lippincott Williams & Wilkins.

DHANAPAL, R., CHANDANAM, S., SWAMY, V., VL, A. B., GUPTA, M. & BASU, S. 2006. Antisteroidogenic activity of *Corallocarpus epigaeus* Benth. ex Hook. tubers in female mice ovaries. Asian Journal of Chemistry, 18, 1013.

DIAS, D. A., URBAN, S. & ROESSNER, U. 2012. A historical overview of natural products in drug discovery. Metabolites, 2, 303-336.

DUMMER, R., ASCIERTO, P. A., GOGAS, H. J., ARANCE, A., MANDALA, M., LISZKAY, G., GARBE, C., SCHADENDORF, D., KRAJSOVA, I. & GUTZMER, R. 2018. Encorafenib plus binimetinib versus vemurafenib or encorafenib in patients with BRAF-mutant melanoma (COLUMBUS): a multicentre, open-label, randomised phase 3 trial. The Lancet Oncology, 19, 603-615.

DUNNILL, P. M. & FOWDEN, L. 1965. The amino acids of seeds of the Cucurbitaceae. Phytochemistry, 4, 933-944.

DYMOCK, W., WARDEN, C. J. H. & HOOPER, D. 1893. Pharmacographia Indica: A history of the principal drugs of vegetable origin, met with in British India, K. Paul, Trench, Trübner & Company, ld.

ENSLIN, P. 1954. Bitter principles of the cucurbitaceae. I.—Observations on the chemistry of cucurbitacin a. Journal of the Science of Food and Agriculture, 5, 410-416.

FECHER, L. A., CUMMINGS, S. D., KEEFE, M. J. & ALANI, R. M. 2007. Toward a molecular classification of melanoma. Journal of Clinical Oncology, 25, 1606-1620.

FERGUSON, J., FISCHER, D. & METCALF, R. 1983. A report of cucurbitacin poisonings in humans. Cucurbit Genetics Cooperative, 36.

FLAHERTY, K. T., INFANTE, J. R., DAUD, A., GONZALEZ, R., KEFFORD, R. F., SOSMAN, J., HAMID, O., SCHUCHTER, L., CEBON, J. & IBRAHIM, N. 2012. Combined BRAF and MEK inhibition in melanoma with BRAF V600 mutations. New England Journal of Medicine, 367, 1694-1703.

FULLER, R. W., CARDELLINA, J. H., CRAGG, G. M. & BOYD, M. R. 1994. Cucurbitacins: differential cytotoxicity, dereplication and first isolation from Gonystylus keithii. Journal of natural products, 57, 1442-1445.

GANESAN, S., PANDI, N. R. & BANUMATHY, N. 2007. Ethnomedicinal survey of Alagarkoil hills (reserved forest), Tamil nadu, India. EJournal of Indian Medicine, 1, 18-18.

GARG, S., KAUL, S. C. & WADHWA, R. 2018. Cucurbitacin B and cancer intervention: Chemistry, biology and mechanisms. International journal of oncology, 52, 19-37.

GNANANATH, K., REDDY, K. R., KUMAR, G. P., KRISHNA, B., REDDY, K. S. & KUMAR, A. S. 2013. Evaluation of antidiabetic activity in *Corallocarpus epigaeus* rhizomes. International Current Pharmaceutical Journal, 2, 53-56.

GRY J, SOBORG I AND ANDERSON HC .2006. Identity, physical and chemical properties, analytical methods. Cucurbitacins in plant food. Ekspressen Tyrk & Kopicenter, Copenhagen, Denmark. 182006.

GUPTA, J., ALI, M., PILLAI, K., VELASCO-NEGUERUELA, A., PÉREZ-ALONSO, M. J. & CONTRERAS, F. Ó. 1997. The Occurrence of Ishwarane and Ishwarone in the Roof Oil of *Corallocarpus epigaeus* Benth. ex Hook. f. Journal of Essential Oil Research, 9, 667-672.

HARITUNIANS, T., GUELLER, S., ZHANG, L., BADR, R., YIN, D., XING, H., FUNG, M. C. & KOEFFLER, H. P. 2008. Cucurbitacin B induces differentiation, cell cycle arrest, and actin cytoskeletal alterations in myeloid leukemia cells. Leukemia research, 32, 1366-1373.

HOCKER, T. L., SINGH, M. K. & TSAO, H. 2008. Melanoma genetics and therapeutic approaches in the 21st century: moving from the benchside to the bedside. Journal of Investigative Dermatology, 128, 2575-2595.

HYLANDS, P. J. & KOSUGI, J. 1982. Bryonoside and bryoside—new triterpene glycosides from Bryonia dioica. Phytochemistry, 21, 1379-1384.

ISHNAVA, K. B. & KONAR, P. S. 2020. In vitro anthelmintic activity and phytochemical characterization of *Corallocarpus epigaeus* (Rottler) Hook. f. tuber from ethyl acetate extracts. Bulletin of the National Research Centre, 44, 1-10.

JACOBS, H., SINGH, T., REYNOLDS, W. F. & MCLEAN, S. 1990. Isolation and 13C-nmr Assignments of Cucurbitacins from Cayaponia Angustiloba, Cayaponia racemosa, and Guraniasubumbellata. Journal of natural products, 53, 1600-1605.

JAGDEEPCHANDRA, S., LAKSHMIDEVI, N., MRUTHUNJAYA, K. & SHIVAPRASAD, H. 2014. Medcinal plants used in tribal and folklore medicine in rural areas of Mysore district. International journal of Biology, Pharmacy and Allied sciences, 3, 797-836.

JAMUNA, S., KARTHIKA, K. & PAULSAMY, S. 2015. Phytochemical and pharmacological properties of certain medicinally important species of Cucurbitaceae family–a review. J. Res. Biol, 5, 1835-1849.

JEYASEELAN, M., ARUMUGAM, T. & THANGARAJ, N. 2014. Evaluation of antioxidant and antiinflammatory activities of *Corallocarpus epigaeus* (Hook. F) rhizomes. Int J Pharm Biomed res, 591, 18-24.

JOHANNESSEN, C. M., BOEHM, J. S., KIM, S. Y., THOMAS, S. R., WARDWELL, L., JOHNSON, L. A., EMERY, C. M., STRANSKY, N., COGDILL, A. P. & BARRETINA, J. 2010. COT drives resistance to RAF inhibition through MAP kinase pathway reactivation. Nature, 468, 968-972.

KANDASAMY, S., CHINNAPPAN, S., THANGASWAMY, S. & BALAKRISHNAN, S. 2020. Facile approach for phytosynthesis of gold nanoparticles from *Corallocarpus epigaeus* rhizome extract and their biological assessment. Materials Research Express, 6, 1250c1.

KARP, G. 2009. Cell and molecular biology: concepts and experiments, John Wiley & Sons.

KARTHIC, V., POONGODI, B., BALAMURUGAN, S., SHANMUGAPRIYA, P., MURUGESAN, S., MANJARI, V., RENGASUNDARI, R., MADHAVAN, R. & BANUMATHI, V. 2017. Phytocompound and Heavy Metal Analysis of Purified *Corallocarpus epigaeus* Benth. ex. hook. (Aagasagarudan Kizhangu) in the aspect of Siddha System of Medicine. International Journal on Applied Bioengineering, 11.

KARTHIC, V., POONGODI, B., SHANMUGAPRIYA, P. & SIVARAMAN, D. 2019. In-silico molecular docking analysis of potential phytotherapeutics from the medicinal herb *Corallocarpus epigaeus* for treating urticaria. Int. J. Trans. Res. Ind. Med, 1, 5-12.

KB, C. S. & NVNA, S. R. 2015. Anti-Hyperlipidaemic Activity of Ethanol Extract of Whole Plant of *Corallocarpus epigaeus* on Wistar rats.

KIRTIKAR, K. & BASU, B. 1935. Indian medicinal plants. Indian Medicinal Plants.

KNOWLES, M. & SELBY, P. 2005. Introduction to the cellular and molecular biology of cancer, Oxford university press.

KOMIYA, Y. & HABAS, R. 2008. Wnt signal transduction pathways. Organogenesis, 4, 68-75.

KOTHAWADE, K. A. & SIDDIQUI, A. 2018. A comprehensive review on pharmacological activity of Vernonia anthelmintica and *Corallocarpus epigaeus*. Asian Journal of Pharmaceutical Education and Research, 7, 28-35.

KOTTAIMUTHU, R. 2008. Ethnobotany of the Valaiyans of Karandamalai, Dindigul District, Tamil Nadu, India. Ethnobotanical leaflets, 2008, 24.

KULIKOVA, K., KIBARDIN, A., GNUCHEV, N., GEORGIEV, G. & LARIN, S. 2012. Wnt signaling pathway and its significance for melanoma development. Sovremennye Tehnologii, 2012, 107-11.

LARUE, L. & DELMAS, V. 2006. The WNT/Beta-catenin pathway in melanoma. Frontiers in Bioscience-Landmark, 11, 733-742.

LEMEN, J., BUFFARD, G., PROVOST, J., TIBERGHIEN, R., FORGACS, P., LAGRANGE, E. & AUROUSSEAU, M. 1969. Relations entre la structure de quelques cucurbitacines leur toxicite et leuractivite laxative. Chem Therapeut, 6, 459-465.

LI, H., ZHU, H., XU, C.-J. & YUAN, J. 1998. Cleavage of BID by caspase 8 mediates the mitochondrial damage in the Fas pathway of apoptosis. Cell, 94, 491-501.

LI, J., ZHANG, Y., OUYANG, D., XU, L., MO, H. & HE, X. 2012. Suppression of STAT3 phosphorylation enhances the cytotoxicity of cucurbitacin B in B16F10 melanoma cells. African Journal of Pharmacy and Pharmacology, 6, 1545-1554.

LI, K., YU, Y., SUN, S., LIU, Y., GARG, S., KAUL, S. C., LEI, Z., GAO, R., WADHWA, R. & ZHANG, Z. 2016. Functional characterisation of anticancer activity in the aqueous extract of Helicteres angustifolia L. Roots. PLoS One, 11, e0152017.

LITO, P., PRATILAS, C. A., JOSEPH, E. W., TADI, M., HALILOVIC, E., ZUBROWSKI, M., HUANG, A., WONG, W. L., CALLAHAN, M. K. & MERGHOUB, T. 2012. Relief of profound feedback inhibition of mitogenic signaling by RAF inhibitors attenuates their activity in BRAFV600E melanomas. Cancer cell, 22, 668-682.

LIU, C., HE, S., ZHANG, J., LI, S., CHEN, J. & HAN, C. 2020. Silencing TCF4 Sensitizes Melanoma Cells to Vemurafenib Through Inhibiting GLUT3-Mediated Glycolysis. OncoTargets and therapy, 13, 4905.

LONG, G. V., WEBER, J. S., INFANTE, J. R., KIM, K. B., DAUD, A., GONZALEZ, R., SOSMAN, J. A., HAMID, O., SCHUCHTER, L. & CEBON, J. 2016. Overall survival and durable responses in patients with BRAF V600-mutant metastatic melanoma receiving dabrafenib combined with trametinib. Journal of Clinical Oncology, 34, 871-878.

MAHESH, R., BABU, V. S., NARAYANA, M. S. V., NAIK, D. N. & MALOTHU, R. 2012. Hepatoprotective activity of leaves of *Corallocarpus epigaeus* in carbon tetrachloride induced rats. Ramesh Malothu. et al International Journal of Biological and Pharmaceutical Research, 3, 567-570.

MENAA, F. 2013. Latest approved therapies for metastatic melanoma: what comes next? Journal of skin cancer, 2013.

MILHAS, D., CUVILLIER, O., THERVILLE, N., CLAVÉ, P., THOMSEN, M., LEVADE, T., BENOIST, H. & SÉGUI, B. 2005. Caspase-10 triggers Bid cleavage and caspase cascade activation in FasL-induced apoptosis. Journal of Biological Chemistry, 280, 19836-19842.

MOSIMANN, C., HAUSMANN, G. & BASLER, K. 2009. β-catenin hits chromatin: regulation of Wnt target gene activation. Nature reviews Molecular cell biology, 10, 276-286.

NADKARNI, K. & NADKARNI, A. 1976. Indian Materia Medica, Vol. I & II. Popular Prakashan Private Limited, Bombay, India.

OBERLIES, N. H., BURGESS, J. P., NAVARRO, H. A., PINOS, R. E., SOEJARTO, D. D., FARNSWORTH, N. R., KINGHORN, A. D., WANI, M. C. & WALL, M. E. 2001. Bioactive Constituents of the Roots of Licania i ntrapetiolaris. Journal of natural products, 64, 497-501.

OMATA, W., TSUTSUMIDA, A., NAMIKAWA, K., TAKAHASHI, A., OASHI, K. & YAMAZAKI, N. 2017. Sequential combination chemotherapy of dacarbazine (DTIC) with carboplatin and paclitaxel for patients with metastatic mucosal melanoma of nasal cavity and paranasal sinuses. Clinical Medicine Insights: Case Reports, 10, CCRep. S39851.

OUYANG, D., ZHANG, Y., XU, L., LI, J., ZHA, Q. & HE, X. 2011. Histone deacetylase inhibitor valproic acid sensitizes B16F10 melanoma cells to cucurbitacin B treatment. Acta Biochim Biophys Sin, 43, 487-495.

PALUNCIC, J., KOVACEVIC, Z., JANSSON, P. J., KALINOWSKI, D., MERLOT, A. M., HUANG, M. L.-H., LOK, H. C., SAHNI, S., LANE, D. J. & RICHARDSON, D. R. 2016. Roads to melanoma: Key pathways and emerging players in melanoma progression and oncogenic signaling. Biochimica et Biophysica Acta (BBA)-Molecular Cell Research, 1863, 770-784.

PARTRIDGE, A. H., BURSTEIN, H. J. & WINER, E. P. 2001. Side effects of chemotherapy and combined chemohormonal therapy in women with early-stage breast cancer. JNCI Monographs, 2001, 135-142.

PATEL, M., ECKBURG, A., GANTIWALA, S., HART, Z., DEIN, J., LAM, K. & PURI, N. 2021. Resistance to molecularly targeted therapies in melanoma. Cancers, 13, 1115.

PONNA, V., RANJANI, R., RAO, M. & SUNDARSANAM, G. 2013. Impact of antidote medicinal plant-*Corallocarpus epigaeus* extract on lipid peroxidation induced by Naja naja snake venom in albino rat. Int J Med Pharm Sci, 3, 23-30.

PRIYAVARDHINI, S., VASANTHA, K., TRESINASORIS, P. & MOHAN, V. 2012. Efficacy of phytochemical and antibacterial activity of *Corallocarpus epigaeus* Hook. f. Int J Pharm Tech Res, 4, 35-43.

REDDY, K., REDDY, C. & TRIMURTHULU, G. 2006. Ethnobotanical survey on respiratory disorders in Eastern Ghats of Andhra Pradesh, India. Ethnobotanical leaflets, 2006, 16.

SANDERS, D., BLESSING, K., HASSAN, G., BRUTON, R., MARSDEN, J. & JANKOWSKI, J. 1999. Alterations in cadherin and catenin expression during the biological progression of melanocytic tumours. Molecular Pathology, 52, 151.

SARANYA, U., SIVAKANESAN, R. & VARNAKULENDRAN, N. 2017. Evaluation of Haemopoietic Activity of the Rhizome of *Corallocarpus epigaeus* Benth. Ex Hook-A Pilot Study. Age, 20, 20-50.

SHRI, C. N., BALAJI, J., VENKATRAMANAN, S. & MADHUMATHI, K. 2010. Pharmacognostical and preliminary phytochemical screening of the root and rhizome of *Corallocarpus epigaeus*. Int J Pharm Biomed Res, 1, 24-27.

SIQUEIRA JR, J. M., PETERS, R. R., GAZOLA, A. C., KREPSKY, P. B., FARIAS, M. R., RAE, G. A., DE BRUM-FERNANDES, A. J. & RIBEIRO-DO-VALLE, R. M. 2007. Anti-inflammatory effects of a triterpenoid isolated from Wilbrandia ebracteata Cogn. Life sciences, 80, 1382-1387.

SIVKUMAR, T., KANNAN, K. & MANAVALAN, R. 2009. Pharmacognostical investigations of *Corallocarpus epigaeus* (Rottler) CB Clark. Lateral, 2, 159-166.

SOWMIYA, K., AISHWARYA, K., NAVAMATHAVAN, R., KIM, H. Y. & NIRMALA, R. 2021. Green synthesis of silver nanoparticles using aqueous rhizome extract of *Corallocarpus epigaeus* for biomedical applications. Applied Science and Convergence Technology, 30, 54-61.

SREEKANTH, C., BAVA, S., SREEKUMAR, E. & ANTO, R. 2011. Molecular evidences for the chemosensitizing efficacy of liposomal curcumin in paclitaxel chemotherapy in mouse models of cervical cancer. Oncogene, 30, 3139-3152.

SUBBIAH, V., LASSEN, U., ÉLEZ, E., ITALIANO, A., CURIGLIANO, G., JAVLE, M., DE BRAUD, F., PRAGER, G. W., GREIL, R. & STEIN, A. 2020. Dabrafenib plus trametinib in patients with BRAFV600E-mutated biliary tract cancer (ROAR): A phase 2, open-label, single-arm, multicentre basket trial. The Lancet Oncology, 21, 1234-1243.

SUNG, H., FERLAY, J., SIEGEL, R. L., LAVERSANNE, M., SOERJOMATARAM, I., JEMAL, A. & BRAY, F. 2021. Global cancer statistics 2020: GLOBOCAN estimates of incidence and mortality worldwide for 36 cancers in 185 countries. CA: a cancer journal for clinicians, 71, 209-249.

SWARNKAR, S. & KATEWA, S. 2008. Ethnobotanical observation on tuberous plants from tribal area of Rajasthan (India). Ethnobotanical leaflets, 2008, 87.

Therapeutic Goods Association: Health Safety Regulation - Substances that may be used in listed medicines in Australia. Government of Australia. 862011.

TUNMANN, P. & STAPEL, G. 1966. On bryodulcoside. 8. On substances found in the root of Bryonia dioica Jacq. Archiv der Pharmazie und Berichte der Deutschen Pharmazeutischen Gesellschaft, 229, 596-598.

UMADEVI, U. & KAMALAM, M. 2012. Pharmacognostical, phytochemical and heavy metal studies on an ethno medicinal plant-*Corallocarpus epigaeus* (rottl. &wild.) Clarke. IJPPR, 4, 117-121.

UTHRAPATHY, S., SHABI, M. M., KRISHNAMOORTHY, G., RAVINDHRAN, D., RAJAMANICKAM, V. G. & PILLAY DUBEY, G. 2011. Efecto analgésico y antiartrítico de *Corallocarpus epigaeus*. Acta bioquímica clínica latinoamericana, 45, 739-756.

VASANTHA, K., PRIYAVARDHINI, S., TRESINA, S. & MOHAN, V. 2012. Antifungal activity of Corrallocarpus epigaeus (Hoo. K.) against cancer. Biosci Discov, 3, 87-90.

VINOD, B. S., MALIEKAL, T. T. & ANTO, R. J. 2013. Phytochemicals as chemosensitizers: from molecular mechanism to clinical significance. Antioxidants & redox signaling, 18, 1307-1348.

WELLBROCK, C. & MARAIS, R. 2005. Elevated expression of MITF counteracts B-RAF–stimulated melanocyte and melanoma cell proliferation. The Journal of cell biology, 170, 703-708.

WIART, C. 2012. The definition and significance of Cucurbitacin B a STAT3 inhibitors. Cancer Letters, 328, 188-188.

World Health Organization 2020 https://gco.iarc.fr/today/online-analysis-table?v=2020&mode=cancer&mode_population=continents&population=900&populations=900&key=asr&sex=0&cancer=39&type=0&statistic=5&prevalence=0&population_group=0&ages_group%5B%5D=0&ages_group%5B%5D=17&group_cancer=0&include_nmsc=1&include_nmsc_other=0.

World Health Organization: WHO Monograph on Selected Medicinal Plants. 4:2662009.

WU, K.-J., GRANDORI, C., AMACKER, M., SIMON-VERMOT, N., POLACK, A., LINGNER, J. & DALLA-FAVERA, R. 1999. Direct activation of TERT transcription by c-MYC. Nature genetics, 21, 220-224.

YANG, A. S. & CHAPMAN, P. B. 2009. The history and future of chemotherapy for melanoma. Hematology/Oncology Clinics, 23, 583-597.

ZAIDIEH, T., SMITH, J. R., BALL, K. E. & AN, Q. 2019. ROS as a novel indicator to predict anticancer drug efficacy. BMC cancer, 19, 1-14.

ZHANG, Y. T., OUYANG, D. Y., XU, L. H., ZHA, Q. B. & HE, X. H. 2013. Formation of cofilin–actin rods following cucurbitacin-B-induced actin aggregation depends on slingshot homolog 1-mediated cofilin hyperactivation. Journal of cellular biochemistry, 114, 2415-2429.

ZHANG, Y., OUYANG, D., XU, L., JI, Y., ZHA, Q., CAI, J. & HE, X. 2011. Cucurbitacin B induces rapid depletion of the G-actin pool through reactive oxygen species-dependent actin aggregation in melanoma cells. Acta Biochim Biophys Sin, 43, 556-567.

ZHANG, Y.-T., XU, L.-H., LU, Q., LIU, K.-P., LIU, P.-Y., JI, F., LIU, X.-M., OUYANG, D.-Y. & HE, X.-H. 2014. VASP activation via the Gα13/RhoA/PKA pathway mediates cucurbitacin-B-induced actin aggregation and cofilin-actin rod formation. PLoS One, 9, e93547.

APPENDIX I

1 L DMEM

Components	Weight/Volume
DMEM powder (GIBCO)	13.5 g
HEPES	5.95 g
$NaHCO_3$	3.75 g
Streptomycin	0.1 g
Penicillin	500 µl

10X PBS

Components	Weight
NaCl	80 g
Na_2HPO_4	14.4 g
KCl	2 g
KH_2PO_4	2.9 g

1X PBS-EDTA (pH 7.4)

Components	Weight
NaCl	8 g
Na_2HPO_4	1.44 g
KCl	0.2 g
KH_2PO_4	0.24 g
EDTA	0.2 g

Trypsin-EDTA (1L)

Components	Weight/Volume
1X PBS-EDTA (Autoclaved)	1000 ml
Trypsin	2 g
Glucose	0.2 g

MTT solution (5mg/ml)

Components	Weight/Volume
MTT	250 mg
Sterile 1X PBS	50 ml

Lysis Buffer for MTT assay

Components	Weight/Volume
SDS	20 g
50% DMF	100 ml

Whole Cell Lysis Buffer

Components	Volume
Tris (pH 7.4)	20 µl
NaCl	50 µl
EDTA	4 µl
Triton X-100	10 µl
DTT	10 µl
PMSF	2.5 µl
Aprotinin	2.5 µl
Leupeptin	2.5 µl
Sodium ortho vanadate	8 µl
Distilled water	916 µl

Bradford's Reagents (200 ml)

Components	Weight/Volume
Brilliant Blue G-250	10 mg
95% ethanol	5 ml
85% orthophosphoric acid	10 ml
Distilled water	185 ml

5X loading dye

Components	Volume
Distilled water	4 ml
0.5 M Tris (pH 6.8)	1 ml
Glycerol	0.8 ml
10% SDS	1.6 ml
B-mercapto ethanol	0.4 ml
0.05% bromophenol blue	0.2 ml

10X TBS (500 ml) pH 7.6

Components	Weight/Volume
Tris	12.1g
NaCl	40 g
Distilled water	500 ml

1X TBST (500 ml)

Components	Volume
10X TBS	50 ml
Distilled water	Make up to 500 ml
Tween 20	2 ml

8X Electrode Buffer (500 ml) pH 8.3

Components	Weight/Volume
Tris	12 g
Glycine	57.6 g
Distilled water	500 ml

1X Electrode Buffer (400 ml)

Components	Volume
8X electrode buffer	50 ml
Distilled water	make up to 400 ml
10% SDS	4 ml

Towbin's Buffer/Transfer Buffer (500 ml)

Components	Weight/Volume
Tris	1.51 g
Glycine	7.2 g
Methanol	100 ml
Distilled water	Make up to 500 ml

Solution A for ECL

Components	Weight/Volume
1M Tris pH 8.5	5 ml
90 mM Para coumaric acid	220 µl
250 mM Luminol	500 µl
Double distilled water	44.3 ml

Solution B for ECL

Components	Weight/Volume
1M Tris pH 8.5	5 ml
30% H2O2	30 µl
Double distilled water	45 ml

4% PFA

Components	Weight/Volume
Para formaldehyde	4 g
1X PBS	100 ml

30% Sucrose solution

Components	Weight/Volume
Sucrose	30 g
1X PBS	100 ml

Citrate buffer (pH 6 adjusted with citric acid)

Components	Weight/Volume
Tri-sodium citrate (dihydrate)	0.147 g
Distilled water	50 ml

Haematoxylin solution

Components	Weight/Volume
Haematoxylin	5 g
Isopropanol	25 ml
Sodium/Potassium alum	50 g
Mercuric oxide	1.2 g
Distilled water	500 ml
Glacial acetic acid	500 µl

0.5% Eosin solution

Components	Weight/Volume
Eosin Y	2.5 g
95% isopropanol	500 ml

Acid Alcohol

Components	Weight/Volume
70% isopropyl alcohol	100 ml
Con. HCl	1 ml

Blueing Solution

Components	Weight/Volume
$NaHCO_3$	0.1 g
$MgSO_4$	1 g
Distilled water	50 ml

APPENDIX II

SDS- Polyacrylamide Resolving Gel

Components	Volume			
	8%	**10%**	**12%**	**15%**
Distilled water	4.6 ml	4 ml	3.3 ml	2.2 ml
30% Acrylamide	2.7 ml	3.3 ml	4 ml	4.9 ml
1.5 M Tris (pH 8.8)	2.5 ml	2.5 ml	2.5 ml	2.5 ml
SDS (10%)	100 µl	100 µl	100 µl	100 µl
APS (10%)	100 µl	100 µl	100 µl	100 µl
TEMED	6 µl	6 µl	6 µl	6 µl

SDS- Polyacrylamide Stacking Gel

Components	Volume
Distilled water	1.7 ml
30% Acrylamide	415 µl
1.5 M Tris (pH 6.8)	315 µl
SDS (10%)	25 µl
APS (10%)	25 µl
TEMED	4 µl

PRESENTATIONS

AWARD

Best poster award in 30th Kerala Science Congress under the subject area Biotechnology, **Aiswarya U S**, Haritha H Nair, Ruby John Anto, Smitha V B, A Study on the Anticancer Potential of the Medicinal Plant *Corallocarpus epigaeus*, held at Govt. Brennan College, Thalasseri, Kannur, Kerala from January 2018, Page No.69.

ORAL PRESENTATIONS

1. **Aiswarya U S**, Haritha H Nair, Jaice Ravindran, Ravi Shankar Lankalapalli, Ruby John Anto, Smitha V B, Isolation identification and characterization of potent anticancer compounds from the medicinal plant *Corallocarpus epigaeus* effective against malignant melanoma**,** International Webinar on Phytochemistry- Impacts and Applications Organized by Kerala Academy of Science, September 11, 2021.

2. **Aiswarya U S**, Haritha H Nair, Jaice Ravindran, Ravi Shankar Lankalapalli, Ruby John Anto, Smitha V B, *Corallocarpus epigaeus*: A Potent Medicinal Plant with Anti-Cancer Property, State Level Seminar on Biotechnology for "Biodiversity Conservation and Utilization" November 2, 2018, Page No. 24-25, Sree Narayana College of Technology, Kollam.

POSTER PRESENTATIONS

1. **Aiswarya U S**, Haritha H Nair, Vikas G, Ravi Shankar Lankalapalli, Ruby John Anto, Smitha V B, Isolation identification and characterization of potent anticancer compounds from the medicinal plant *Corallocarpus epigaeus* effective against melanoma, 33rd Kerala Science Congress, January 2021

2. **Aiswarya U S**, Haritha H Nair, Vikas G, Ravi Shankar Lankalapalli, Ruby John Anto, Smitha V B, Isolation and identification of potent anticancer compounds from the plant, *Corallocarpus epigaeus*, 32nd Kerala Science Congress, January 2020

3. **Aiswarya U S**, Haritha H Nair, Jaice Ravindran, Ravi Shankar Lankalapalli, Ruby John Anto, Smitha V B, Evaluation of the Medicinal Plant *Corallocarpus epigaeus* for Anti-Cancer Property, 8th Annual meeting of Indian Academy of Biomedical Sciences & conference on Deliberation on Translation of Basic Scientific Insights into Affordable Health Care Products February 25-27,2019, Page No. 174-175.

4. **Aiswarya U S**, Haritha H Nair, Jaice Ravindran, Ravi Shankar Lankalapalli, Ruby John Anto, Smitha V B, Tubers of the Medicinal Plant *Corallocarpus epigaeus* Possess Potent Anti-Cancer Principles Effective against Hepatocellular Carcinoma Cells, 3 rd International Conference on "Nutraceuticals and Chronic Diseases" September14-16, 2018.

5. **Aiswarya U S**, Haritha H Nair, Ravi Shankar L, Ruby John Anto, Smitha V B, A Bioactive Fraction from the Medicinal Plant *Corallocarpus epigaeus* Induces Apoptosis in Hepatocellular Carcinoma cells, National Seminar on New Horizons in Cancer Treatment and Prevention: From Bench to Bedside, March 2018, ISBN 978-93-5300-765-2, Page No. 13-14.

6. **Aiswarya U S**, Haritha H Nair, Ruby John Anto, Smitha V B, FFC, a potent fraction from the medicinal plant, *Corallocarpus epigaeus* induces cytotoxicity in hepatocellular carcinoma via induction of apoptosis, 7th International Conference on Translational Cancer Research (7th ICTCR 2018) , February 2018, Page No.78.

7. **Aiswarya U S**, Haritha H Nair, Ruby John Anto, Smitha V B, A Study on the Anticancer Potential of the Medicinal Plant *Corallocarpus epigaeus,* 30th Kerala Science Congress, January 2018, Page No.69. **Best Poster Award.**

PUBLICATIONS

1. **Sreekumar Usha Devi Aiswarya**, Gowda Vikas, Nair Hariprasad Haritha, Vijayasteltar Belsamma Liju, Anwar Shabna, Mundanattu Swetha, Tennyson Prakash Rayginia, Chenicheri Kizhakkeveettil Keerthana, Lekshmi Raghu Nath, Mullan Vellandy Reshma, Sankar Sundaram, Nikhil Ponnoor Anto, Ravi Shankar Lankalapalli*, Ruby John Anto* and Smitha Vadakkeveettil Bava*, Cucurbitacin B, Purified and Characterized From the Rhizome of Corallocarpus epigaeus Exhibits Anti-Melanoma Potential, *Frontiers in Oncology*, 2022, 12:903832. DOI: 10.3389/fonc.2022.903832 (Impact Factor: 5. 738).

2. A Shabna, Jayesh A, Vinod V, Minakshi S, V B Liju, Archana P R, N A Amrutha, Vijai V Alex, M Swetha, **Sreekumar U Aiswarya**, S Jannet, Uma Subramanian Unni, Sankar Sundaram, Daisy R Sherin, Nikhil P Anto, Smitha V Bava, Sadasivan Chittalakkottu, Sophia Ran, and Ruby John Anto*, Pharmacological attenuation of melanoma by tryptanthrin pertains to the suppression of MITF-M through MEK/ERK signaling axis, *Cell. Mol. Life Sci.* 2022, 79, 478. DOI*:* https://doi.org/10.1007/s00018-022-04476-y (Impact Factor: 9.207).

3. M Swetha, C.K. Keerthana, Tennyson P Rayginia, Lekshmi R Nath, Nair Hariprasad Haritha, Anwar Shabna, Kalishwaralal Kalimuthu, Arun Kumar Thangarasu, **Sreekumar U Aiswarya**, Somaraj Jannet, Sreekumar Pillai, Kuzhuvelil B Harikumar, Sankar Sundaram, Nikhil P Anto, Dee H Wu, Ravi Shankar L, Rheal Towner, Noah Isakov, S S. Deepa and Ruby John Anto*, Augmented efficacy of uttroside B over sorafenib in a murine model of human hepatocellular carcinoma, *Pharmaceuticals*, 2022, 15, 636. DOI: https://doi.org/10.3390/ph15050636. (Impact Factor: 5.215).

4. Lekshmi R Nath, M Swetha, Vinod V, Arun Kumar T, Haritha H Nair, Shabna A, **Sreekumar U Aiswarya**, T P Rayginia, C K Keerthana, Kalishwaralal Kalimuthu, Sankar S, Ravi Shankar L, Sreekumar Pillai, Rheal Towner, Noah Isakov and *Ruby John Anto, Blockade of uttroside B-induced autophagic pro- survival signals augments its chemotherapeutic efficacy against hepatocellular carcinoma, *Frontiers in Oncology*, 2022, 12:812598. DOI: 10.3389/fonc.2022.812598. (Impact Factor: 5. 738).

5. Haritha H Nair, Akbar N, Vinod V, Nikhil P Anto, VB Liju, Vijai V Alex, Amrutha Nisthul A, **Sreekumar U Aiswarya**, Swetha M, BS Vinod, Sankar Sundaram, Maria V G, Thomas Herlevich, Nesteena K N, Smitha V B, Sadasivan C, Maria Zajac-Kaye and *Ruby John Anto, Targeting thymidylate synthase enhances the chemosensitivity of triple-negative breast cancer towards 5-FU- based combinatorial therapy, *Frontiers in Oncology*, 2021, DOI:10.3389/fonc.2021.656804. (Impact Factor: 5. 738).

frontiers | Frontiers in Oncology

ORIGINAL RESEARCH
published: 08 June 2022
doi: 10.3389/fonc.2022.903832

Cucurbitacin B, Purified and Characterized From the Rhizome of *Corallocarpus epigaeus* Exhibits Anti-Melanoma Potential

Sreekumar Usha Devi Aiswarya[1,2], *Gowda Vikas*[3], *Nair Hariprasad Haritha*[2], *Vijayasteltar Belsamma Liju*[2,4], *Anwar Shabna*[2], *Mundanattu Swetha*[2], *Tennyson Prakash Rayginia*[2], *Chenicheri Kizhakkeveettil Keerthana*[2], *Lekshmi Raghu Nath*[2,5], *Mullan Vellandy Reshma*[6,7], *Sankar Sundaram*[8], *Nikhil Ponnoor Anto*[4], *Ravi Shankar Lankalapalli*[3,7]*, *Ruby John Anto*[2]* *and Smitha Vadakkeveettil Bava*[1]*

[1] Department of Biotechnology, University of Calicut, Malappuram, India, [2] Division of Cancer Research, Rajiv Gandhi Centre for Biotechnology, Thiruvananthapuram, India, [3] Chemical Sciences and Technology Division, Council for Scientific and Industrial Research (CSIR)-National Institute for Interdisciplinary Science and Technology (CSIR-NIIST), Thiruvananthapuram, India, [4] The Shraga Segal Department of Microbiology-Immunology and Genetics, Faculty of Health Sciences, Ben-Gurion University of the Negev, Beer Sheva, Israel, [5] Department of Pharmacognosy, Amritha School of Pharmacy, Amritha Vishwa Vidyapeetham, Amrita Institute of Medical Sciences (AIMS) Health Science Campus, Ponekkara P.O, Kochi, India, [6] Agro-Processing and Technology Division, Council for Scientific and Industrial Research (CSIR)-National Institute for Interdisciplinary Science and Technology (CSIR-NIIST), Thiruvananthapuram, India, [7] Academy of Scientific and Innovative Research (AcSIR), Ghaziabad, India, [8] Department of Pathology, Government Medical College, Kottayam, India

OPEN ACCESS

Edited by:
Balaji Krishnamachary, Johns Hopkins University, United States

Reviewed by:
Chandra K. Singh, University of Wisconsin-Madison, United States
Rolando Perez-Lorenzo, Columbia University, United States

***Correspondence:**
Ravi Shankar Lankalapalli
ravishankar@niist.res.in
Ruby John Anto
rjanto@rgcb.res.in
Smitha Vadakkeveettil Bava
smithanishad@gmail.com

Specialty section:
This article was submitted to Pharmacology of Anti-Cancer Drugs, a section of the journal Frontiers in Oncology

Received: *24 March 2022*
Accepted: *17 May 2022*
Published: *08 June 2022*

Citation:
Aiswarya SUD, Vikas G, Haritha NH, Liju VB, Shabna A, Swetha M, Rayginia TP, Keerthana CK, Nath LR, Reshma MV, Sundaram S, Anto NP, Lankalapalli RS, Anto RJ and Bava SV (2022) Cucurbitacin B, Purified and Characterized From the Rhizome of Corallocarpus epigaeus Exhibits Anti-Melanoma Potential. Front. Oncol. 12:903832. doi: 10.3389/fonc.2022.903832

The ethnomedicinal plant from the Cucurbitaceae family, *Corallocarpus epigaeus*, or its bioactive derivatives have been widely utilized in traditional medicine owing to their distinct applications against various human ailments and have lured the interest of ethnobotanists and biochemists. Here, we report for the first time, the anti-cancer potential of a bio-active fraction isolated from the dried rhizome of *C. epigaeus*, and the bioactive principle identified as cucurbitacin B (Cu-B). The purification processes involving the utilization of multiple organic extracts of *C. epigaeus* rhizome powder, yielded Cu-B from the Ethyl acetate Cytotoxic Fraction (ECF), obtained by the chromatographic separation of the ethyl acetate extract. Amongst the various cancer lines tested, melanoma cells exhibit maximal sensitivity towards the Cu-B-containing ECF fraction. Cu-B induces an apoptotic mode of cell death initiated intrinsically as well as extrinsically in A375 melanoma cells whilst remaining comparatively less toxic to normal skin fibroblasts. *In vivo* studies involving a NOD-SCID murine model of human melanoma demonstrate the ability of Cu-B to attenuate tumor growth, while being pharmacologically safe *in vivo*, as assessed in *Swiss albino* mice. Furthermore, Cu-B inhibits MEK 1/2 as well as the constitutive and EGF-induced ERK 1/2 activation, indicating a definitive involvement of MAPK signal transducers in regulating Cu-B-mediated anti-melanoma activity. Together, our study demonstrates the anti-melanoma potential of *C. epigaeus*-derived Cu-B, which indicates the Cucurbitaceae succulent as a prospective source for deriving potent and pharmacologically safe anti-cancer compounds.

Keywords: *Corallocarpus epigaeus*, Cucurbitacin B, melanoma, apoptosis, NMR spectroscopy, mass spectrometry

INTRODUCTION

Corallocarpus epigaeus (Rottl. & Willd.) C. B. Clarke is a popular medicinal plant from the Cucurbitaceae family, notably prescribed in traditional medicine as a remedy for acute dysentery, venereal diseases, skin diseases, and snake bite (1). Despite its significance in traditional medicine, there are no comprehensive reports on the isolation of phytochemical constituents from *C. epigaeus*. Reports on the isolation of *N*-methyl asparagine from *C. epigaeus* seeds and essential oils like ishwarane and ishwarone from the roots are documented (2, 3). Volatile compounds from the roots and rhizomes of *C. epigaeus* have been detected by GC-MS analysis in comparison with standard phytochemical libraries for identification (3–5). In addition, there are reports on the identification of a pyridine carboxylic ester (corallocarpenoyl ester), an aliphatic C_{32} keto diol (dotriacont-22, 25-diol-10-one), a sesterpene lactone (corallocarpscalarolide), and a *p*-hydroxybenzoyl ester (designated as epigaeusyl ester) from the roots of *C.* epigaeus (6). Furthermore, a glycoside termed bryonin is purified from *C. epigaeus* roots (7). Organic solvent extracts of various parts of the plant are shown to possess a broad range of pharmacological properties (8). A couple of reports indicate that the ethanol extracts of *C. epigaeus* induce cytotoxicity in cancer cells (9, 10). However, a thorough investigation of the anti-cancer potential of *C. epigaeus* or its purified derivatives remains elusive.

In the present study, we report, the potent anti-cancer activity exhibited by the ethyl acetate extract of C. *epigaeus* dried rhizome and identify the anticancer principle in the extract as the triterpenoid, cucurbitacin B (Cu-B). Our studies demonstrate Cu-B as an efficacious agent against melanoma, compared to cancers of other tissue origins. Melanoma is the most deadly among skin cancer subtypes, the incidence, and mortality of which have been increasing over the past four decades (11). In melanoma, constitutive activation of MAP Kinase (MAPK) signaling *via* the RAS-B RAF -MEK-ERK signaling axis has been widely implicated in the initiation and development of cancer due to activation mutations of B-RAF and RAS genes. The development of small-molecule inhibitors of B-RAF, and MEK has made significant progress in melanoma chemotherapy. However, acquired resistance poses serious limitations to the therapeutic benefit of these small molecule inhibitors (12). A previous study has reported the ability of Cu-B to inhibit B-RAF and MEK by binding to the hydrophobic pocket of B-RAF receptor and allosteric site of MEK *via* molecular docking studies and has indicated the anti-melanoma potential of Cu-B by targeting the MAPK pathway (13). Our study indicates that Cu-B targets the MAPK pathway and evokes programmed cell death in melanoma cells by the induction of the apoptotic machinery. The pharmacological safety of Cu-B is ensured by its treatment on the normal skin fibroblasts. *In vivo* xenograft and toxicological studies corroborated the anti-melanoma efficacy and pharmacological safety of Cu-B. Taken together, our study reports the isolation and characterization of Cu-B from *C. epigaeus* rhizome and its prospective anti-melanoma potential.

MATERIALS AND METHODS

Reagents and Antibodies

Cell culture reagents such as Dulbecco's Modified Eagle Medium (DMEM) (GIBCO, 12800-017) and streptomycin sulfate (GIBCO, 11860-038) were obtained from Invitrogen Corporation (Grand Island, USA). Poly Excel HRP/DAB detection system universal kit (PathnSitu Biotechnologies Pvt. Ltd, India, OSH001) was used for immunohistochemistry experiments. Cucurbitacin B and MTT reagent were purchased from TCI Chemicals (India) Pvt. Ltd (D0801) and Amersham ECL Plus™ Western blotting reagents (PRPN 2132) were purchased from GE Healthcare Life Sciences (Piscataway, USA). Annexin V apoptosis detection kit (sc4252AK) was purchased from Santa Cruz Biotechnology (Santa Cruz, CA, USA). Antibodies against, Caspase 9 (9508S), Caspase 8 (4790S), Caspase 7 (12827S), Bid (2002S), p-P53 (9281S), PARP (9532S), p-ERK1/2 (4370S), ERK (9108S), p-STAT3 (9136S), β-actin (12620S) and p-MEK1/2 (9121S) were obtained from Cell Signalling Technologies (Beverly, MA, USA) and the antibody against C-MYC (sc764), Cyclin-D1 (sc8396), PCNA (sc25280) were purchased from Santa Cruz Biotechnology (Santa Cruz, CA, USA).Antibody against Caspase 3 (74T2) and ECL reagent (Pierce™ ECL western blotting substrate 32109) were purchased from ThermoFisher Scientific (Waltham, Massachusetts, United States) Antibody against MITF-M (ab12039) and Cellular ROS kit (ab113851) were purchased from Abcam (Cambridge, United Kingdom). Anti-caspase 10 (BD 51-9000066) antibody was purchased from BD Bioscience. DeadEnd™ Colorimetric TUNEL System from Promega (G7132) was procured from Addgene (Cambridge, MA, USA). An antibody against B-RAF^{V600E} (SAB 5600047), anti-rabbit antibody, anti-mouse antibody, and silica gel for column chromatography were obtained from Sigma Chemicals (St. Louis, MO, USA). EGF was purchased from Genscript (New Jersey, U.S). Organic solvents and TLC sheets were purchased from Merck (Germany). All other chemicals and an antibody against Vinculin (V9131) were purchased from Sigma Chemicals (St. Louis, MO, USA) unless otherwise mentioned.

Cell Lines

The lung cancer cell line, H1299, and normal skin fibroblast, FS were gifts from Prof. B.B. Agarwal to RJA. The cancer cell lines viz. colon (HCT-116), breast (MDA-MB-231), liver (HEP 3B), and cervical (HeLa) were procured from NCCS, Pune, India. Melanoma cell lines with different mutation status viz. A375 (B-RAF), SK-MEL-2 (N-RAS), and SK-MEL-28 (B-RAF) were procured from NCCS, Pune, India. All the cells were routinely maintained in a complete medium, which contained DMEM, 10% FBS, and 2mg/ml Amphotericin B. The cells were incubated at 37°C and 5% CO_2 atmosphere. Mycoplasma tests were performed on parent cell lines every 6 months. Cell lines passage between 3-6 times post-revival, were used for all experiments.

Plant Specimens

Fresh Rhizomes of *C. epigaeus* collected in January 2017 from Nagamalai, Madhurai were identified and authenticated by Dr. Pradeep Kumar, Curator, Department of Botany, University of Calicut, and a voucher specimen has been deposited at the Department of Botany, University of Calicut (VOUCHER NO: CALI 6891).

Preparation of Extracts and Isolation of ECF

Hexane, ethyl acetate, and methanol extracts were prepared by polarity gradient successive extraction of the dried rhizome powder. Among the three organic extracts of the rhizome, ethyl acetate extract was found to be the most cytotoxic. To isolate the active principle, we subjected the ethyl acetate extract to column fractionation, which yielded 11 fractions. Chromatographic separations were carried out by conventional column chromatography on silica gel (100-200 and 230-400 mesh).We tested the cytotoxic activity of each fraction among which, four fractions (Fraction 6 to 9) were found to be highly cytotoxic. As they showed similar cytotoxic profile as well as TLC pattern, we pooled them together and designated them as ECF (Ethyl acetate Cytotoxic Fraction).

Nuclear Magnetic Resonance Spectroscopic Analysis

^{1}H and ^{13}C NMR were recorded on a Bruker ASCENDTM-500 spectrometer at 500 and 125 MHz, respectively using CDC_{l3} and acetone-d6 solvents. TOCSY spectrum was acquired with an 80 ms mix time. NMR data are reported as follows: chemical shifts in ppm (δ) with integration, coupling constants in Hz. ^{1}H, ^{13}C, and 2D NMR data were used to elucidate the structure of the compounds.

Mass Spectrometry

Higher Resolution Mass Spectrometry (HRMS) analysis was recorded to determine the molecular formula of the compounds using a Thermo Scientific Exactive-Liquid Chromatography-Mass Spectrometry (LCMS) instrument by electrospray ionization method with ions given in *m/z* using Orbitrap analyzer.

Ultra-High Performance Liquid Chromatography Profiling of ECF Extract From *C. epigaeus*

The sample was injected into the analytical Nexera UHPLC system equipped with a reverse-phase Shim-pack GWS 5μ C18 column 250 × 4.6 mm ID connected to a PDA detector (SPD-M20A) and an autosampler (SIL-30AC). ECF fraction (3 mg/ml) and the isolated pure compound (2 mg/ml) were dissolved in acetonitrile: water (1:1) and filtered through a 0.2 μm nylon filter. The sample injection volume was 20 μL, and the C18 column temperature was 35°C. The mobile phase system consisted of water: acetic acid (100:1) (A) and acetonitrile (B). A step gradient program was used for this analysis as follows: 0% B at 0 min to 40% B at 20 min, 40 to 50% at 30 min, 50 to 60% at 40 min, 60 to 80% at 50 min, 80 to 100% at 60 min, then maintaining at 100% B from 60 to 65 min at a flow rate of 1 ml/min, monitored at 254 nm.

MTT Assay

The cells were seeded in 96-well plates (2000 cells/well), incubated overnight, and treated with different concentrations of plant extracts, ECF and Cu-B. After 72 h the sample solution was flicked off and Fresh media containing 25 μL of 3-(4, 5-Dimethylthiazol-2-yl)-2,5-Diphenyltetrazolium Bromide (MTT) solution (5 mg/mL in PBS) was added to the wells and incubated for 2h. At the end of incubation, lysis buffer (20% sodium dodecyl sulfate in 50% dimethylformamide) was added to the wells (0.1 mL/well) and incubated for another 1 h at 37°C. At the end of incubation, the optical density was measured at 570 nm using an ELISA plate reader (Bio-Rad). The relative cell viability in percentage was calculated as (A570 of treated cells/A570 of untreated cells) X 100. The IC50 values were extrapolated from polynomial regression analysis of experimental data.

Clonogenic Assay

Clonogenic assay or colony formation assay is an *in vitro* cell survival assay based on the ability of a single cell to grow into a colony. The colony is defined to consist of at least 50 cells. The assay essentially tests every cell in the population for its ability to undergo "unlimited" division. Briefly, 500 cells were seeded in 6-well plates and treated with different concentrations of ECF. After 72 h, media along with ECF was removed, supplied with fresh medium, and incubated for 1 week. The developed clones were fixed in glutaraldehyde (6%) and stained using crystal violet (0.5%). The plate was incubated for 30 min at room temperature, followed by rinsing with tap water. After drying the plate, colonies were counted and compared with the untreated control.

Annexin V-Propidium Iodide Staining

Apoptotic cells were detected with the help of a fluorescent microscope by Annexin V apoptosis detection kit according to the manufacturer's protocol (Santa Cruz, CA, USA). Briefly, the cells were seeded in 96-well plates and treated with ECF as in the MTT assay, but for 16 h. The cells were then washed with PBS, followed by 1X assay buffer, after which, 5 μL of Annexin V FITC and 10 μL of propidium iodide per 100 μL assay buffer was added, followed by incubation in the dark for 15min. The cells were then washed with PBS and immediately photographed using a fluorescent microscope, Nikon inverted fluorescent microscope (TEEclipse 300).

Fluorescent Activated Cell Sorting Analysis for Apoptosis

The extent of apoptosis induced by ECF and Cu-B was estimated by FACS using Annexin V FITC apoptosis kit (Santa Cruz, CA, USA). Briefly, the cells were seeded in 60mm culture plates, and incubated with different concentrations of ECF and Cu-B. After 16 h, cells were trypsinized and the pellets were washed with PBS and suspended in 100 μL 1 X assay buffer. To the buffer, 5 μL of FITC conjugated Annexin V and 10 μL of propidium iodide were added and incubated for 15 min in dark at room temperature.

The cells were then analyzed by flow cytometry to get the percentage of apoptotic cells (FACS Aria™, BD Bioscience)

Flow Cytometry and Cell Cycle Analysis

Cell cycle analysis helps in differentiating the distribution of a population of cells to the different stages of the cycle. Briefly, cells were treated with different concentrations of Cu-B and incubated for different time periods (24 h and 48 h). After incubation, the cells were trypsinized and the pellets were washed with PBS, and fixed in 70% ice-cold ethanol treated with 100 mg/ml RNAase A and 50 mg/ml propidium iodide, followed by flow cytometric analysis (BD Biosciences).

Fluorescent Microscopy for Reactive Oxygen Species

ROS levels within the cells in response to Cu-B were determined by staining the cells using H2DCF-DA according to the manufacturer's protocol. Briefly, the cells were seeded in 60 mm plates, kept overnight, and treated with different concentrations of Cu-B for 6 h followed by trypsinization. The cell pellets were washed with PBS, re-suspended in DCFDA containing assay buffer, and incubated for 30 min. After incubation, the cells were washed with PBS and observed and quantified using a Nikon inverted fluorescent microscope (TEEclipse 300).

Immunoblot Analysis

The cells were treated with the indicated concentration of ECF/Cu-B. The whole-cell lysates of drug treated cells/Tissue extracts from Cu-B treated mice, were electrophoresed by SDS/PAGE, and electrotransferred to PVDF membranes, the membranes were blocked with 5% milk for 60 min, washed using TBST and immunoblotted with the appropriate antibodies (14). The bands were visualized using an enhanced chemiluminescence kit (Pierce™ ECL western blotting solution) as per the manufacturer's protocol.

Animal Experiments

Toxicological Analyses

The toxicological analysis of the active fraction ECF and Cu-B were performed in 6-8 weeks old male *Swiss albino* mice as per protocol (IAEC/669/RUBY/2018 and IAEC/849/Ruby/2021) approved by the Institutional Animal Ethics Committee, Rajiv Gandhi Centre for Biotechnology.

Acute toxicity: Doses of 0, 0.25, and 1.25mg/Kg of active fraction ECF and 0, 0.05, and 0.15 mg/Kg of Cu-B were given as a single intraperitoncinsiseal injection to each group of 5 animals. The mice were observed continuously for 1 h, for any gross behavioral changes and death, and then intermittently for the next 6 h and 24 h. The behavioral parameters monitored were convulsion, hyperactivity, sedation, grooming, food and water intake, etc. The animals were observed routinely for the next 7 days from the day of treatment, after which, the animals were euthanized. The liver tissue was verified by histopathologic evaluation using H&E staining and the serum was used to perform Liver Function Test (14).

Sub-chronic toxicity: Doses of 0, 0.25, and 1.25mg/Kg of active fraction ECF and 0, 0.05, and 0.15 mg/Kg of Cu-B were given as intraperitoneal injections on alternate days for 3 months. Each group consists of 5 animals. Animals were euthanized after 3 months. Liver tissues were collected and toxicity was measured as described above.

In Vivo Xenograft Model

A melanoma xenograft study was performed in male NOD-SCID mice following the approved guidelines of the Institute Animal Ethics Committee of Rajiv Gandhi Centre for Biotechnology, Thiruvananthapuram (IAEC/818/RUBY/2020). A375 cells ($1X10^6$) were subcutaneously injected into the flank region of the mice. 5 days post the cell injection, the animals were divided into 3 groups. Cu-B being hydrophobic was encapsulated in the liposomal formulation, which was prepared by vacuum rotary evaporation of a mixture of 1 mg Cu-B, 9 mg phosphatidylcholine, and 1.16 mg cholesterol, dissolved in a 3:1 mixture of chloroform and methanol. 0.05 mg/Kg of liposomal Cu-B (corresponding to the IC50 in A375), was prepared by dissolving the liposome in 1X PBS and administered intradermally and intraperitoneally to the animals in groups 2 and 3 respectively, on alternative days for a period of 4 weeks. Group 1 was kept as vehicle control. The tumor size was measured weekly and the corresponding tumor volume was calculated as per the formula, (length x $width^2$)/2 (15). At the end of the experiment, the animals were euthanized and tumor tissues were collected.

Histology and Immunohistochemistry

The tumor and liver tissues from mice were fixed and sectioned and stained using Hematoxylin and eosin (H & E). Immunolocalization of specific proteins in the tissue sections was done using Poly Excel HRP/DAB detection system universal kit for mouse and rabbit primary antibodies as per the manufacturer's protocol. The tissues were subjected to an immunohistochemical analysis against, PCNA (Proliferating Cell Nuclear Antigen), B-RAF^{V600E}, p-MEK1/2, p-ERK1/2, p-STAT3, c-MYC, Cyclin-D1 and β-Catenin. All the immunohistochemistry images were taken in DMi8 Inverted Fluorescence Research Microscope with a DMC 2900 Digital Camera.

TUNEL Assay

TUNEL assay was performed to detect apoptosis in formalin-fixed, paraffin-embedded xenograft tumor tissue sections using Dead End Colorimetric TUNEL System (Promega) following the manufacturer's instructions.

Statistical Analysis

For the flow cytometry, data analysis was performed using the BD FACS Diva software version 5.0.2. The statistical analysis was performed using Graph Pad Prism software Inc. (version6.0, San Diego, CA, USA) and the quantification of Western blot was carried out using ImageJ software, version1.8.0. Statistical significance was defined as $p < 0.05$. The error bars represent SD, taken from three independent experiments.

RESULTS

ECF, a Bioactive Fraction From *C. epigaeus* Rhizome Exhibits Anti-Melanoma Activity

To investigate the potential anti-cancer ability of *C. epigaeus*, the rhizome part was preferred, due to its multiple applications in traditional medicine against various ailments. A polarity gradient extraction of *C. epigaeus* dried rhizome powder was performed and the cytotoxicity analysis using the three organic extracts (hexane, ethyl acetate, and methanol) was conducted in cancer cell lines of various tissue origins. The assessment of cell viability in the indicated cancer cells demonstrated the ethyl acetate extract as the most potent fraction which exhibited substantial cytotoxicity with an IC50 around 0.05μg/ml, particularly in the melanoma cell line, A375. The methanol extract also possessed the ability to induce death, most notably in A375 (IC50 of 0.15 μg/ml) whereas the hexane fraction was found to be non-toxic to all cell lines (**Figures 1A–C**). The ethyl acetate extract was considered for further studies to isolate and purify one or more potential anticancer principle(s). We subjected the ethyl acetate extract to silica gel column chromatography, which yielded a bioactive fraction, and was designated as "ECF" [the isolation of ECF has been detailed in the methodology section]. We tested the cytotoxic ability of ECF against various human cancer cell lines using a cell viability assay. The melanoma cell line, A375 displayed maximal sensitivity towards ECF (IC50-0.015 μg/ml) (**Figure 1D**). To validate the anti-melanoma efficacy of ECF, we tested it on different melanoma cell lines viz. A375, SK-MEL-2, and SK-MEL-28. Interestingly, all the melanoma cell lines selected for this study displayed considerable sensitivity towards ECF. The cell line, A375 was repeatedly observed as the most sensitive to ECF and was picked for further studies (**Figure 1E**). Prior to the studies in A375, we tested the biological safety of the ECF, by treating normal skin fibroblast cells, FS, and found that the IC50 concentration of ECF in these cells was three times higher than that in A375 cells (**Figure 1F**). We further studied the ability of ECF to inhibit the proliferative propensity of A375 cells using a clonogenic assay. The widely studied bio-active phytochemical curcumin (9 μg/ml), was used as a positive control. The result indicated a significant reduction in the number and size of the colonies formed, demonstrating the anti-melanoma potential of ECF (**Figure 1G**). The results suggest *C. epigaeus*-derived ECF as a highly efficacious bioactive fraction potent to kill melanoma cells.

ECF Induces Caspase-Dependent Apoptosis in Melanoma Cells

Next, to analyze the mode of cell death induced by ECF in melanoma, we tested the efficacy of ECF to induce apoptosis using FITC-Annexin V/PI staining. ECF treatment led to a significant hike in the number of FITC/PI+ apoptotic cells in comparison to the untreated control (**Figure 2A**). The extent of apoptosis induced by ECF was further estimated by FACS analysis of the Annexin V–FITC/PI double-stained cells. The apoptotic cell population was increased from 2.4% to 6.3% and 34.3% respectively when treated for 16 h with 0.01 μg/ml and 0.015 μg/ml of ECF. A375 cells treated with curcumin (9 μg/ml) were used as a positive control (**Figure 2B**). We further tested the cleavage of procaspases, a marker of the apoptosis program, using immunoblotting. Apoptosis is mediated by cysteine proteases termed caspases, which are functionally classified into initiators and executioners. Initiator caspases 8 and 9, activated by intrinsic or extrinsic apoptotic stimuli, subsequently activate executioner caspases, which in turn cleave the cellular death substrates, eventually resulting in apoptosis. ECF treatment led to the cleavage of the initiator caspase 9 (**Figure 2C**) while caspase 8, associated with extrinsic stimuli, remained unaffected (**Figure 2D**). Further, we tested the activation of BID, a specific proximal substrate of caspase 8 in the death receptor-mediated extrinsic apoptotic signaling pathway and a mediator of caspase 8-induced mitochondrial damage (16). Strikingly, we noticed an activation of BID upon ECF treatment, even in the absence of caspase 8 activation (**Figure 2E**). Previous reports indicate the ability of initiator caspase 10 to cleave and activate BID (17). Indeed, we observed a significant reduction in the procaspases 10 level indicating caspase 10 activation (**Figure 2E**) by the fraction. Furthermore, ECF induced the cleavage of executioner caspases, 7and 3, as well as the substrate of executioner caspases, Poly ADP-Ribose Polymerase (PARP) (**Figures 2F–H**). Together, these data confirm that the cytotoxicity induced by ECF in melanoma cells involves caspase-dependent apoptosis.

ECF is Pharmacologically Safe, *In Vivo*

To ascertain the biological safety of ECF, we conducted acute and sub-chronic toxicity studies in *Swiss albino* mice. For this, we did a mass spectrometry analysis of the ECF fraction and calculated the optimal dose using the Castanas method, taking the molecular weight corresponding to the base peak obtained as 581, which corresponds to a sodium adduct of 558, assuming that this compound is responsible for the cytotoxic effect of the fraction (18). We selected two doses of ECF, the optimal dose and five times the optimal dose [0.25 and 1.25 mg/kg], for the drug-induced toxicity evaluation. The murine blood was collected to quantitate AST, ALT, and ALP, the elevated levels of which are indicative of liver toxicity. Histopathological analysis of mice liver tissues was also performed using H & E staining. Notably, no behavioral changes such as convulsion, hyperactivity, sedation, grooming, food and water intake, etc. were observed in the mice upon ECF treatment. In addition, no significant changes were observed in the body weight of the animals. The serum analysis, as well as histopathological evaluation of liver sections of the mice studied, did not show a significant toxicological change in any of the parameters studied (**Figures S1A–F**), indicating that ECF is pharmacologically safe *in vivo*.

The Triterpenoid, Cucurbitacin B, Is the Anticancer Principle in ECF

We further focused on the isolation, purification, and identification of the anticancer compound in ECF. Column chromatography of

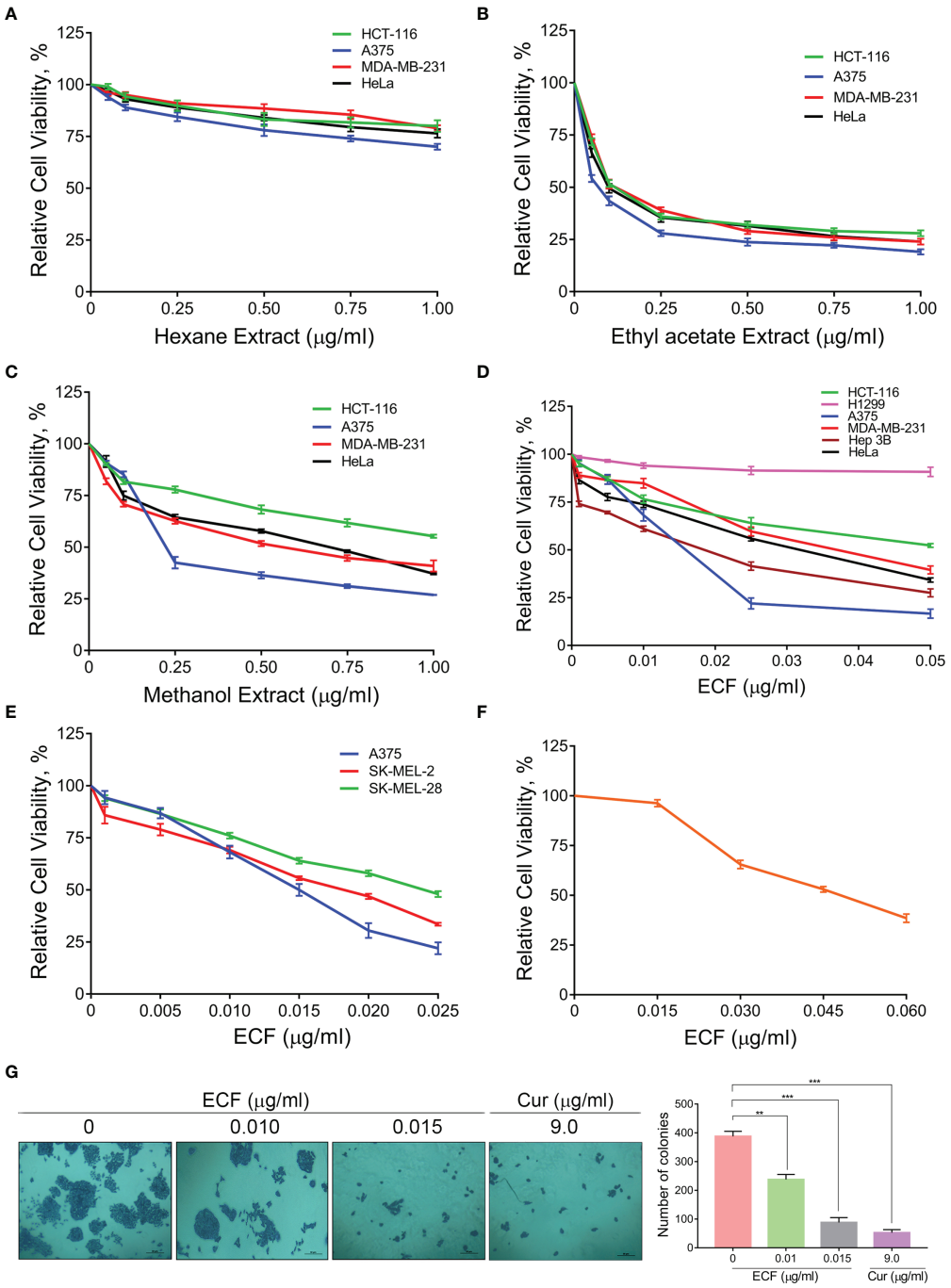

FIGURE 1 | ECF, a bioactive fraction of *C. epigaeus* rhizome induces cytotoxicity in melanoma cells **(A–C)** Cytotoxicity assessment of the *C. epigaeus* rhizome-derived organic extracts on cancer cells of various tissue origins. **(D)** Cell viability analysis upon treatment by ECF bioactive fraction as assessed in various cancer cell lines. **(E, F)** Cytotoxicity induced by ECF on melanoma cell lines in comparison to normal skin fibroblast, FS cells. **(G)** ECF inhibits the proliferative potential of A375 cells. Data are representative of three independent experiments (Mean±SEM) and P-values are calculated using one way ANOVA. ***P ≤0.001, **P ≤0.01 and ns ≥ 0.05.

ECF led to a major product with polar characteristics. An initial observation by ^{1}H NMR indicated a triterpene pattern with polar functional groups for the isolated compound (**Figure 3A**). The compound was found to have structural similarities with cucurbitacins, which are abundantly oxygenated triterpenes. Initially, an HR-ESI-MS analysis was carried out to match the list of already isolated cucurbitacins from the family of Cucurbitaceae. The molecular formula of the *C. epigaeus*-derived cucurbitacin was determined as $C_{32}H_{46}O_8$ as per the HR-ESI-MS analysis which exhibited ions at 581.3113 (M+Na)+ along with a corresponding

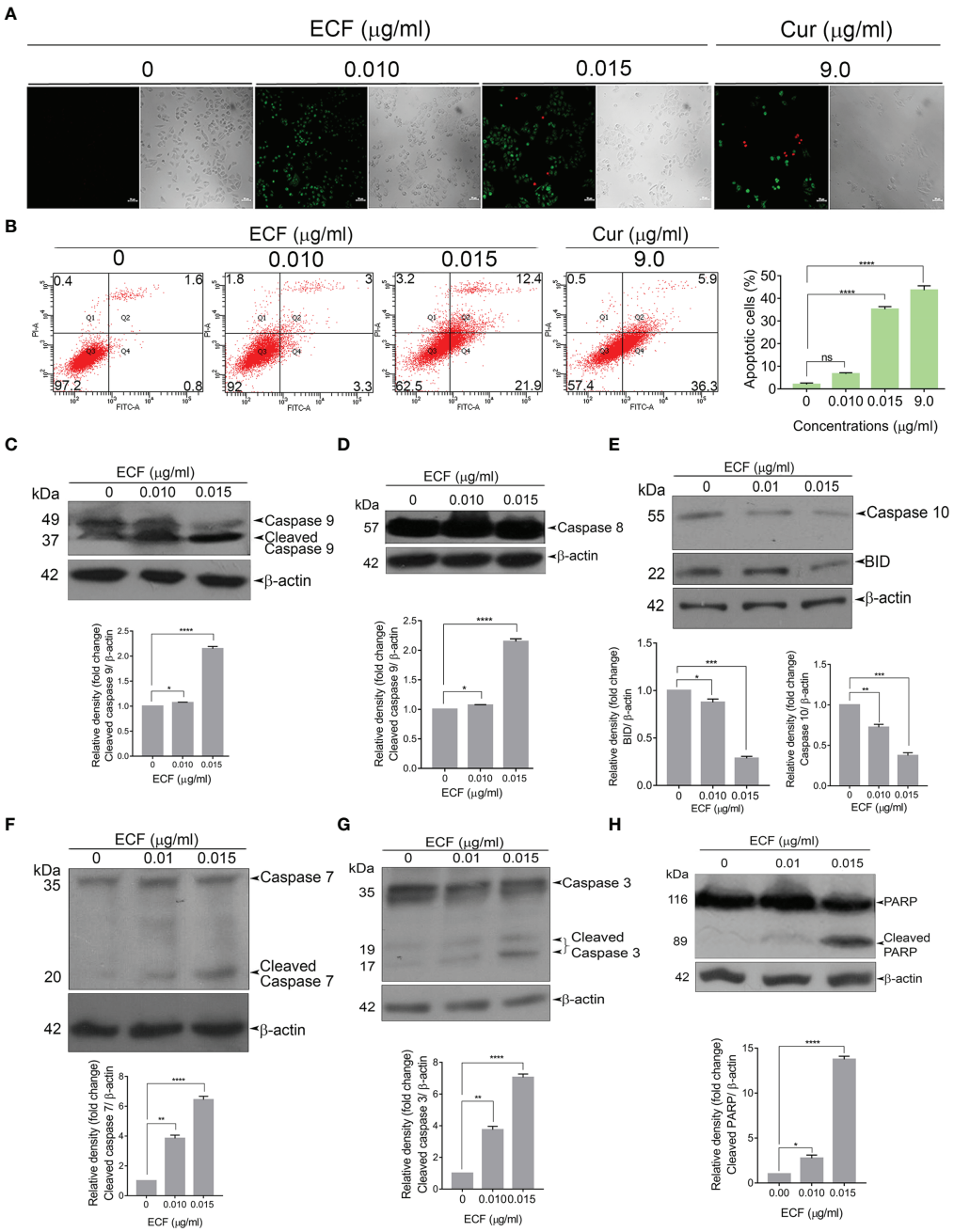

FIGURE 2 | ECF triggers apoptotic mode of cell death in melanoma **(A, B)** ECF induces apoptosis in A375 cells as assessed by Annexin/PI staining, and was quantitated by FACS analysis. **(C–H)** ECF potentiates the activation of caspases and cleavage of PARP in A375 cells as analyzed by immunoblotting. Data are representative of three independent experiments (Mean±SEM) and P-values are calculated using one way ANOVA. ****P ≤0.0001, ***P ≤0.001, **P ≤0.01, *P ≤0.1and ns ≥ 0.05.

dimer peak at 1139.6336 (2M+Na)+ (**Figure 3B**). The ^{13}C NMR exhibited three ketone functional groups at δC 202.50, 212.19, and 213.08 ppm, and one among these three carbonyls is a part of α, β-unsaturated system that appears at δH 6.4 (d, J = 16.5 Hz) and 7.0 (d, J = 16 Hz) in the ^{1}H NMR (**Figure 3C**). The presence of δC 170.32 indicated the presence of an ester group and the presence of nine methyl groups in ^{13}C NMR. Together, the spectral data indicated the identity of the polar compound as cucurbitacin B (purity 99.99%) (**Figure 3D**). Gratifyingly, the ^{1}H and ^{13}C NMR were found to be in perfect agreement with published literature (**Table S1**) for Cu-B (19). This is the first report indicating the presence of Cu-B from *C. epigaeus*. UHPLC profiling was conducted to ascertain the purity of the isolated Cu-B, which exhibited a peak at 31.8 min at 254 nm. The chromatograms of

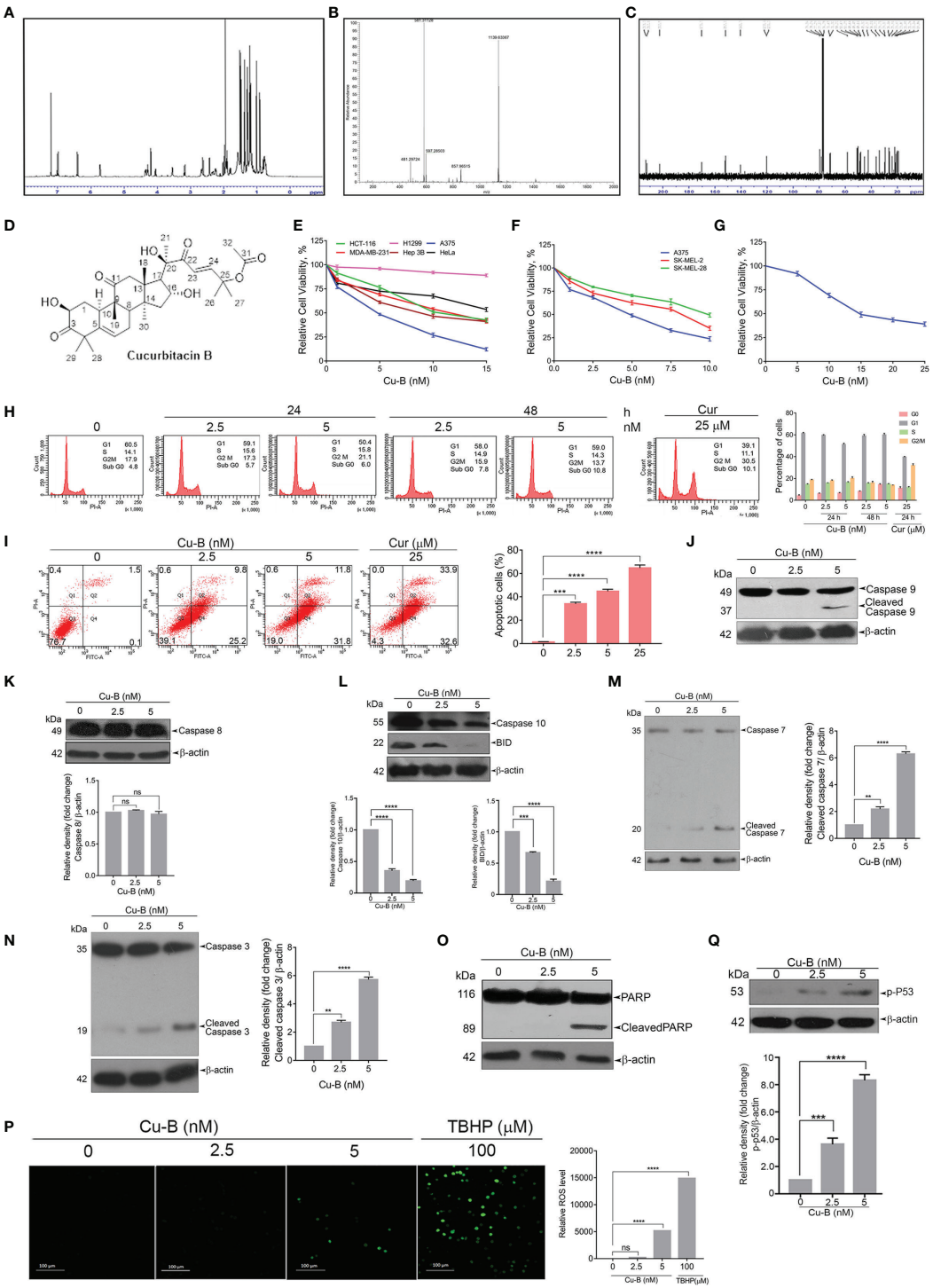

FIGURE 3 | Purification and structural elucidation of Cu-B from ECF fraction of *C. epigaeus* rhizome **(A–D)** ^{1}H NMR, HR-ESI-MS, ^{13}C NMR data, and structure of *C. epigaeus*-derived Cu-B. **(E–G)** Cytotoxicity assessment of Cu-B in melanoma cell lines and normal fibroblast cells **(H)** Cu-B does not affect any phases of the cell cycle in A375 cells as demonstrated by flow cytometry. **(I)** The extent of apoptosis induced by Cu-B was quantitated by Annexin V/PI FACS analysis **(J–O)** Cu-B treatment induces activation of caspases and cleavage of PARP in A375 cells as analyzed by immunoblotting. Cu-B promotes the cleavages of caspase-10 and Bid as analyzed by immunoblotting. **(P)** ROS production in response to Cu-B treatment in A375 cells as detected by fluorescence microscopy. **(Q)** Cu-B potentiates p53 activation in A375 cells as analyzed by immunoblotting. Data are representative of three independent experiments (Mean±SEM) and P-values are calculated using one-way ANOVA. ****P ≤0.0001, ***P ≤0.001, **P ≤0.01 and ns ≥ 0.05.

Cu-B and its presence in ECF were confirmed by spiking the bioactive fraction with pure cucurbitacin B (**Figures S2A, B**).

Cucurbitacin B Possesses Potent Anti-Melanoma Activity

Owing to the potent anticancer activity of ECF against melanoma cell lines, we sought to explore the anti-melanoma efficacy of Cu-B *in vitro*. In line with the observation in ECF fraction (refer to **Figure 1D**) we observed increased sensitivity of the melanoma cells to Cu-B in comparison to cancer cells of other tissue origins (**Figure 3E**). Melanoma is classified into several molecular subgroups based on genomic alterations, among which B-RAF and NRAS mutated melanomas are the most common (20). Therefore, we selected melanoma cell lines, which belong to the two molecular subgroups, with B-RAF/NRAS mutation status viz. A375 cells [B-RAF mutation], SK-MEL-2 [NRAS mutation] and SK-MEL-28 [B-RAF mutation]. Cu-B induced potent cytotoxicity in all the three cell lines chosen for the study, irrespective of the mutation status (**Figure 3F**). Again A375 cell line, which exhibited maximal sensitivity to Cu-B (IC50-5nM), was selected for further studies. To confirm the biological safety, we tested the cytotoxic effect of Cu-B on normal skin fibroblasts and the IC50 concentration was found to be thrice that observed in the melanoma cell line, A375 (**Figure 3G**).

To delineate the mode of cell death induced by Cu-B in A375 cells, we analyzed whether Cu-B induces any cell cycle-specific effects by flow cytometry, and it was found that Cu-B did not interfere with any phases of the cell cycle even after prolonged treatment for 48 h (**Figure 3H**). Notably, there was an augmentation in the number of cells at the sub G0 phase, which was an indication of apoptosis. To quantitate the extent of apoptosis induced by Cu-B, we conducted FACS analysis of the Cu-B treated, Annexin V–FITC/PI double-stained cells. It was interesting to see that the apoptotic cell population increased from 1.6% to 35% and 43.6% respectivelywhen treated with 2.5 nM and 5 nM of Cu-B for 16 h. A375 cells treated with 25 μM curcumin were used as positive control (**Figure 3I**). To ascertain the Cu-B-mediated apoptotic mode of cell death in melanoma, we performed immunoblot analysis focusing on cleaved activated caspases and PARP, which are effective markers of apoptosis. We found a dose-dependent cleavage of the initiator caspase 9 as well as the effector caspases, 3 and, 7 (**Figures 3J, M, N**). Interestingly, Cu-B failed to induce the cleavage of caspase 8, as observed upon ECF treatment (**Figure 3K**), and in line with the data obtained with ECF, we observed activation of caspase 10 and BID in A375 cells indicating the involvement of the death receptor pathway in Cu-B induced apoptosis (**Figure 3L**). Furthermore, Cu-B triggered a noticeable cleavage of PARP, marking apoptotic cell death (**Figure 3O**). Previous reports have demonstrated the ability of chemotherapeutic drugs to induce apoptosis in cancer cells by triggering DNA damage as a result of increased ROS production (21). To investigate whether Cu-B elevates ROS production in A375 cells, a ROS-sensitive H2DCF-DA assay was employed. Cu-B treatment in A375cells triggered the oxidation of H2DCF-DA by ROS to dichlorofluorescein (DCF), which further led to the generation of green fluorescence, the intensity of which was quantified by confocal microscopy (**Figure 3P**). Moreover, we observed an increase in the phosphorylation of p53 in response to Cu-B (**Figure 3Q**). These results indicate that Cu-B augments ROS production in A375 cells, subsequently leading to intrinsic apoptosis, signaled by DNA damage-induced p53 signaling. Together, our data demonstrate the cell death mechanism through which *C. epigaeus*-derived Cu-B targets melanoma cells with the involvement of extrinsic and intrinsic apoptotic pathways.

Cucurbitacin B Targets MAPK Signaling in Melanoma

The constitutive activation of RAS-RAF-MEK-ERK signaling axes has been widely implicated in the initiation and development of melanoma *via* the activation of mutant RAF and RAS proteins (22). We tested the effect of Cu-B on MAPK signaling firstly by analyzing the expression status of B-RAF protein in A375 cells, which endogenously harbor a B-RAF mutation. The result revealed a significant down-regulation of the mutant B-RAF^{V600E} protein (**Figure 4A**). Further, we looked for the activation of MEK and ERK by immunoblot analysis of MEK1/2 and ERK1/2 phosphorylation. Notably, Cu-B treatment ablated the constitutive phosphorylation of MEK1/2 and ERK1/2 (**Figures 4B, C**), indicating Cu-B-mediated suppression of B-RAFV600E downstream kinase activity. We further analyzed the status of phospho-STAT3, a major transcription factor that stays downstream of the RAF pathway and is involved in maintaining cell proliferation and survival in melanoma (23). Active ERK is reported to phosphorylate Ser^{727} residue of STAT3 (24). We observed a significant down-regulation in the levels of phospho-STAT3 upon Cu-B treatment of A375 cells (**Figure 4D**). We also tested the effect of Cu-B on the expression statuses of c-MYC, and Cyclin-D1, the major downstream targets in the MAPK pathway. Notably, the Cyclin-D1 protein levels remained unaltered, however, a down-regulation in the c-MYC levels was observed (**Figure 4E**). In addition, we analyzed the expression levels of MITF-M, and β-catenin in A375 cells, however, Cu-B treatment did not affect their statuses in melanoma (**Figure 4F** and **Figure S4A**). The serum analysis, as well as histopathological evaluation of liver sections from Cu-B-treated mice did not reveal any noticeable toxicological changes in any of the parameters tested (**Figures S3A-F**), indicating the pharmacological safety of Cu-B. Collectively, our data demonstrate the key factors which are targeted by Cu-B to exert its potency against melanoma.

Cucurbitacin B Suppresses Melanoma Growth in a NOD-SCID Tumor Model

The anti-melanoma efficacy of Cu-B was tested *in vivo* using a xenograft model of human melanoma in NOD-SCID mice using A375 cells. The development of the A375-induced tumor and drug treatment regimen in the NOD-SCID murine model has been detailed in the methodology. Following the regimen, the tumors from the animals were excised for further analysis. Firstly, we observed that the ID administration of Cu-B was

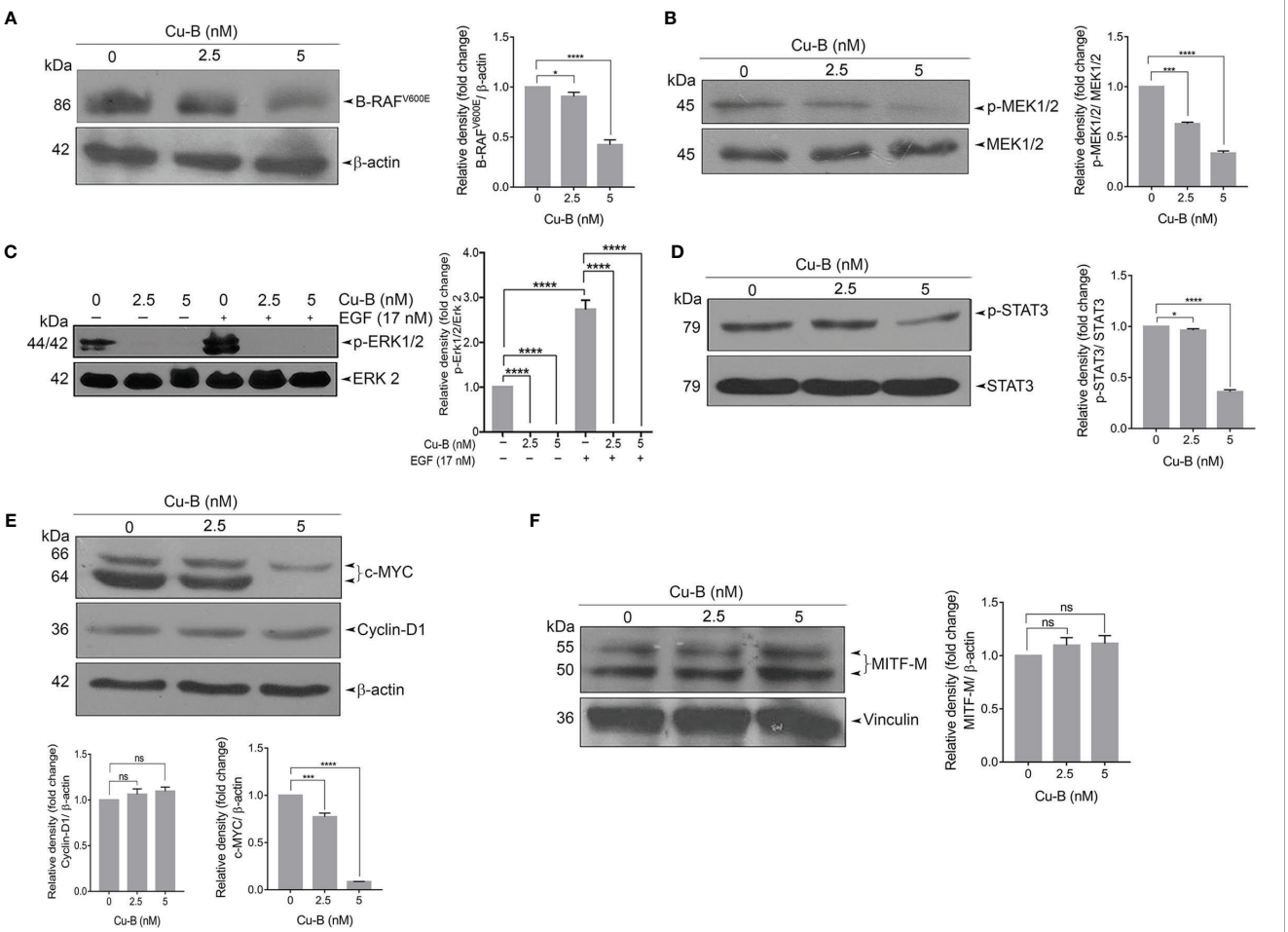

FIGURE 4 | The effect of Cu-B on the key survival signals in melanoma **(A, B)** Cu-B diminishes B- RAF^{V600E} and p-MEK1/2 expressions in A375 cells. **(C)** Cu-B down-regulates the constitutive and EGF-induced phosphorylation of ERK1/2 in A375 cells. **(D, E)** Cu-B reduces the expressions of p-STAT 3 and c-MYC, but not Cyclin-D1, in A375 cells. **(F)** Cu-B treatment unalters MITF-M levels in A375 cells. Data are representative of three independent experiments (Mean±SEM) and P-values are calculated using one-way ANOVA. ****P ≤0.0001, ***P ≤0.001, *P ≤0.1and ns ≥ 0.05.

more effective, as evidenced by the significant reduction in tumor volume, compared to that of IP drug administration (**Figures 5A, B**). The body weight of the animals was routinely checked and no significant change between the groups was observed (**Figure 5C**). Histopathological analysis indicated substantial destruction of tumor cells in Cu-B-treated mice-derived tissues, which correlated with the considerable tumor reduction (**Figure 5D**). Immunohistochemical analysis for the expression of PCNA in tumor sections derived from Cu-B-treated (ID) animals showed a significant decline in the PCNA expression, which authenticated the ability of Cu-B to inhibit tumor cell proliferation. Induction of apoptosis in the tissue sections in response to Cu-B was confirmed by the TUNEL assay (**Figures 5E, F**).

The decisive role of the MAPK pathway as observed *in vitro* was validated in the *in vivo* tumor samples. We observed a significant down-regulation in the expression of the key components of the MAPK pathway, p-ERK1/2, and p-MEK1/2, in the lysates of Cu-B-treated mice tissues in comparison to the vehicle control (**Figures 5G, H**). In line with this observation, a strong inhibition in the expression of c-MYC and p-STAT3, a critical downstream target of ERK, supported our *in vitro* data (**Figure 5I**). However, MITF-M, Cyclin-D1, and β-catenin levels were unaltered upon Cu-B treatment (**Figure 5J** and **Figures S4B, C**). The immunohistochemical analysis of the tissue sections authenticated the results obtained from immunoblot analysis (**Figure 5K**). Together, our studies involving a murine model of human melanoma indicate the *in vivo* therapeutic efficacy of Cu-B against melanoma by targeting the MAPK pathway.

DISCUSSION

Systematic analysis of the bioactive compounds derived from plants of ethnobotanical significance has paved the way for novel

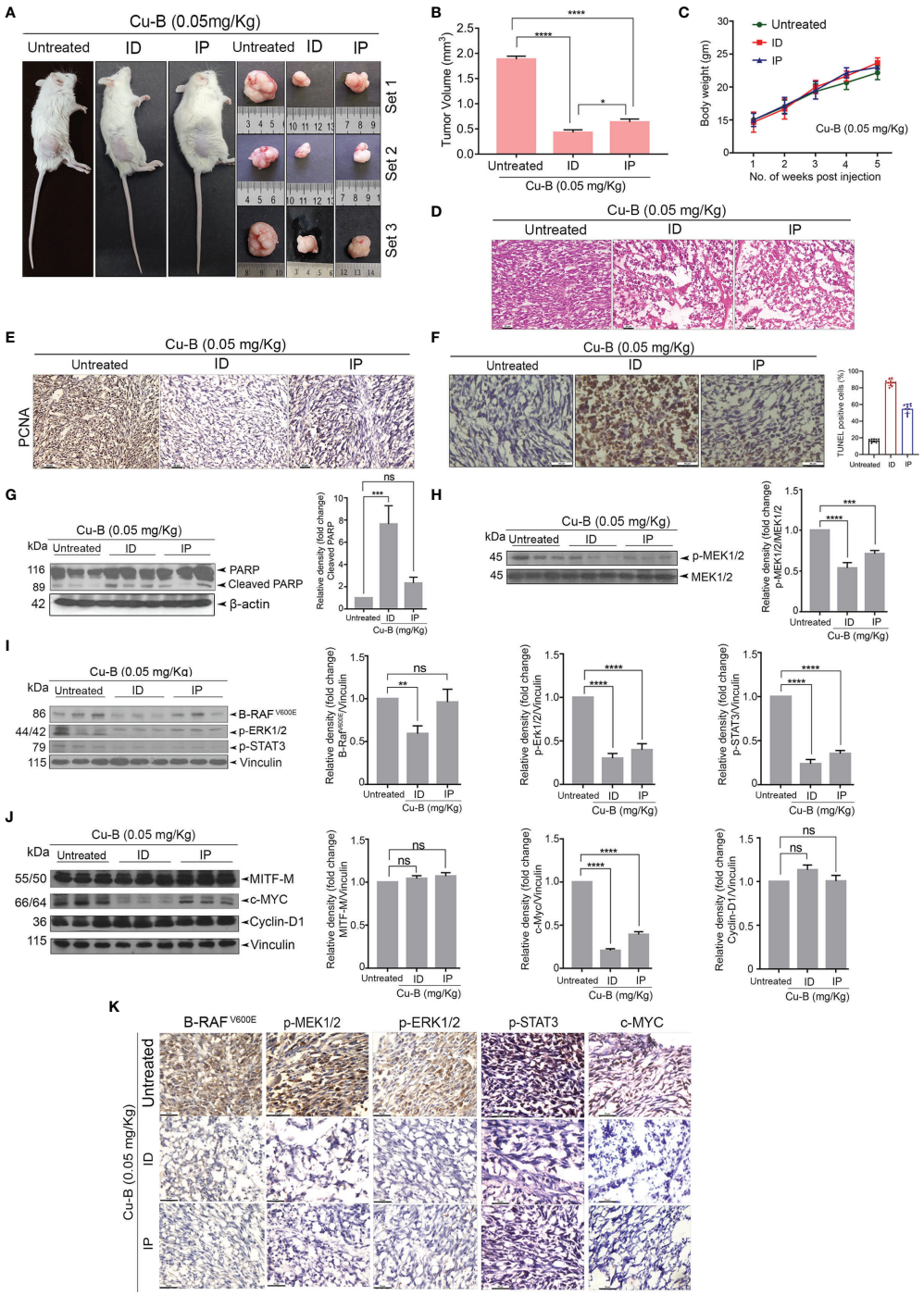

FIGURE 5 | Cu-B suppresses tumor development in a NOD-SCID murine model of human melanoma **(A)**. Representative photographs of Cu-B treated NOD-SCID mice bearing A375 xenografts and the excised tumors. **(B)** Cu-B represses the tumor volume in Cu-B treated melanoma-bearing mice. **(C)** Cu-B treatment unalters the bodyweights of mice throughout the study period. **(D)** Histopathological evaluation of tumor tissue isolated from mice groups. Formalin-fixed cryosections were H and E stained. **(E)** IHC analysis on the expression of PCNA in tumor tissues of mice groups**. (F)** The apoptosis induced by Cu-B in the tumor tissues was confirmed by TUNEL assay **(G)** Immunoblot analysis demonstrating enhanced cleavage of PARP in the tumor lysates of Cu-B treated mice. **(H–J)** Immunoblot analysis showing the effect of Cu-B on key survival signals in melanoma, B- RAF^{V600E}, p-MEK1/2, p-ERK1/2, p-STAT3, c-MYC, Cyclin-D1, and MITF-M, as evidenced in the tumor lysates. **(K)** IHC analysis on the expression of B- RAF^{V600E}, p-MEK1/2, p-ERK1/2, p-STAT3, and c-MYC in tumor tissues of mice groups. Data are representative of three independent experiments (Mean±SEM) and P-values are calculated using one-way ANOVA. ****P ≤0.0001, ***P ≤0.001, **P ≤0.01, *P ≤0.1 and ns ≥ 0.05.

lead structures and has largely progressed as drugs against many diseases including cancer (25). The present study was designed to explore the potential anti-cancer activity of *C. epigaeus*, focusing on the rhizome part which is widely being utilized in ethnomedicine. Our study also intended to isolate the principle, if any, which contributes to the anticancer potential of *C. epigaeus* rhizome. Our studies revealed the potent anticancer property of the ethyl acetate extract of *C. epigaeus* rhizome and isolated a cytotoxic fraction, ECF, which yielded Cu-B as the bio-active ingredient. We used cancer cell lines of various tissue origins to screen their sensitivity towards organic extracts of the rhizome, ECF and Cu-B. Amongst the cancer cell lines of various tissue origins, which we employed for the drug screening, the melanoma cell line, A375 was found to be the most sensitive towards ECF and Cu-B. Hence, we tested the cytotoxic potential of Cu-B in melanoma cell lines belonging to two molecular subgroups, based on the difference in their mutation status in RAS and RAF genes. Moreover, in normal skin fibroblast, Cu-B induced 50% cell death only at a concentration three times than in the melanoma cell line.

A literature survey shows that there are up to 40 known cucurbitacins or their derivatives which are essentially classified into 12 groups. Group B cucurbitacins have been shown to possess potent anticancer activity in a variety of cancers *in vitro* and *in vivo* (26). However, this is the preliminary report demonstrating the molecular mechanism underlying the efficacy of Cu-B against human melanoma *in vitro* and *in vivo*. In the melanoma cell line A375, Cu-B induced potent cytotoxicity with an IC50 value of 5 nM. Moreover, analysis of Cu-B induced cytotoxic mechanism in A375 cells showed that the drug potentiates apoptosis involving both the intrinsic and extrinsic pathways. Activation of initiator and executioner caspases, 9 and 3 respectively as well as cell-surface death receptor-mediated caspase 10 and Bid underscore the significant role of mitochondrial pathway in Cu-B induced apoptosis. Our investigation of the underlying reason for the augmented sensitivity of melanoma cells to Cu-B revealed that the drug down-regulates MAPK signaling, involved in cell proliferation.

Melanoma is a subtype of skin cancer, partly driven by the MAPK signaling pathway through RAS-RAF-MEK-ERK signaling, which concludes in the activation of ERK, and regulates p-STAT, MITF-M, c-MYC, and other transcription factors, resulting in alteration of cell proliferation and survival. The most prevalent gene mutations identified in melanoma are B-RAF, RAS, and NF-1, all of which cause constitutive MAPK signaling (20). Evaluation of the cytotoxic potential of Cu-B in melanoma cell lines viz. SK-MEL-2 and SK-MEL-28 with N-RAS and B-RAF mutation respectively revealed that the compound is highly efficacious against the melanoma cell lines, irrespective of the mutation status. In fact, elucidation of the key mutations that drive melanoma progression has resulted in targeted therapies using small-molecule inhibitors of B-RAF and MEK either alone or in combination and has made significant progress in the treatment of melanoma (20, 27). However, acquired resistance poses serious limitations to the success of these small-molecule kinase inhibitors in the clinic (12, 28). A previous study conducted in the human melanoma xenograft model had shown that melanoma cells can transcriptionally up-regulate the B-RAF molecule to compensate for the inhibition by, the B-RAF^{V600E} inhibitor, vemurafenib (29). The present study demonstrates the efficacy of Cu-B, in suppressing the expression of mutant B-RAF^{V600E} protein as well as inhibiting the B-RAF^{V600E} kinase activity as evidenced by inhibition of

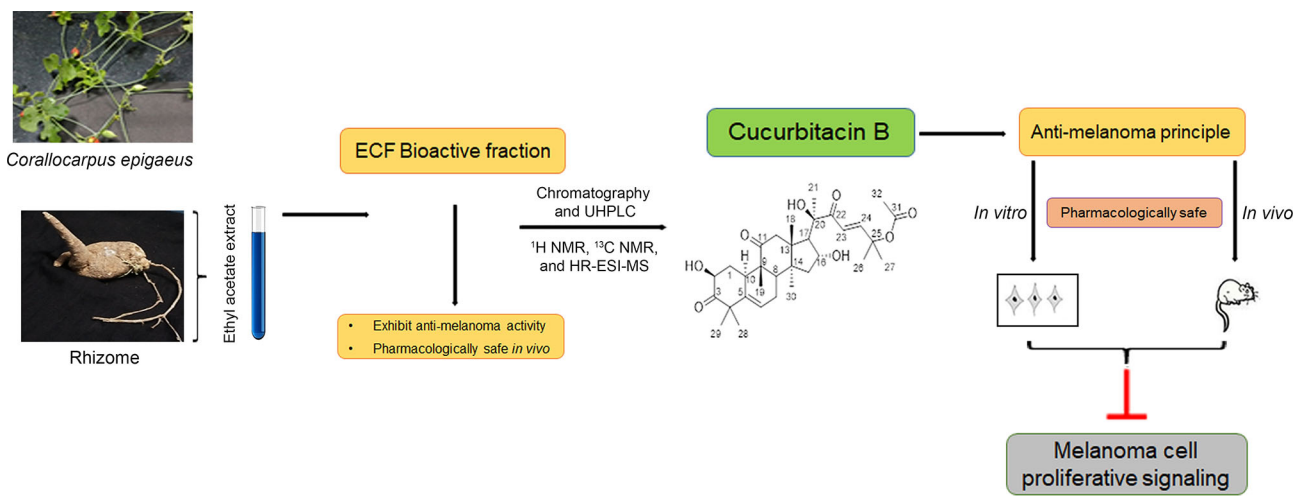

FIGURE 6 | Schematic representation highlighting the isolation process and characterization of the anti-melanoma principle, Cucurbitacin B from the rhizome of *C. epigaeus*. Briefly, ethyl acetate extract of *C. epigaeus* rhizome, was fractionated using column chromatography, which yielded purified Cu-B and the isolated anti-cancer principle was characterized and verified using ^{1}H NMR, ^{13}C NMR and HR-ESI-MS analysis. *In vitro* and *in vivo* studies validated the potential of Cu-B to attenuate melanoma by targeting critical proliferative signals. The pharmacological safety of ECF and ECF-derived Cu-B were assured in *Swiss albino* mice.

MEK1/2 phosphorylation. Moreover, Cu-B inhibited both the constitutive as well as EGF-induced ERKphosphorylation, indicating the role of MAPK signaling in regulating the chemotherapeutic potency of Cu-B against melanoma. As RAF inhibitors have been found to relieve the ERK1/2- dependent feedback inhibition of MAPK signaling, inhibition of MEK1/2 along with B-RAF is considered a promising strategy in the treatment of B-RAF -mutated melanoma and MEK inhibition has proved to be beneficial for NRAS-mutated melanoma (30–32). Indeed, molecular docking studies have revealed that cucurbitacins show a significant binding towards the crystal structure of RAF and MEK, comparable to that of the standard B-RAF and MEK inhibitors, imparting cucurbitacins the ability to inhibit the ERK activation in melanoma cells (33). In line with the ability of Cu-B to inhibit MAPK signaling, we also demonstrate the efficacy of Cu-B in down-regulating the downstream effector transcription factors of ERK, such as p-STAT-3 and c-MYC in A375 cells. In melanoma cells harboring B-RAF^{V600E} mutation, MITF-M down-regulated by B-RAF signaling is considered a crucial event for the progression of melanoma (34). However, our study did not find any significant variation in the expression of MITF-M in response to Cu-B at the concentrations investigated. Furthermore, our study using a tumor xenograft model in NOD-SCID mice harboring the B-RAF^{V600E} mutated A375 cells, resulted in substantial inhibition of tumor growth without any apparent toxicity and corroborated our *in vitro* data on the molecular mechanism underlying the anti-melanoma activity of Cu-B. Taken together, the data highlights the potent anti-melanoma activity of Cu-B, involving potentiation of apoptotic cell death and suppression of proliferation by the inhibition of MAPK signaling. Studies are in progress to elucidate the role of Cu-B in modulating key mutations in other genes which cause de-regulated MAPK signaling, viz. RAS and NF-1. Further, the anti-melanoma efficacy of Cu-B has to be evaluated using patient-derived melanoma xenograft model and using patient-derived melanoma cells so that the compound can be effectively translated from bench to bedside.

The current study, which explains the derivation of the anti-cancer principle, Cu-B, from *C. epigaeus* and its prospective anti-melanoma efficacy is briefed in a schematic representation (**Figure 6**). To summarize, we report a hidden anti-cancer property displayed by Cu-B, purified from the Cucurbitaceae succulent, *C. epigaeus*, against melanoma. This is the first study reporting the isolation and identification of cucurbitacin B from *C. epigaeus* and also demonstrating its anti-melanoma potential, *in vitro* and *in vivo*. Our study demonstrates the necessity of advancing Cu-B, as a candidate drug against melanoma, which is the most aggressive and treatment-resistant cancer, and accounts for 75% of all skin cancer-related deaths (30).

DATA AVAILABILITY STATEMENT

The original contributions presented in the study are included in the article/**Supplementary Material**. Further inquiries can be directed to the corresponding authors.

ETHICS STATEMENT

The animal study was reviewed and approved by 326/GO/ReBiBt/S/2001/CPCSEA.

AUTHOR CONTRIBUTIONS

Conception and design: RA and SB. Development of methodology: RA, SB and RL. Acquisition of data: AS, GV, LN, SA, MS, TR, and CK. Data editing and Figure arrangement: NH and VL. Isolation Identification and characterization of the compound: RL and MR. Verification of Histopathological data: SS. Review and editing of the manuscript: RA, SB, and NA. All authors contributed to the article and approved the submitted version.

FUNDING

This work was supported by the Institutional fund by DBT, Government of India, and extramural grant by KSCSTE Thiruvananthapuram, Kerala to RA (Grant number: 025/SRSLS/2014/CSTE), and extramural grant by KSCSTE Thiruvananthapuram, Kerala to SB (Grant number: 025/SRSLS/2014/CSTE).

ACKNOWLEDGMENTS

We acknowledge KSCSTE, DST-SERB, and DBT, Government of India for funding. We acknowledge the immense help provided by Jannet S for the successful completion of this work. We thank Dr. Vishnu Sunil Jaikumar, Dr. Archana S, and Dr. Arya Aravind for the help rendered in animal work. We also acknowledge the immense help provided by the RGCB Animal house facility and Instrumental facility for the successful completion of the experiments.

SUPPLEMENTARY MATERIAL

The Supplementary Material for this article can be found online at: https://www.frontiersin.org/articles/10.3389/fonc.2022.903832/full#supplementary-material

REFERENCES

1. Kirtikar K, Basu B. Indian Medicinal Plants. *Indian Med Plants*. Allahbad, India: Lalit Mohan Basu (1935).
2. Dunnill PM, Fowden L. The Amino Acids of Seeds of the Cucurbitaceae. *Phytochemistry* (1965) 4(6):933–44. doi: 10.1016/S0031-9422(00)86271-8
3. Gupta J, Ali M, Pillai KK, Velasco-Negueruela A, Pérez-Alonso MJ, Contreras FÓ. The Occurrence of Ishwarane and Ishwarone in the Roof Oil of Corallocarpus Epigaeus Benth. Ex Hook. F. *J Essential Oil Res* (1997) 9 (6):667–72. doi: 10.1080/10412905.1997.9700808
4. Kandasamy S, Chinnappan S, Thangaswamy S, Balakrishnan S. Facile Approach for Phytosynthesis of Gold Nanoparticles From Corallocarbus

Epigaeus Rhizome Extract and Their Biological Assessment. *Mater Res Express* (2020) 6(12):1250c1. doi: 10.1088/2053-1591/ab608f
5. Karthic VM, Poongodi B, Balamurugan S, Shanmugapriya P, Murugesan S, Manjari V, et al. Phytocompound and Heavy Metal Analysis of Purified Corallocarpus Epigaeus Benth. Ex. Hook.(Aagasagarudan Kizhangu) in the Aspect of Siddha System of Medicine. *Int J Appl Bioeng* (2017) 11(2):31–7.
6. Ali M, Gupta J. Chemical Constituents of Corallocarpus Epigaeus Rhizomes. *J Med Aromat Plant Sci* (1996) 18(4):791–4.
7. Dymock W, Warden CJH, Hooper D. *Pharmacographia Indica: A History of the Principal Drugs of Vegetable Origin, Met With in British India* Vol. 3. K Paul, editor. London: Trench, Trübner & Company, ld (1893).
8. Jamuna S, Karthika K, Paulsamy S. Phytochemical and Pharmacological Properties of Certain Medicinally Important Species of Cucurbitaceae Family–a Review. *J Res Biol* (2015) 5(6):1835–49.
9. Banotha CS, Nayakanti D, Nandyalac VN, Orugantic SK, Kanalad JR, Sanakattula S, et al. Evaluation of In-Vitro Anti-Cancer Activity of Ethanolic Extract of Corallocarpus Epigaeus on Chronic Myeloid Leukaemia K562 Cell Lines. *J Compr Pharm* (2015) 2(1):8–13
10. Bhavani M, Leelavathi S. Investigation on *In Vitro* Cytotoxic Activity of a Selected Wild Cucurbitaceae Plant Corallocarpus Epigeaus Against Cancer. *Int J Pharm Sci Res* (2015) 6(8):3554–57. doi: 10.13040/IJPSR.0975-8232.6(8).3554-57
11. Sung H, Ferlay J, Rebecca ME, Siegel L, Laversanne M, Soerjomataram I. Global Cancer Statistics 2020: GLOBOCAN Estimates of Incidence and Mortality Worldwide for 36 Cancers in 185 Countries. *CA: Cancer J Clin* (2021) 71(3):209–49. doi: 10.3322/caac.21660
12. Long GV, Weber JS, Infante JR, Kim KB, Daud A, Gonzales R, et al. Overall Survival and Durable Responses in Patients With BRAF V600-Mutant Metastatic Melanoma Receiving Dabrafenib Combined With Trametinib. *J Clin Oncol* (2016) 34(8):871–8. doi: 10.1200/JCO.2015.62.9345
13. Ahmed MS, Kopel LC, Halaweish FT. Structural Optimization and Biological Screening of a Steroidal Scaffold Possessing Cucurbitacin-Like Functionalities as B-Raf Inhibitors. *ChemMedChem* (2014) 9(7):1361–7. doi: 10.1002/cmdc.201300523
14. Nath LR, Gorantla JN, Joseph SM, Antony J, Thankachan S, Menon DB, et al. Kaempferide, the Most Active Among the Four Flavonoids Isolated and Characterized From Chromolaena Odorata, Induces Apoptosis in Cervical Cancer Cells While Being Pharmacologically Safe. *RSC Adv* (2015) 5(122):100912–22. doi: 10.1039/C5RA19199H
15. Sreekanth CN, Bava SV, Sreekumar E, Anto RJ. Molecular Evidences for the Chemosensitizing Efficacy of Liposomal Curcumin in Paclitaxel Chemotherapy in Mouse Models of Cervical Cancer. *Oncogene* (2011) 30(28):3139–52. doi: 10.1038/onc.2011.23
16. Li H, Zhu H, Xu CJ, Yuan J. Cleavage of BID by Caspase 8 Mediates the Mitochondrial Damage in the Fas Pathway of Apoptosis. *Cell* (1998) 94(4):491–501. doi: 10.1016/S0092-8674(00)81590-1
17. Milhas D, Cuvillier O, Therville N, Clavé P, Thomsen M, Levade T, et al. Caspase-10 Triggers Bid Cleavage and Caspase Cascade Activation in FasL-Induced Apoptosis. *J Biol Chem* (2005) 280(20):19836–42. doi: 10.1074/jbc.M414358200
18. Antony J, Saikia M, Nath L, Katiki MR, Murty MS, Paul A, et al. DW-F5: A Novel Formulation Against Malignant Melanoma From Wrightia Tinctoria. *Sci Rep* (2015) 5(1):1–15. doi: 10.1038/srep12662
19. Jacobs H, Singh T, Reynolds WF, McLean S. Isolation and 13C-Nmr Assignments of Cucurbitacins From Cayaponia Angustiloba, Cayaponia Racemosa, and Guraniasubumbellata. *J Nat Prod* (1990) 53(6):1600–5. doi: 10.1021/np50072a037
20. Amann VC, Ramelyte E, Thurneysen S, Pitocco R, Bentele-Jaberg N, Goldinger SM, et al. Developments in Targeted Therapy in Melanoma. *Eur J Surg Oncol (EJSO)* (2017) 43(3):581–93. doi: 10.1016/j.ejso.2016.10.014
21. Zaidieh T, Smith JR, Ball KE, An Q. ROS as a Novel Indicator to Predict Anticancer Drug Efficacy. *BMC Cancer* (2019) 19(1):1–14. doi: 10.1186/s12885-019-6438-y
22. Paluncic J, Kovacevic Z, Jansson PJ, Kalinowski D, Merlot AM, Huang ML, et al. Roads to Melanoma: Key Pathways and Emerging Players in Melanoma Progression and Oncogenic Signaling. *Biochim Biophys Acta (BBA)-Mol Cell Res* (2016) 1863(4):770–84. doi: 10.1016/j.bbamcr.2016.01.025
23. Becker TM, Boyd SC, Mijatov B, Gowrishankar K, Snoyman S, Pupo GM, et al. Mutant B-RAF-Mcl-1 Survival Signaling Depends on the STAT3 Transcription Factor. *Oncogene* (2014) 33(9):1158–66. doi: 10.1038/onc.2013.45
24. Carpenter RL, Lo H-W. STAT3 Target Genes Relevant to Human Cancers. *Cancers* (2014) 6(2):897–925. doi: 10.3390/cancers6020897
25. Dias DA, Urban S, Roessner U. A Historical Overview of Natural Products in Drug Discovery. *Metabolites* (2012) 2(2):303–36. doi: 10.3390/metabo2020303
26. Garg S, Kaul SC, Wadhwa R. Cucurbitacin B and Cancer Intervention: Chemistry, Biology and Mechanisms. *Int J Oncol* (2018) 52(1):19–37. doi: 10.3892/ijo.2017.4203
27. Berger M, Richtig G, Kashofer K, Aigelsreiter A, Richtig E. The Window of Opportunities for Targeted Therapy in BRAFwt/NRASwt/KITwt Melanoma: Biology and Clinical Implications of Fusion Proteins and Other Mutations. *Giornale Ital Dermatol Venereol: Organo Ufficiale Soc Ital Dermatol Sifilogr* (2018) 153(3):349–60. doi: 10.23736/S0392-0488.18.05970-9
28. Johannessen CM, Boehm JS, Kim SY, Thomas SR, Wardwell L, Johnson LA, et al. COT Drives Resistance to RAF Inhibition Through MAP Kinase Pathway Reactivation. *Nature* (2010) 468(7326):968–72. doi: 10.1038/nature09627
29. Das Thakur M, Salangsang F, Landman AS, Sellers WR, Pryer NK, Levesque MP, et al. Modelling Vemurafenib Resistance in Melanoma Reveals a Strategy to Forestall Drug Resistance. *Nature* (2013) 494(7436):251–5. doi: 10.1038/nature11814
30. Ascierto PA, Schadendorf D, Berking C, Agarwala SS, van Herpen CM, Queirolo P, et al. MEK162 for Patients With Advanced Melanoma Harbouring NRAS or Val600 BRAF Mutations: A Non-Randomised, Open-Label Phase 2 Study. *Lancet Oncol* (2013) 14(3):249–56. doi: 10.1016/S1470-2045(13)70024-X
31. Lito P, Pratilas CA, Joseph EW, Tadi M, Halilovic E, Zubrowski M, et al. Relief of Profound Feedback Inhibition of Mitogenic Signaling by RAF Inhibitors Attenuates Their Activity in BRAFV600E Melanomas. *Cancer Cell* (2012) 22(5):668–82. doi: 10.1016/j.ccr.2012.10.009
32. Flaherty KT, Infante JR, Daud A, Gonzalez R, Kefford RF, Sosman J, et al. Combined BRAF and MEK Inhibition in Melanoma With BRAF V600 Mutations. *N Engl J Med* (2012) 367(18):1694–703. doi: 10.1056/NEJMoa1210093
33. Ahmed MS, Halaweish FT. Cucurbitacins: Potential Candidates Targeting Mitogen-Activated Protein Kinase Pathway for Treatment of Melanoma. *J Enzyme Inhib Med Chem* (2014) 29(2):162–7. doi: 10.3109/14756366.2012.762646
34. Wellbrock C, Marais R. Elevated Expression of MITF Counteracts B-RAF–stimulated Melanocyte and Melanoma Cell Proliferation. *J Cell Biol* (2005) 170(5):703–8. doi: 10.1083/jcb.200505059

Conflict of Interest: The authors declare that the research was conducted in the absence of any commercial or financial relationships that could be construed as a potential conflict of interest.

Supplementary Materials

Supplementary Figures.

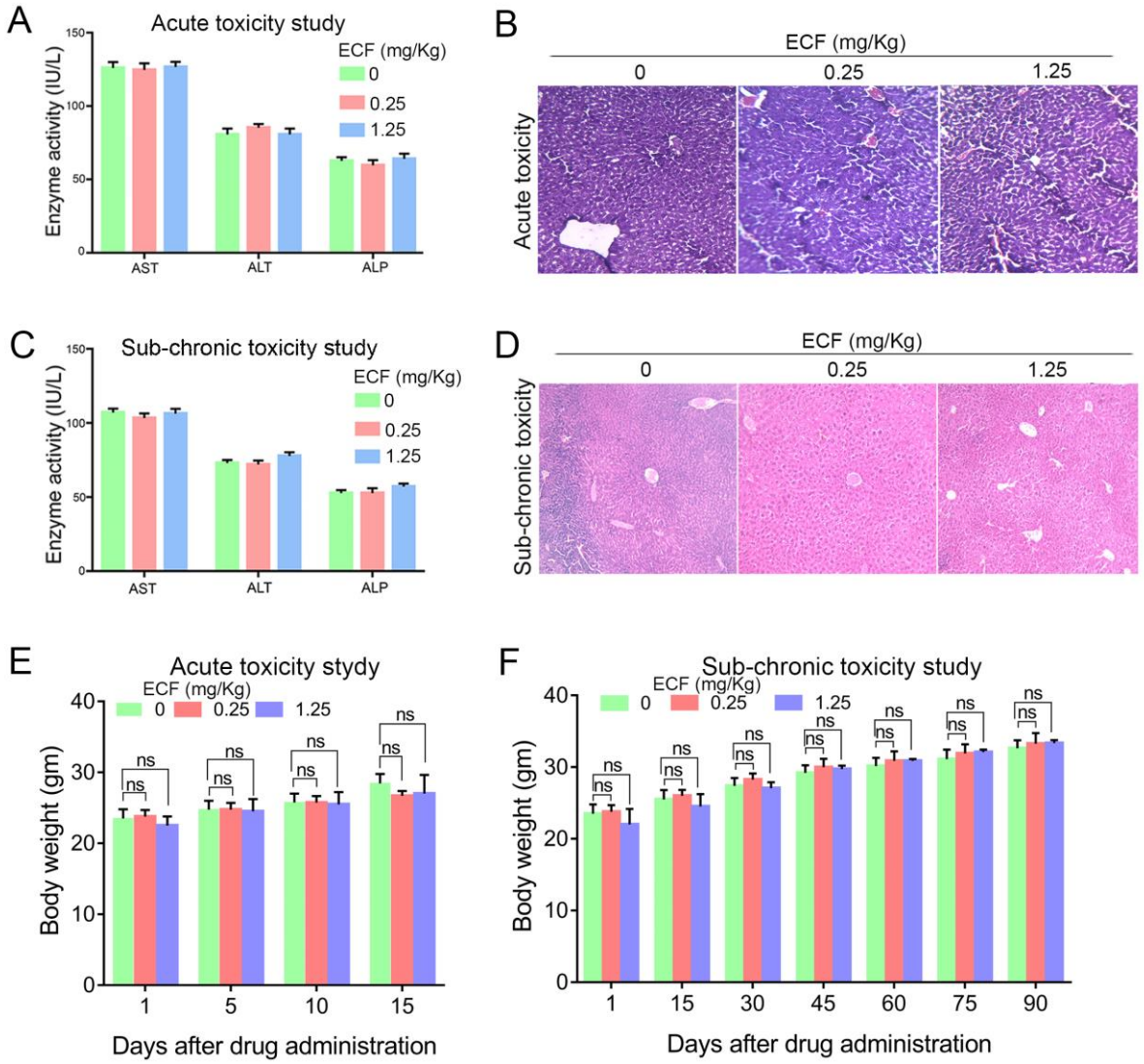

Supplementary Figure 1. Pharmacological safety of ECF, (A-D) Toxicity analysis upon ECF treatment *in vivo.* Graphical representation of AST, ALT, and ALP activities in response to ECF treatment. H&E stained liver tissues of mice treated with ECF. **(E)** Representation of body weight (5 days intervals) of animals of the acute toxicity study. **(F)** Representation of body weight (14 days interval) of animals of the sub-chronic toxicity study.

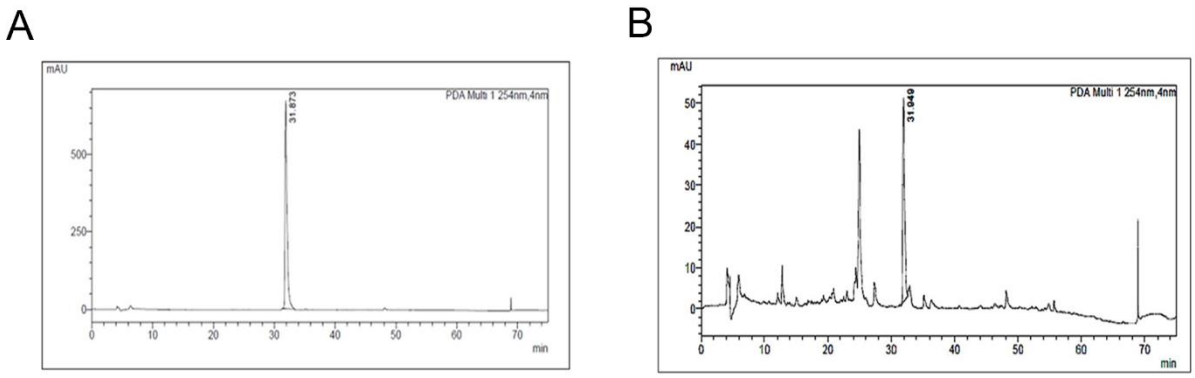

Supplementary Figure 2. UHPLC chromatograms of cucurbitacin B and its presence in ECF fraction, (A-B) ECF fraction (3 mg/ml) and the isolated pure compound (2 mg/ml) were dissolved in acetonitrile:water (1:1) and filtered through a 0.2 µm nylon filter. The sample injection volume was 20 µL, and the C18 column temperature was 35 °C. The mobile phase system consists of water:acetic acid (100:1) (A) and acetonitrile (B). A step gradient program was used for this analysis as follows: 0% B at 0 min to 40% B at 20 min, 40 to 50% at 30 min, 50 to 60% at 40 min, 60 to 80% at 50 min, 80 to 100% at 60 min, then maintaining at 100% B from 60 to 65 min at a flow rate of 1 ml/min, monitored at 254 nm.

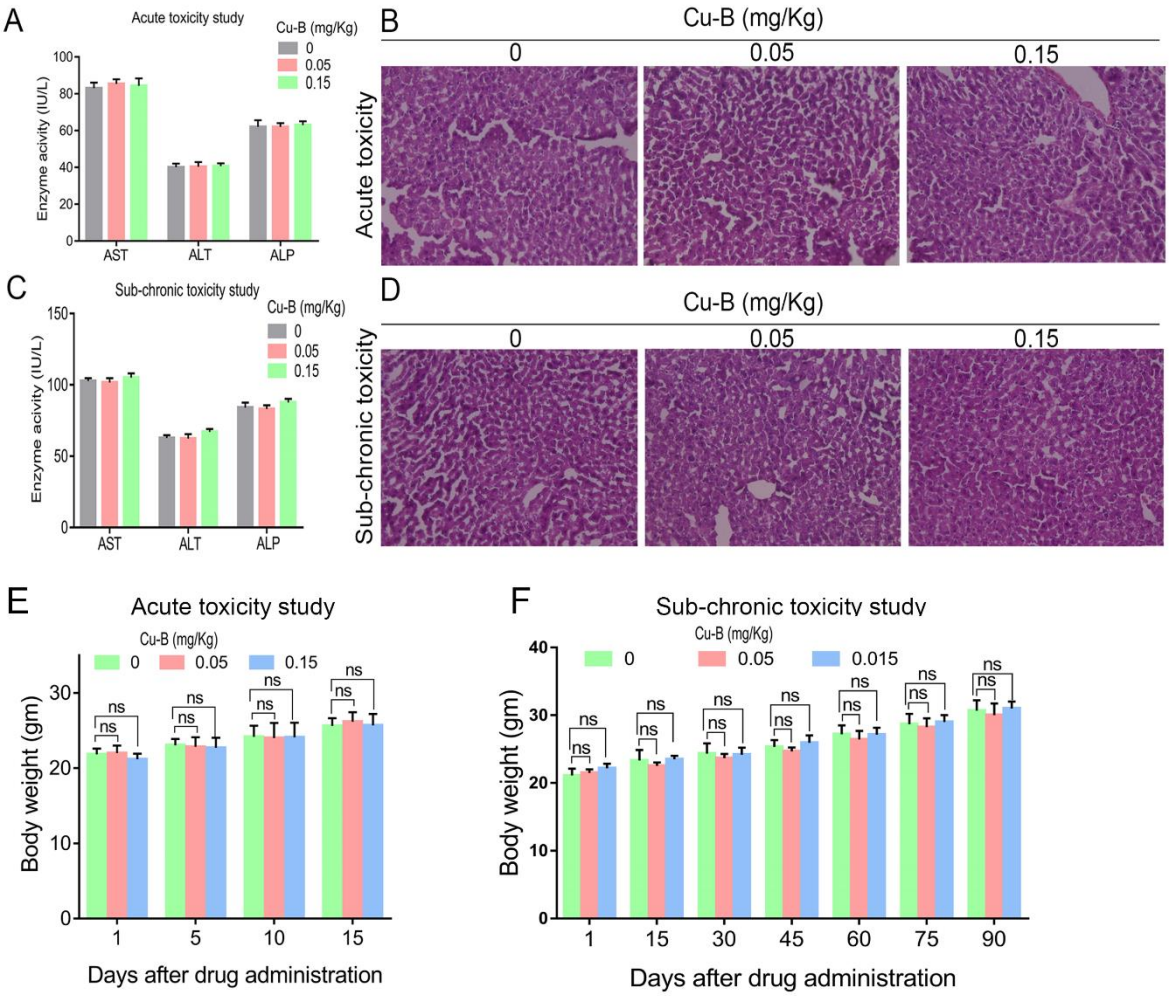

Supplementary Figure 3. Pharmacological safety of Cu-B, (A-D) Acute and sub-chronic toxicity analysis upon Cu-B treatment in *Swiss albino* mice. Graphical representation of AST, ALT, and ALP activities in response to Cu-B treatment. H&E stained liver tissues of mice treated with Cu-B. **(E)** Representation of body weight (5 days intervals) of animals of the acute toxicity study. **(F)** Representation of body weight (14 days interval) of animals of the sub-chronic toxicity study

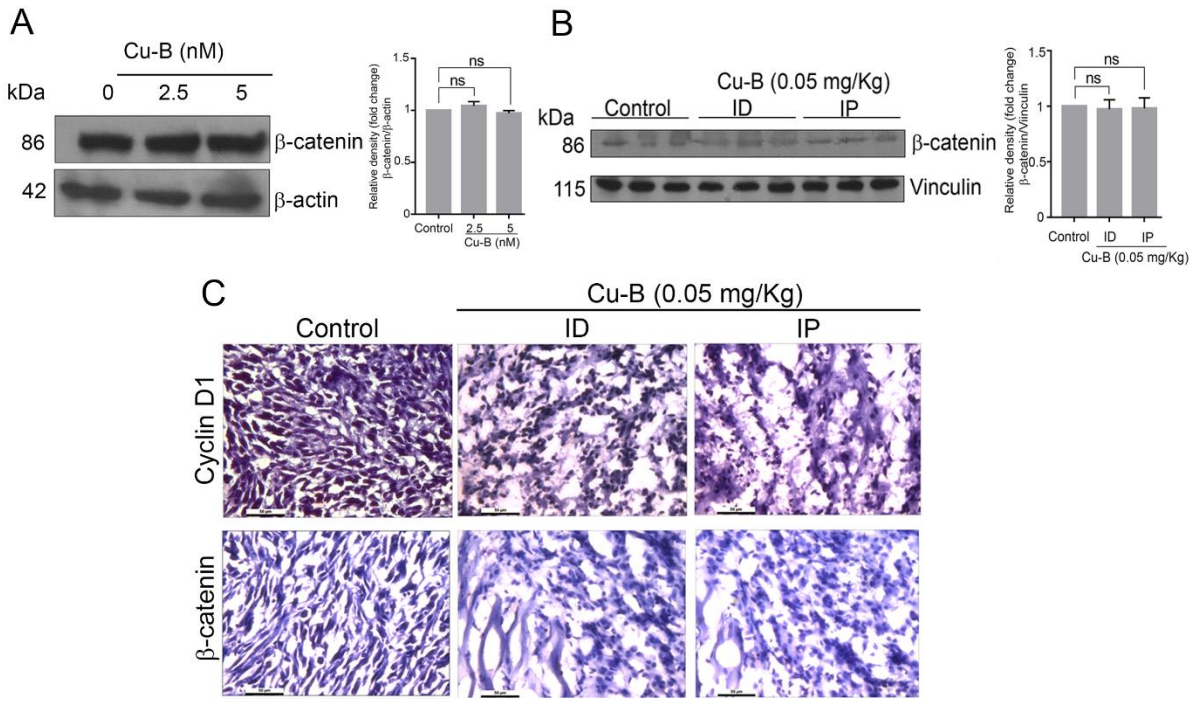

Supplementary Figure 4. The effect of Cu-B on the key survival signals in melanoma, (A) Cu-B treatment unalters β-catenin levels in A375 cells (B) Cu-B does not change β-catenin levels *in vivo* as evidenced in the tumor lysates (C) IHC analysis on the expression of Cyclin D1 and β-catenin in tumor tissues of mice groups. Data are representative of three independent experiments (Mean±SEM) and P-values are calculated using one-way ANOVA. ns ≥ 0.05.

Supplementary Table

Carbon No.	^{1}H (ppm)	^{13}C (ppm)
1	2.30, 1.24	36.01
2	4.36	71.65
3	-	213.08
4	-	50.25
5	-	140.36
6	5.7 (t, *J* = 3.5 Hz, 1H)	120.46
7	1.90 (d, *J* = 7 Hz), 2.42 (d, *J* = 7 Hz)	23.87
8	1.98	42.37
9	-	48.45
10	2.67	33.73
11	-	212.19
12	3.17 (d, *J* = 14.5 Hz), 2.62 (d, *J* = 14.5 Hz)	48.66
13	-	50.69
14	-	48.11
15	1.89, 1.47	45.32
16	4.36	71.3
17	2.5	58.2
18	0.91 (s, 3H)	19.86
19	1.01 (s, 3H)	20.06
20	-	78.24
21	1.35 (s, 3H)	23.93
22	-	202.5
23	6.39 (d, *J* = 16.5 Hz)	120.29
24	7.0 (d, *J* = 16.0 Hz)	152.03
25	-	79.34
26	1.50 (s, 3H)	26.46
27	1.57 (s, 3H)	25.91
28	1.2 4(s, 3H)	29.37
29	1.28 (s, 3H)	21.26
30	1.3 (s, 3H)	18.91
31	-	170.32
32	1.94 (s, 3H)	21.95

Supplementary Table 1. ^{1}H and ^{13}C NMR of cucurbitacin B, in $CDCl_3$, isolated from the ethyl acetate extract of *Corallocarpus epigaeus.*

frontiers | Frontiers in Oncology

TYPE Correction
PUBLISHED 12 August 2022
DOI 10.3389/fonc.2022.989283

OPEN ACCESS

EDITED AND REVIEWED BY
Balaji Krishnamachary,
Johns Hopkins University,
United States

*CORRESPONDENCE
Ravi Shankar Lankalapalli
ravishankar@niist.res.in
Ruby John Anto
rjanto@rgcb.res.in
Smitha Vadakkeveettil Bava
smithanishad@gmail.com

SPECIALTY SECTION
This article was submitted to Pharmacology of Anti-Cancer Drugs, a section of the journal Frontiers in Oncology

RECEIVED 08 July 2022
ACCEPTED 19 July 2022
PUBLISHED 12 August 2022

CITATION
Aiswarya SUD, Vikas G, Haritha NH, Liju VB, Shabna A, Swetha M, Rayginia TP, Keerthana CK, Nath LR, Reshma MV, Sundaram S, Anto NP, Lankalapalli RS, Anto RJ and Bava SV (2022) Corrigendum: Cucurbitacin B, purified and characterized from the rhizome of *Corallocarpus epigaeus* exhibits anti-melanoma potential. *Front. Oncol.* 12:989283. doi: 10.3389/fonc.2022.989283

Corrigendum: Cucurbitacin B, purified and characterized from the rhizome of *Corallocarpus epigaeus* exhibits anti-melanoma potential

Sreekumar Usha Devi Aiswarya[1,2], Gowda Vikas[3], Nair Hariprasad Haritha[2], Vijayasteltar Belsamma Liju[2,4], Anwar Shabna[2], Mundanattu Swetha[2], Tennyson Prakash Rayginia[2], Chenicheri Kizhakkeveettil Keerthana[2], Lekshmi Raghu Nath[2,5], Mullan Vellandy Reshma[6,7], Sankar Sundaram[8], Nikhil Ponnoor Anto[4], Ravi Shankar Lankalapalli[3,7]*, Ruby John Anto[2]* and Smitha Vadakkeveettil Bava[1]*

[1]Department of Biotechnology, University of Calicut, Malappuram, India, [2]Division of Cancer Research, Rajiv Gandhi Centre for Biotechnology, Thiruvananthapuram, India, [3]Chemical Sciences and Technology Division, Council for Scientific and Industrial Research (CSIR)-National Institute for Interdisciplinary Science and Technology (CSIR-NIIST), Thiruvananthapuram, India, [4]The Shraga Segal Department of Microbiology-Immunology and Genetics, Faculty of Health Sciences, Ben-Gurion University of the Negev, Beer Sheva, Israel, [5]Department of Pharmacognosy, Amritha School of Pharmacy, Amritha Vishwa Vidyapeetham, Amrita Institute of Medical Sciences (AIMS) Health Science Campus, Ponekkara P.O, Kochi, India, [6]Agro-Processing and Technology Division, Council for Scientific and Industrial Research (CSIR)-National Institute for Interdisciplinary Science and Technology (CSIR-NIIST), Thiruvananthapuram, India, [7]Academy of Scientific and Innovative Research (AcSIR), Ghaziabad, India, [8]Department of Pathology, Government Medical College, Kottayam, India

KEYWORDS

***corallocarpus epigaeus*, cucurbitacin B, melanoma, apoptosis, NMR spectroscopy, mass spectrometry**

A Corrigendum on:

Cucurbitacin B, purified and characterized from the rhizome of Corallocarpus epigaeus exhibits anti-melanoma potential

By Aiswarya SUD, Vikas G, Haritha NH, Liju VB, Shabna A, Swetha M, Rayginia TP, Keerthana CK, Nath LR, Reshma MV, Sundaram S, Anto NP, Lankalapalli RS, Anto RJ and Bava SV (2022). *Front. Oncol.* 12:903832. doi: 10.3389/fonc.2022.903832

10.3389/fonc.2022.989283

In the published article, there was an error in Figure 2 as published. The blot quantification graph of Figure 2C was duplicated in place of the graph for Figure 2D. The corrected Figure 2 appears below.

The authors apologize for this error and state that this does not change the scientific conclusions of the article in any way. The original article has been updated.

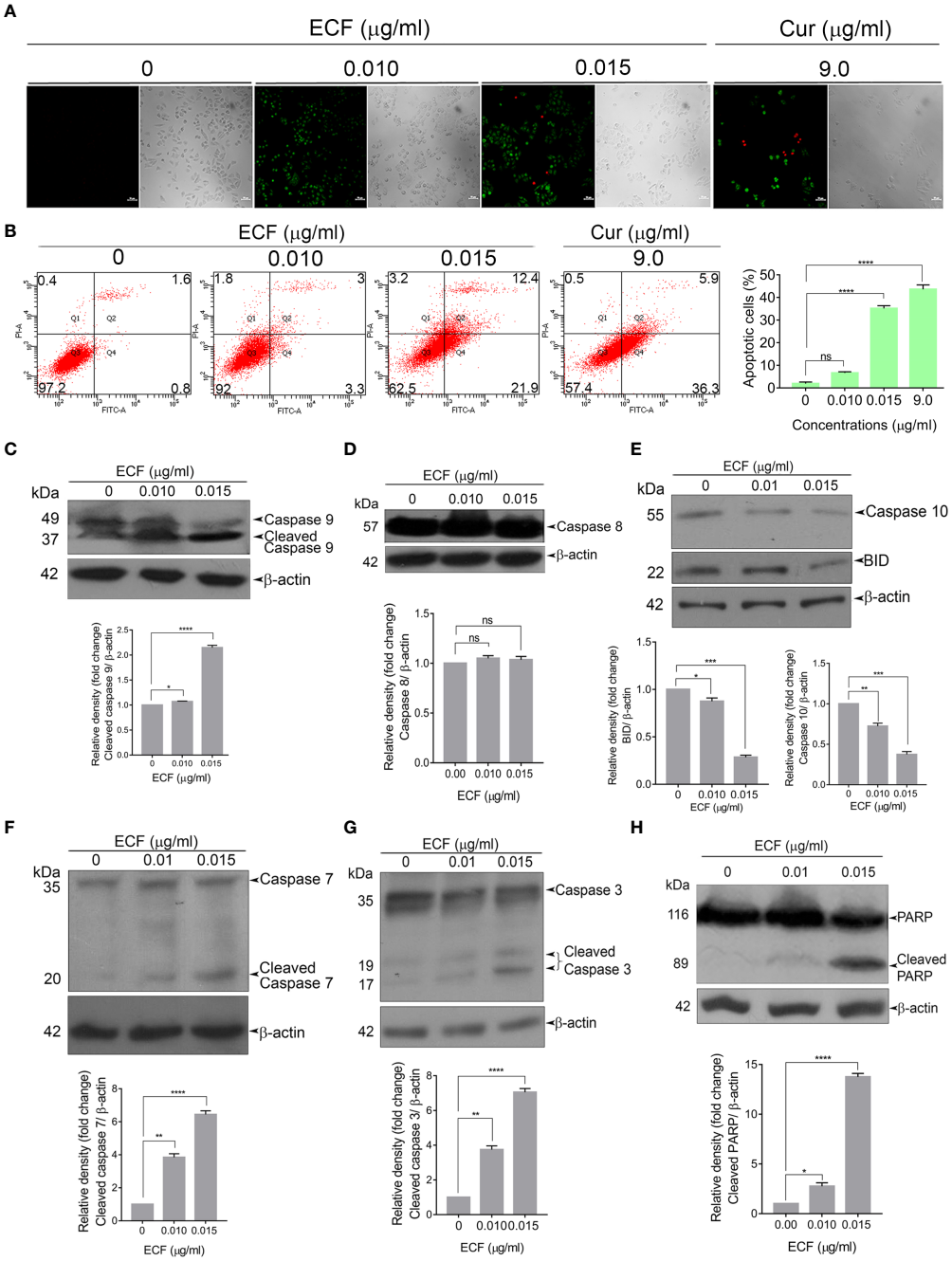

FIGURE 2
ECF triggers apoptotic mode of cell death in melanoma **(A, B)** ECF induces apoptosis in A375 cells as assessed by Annexin/PI staining, and was quantitated by FACS analysis. **(C–H)** ECF potentiates the activation of caspases and cleavage of PARP in A375 cells as analyzed by immunoblotting. Data are representative of three independent experiments (Mean ± SEM) and P-values are calculated using one-way ANOVA. ****P ≤ 0.0001, ***P ≤ 0.001, **P ≤ 0.01, *P ≤ 0.1and ns ≥ 0.05.

10.3389/fonc.2022.989283

Publisher's note